UNIVERSIDAD DE CHILE
FACULTAD DE CIENCIAS FÍSICAS Y MATEMÁTICAS
DEPARTAMENTO DE GEOLOGÍA

INSIGHTS ON THE HOLOCENE CLIMATE OF SOUTHERNMOST SOUTH AMERICA FROM PALEOGLACIER RECONSTRUCTIONS IN PATAGONIA AND TIERRA DEL FUEGO (46°-55°S)

TESIS PARA OPTAR AL GRADO DE DOCTOR EN
CIENCIAS MENCIÓN GEOLOGÍA

SCOTT ANDREW, REYNHOUT

PROFESOR GUÍA:
MAISA ROJAS CORRADI

MIEMBROS DE LA COMISIÓN:
VALENTINA FLORES AQUEVEQUE
MICHAEL KAPLAN
ESTEBAN SAGREDO TAPIA
GABRIEL VARGAS EASTON

SANTIAGO DE CHILE
2019

RESUMEN DE LA TESIS PARA OPTAR AL GRADO DE:
Doctor en Ciencias, mención Geología
POR: Scott Andrew Reynhout Reynhout
FECHA: 03/09/2019
PROFESOR GUIA: Maisa Rojas Corradi

"INSIGHTS ON THE HOLOCENE CLIMATE OF SOUTHERNMOST SOUTH AMERICA FROM PALEOGLACIER RECONSTRUCTIONS IN PATAGONIA AND TIERRA DEL FUEGO (46°-55°S)"

This dissertation presents preliminary and final results of four paleoglacier reconstructions in the regions of Patagonia and Tierra del Fuego (46°-55°S), with the objective of identifying trends in Holocene climate in southernmost South America. Two complete chronologies and one partial chronology of Holocene glacier fluctuations are determined by geomorphologic mapping, cosmogenic surface exposure dating of glacial landforms, dendroglaciology, and radiocarbon dating. Former glacier surfaces from four sites across the region are reconstructed to evaluate spatial variability of equilibrium-line altitude depression associated with age-constrained glacier advances.

Glaciar Torre (Chapter 3; 49.3°S / 73.0°W) advanced to pre-Holocene maxima at c. 17 ka and c. 13 ka, coincident with the onset of the Last Glacial Termination and the end of the Antarctic Cold Reversal, respectively. While the record at the Dalla Vedova glacier (Chapter 4; 54.6°S / 69.1°W) is less well-constrained, the few dates available suggest potentially synchronous advances occurred at these times. Glaciar Torre subsequently readvanced several times in the Holocene, registering progressively less-extensive advances at 9.4 ka, 6.8 ka, 6.1 ka, 4.5 ka, and 0.5 ka. Preliminary ages of glacier advances from Cerro Castillo (Chapter 5; 46.1°S / 72.2°W) show advances from c. 10-8 ka and at c. 2.3 ka; an additional six glacier advances occurred between these dates, although no numerical age constraint yet exists for these advances. Paleoglacier reconstructions at Glaciar Torre, Cerro Castillo (Chapter 5), and an already dated glacier advance at Río Tranquilo (47.5°S / 72.4°W), show that Holocene advances in Patagonia corresponded to snowline depressions of 160-200 m. On the other hand, the earliest dated Holocene advance of the Dalla Vedova glacier in Tierra del Fuego occurred at 0.9 ka, which coincided with a much smaller snowline depression of 65 m.

The directly dated early Holocene glacier maxima observed in this study have not been previously defined in Patagonia; subsequent glacier advances align well with well-constrained glacier advances in the region. These data collectively define a new pattern of Holocene glaciation in Patagonia and suggest the older "Neoglacial" model must be reconsidered. The glacial sequence identified at Glaciar Torre corresponds to cold/wet periods inferred from other paleoenvironmental proxies, tentatively linked to the Southern Annular Mode (SAM). Patagonian glaciers therefore seem to have responded coherently to persistent SAM-like phases throughout the Holocene, which may also explain the out-of-phase advances observed in the Cordillera Darwin, which is inferred as a consequence of enhanced precipitation superposed upon generalized warming during positive SAM-like phases.

RESUMEN DE LA TESIS PARA OPTAR AL GRADO DE:
Doctor en Ciencias, mención Geología
POR: Scott Andrew Reynhout Reynhout
FECHA: 03/09/2019
PROFESOR GUIA: Maisa Rojas Corradi

"NUEVOS CONOCIMIENTOS DEL CLIMA DE PATAGONIA Y TIERRA DEL FUEGO (46°-55°S) EN EL HOLOCENO BASADOS EN RECONSTRUCCIONES PALEOGLACIALES"

En esta tesis se aborda el análisis de los controles fundamentales sobre cambios climáticos holocénicos en las regiones de Patagonia y Tierra del Fuego (46°-55°S) en base del registro glacial. Mapeo geomorfológico se combina con técnicas geocronológicas para evaluar nuevamente la cronología glacial de la zona de estudio. A su vez, cronologías nuevas y preexistentes se utilizan para modelar cambios históricos en las alturas de las líneas de equilibrio ("ELA") desde los 18,000 años antes del presente hasta tiempos modernos.
Glaciar Torre (Capítulo 3; 49.3°S / 73.0°O) registró avances pleistocenos a los 17.1 ka y 13.5 ka, que coincidieron con el inicio de la terminación del último máximo glacial y la "Inversión Fría Antártica", respectivamente. Trazas de avances glaciales que corresponden a estos eventos quedaban al frente del Glaciar Dalla Vedova (Capítulo 4; 54.6°S / 69.1°O). Los paralelos entre sitios sugieren que ambas regiones estaban sujetas a cambios climáticos síncronos durante el fin del pleistoceno.

En cambio, el registro glacial de Patagonia continental demuestra un patrón distinto que sus equivalentes en la Isla Grande de Tierra del Fuego durante el Holoceno. Glaciar Torre registró avances a los 9.7 ka, 6.8 ka, 6.1 ka, 4.5 ka, y 0.5 ka, cada uno de una magnitud decreciente. Este patrón se replica en Cerro Castillo (Capítulo 5; 46.1°S / 72.2°O), donde el sistema glacial registró al mínimo 8 avances decrecientes entre los ~10.5-8.4 ka y ~2.7-1.8 ka. El patrón decreciente de avances desde el Holoceno temprano aparece también en Río Tranquilo (47.5°S / 72.4°O). Reconstrucciones de estos glaciares revelan que avances holocénicos en Patagonia correspondieron a depresiones en la ELA de 160-200 m. Por otra parte, el avance glacial más extenso en Dalla Vedova ocurrió a los 0.9 ka, y correspondió a una depresión menor en la ELA de 65 m.

Los avances extensos en el Holoceno temprano aún no han sido reconocidos en Patagonia. Avances subsecuentes son paralelas a eventos previamente reconocidos en la región, y junto con los avances en el Holoceno temprano definen un patrón nuevo de glaciación holocénica en Patagonia; en base de estos nuevos datos, se sugiere que el modelo "Neoglacial" merece reevaluación.

El nuevo patrón decreciente de avances glaciales holocénicos en Patagonia paralela el de los glaciares en Nueva Zelandia, y se opone al patrón creciente en el hemisferio norte. Se propone que cambios en la intensidad de insolación del verano puede explicar este fenómeno. La nueva cronología glacial del Holoceno en Patagonia corresponde a eventos "fríos/húmedos" registrado por otros archivos paleoclimáticos, vinculados a cambios parecidos al funcionamiento moderno del Modo Anular del Sur / oscilación antártica (SAM). El SAM puede explicar la cadencia de avances glaciales en Patagonia, y también el avance desfasado en Tierra del Fuego, por cambios sistemáticos en temperatura y precipitación a lo largo de ambas regiones.

Para los huérfanos
dónde estén y quiénes sean

AGRADECIMIENTOS

Este trabajo no habría sido posible si no fuera por el aporte financiero de las dos encarnaciones del Núcleo Milenio Paleoclima y el programa de Becas de Doctorado de la Comisión Nacional de Investigación Científica y Tecnológica, FONDECYT 1160488, FONDECYT 1171773, FONDECYT 1180717, FONDAP-CONCIYT 15110009, NSF-EAR 09-02363, y NSF-EAR 18-04816. A mi profesora guía, Maisa, muchas gracias por su ayuda y todas las largas conversaciones. Gracias a los Drs. Sagredo y Kaplan, quienes me regalaron la oportunidad de hacer estos años de estudios. Finalmente, agradezco todos los comentarios de la comisión y de todxs mis co-autores, que me ayudaron en producir y mejorar el producto final.

TABLE OF CONTENTS

TABLE INDEX

CHAPTER 3

Article: Holocene glacier fluctuations in Patagonia are modulated by summer insolation intensity and paced by Southern Annular Mode-like variability

CHAPTER 4

CHAPTER 5

FIGURE INDEX

CHAPTER 1

CHAPTER 2

CHAPTER 3

Article: Holocene glacier fluctuations in Patagonia are modulated by summer insolation intensity and paced by Southern Annular Mode-like variability

CHAPTER 4

CHAPTER 5

CHAPTER 6

Chapter 1 – Introduction

1.1 Preface

Understanding modern climate change requires knowledge of past climate variability, to place the present trend towards a warmer globe in context. The global instrumental climate record, while useful, only extends over (at maximum) the last two centuries and possesses a strong regional bias—more remote areas are less likely to have dense, high-quality networks of weather stations necessary for detailed instrumental analysis. "Proxies" for past climates in the geological record therefore provide unique insights into changes in the past and are key tools in the investigation of the mechanisms by which Earth's climate system functions.

Glaciers are masses of frozen water that persist from year to year and flow under their own weight. Their composition is sensitive to changes in baseline climate conditions, and their mass means that they act as a type of "low pass" filter of climate, responding to changes in baseline climate over the scale of tens to tens of thousands of years (Mackintosh et al., 2017). The geological record of past glacier volume therefore serves as a powerful proxy for climate change when observational records do not exist. Southernmost South America (defined hereafter as the southern South American continent between 40°-54°S) hosts the greatest ice volume outside of the polar regions including Greenland. Patagonia (46°-53°S) and Tierra del Fuego (53°-55°S) sit astride the Southern Ocean as the only continental landmass interrupting southern westerly circulation at these latitudes. The glaciers of southern South America therefore retain a perspective—unique in the world—of the terrestrial climatic response to changes in this dominant feature of global climate.

Despite the long-recognized record of glacial fluctuations preserved in the region (Caldenius, 1932), assigning an absolute chronology to these glaciations remains a topic of active investigation. On the scale of glacial cycles, Patagonian ice grew and disappeared broadly in concert with global glacial and interglacial stades, respectively (Denton et al., 1999; Hein et al., 2010, 2017), although some exceptions exist (e.g. García et al., 2019). Recent research has focused on clarifying the Patagonian glacier response to the turbulent Last Glacial Termination (LGT; García et al., 2012; Hall et al., 2013; Bendle et al., 2017; Sagredo et al., 2018; Martin et al., 2019). During the LGT, the Patagonian glacial record in Patagonia closely aligns with changes preserved in the Antarctic ice core record at the onset of the deglaciation (Denton et al., 2010) and the Antarctic Cold Reversal (Sagredo et al., 2018). In the Northern Hemisphere, episodic cold periods during the LGT seemingly occurred out-of-phase with 'Antarctic-style' southern records (Denton et al., 2010). The contrasting behavior of Northern and Southern Hemisphere glaciers during this time heavily informs the discussion of mechanisms behind abrupt climate changes.

With regards to the Holocene, various conflicting models have been proposed to characterize regional glacier variability in Patagonia (Mercer, 1982; Glasser et al., 2004; Aniya, 2013; Kaplan et al., 2016). While differing in the timing of specific glacier advances, each model conforms to a 'Hypsithermal-Neoglacial' model characteristic of the Northern Hemisphere (Porter and Denton, 1967; Denton and Karlén, 1973), where an early Holocene thermal maximum is subsequently followed by renewed glacial activity in the middle to late Holocene. However, in contrast to the progressively more-extensive Neoglacial advances in the Northern Hemisphere (Menounos et al., 2009; Ivy-Ochs et al., 2009; Nesje, 2009), to date, existing data have indicated that Patagonian glaciers appear to reach their maximum Holocene extent at the beginning of the South American "Neoglacial" in the mid-Holocene, c. 6-5 ka (ka = 1,000 years before present; Porter, 2000; Kaplan et al., 2016). None of these patterns, therefore, conform easily to established chronologies in other parts of the globe (Solomina et al., 2015): the Patagonian record, as recorded in current literature, appears to differ from Northern Hemisphere records in the timing and magnitude of glacial advances, and similarly departs from other Southern Hemisphere records in New Zealand (Schaefer et al., 2009; Putnam et al., 2012; Kaplan et al., 2013).

A weakness of the Patagonian paleoglacial record is its reliance on sparse and often incomplete chronologies using inadequate applications of geochronological methods. The proposed Hypsithermal-Neoglacial models for regional Holocene glaciation are to some degree based on decades-old work using radiocarbon minimum-limiting age bracketing (Mercer, 1976; Aniya, 2013), which have been shown in certain cases to have underestimated the true age of glacial landforms by up to 10,000 years (Strelin et al., 2014; Kaplan et al., 2016). Furthermore, these models generally ignore preexisting evidence of glacier advances during the early Holocene (Röthlisberger, 1986; Harrison et al., 2012). Newer methods that can directly date Holocene or postglacial landforms have only recently begun to be applied to the Patagonian glacial record (Kaplan et al., 2016), and even then, most studies have focused on landforms associated with the LGT (Sagredo et al., 2018).

In summary, despite the regional and global importance of Patagonia's terrestrial glacial record, additional work is required to resolve doubts surrounding the existing Holocene paleoglacier literature describing the region. This doctoral thesis aims to address this issue by applying terrestrial cosmogenic nuclide surface exposure dating (TCN-SED) to paleoglacial landforms preserved in several sites across southern Patagonia and Tierra del Fuego. The principal goal is to use direct dating to time the response of glaciers to regional Holocene climate change. Through this work, I will address the following questions:

- Have glaciers in southernmost South America (Patagonia and Tierra del Fuego) varied in a way that corresponds to a previously-proposed model of regional Holocene climate variability?
- Did glaciers in Patagonia and Tierra del Fuego advance and retreat in synchrony, or are there spatial variations in the magnitude and/or timing of glacial advances?

- Can the structure of glacier variability in southernmost South America reveal insights into the nature of regional climate change over the Holocene?

I outline the structure of the thesis below.

Chapter 1 reviews the key assumptions necessary in the use of glaciers as paleoclimate proxies. The climate sensitivity of glaciers is discussed, as are the process of identifying past glacier extent, the methods commonly used to determine an absolute chronology of glacial events, and the climatic interpretation of past glacier variations.

Chapter 2 introduces the study area, both in physical and historical terms. The chapter begins with a review of the geology and climatology of southern Patagonia. A summary of the historical development of paleoglacier studies in the area follows, with special emphasis on a critical analysis of the prior literature. Complementary paleoclimate proxies in the area are also considered.

Chapter 3 presents a paleoglacier chronology from southern Patagonia constructed as part of this thesis. It includes an article submitted to *Quaternary Science Reviews* in January 2019, titled "Holocene glacier fluctuations in Patagonia are modulated by summer insolation intensity and paced by Southern Annular Mode-like variability." In this article, ^{10}Be surface exposure dating of glacial moraines are applied to a moraine sequence near Monte Fitz Roy, Argentina. LGT and Holocene events are captured in this chronology, notably two advances that predate the previously-identified onset of the "Neoglacial" in Patagonia.

Chapter 4 presents a paleoglacier chronology in Tierra del Fuego, in preparation for publication. ^{10}Be surface exposure dating of moraines of the Glaciar Dalla Vedova in the Cordillera Darwin is combined with radiocarbon dating of bog cores and dendrochronologic surface exposure dating to constrain the glacial history of this region. In addition to newly identified LGT moraines, a Holocene glacier advance asynchronous with respect to Patagonia is presented. The chapter concludes with a discussion of the climate significance of asynchronous glaciation between Patagonia and Tierra del Fuego, as well as implications for methodology and future studies.

Chapter 5 presents ELA reconstructions of the glaciers studied within this study, based on the geomorphology and preexisting glacial chronologies, as well as one new chronology presented in this chapter. These results are placed in the context of other paleoclimate proxies in Patagonia as well as New Zealand, and are used to interpret our new chronologies in a regional climate context.

Chapter 6 concludes with a summary and discussion of the results of this thesis.

1.2 Theoretical framework

1.2.1 Glacier response to climate change

Glaciers, as masses of ice that flow, form where climate conditions at the earth's surface enable the preservation of solid precipitation for more than one hydrological year (Benn and Evans, 2014). Glaciers may be thought of as consequences of the interaction between topography and climate. While the relationships between surface topography, climate, and glaciers are complex and involve many feedbacks, on short (10^4 year) time scales, alpine valley glaciers exert a minimal effect on the baseline topography (MacGregor et al., 2000). They therefore reflect the effect of both local and regional climate factors on the land surface.

Glaciers may be broadly classified by their morphology and relationship with topography (Benn and Evans, 2014). Glaciers unconstrained by topography—that is, glaciers of great size that completely cover the landscape—are most commonly known as *ice sheets* or *ice caps* and are often of continental scale. Glaciers constrained by surrounding and underlying topography carry a variety of classifications based upon their specific setting and size. Features of in this category, such as *ice fields*, *valley glaciers*, and *cirque glaciers* are among those glaciers common to alpine environments. *Ice shelves* form from floating ice. While general principles of mass balance and glacial erosion and deposition apply to all moving bodies of terrestrial ice, this discussion focuses on principles applying to glaciers constrained by topography, specifically with regards to climate (1.2.1.2) and glacier landsystems (1.2.2.2).

1.2.1.1 Glacier mass balance and steady states

Solid precipitation is necessary to grow a body of ice. Subzero temperatures and a source of atmospheric moisture are prerequisites for solid precipitation, so ice mass *accumulation* is dependent upon the existence of cold, wet conditions for at least part of a solar year. Accumulation is counteracted by *ablation*, a term that incorporates all processes by which ice is lost. Glaciers exist in a balance between accumulation and ablation, a concept referred to as *mass balance*. If accumulation exceeds ablation, a glacier will gain net mass; if ablation exceeds accumulation, a glacier will lose net mass (Benn and Evans, 2014).

As temperature declines with increasing altitude in the troposphere, accumulation dominates at higher altitudes and ablation dominates at lower altitudes. The elevation of the glacier surface where net annual accumulation is equivalent to net annual ablation is known as the *equilibrium line altitude* (ELA; Oerlemans, 2001). As the physical *equilibrium line* is difficult to determine for modern glaciers and impossible to directly determine for past glaciers, a more meaningful metric for discussion of prior glaciation is the *steady-state ELA*, which is the average altitude where net accumulation equals net ablation for a glacier with zero net mass balance (Benn and Evans, 2014).

Glaciers transfer mass above the ELA to the ablation area below by moving downward with gravity, via internal deformation, deformation of the bed, or sliding at the glacier-bed interface (Benn and Evans, 2014). The loss of mass above the ELA is counterbalanced by accumulation, while the gain of mass below the ELA is compensated

for by ablation. In the special case where the effects of glacier redistribution downhill are exactly compensated by accumulation and ablation, the glacier is said to possess zero net mass balance, generating a 'steady state' glacier morphology with characteristic thickness and length (Benn and Evans, 2014). Glaciers advance and thicken in response to a positive perturbation in net mass balance and are said to "retreat" (or contract) in response to negative net mass balance.

Mass balance does not necessarily vary evenly with altitude, often exhibiting pronounced differences in the rate of mass balance change with altitude between the accumulation and ablation areas (Benn and Evans, 2014). This concept can be expressed as the *mass balance gradient*, which represents the rate at which mass balance changes with altitude (Furbish and Andrews, 1984; Oerlemans and Hoogendoorn, 1989; Figure 1.1).

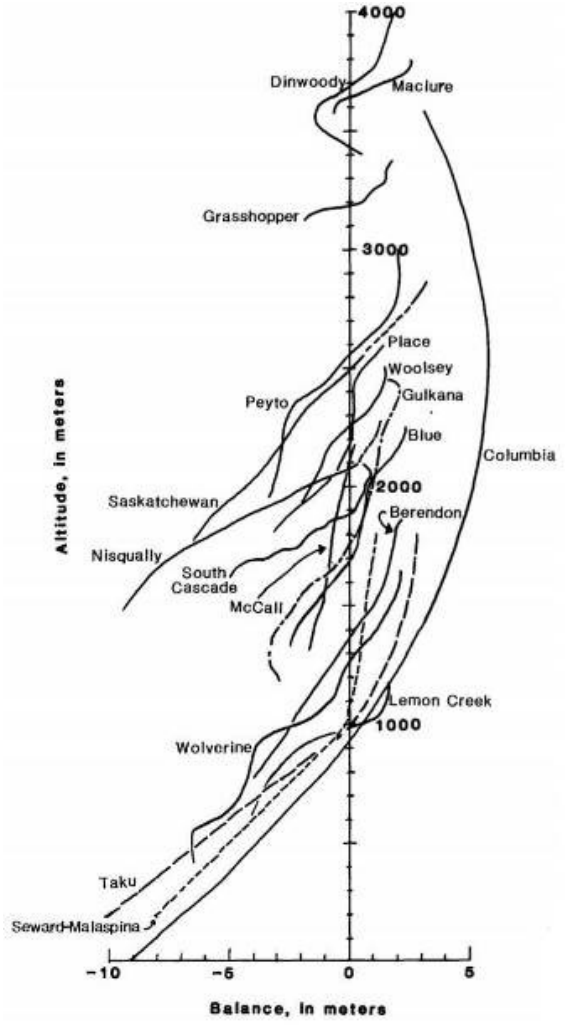

Figure 1.1. Annual measured mass balance gradients from selected North American glaciers. From Mayo (1984).

Changes in glacier length and height are relatively straightforward to evaluate via glacier geomorphology (see 1.2.2.2), historical records, and direct observation. However, the response of the glacier terminus to perturbed mass balance varies greatly, depending on factors such as glacier thermal regime, bed morphology, hypsometry, and the climatic setting of the glacier itself (Oerlemans, 2001; Cuffey and Paterson, 2010; Strelin et al.,

2014). On the other hand, variability in the ELA depends solely on changes in local climate, independent of a glaciers' morphometry or flow dynamics (Benn and Evans, 2014). The evaluation of paleo-ELA is thus a chief goal of many studies intending to evaluate the magnitude of climate perturbations.

Achieving steady state mass balance requires unvarying climate to produce a consistent glacier mass balance gradient. Changes in baseline conditions of temperature or precipitation will affect the mass balance gradient, and therefore alter glacier mass balance. This produces a new quasi-steady state to which the glacier will adjust via changes in thickness and length. The time necessary for a glacier to adjust from the initial steady state to a new steady state has been termed the *response time* (Jóhannesson et al., 1989; Bahr et al., 1998); the *reaction time* refers to the time between the change in steady state conditions and the initial reaction of the glacier terminus. Response times vary from the decadal to centennial scale (Oerlemans, 2001), recording long-term climate trends at the submillennial timescale.

Large interannual variability in climate suggests that true, interannual steady state conditions in *mean specific glacier mass balance* (the sum of glacier mass balance over the whole glacier; Benn and Evans, 2014) is unlikely to exist for long periods of time. A steady state must exist, however, at the change point between long-term (greater than decadal) mass balance trends. The inflection point at which long-term positive mass balance changes to negative (and vice versa) reflects a transient steady state when mass balance must equal zero. At this time, the steady-state ELA was achieved, however briefly.

In terms of glacier morphology, the change from positive to negative mass balance in a glacier is marked by the culmination of a glacier advance. The age of this culmination postdates the actual change in mass balance by the reaction time. Landforms that mark the maximum advance of a glacier (see section 1.2.2.2) therefore mark a time at which a steady-state ELA existed. This has important implications for the use of past glacier extent to reconstruct climate: the culmination of a glacier advance is geologically identifiable and represents a climatically significant event and corresponds with a quantifiable variable present within all glacier systems.

The key assumption behind the use of past glacier extent for climate reconstructions is the presumption of total climatic control over changes in glacier morphometry. Notable real-life counterexamples include calving and surging glaciers, whose form variations depend on non-climatic factors (Meier and Post, 1987; Raymond, 1987; Benn et al., 2007). Furthermore, modeling studies suggest that individual glacier advances and retreats can be attributed to interannual climate fluctuations characteristic of the internal variability of the climate system, requiring no net climate change (Reichert and Bengtsson, 2002; Roe and O'Neal, 2009). These factors highlight the importance to paleoclimate studies of incorporating either multiple glacier chronologies or cross-correlation with independent paleoclimate proxies to reproduce findings and test conclusions or hypotheses about past climate based on glacial records.

In summary, climate-sensitive glaciers respond to climate changes by adapting their morphology to the new mass balance gradient. The culmination of a glacier advance closely follows a transient steady state in glacier mass balance. Individual glacier advances are therefore of great climatic significance, as they mark a turning point in long-term climate, and permit the use of a standardized metric—changes in the steady state ELA—to help quantify the climate conditions at this point.

1.2.1.2 Accumulation and ablation processes

Accumulation refers to the sum of factors that add solid water mass to a glacier. Solid precipitation onto the glacier surface is by far the largest contributor at the whole-glacier scale. However, other factors may be locally important on the glacier surface, such as windblown snow, avalanching, freeze-on of liquid water and superimposed ice, and direct accumulation of advected water droplets onto the glacier surface (rime ice).

Ablation incorporates a variety of factors, and is at the surface of a glacier perhaps best conceived in terms of *energy balance* (Hock, 2005):

$$Q_N + Q_H + Q_L + Q_G + Q_R + Q_M = 0$$

where Q_N represents the net shortwave and longwave radiation fluxes, Q_H and Q_E are sensible and latent heat transfer, Q_G is ground heat transfer, Q_R is energy advected by rain-on-snow events, and Q_M is energy used to melt or freeze water. These components, and their significance for the interpretation of paleoglacier records, are summarized below.

The radiative fluxes (Q_N) incorporate all radiation received and emitted at the glacier surface and can be separated into *shortwave* and *longwave* components. Shortwave radiation is predominantly solar radiation in the ultraviolet to near-infrared spectrum, from roughly 0.2-4 μm; longwave radiation is principally thermal radiation in the 4-120 μm spectrum. Broadly speaking, radiative fluxes are the most important component of surface energy mass balance (Hock, 2005). Radiation can be written as:

$$Q_N = (I + D_s + D_t)(1 - \alpha) + L_s^{\downarrow} + L_s^{\uparrow} + L\uparrow$$

(I + Ds + Dt) is known as global radiation, and incorporates direct solar (shortwave) radiation I, the scattered and backscattered diffuse sky radiation D_s, and radiation reflected from surrounding topography D_t. α refers to albedo (the reflectivity of a surface in the shortwave spectrum). $L_s^{\downarrow} + L_s^{\uparrow}$ are the incoming longwave radiative fluxes from the sky and surrounding topography, respectively, while L↑ is the emitted longwave radiative flux.

Direct solar radiation is at a first order a function of total solar irradiance, which has deviated from the long-term average by 1-2 W m^{-2} over the Holocene (Steinhilber et al., 2009). Changes in the earth's orbital parameters provoke changes in the *seasonality*

(degree of difference between summer and winter) of solar energy distribution at millennial timescales. The seasonality of *insolation* (**in**coming **sol**ar radi**ation**) in the northern and southern hemispheres' midlatitudes has varied in an antiphased pattern over the Holocene (Figure 1.2), with the southern (northern) hemisphere experiencing progressively greater (lower) seasonality with the passage of time (Laskar et al., 2004). Long-term changes in summer insolation are of particular interest, given posited relationship between summer insolation and the solar modulation of glacial cycles (Kaufman et al., 2004; Huybers, 2006).

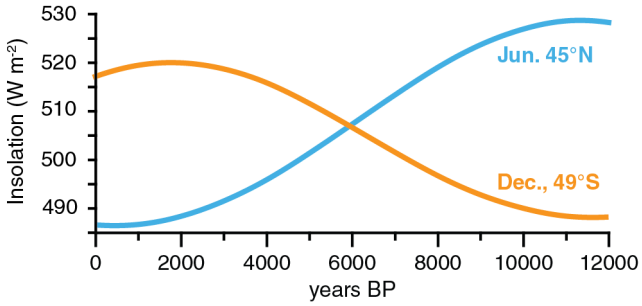

Figure 1.2. Summer insolation trends over the Holocene in the Northern Hemisphere (21 June, blue) and in the Southern Hemisphere (21 December, orange) midlatitudes.

Global radiation is insensitive to temperature but highly affected by atmospheric transmissivity (aerosols and clouds). The incoming longwave fluxes $L_s^{\downarrow} + L_s^{\uparrow}$ vary as functions of both the quantity and temperature of water vapor in the atmosphere and are therefore also highly affected by atmospheric transmissivity.

Sensible heat flux (Q_H) is the direct transfer of heat from one medium to the other, or the transfer of molecular momentum between the atmosphere to the ice surface. It is directly related to the temperature gradient between the ice surface and the atmosphere and is strongly affected by wind strength and roughness at the ice surface. Latent heat flux (Q_L) incorporates heat transfer associated with phase changes; this is also proportional to temperature and wind speed, as well as relative humidity. The turbulent fluxes are generally of lesser daily importance relative to the radiative fluxes, with some exceptions in the maritime midlatitudes and high altitudes (Anderson et al., 2010; Vargo et al., 2018).

In the context of surface energy mass balance, ground heat transfer (Q_G) refers to energy transferred from the surface of the glacier to the ice beneath. Effectively, for a glacier this is equivalent in other formulations to the energy used to change the temperature of the ice. This is principally a function of conduction as well as near-surface penetration of shortwave radiation, and therefore is also controlled by the gradient in ice:atmosphere temperature.

Rain-on-snow events (Q_R) generally have little effect on a glacier's surface energy balance (Hock, 2005), although in maritime environments they can have a significant transient impact on mass balance (Hay and Fitzharris, 1988).

1.2.1.3 Temperature and precipitation: How do they fit?

On a first-order level, temperature plays a crucial role on spatial distribution of glaciers by exerting a fundamental control over the amount of accumulation and magnitude of ablation. Temperature exerts a strong control of ablation over glacier mass balance on the interannual scale (Braithwaite, 1981; Oerlemans and Fortuin, 1992; Ohmura et al., 1992; Hock, 2005), although the magnitude of the relationship differs from glacier to glacier. For some glaciers, variations in precipitation (Mayo and March, 1990; Hooker and Fitzharris, 1999; Nesje and Matthews, 2012) may contribute to observed changes in glacier mass balance.

A glacier's response to a given temperature and precipitation change can be quantified as the *glacier mass balance sensitivity* to climate change, which evaluates a glacier "response" to a hypothetical climate change. The glacier response can be expressed in a variety of ways, for example as melt per unit change of temperature (Mackintosh et al., 2017) or as change in ELA (ΔELA; Sagredo et al., 2014). A range of mass balance sensitivities arise from regional differences in climate and is an important factor to consider when interpreting paleoglacier variations.

1.2.2 Glacial geology

Glaciers play an important role in shaping the alpine environment. As agents of erosion, debris transport, and sedimentation, the processes involved in glacial activity are distinct from fluvial systems or mass wasting, producing a characteristic glacial landscape. The distinctive impact of glaciation on the landscape and earth materials can be used to reconstruct the past behavior of glaciers—glacier geomorphology is therefore the foundation of the use of glacier extent as an indicator of climate change.

1.2.2.1 Glacial erosion and transport

Glaciers erode via *plucking/quarrying* (direct entrainment of rock into the glacier base) and *abrasion* (physical erosion of the substrate by materials transported within a glacier; Benn and Evans, 2014). The relative importance of both processes depends highly upon conditions at the base of the glacier, with the basal thermal state of a glacier playing a critical role. Temperate glaciers, where basal ice is at the pressure-melting point, facilitate erosion by abrasion due to high ice velocities of sliding glaciers, and facilitate quarrying via the concentration of pressure on a base segmented by subglacial erosion channels. Cold-based glaciers do not slide at the base, minimizing abrasion. Hallet et al. (1996) demonstrate glacier thermal state—fundamentally controlled by climate—results in glacial erosion rates several orders of magnitude different, from 0.01 mm yr^{-1} in arctic Greenland to 100 mm yr^{-1} in maritime Alaska.

High rates of temperate glacier erosion have been proposed by various authors (Montgomery, 2002; Foster et al., 2008; Egholm et al., 2009) to control the distribution of alpine topography. Most notably, this is seen in the close correspondence between modern and paleo equilibrium line altitudes and maximum topography along the western margin of the Americas (Figure 1.3). The implication is that the limit of glaciation exerts an upper limit on topography, a hypothesis known as the "glacial buzzsaw" (Mitchell and Montgomery, 2006).

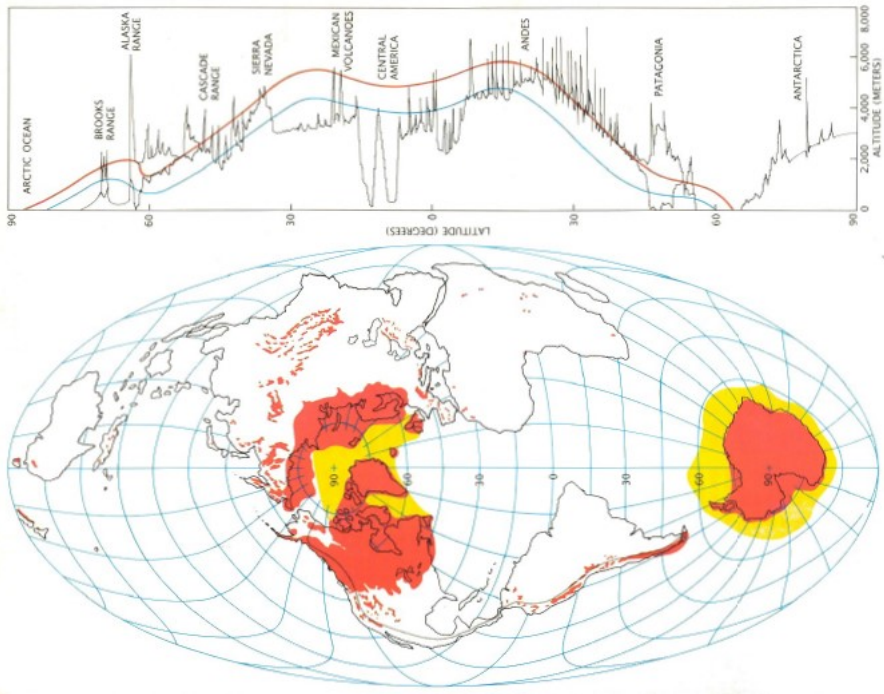

Figure 1.3. Topographic swath profile along the western margin of North America, showing peak elevation (black line), modern ELA (red), and ELA at the Last Glacial Maximum c. 26.5-19 ka (blue). From Broecker and Denton (1990)

As proposed basal ice velocity purportedly plays a key role in governing the rate of erosion, maximum glacial erosion rates should occur at the depth of the ice below the equilibrium line, where ice flux is greatest (Hallet et al., 1996). Debris generated at the base is incorporated into the glacier in a *basal tractive zone* in contact with the substrate, or as suspended load in the body of the glacier. Suspended debris that makes its way to the glacier surface mixes with rockfall debris and is transported as supraglacial debris. Subglacial drainage is also a significant transport process in temperate glaciers.

1.2.2.2 Glacial deposition and glacigenic landforms

Downglacier from the zone of maximum glacial erosion, deposition of glacigenic sediment becomes progressively more important in shaping the glacial landscape. The sediment-landform associations characteristic of alpine valley glaciers have been collectively labelled the *glaciated valley landsystem* (Boulton and Eyles, 1979; Eyles et al., 1983). This environment is distinctive due to the valley walls surrounding a glacier,

which act as a source of sediment and to constrain deposition and landform creation. This landsystem is also encountered at the outlets of mountain and plateau ice fields, forming a component of these distinct landsystems.

The glaciated valley landsystem is in fact an agglomeration of several different sediment-landform associations and depositional environments (Benn and Evans, 2014). For a previously glaciated landscape, sediments and landforms from the *subglacial* and *supraglacial* (beneath the glacier and on top of the glacier, respectively) environments will be encountered within the past ice margin. *Ice-marginal* sediments and landforms are found at the past ice margin, while *proglacial* (ice-distal) and *subaquatic* sediments and landforms will be found outside the past ice margin (Benn and Evans, 2014). Moreover, these associations are often found tightly spaced and will evolve over time depending on the relative position of the glacier. For instance, a glacier advancing over a fixed point in space may deposit at this point a succession of facies, from proglacial, to ice-proximal, to sub- or supraglacial.

Of particular interest for paleoclimate reconstructions are ice-marginal sediments and landforms. These sediment-landform associations commonly mark past glacier termini, or the point in space where a glacier ceases to grow in length and begins to recede. As discussed in section 1.2.1.1, these moments in the evolution of a glacier carry climatic significance. Careful study of glacial ice-marginal features therefore permits the reconstruction of past ice margins and is the first step towards paleoclimate reconstruction using glaciers.

Ice-marginal moraines are depositional landforms created at the edge of a glacier. When well-preserved, they often form a near-continuous arcuate ridge of glacigenic sediment that demarcates a past ice margin (Benn and Evans, 2014). Often labeled *terminal* or *lateral moraines* depending on their position relative to the ice body, ice-marginal moraines are perhaps better classified by the four principal mechanisms by which they are produced (Benn and Evans 2010). *Push* and *squeeze* moraines are formed by the physical “bulldozing” of sediment by an advancing glacier on the annual time scale. *Ice-marginal glacitectonic landforms* are formed by brittle and/or ductile displacement of ice-marginal and proglacial material, which are provoked by the stresses produced by a glacier. *Dump moraines* encompass a range of forms produced by the gravity-driven accumulation of supraglacial debris at a glacier terminus, while the related *latero-frontal fans and ramps* form by the wet-based evacuation of supraglacial debris via glaciofluvial processes and debris flows.

Moraine formation depends on the availability of sediment and ice flux. The relative abundance of each governs the diverse possible configurations of sediment-landform associations in valley glaciers, which may have limited moraine development or none at all (Figure 1.4). Where moraines do not exist, *trimlines* can aid the identification of past glacier limits. A trimline is the vertical boundary between a surface that has been more recently covered with ice (lower) from a surface that was not covered (upper). They may be defined either by changes in vegetation for recently deglaciated surfaces to changes in surface weathering and regolith.

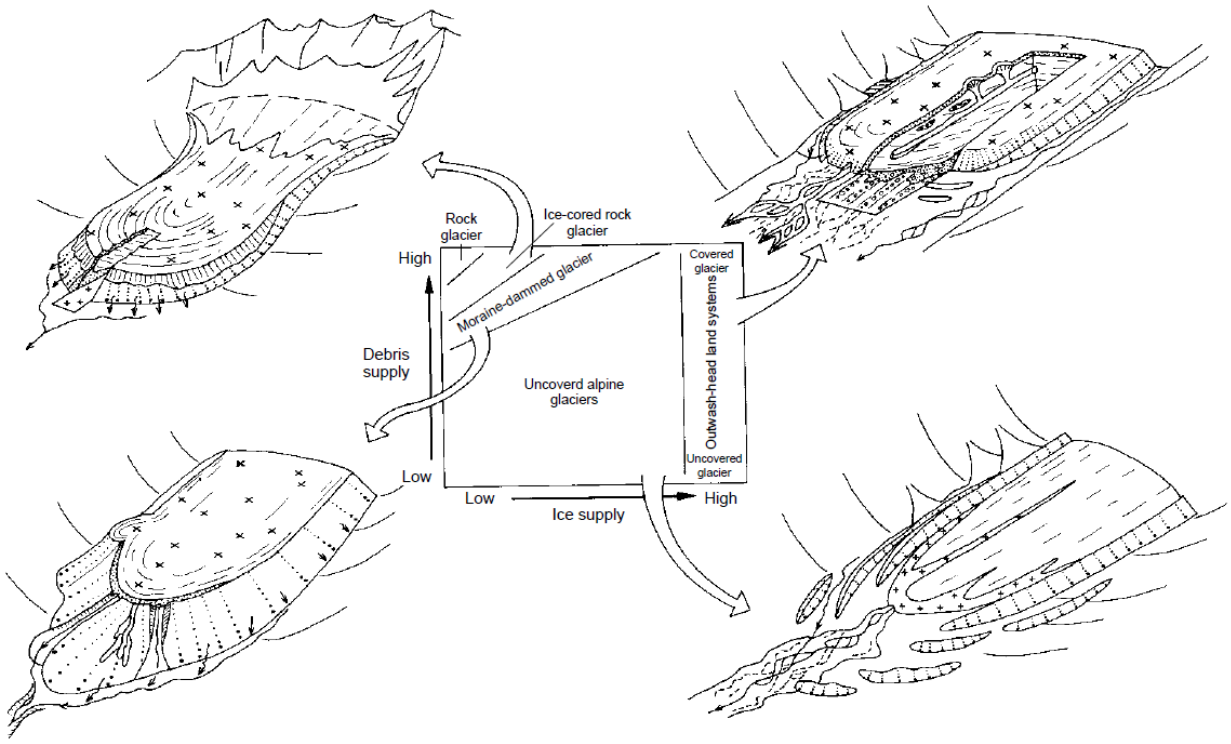

Figure 1.4. Idealized glaciated valley landsystems and their inferred relationships to ice and sediment flux. From Evans (2015).

Together, ice-marginal landforms allow for the reconstruction of past ice limits. Their identification forms the basis of studies that use paleoglacier extent to infer past climate.

1.2.3. Dating glacial events by bracketing

On historical timescales, glaciologists can use archival images from satellites, aerial surveys, or even historical photographs or paintings to reconstruct past glacier extent. At timescales longer than several hundred years—or where there exist no documented records of the past size of the glacier—paleoenvironmental reconstructions of past ice limits is the only method by which paleoglaciers may be visualized. These reconstructions, however, alone do not provide the absolute chronological information necessary to determine the timing of glacier advances or retreats. A number of geochronological methods have been devised to tract this problem, which has become a discipline unto itself.

1.2.3.1 Principles

Bracketing involves determining the absolute age of events stratigraphically above and below a sedimentary sequence of interest (Figure 1.5). Dating the upper event yields a *minimum limiting age*, or the age before which deposition of the sequence of interest must have occurred. A minimum age of glacier retreat is obtained from material

overlying glacial sediment or from the surface between a glacial moraine and the present-day glacier margin. Dating an event below (or sometimes within) glacial sediment yields a *maximum limiting age*, establishing the age after which deposition of the sequence of interest must have occurred. However, both methods are limited by their "one-sidedness" in that while they constrain glacial advance, in the absence of a minimum-limiting age overlying a glacial sequence they cannot give the whole history of a glacial advance-retreat cycle—the elusive *bracketed limiting age*.

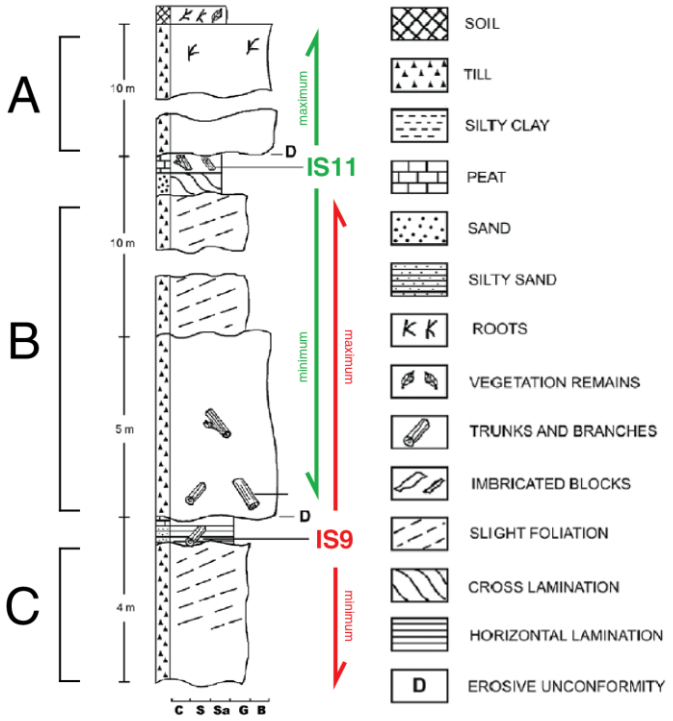

AMS radiocarbon dates of samples collected in the internal moraines of Ema Glacier (for locations see Figs. 4 and 5)

Sample	Radiocarbon age (14C y BP)	13C/14C (‰)	Corrected age (14C y BP)	Lab no.
1S1	465±75	−26.97	379±75	Ua — 13 419
1S2	335±70	−26.86		Ua — 13 420
1S9	3135±75	−26.20		Ua — 13 421
1S10	1315±75	−27.85	1288±75	Ua — 13 422
1S11	1330±65	−27.11		Ua — 13 423
1S12	315±70	−25.66	251±70	Ua — 13 424
1S13	695±95	−28.78		Ua — 13 425

The fourth column shows the corrected age considering the tree ring lifespan age (Fidel Roig, personal communication). All ages were obtained at the Tandem Laboratory, University of Uppsala, Sweden.

Figure 1.5. Example of the application of bracketing to glacial stratigraphy. Sample IS11 is interpreted to reflect nonglacial conditions between the deposition of till A and till B; it serves as both a maximum-limiting age of till A and a minimum limiting age of till B. Sample IS9 is interpreted to date nonglacial conditions between the deposition of till B and till C, giving a maximum limiting age of till B and a minimum limiting age of till C. Till B is therefore bracketed by samples IS11 and IS9; it can be inferred that a glacier advanced and retreated from the position of the stratigraphic column between 1330 and 3135 ^{14}C years BP. Adapted from (Strelin et al., 2008).

Bracketing of glacial sediments in Patagonia has been done using dendrochronology, radiocarbon dating, luminescence dating, potassium-argon/argon-argon dating, and

physical cross-referencing of known strata (tephrochronology). These methods are summarized below.

1.2.3.2 Radiocarbon

Many investigations of paleoglacier fluctuations have been conducted using *radiocarbon* (often abbreviated *^{14}C*) limiting ages of organic matter that post- or predates glacial retreat. Interactions between the atmosphere and galactic cosmic radiation produce *carbon-14*, the radioactive isotope of carbon, which is subsequently taken up by photosynthesizing organisms as carbon dioxide and distributed through the food chain. While alive, an organism's ratio of ^{14}C to ^{12}C is in equilibrium with that of its environment. Radiocarbon dating measures ^{14}C to determine the age of death of an organism, when it ceases to be in equilibrium with its environment as ^{14}C decay is not compensated.

The measured ratio of $^{14}C/^{12}C$ is used to determine the *radiocarbon age* of the death of an organism by the following equation:

$$Age\left(^{14}C\ years\right) = -8033\ln(Fm)$$

where -8033 is the ^{14}C mean-life using the nonstandard ^{14}C half-life of 5568 years of (Libby, 1961), and *Fm* is the corrected fraction modern: the ratio of sample $^{14}C/^{12}C$ to a corrected "modern" ratio. This is therefore the age of death of an organism, assuming a ^{14}C half-life of 5568 years and a constant ratio of atmospheric $^{14}C/^{12}C$.

The radiocarbon age must be corrected further to yield a calendar age, as the true half-life of ^{14}C is 5730 years (Godwin, 1962), and the ratio of atmospheric $^{14}C/^{12}C$ has varied in the past. Past ratios of $^{14}C/^{12}C$ can be determined by cross-dating organic material of a known age. Numerous cross-datings are integrated in *calibration curves*, which model past variations of $^{14}C/^{12}C$. As new data and uncertainties surrounding $^{14}C/^{12}C$ ratios are continuously added to the scientific literature, curves are continuously updated (Stuiver et al., 1998; Reimer et al., 2009, 2013). Given the inconstant nature of calibrations, ages derived from radiocarbon dating are reported as both *^{14}C years BP* (the analytical age) and as *cal years BP* (the age according to the chosen calibration curve).

Additional uncertainties come from heterogeneities in global $^{14}C/^{12}C$. Atmospheric radiocarbon is only well-mixed with the ocean near the surface; deep water originating from outside the photic zone are depleted in ^{14}C and will affect marine organisms affected by upwelling, as well as terrestrial biota reliant upon these organisms for food (Ascough et al., 2005). Marine fossils may require an additional correction for this *marine reservoir effect*. Furthermore, atmospheric $^{14}C/^{12}C$ varies slightly between the northern and southern hemispheres (Rodgers et al., 2011), so hemispheric-specific calibration curves may be appropriate in some regions (e.g. Hogg et al., 2013).

Radiocarbon dating in the glacial context is principally limited by the indirect nature of the chronologies, which can only say *a priori* when a glacier was *not*. Their utility is highly dependent upon the site-specific sensitivity of the dating sites. For instance, ^{14}C-dateable material exists in ice-proximal contexts (e.g., proglacial lakes) that are highly sensitive to variations in glacier extension. However, other contexts—such as radiocarbon dating of vegetation colonization on glacial landforms—the absolute date of vegetation death does not necessarily correspond to a glacial event. Bracketing radiocarbon dates therefore must be considered carefully in terms of their sampling context.

Wood and charcoal are common macrofossils associated with terrestrial glacial sediment and are frequently dated in paleoglacier studies. However, woody plants contain internal zonation of ^{14}C, wherein only the live sapwood exists in atmospheric equilibrium—the heartwood has ceased to exchange carbon with the atmosphere and the ^{14}C radiometric clock of heartwood has begun prior to the actual death of the tree. Sampling should ideally target sapwood, as heartwood may potentially overestimate the death date by the lifespan of the tree. Logistically, radiocarbon dating is also limited by the need for appropriate stratigraphic sections, as well as the need for organic matter to be preserved within these sections.

1.2.3.3 Optically-stimulated luminescence dating

Luminescence dating utilizes a geologic 'clock' resulting from the ability of certain minerals, such as quartz and feldspar, to retain energy within their crystal structure (Duller, 2004). Ionizing radiation and galactic cosmic radiation result in electrons becoming trapped in an excited state. This energy will increase predictably with time, until the crystal is stimulated, when the energy is released as light (luminescence). To utilize the amount of stored energy as a geochronometer, the source material must first be 'reset' by exposure to heat, pressure, or light, which starts the geologic clock.

Various methods exploit the processes by which prior energy in the mineral is 'reset,' therefore starting the clock. The most common method applied to glacially-associated sediments in Patagonia, known as *optically stimulated luminescence (OSL)*, uses the last exposure of a material to sunlight as the resetting event ("bleaching"). Dates provided with this method are therefore burial dates of a material.

Eolian sediments are uniformly exposed to the atmosphere when transported, and therefore are ideal candidates for application of the method. OSL has been successfully used to date dune sands (Olley et al., 1998) as well as loess (Zárate, 2003), although their use for fluvial sediments are complicated by partial bleaching of individual grains (Wallinga, 2002). Partial bleaching is particularly problematic for glacigenic sediment (Rhodes, 2011), so dating of glacial deposits often follows indirect bracketing procedures, wherein glacial till is dated by obtaining maximum and minimum limiting ages of confining sediment packages.

1.2.3.3 Potassium-argon and argon-argon dating

Both *potassium-argon (K-Ar)* and *argon-argon (^{40}Ar-^{39}Ar)* dating rely on the decay of the radioactive ^{40}K to the stable ^{40}Ar. ^{40}Ar escapes from earth material while it is molten but becomes trapped in crystal lattices when solid. Crystallization time is therefore the closure event that beings the molecular clock. The two methods differ in the way ^{40}K is determined (Kelley, 2002). ^{39}K is proportional to ^{40}K, so K-Ar dating directly measures ^{39}K by flame photometry or atomic absorption spectrometry. This, however, requires the separation of one sample into two aliquots with two separate methods of measurement, introducing greater internal error. In ^{40}Ar-^{39}Ar dating, the sample is irradiated prior to measurement, resulting in the transmutation of ^{39}K to ^{39}Ar. The calculation of ^{40}K is therefore achieved via the measurement of ^{39}Ar alongside ^{40}Ar, improving internal precision.

As glacigenic sediments do not undergo crystallization during the process of deposition, both K-Ar and ^{40}Ar-^{39}Ar methods are not used to directly date glacial deposits. They are used instead to date lava flows that bracket glacial sediments; in this capacity these methods have been instrumental in defining the Quaternary and Neogene glacial history of Patagonia (Mercer, 1982; Singer et al., 2004).

1.2.3.4 Tephrochronology

Glacigenic sediments are highly localized in context. On the regional (and often local) scale, glacial deposits violate the stratigraphic principle of lateral continuity, meaning that events that happen in one valley are not easily extrapolatable to other valleys. Tephra, on the other hand, is often distributed regionally, possesses a unique chemical footprint, and can be both directly and indirectly dated. Tephras in the Quaternary sedimentary record can therefore be used as stratigraphic indicators for bracketing purposes.

The high concentration of historically active volcanoes in Patagonia make the area well-suited for the development of tephra-based chronologies, and extensive work has been conducted towards this goal (e.g. Naranjo and Stern, 2004; Stern, 2008; Fontijn et al., 2016).

1.2.4 Dating glacial events with surface exposure dating

The methods mentioned in the last section apply to packages of glacial sediment. Fundamentally, the methods described depend upon the exposure of numerous stratigraphic sections, or the extraction of sediment cores. Exposures of sedimentary sequences are not always available where needed, and the digging of test pits or core retrieval is often impractical. Furthermore, the information gained from these sections gives a highly detailed description only of what transpired at the sample site. Information on specific locations of ice margins, for example, is often impossible to extrapolate from a single stratigraphic section.

Glacial landforms, on the other hand, are widely-distributed in alpine areas, and dating the formation of ice-marginal landforms can give precise information on former ice extent. In circumstances where sediment-landform associations are strong, dating the sediment that makes up a landform can sometimes determine the age of a landform (e.g. optical dating of fluvial sands making up a fluvial terrace). When this is not possible, methods specific to the formation of landforms become necessary.

1.2.4.1 Terrestrial cosmogenic nuclide surface exposure dating

Cosmogenic nuclides are particles produced by interactions between the earth system and galactic cosmic radiation. Radiocarbon dating utilizes one such nuclide, atmospheric ^{14}C, which is produced by absorption of daughter neutrons by ^{14}N (Libby, 1961). Gosse and Phillips (2001) define a *terrestrial cosmogenic nuclide (TCN)* as "a nuclide produced by the interaction of secondary cosmic radiation with exposed target atoms in earth-surface materials," thus differentiating cosmogenic nuclides accumulating in solid earth material (*in situ*) from those produced in the atmosphere. Certain nuclides are only produced via cosmogenic interactions and are furthermore produced at known rates in common materials. By measuring the concentrations of these nuclides at the earth's surface, they can be used as geochronometers. All TCN-based surface exposure dating methods (hereafter referred to as TCN-SED) function on this principle. The reader is referred to Gosse and Phillips (2001) and Dunai (2010) for a comprehensive review of principles behind geologic applications of TCN; this section will focus on the use of *beryllium-10 (^{10}Be)* for surface exposure dating.

Galactic cosmic radiation refers to highly-energetic nucleons (1-10^{10} GeV, occasionally >10^{20} eV) mostly originating from outside the solar system but within the galaxy (Gosse and Phillips, 2001). Once these nucleons (*primary GCR*) enter the atmosphere, they interact with the nuclei of atoms to form energetic daughter particles (*secondary radiation*). These secondary products—a mixture of nucleons and mesons—in turn react with other atoms in the atmosphere, resulting in a cascade of energized particles (Figure 1.6). Some of these particles reach the earth's surface, where they produce terrestrial cosmogenic nuclides.

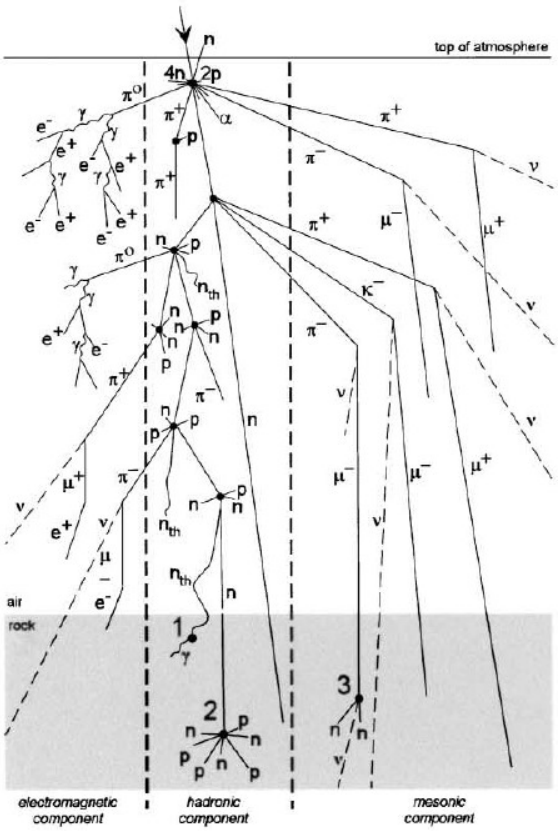

Figure 1.6. From Gosse & Phillips (2001). Secondary radiation cascade resulting from interactions between primary GCR and the atmosphere. "2" represents ^{10}Be production from ^{16}O at the earth's surface.

^{10}Be is a nuclide principally produced via two main processes: neutron spallation and muon capture. Nuclide production via neutron spallation occurs when a high-energy (> 10 MeV) neutron strikes a target nucleus and "spalls" off pieces of the nucleus; the products are several lighter particles and a lighter residual nucleus (Templeton, 1953). Slow negative muons may be captured by positively charged nuclei, and this process comprises the majority of muonic production (Lal, 1988). At the earth's surface, neutron spallation is by far the principal contributor to ^{10}Be production, but the low reactivity (and therefore deeper penetration) of muons leads the muonic component to dominate ^{10}Be production at depth (Figure 1.7).

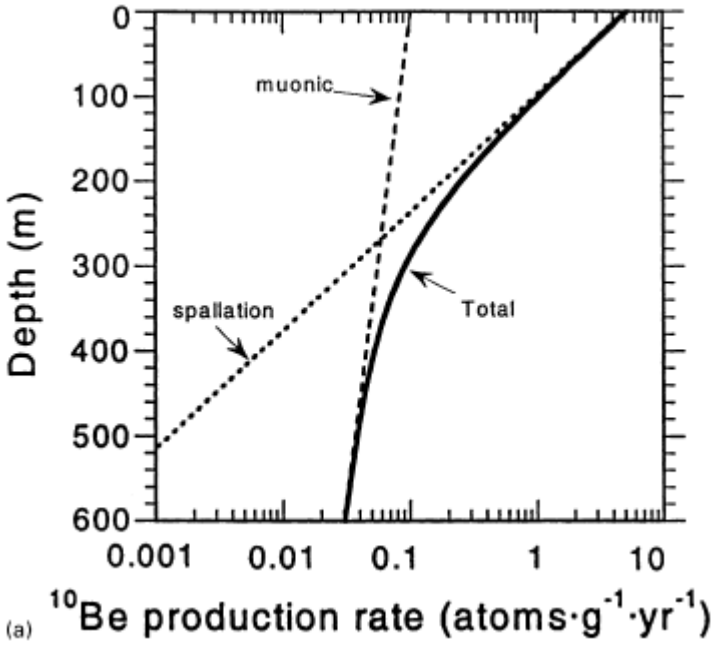

Figure 1.7. Production-depth relationship of ^{10}Be for the muonic and nucleogenic components. From Gosse and Phillips (2001).

^{10}Be production can occur via reactions with ^{16}O, ^{28}Si, ^{9}Be, ^{10}B, and ^{13}C (Gosse and Phillips, 2001); any earth material containing these elements may be conceivably used for ^{10}Be dating. However, most studies utilizing ^{10}Be for geochronologic purpose use quartz (SiO_2) as a target mineral, owing to its simple chemistry, worldwide abundance, and resistance to chemical weathering. The long half-life of ^{10}Be (1.36±0.07 Ma) makes it ideally suited for Quaternary studies, as in most geomorphologic contexts surfaces have not been long enough for the production of ^{10}Be to reach secular equilibrium with decay.

The relationship between cosmogenic nuclide concentration and age is given by the following equation (Balco, 2011):

$$N_{10} = \frac{P_{10}}{\lambda_{10}}\left[1 - e^{-\lambda_{10} t}\right]$$

where N_{10} is the ^{10}Be concentration in quartz (atoms g^{-1}), P_{10} is the ^{10}Be production rate (atoms g^{-1} yr^{-1}) in quartz at the sample site, λ_{10} is the ^{10}Be decay constant (4.99 x 10^{-7} yr^{-1}), and t is the exposure time in years. N_{10} is measured by accelerator mass spectrometer (AMS) and λ_{10} is known, so to solve for t it is first necessary to know P_{10}, the local production rate of ^{10}Be.

Primary variability of ^{10}Be production rates

The primary GCR flux is assumed to be constant since 10 Ma (Gosse and Phillips, 2001), although variations at timescales longer than the analytical period (150-700 Myr; Lavielle et al., 1999), as well as extreme punctual events (Lal, 1987), are known to have occurred. The principal modulator of GCR flux to the upper atmosphere is instead

variability in the interplanetary magnetic field, which acts as a shield of GCR. Interplanetary magnetic field intensity has an inverse effect on received GCR flux. A key factor influencing variations on this magnetic field is solar output, which has a measurable effect on present and historical ^{10}Be production (Beer et al., 1991; Steinhilber et al., 2008), although the low amplitude of modern solar output variations and the poor understanding of long-term variations in solar output suggests the net effect integrated over tens of thousands of years is small (Gosse and Phillips, 2001).

The earth's geomagnetic field also affects the accumulation of secondary GCR at the surface, although the effect is not equally felt. Incoming primary GCR must meet a minimum *rigidity* (momentum of a particle per charge) value to pass through the geomagnetic field and enter the atmosphere. This value is a function of latitude—and to a lesser extent altitude—due to the configuration of the geomagnetic dipole, as steeper field lines near the poles result in permitted particle rigidity below the necessary threshold to produce TCN (Gosse and Phillips, 2001). This implies that above a certain latitude (~58°, less at higher elevations) TCN accumulation is unaffected by geomagnetic field variations (Lal, 1991). Gosse and Phillips (2001) modeled the latitudinal effect on long-term perceived production rates based on a 200-kyr record of relative variations in geomagnetic field intensity (Guyodo and Valet, 1999). They showed that significant differences between the time-averaged production rate and the actual production rate would be perceptible for latitudes <30°; however, long term relative variation at 45° is less than 0.05 and is negligible at 60°.

Secondary variability of ^{10}Be production rates

Variation in the geographic position of the dipole axis will shift geomagnetic latitude, affecting long-term sensitivity to dipole intensity changes. Non-dipole related variations in the geomagnetic field may also affect local production rates; alternative production scaling methods incorporating these effects have been produced (see next section). Furthermore, variations in solar output modulate secondary cosmic ray flux, so the in-situ production rate will have changed over time.

Finally, as the intensity of the GCR cascade varies as a function of atmospheric depth, changes in surface elevation or mean atmospheric pressure affect production rates. High-elevation sites receive more secondary high-energy GCR, as the GCR cascade is less-attenuated by the atmosphere. Systematic variations in atmospheric pressure with latitude has a similar effect, where high-latitude sites will have higher production rates than low-latitude sites, all factors being equal. Of note are long-term longitudinal variations in pressure (Stone, 2000), although caution must be used to avoid circularity when applying climate-dependent production rates to applications of cosmogenic dating to paleoclimate studies.

Scaling models

Ideally, each site where TCN-SED is utilized would also determine the local production rate for the studied nuclide, whereby a surface would be measured for its TCN concentration while also being independently dated by another method. While cross-dating would control for all spatial variability in production rates, it would not account

for temporal variability, and would prohibit the use of TCN-SED as an independent geochronologic method. Various *scaling models* have been developed, which by attempting to correct for spatial and/or temporal variability in production rates permit the estimation of local production rates for age calculations.

The muonic component of ^{10}Be production at the surface is a small percentage of spallation production, so a simple elevation-based scaling is most often used, considering geomagnetic effects to be negligible (Balco et al., 2008). Multiple scaling models for spallation exist, which may be divided into time-independent and time-dependent models.

Time-independent models do not account for secular variations in the geomagnetic field or atmospheric depth, modeling ages solely as a function of spatial variability in production rate. The model of Lal (1991) determines production rate as a function of geomagnetic latitude and altitude, based on measurements of contemporary GCR flux from film emulsions and neutron detectors. The closely-related model of Stone (2000) utilizes the same scaling relationships, the principal change being the articulation of atmospheric depth in terms of pressure rather than altitude.

Time-dependent models address the principal deficiency of their time-independent counterparts by modeling past variations in the geomagnetic field. These models depend not on latitude and altitude, but rather cutoff rigidity and atmospheric pressure, defined on the basis of neutron monitor measurements (Dunai, 2001; Desilets and Zreda, 2003; Lifton et al., 2005; Desilets et al., 2006). These scaling factors are then combined with corrections for secular variability in the geomagnetic field. Lifton et al. (2005) additionally incorporate corrections for solar modulation and historical variation in solar output. Balco et al. (2008) returned to the original altitudinal scaling of Lal (1991) while adding a paleomagnetic correction from Nishiizumi et al. (1989). Lifton et al. (2014) forego purely empirical scaling, instead relying on modeled neutron flux (Sato et al., 2008) with newer corrections for both geomagnetic and solar variation.

Local production rate calibration

The global averaged production rate using the scaling methods described above yields a range between 4.26±0.21 atoms g^{-1} a^{-1} (Lm scaling of Balco et al., 2008) and 4.95±0.24 atoms g^{-1} a^{-1} (Li scaling of Lifton et al., 2005; ranges from Balco et al., 2008). However, production rates derived from local sites often differ from these global values. Using the Balco et al. (2008) scaling scheme, midlatitude production rates are 12% lower in northeastern North America (Balco et al., 2009), 13% lower in New Zealand (Putnam et al., 2010), and 15% lower in Patagonia (Kaplan et al., 2011).

"Tertiary" variability of ^{10}Be production rates – local effects

Production rates are given for a horizontal planar surface with an unobstructed horizon. As incident secondary radiation is assumed to be isotropic, a sloped surface or an obstructed horizon will affect the in-situ production rate. Where a sample does not fit the flat and unobstructed ideal, correction for *topographic shielding* must be done.

Shielding corrections are typically made for topographic obstructions alone, although other potentially important sources of shielding error include forest canopy or burial by snow or sediment. Canopy cover has a maximum potential effect on production rates of ~4% (Cerling and Craig, 1994), but in most cases is likely minimal. Snow cover can potentially alter reported ages significantly in areas of high accumulation where it persists for much of the year (Benson et al., 2004), but its effect is difficult to independently verify, and presents a degree of circularity when applied to glacial systems. Burial by sediment is also a potential source of shielding bias.

While effects of surface erosion and burial are typically difficult to evaluate in the field, standardized field procedures have been developed to minimize their potential effects. In terms of moraine dating, decades of work have led to sampling heuristics aimed at minimizing so-called "geologic scatter" (Balco et al., 2011). Samples of larger dimensions are preferred to avoid burial effects. Samples are taken only from moraine crests to avoid potential toppling or burial, while sampling surfaces without apparent evidence of mass loss are favored to avoid effects of surface erosion.

1.2.5 Dendroglaciology

Landform stabilization ages can be constrained by the ages of the oldest living tree on the landform (Sigafoos and Hendricks, 1969; Luckman, 2000), a process that has been termed *dendroglaciology*. This age represents a minimum age of landform formation, plus a correction made for the interval between final stabilization of the landform and tree germination (*ecesis*). Corrections are also often necessary due to sampling height error (McCarthy et al., 1991).

The most significant uncertainty underlying this method is the determination of ecesis and the assumption that living trees represent the first generation of trees grown on a new surface. Ecesis is reliably determined only with independent control on local tree establishment; dendroglaciology therefore requires calibration and the uncertainties that accompany extrapolation of ecesis values from one location to another. Furthermore, in humid climates degradation of dead trees can occur rapidly enough to erase evidence of prior generations of trees, complicating the first-generation assumption.

1.2.6 ELA reconstruction

Most of paleoglacier studies in Patagonia have remained crude in the sense that little effort has been made to reconstruct paleo-equilibrium line altitudes (ELAs) for past glacier extents. Although ELA reconstructions provide a more robust metric of the magnitude of a glacial advance than simple fluctuations in length, few studies have utilized this method to derive a more comprehensive climate signal from past glacier extents (e.g. Wolff et al., 2013), as has been done in New Zealand (Putnam et al., 2012; Kaplan et al., 2013).

Intricacies of this method, as well as its application to the study area, are discussed further in Chapter 5.

* * *

Chapter 2 – Setting and prior work

This chapter introduces the geology, climatology, and prior work conducted on the paleoglacial history of the study area. The chapter also provides a review of prior studies, and a comparison is made with other paleoclimate proxies.

2.1 Geographic and tectonic framework

2.1.1 Geographic features of the study area

At present, the southern Andes present a continuous topographic barrier along the Pacific coast of South America, generally declining in maximum elevation from >6000m at the southern Andes' northern boundary with the southern flat slab zone at 25°S, to <3000m in the Fuegian Andes at 55°S (Montgomery et al., 2001). The Patagonian Andes, defined here as the southern Andes south of 42°S, can be divided into two sections, based on the present location of the Chile Triple Junction (CTJ) off the Taitao Peninsula (46.5°S). The CTJ separates the Nazca Plate from the Antarctic plate, both of which are subducting obliquely under the South American plate (Ramos, 2005).

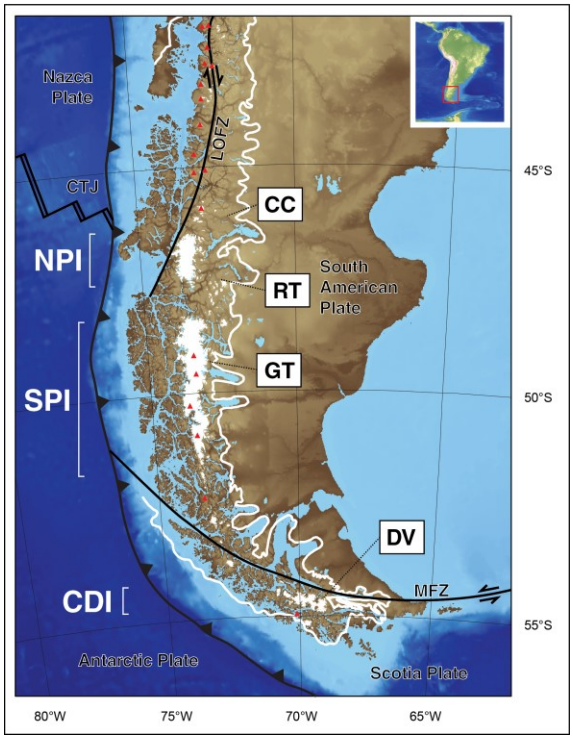

Figure 2.1. Shaded elevation map of the study area, highlighting key tectonic and geographic features. Plate margins and major tectonic features are shown as black lines. Modern ice bodies are shown as white polygons, and the reconstructed ice limit at the Last Glacial Maximum c. 26.5-19 ka is shown as a thick white line. Active volcanoes are shown as red triangles. LOFZ = Liquiñe-Ofqui Fault Zone, CTJ = Chile Triple Junction, MFZ = Magallanes Fault Zone, NPI = North Patagonian Icefield, SPI = South Patagonian Icefield, CDI = Cordillera Darwin Icefield, CC = Cerro Castillo (Chapter 5), RT = Río Tranquilo (Chapter 5), GT = Glaciar Torre (Chapter 3), DV = Dalla Vedova (Chapter 4).

To the north, the Northern Patagonian Icefield (NPI) and Southern Patagonian Icefield (SPI) comprise the largest ice fields outside of the poles, dominating the Patagonian Andes south of 46°S. Following the NPI/SPI, the other principal body of ice in the region is the Cordillera Darwin Icefield (CDI), along the southern margin of the island of Tierra del Fuego. Additional concentrations of modern glaciers can be found at Isla Santa Inés and Isla Hoste in the Fuegian archipelago, the Gran Campo Nevado south of the SPI, and the Queulat ice cap north of the NPI.

During the Last Glacial Maximum (LGM; 26.5-19 ka; Clark et al. 2009) these ice bodies were united in to a large body of ice, often referred to as the Patagonian Ice Sheet (PIS; 39°-55°S, Sugden et al., 2002). Large outlet glaciers extended into the arid area of Patagonia to the east and out onto the continental shelf to the west (Mcculloch et al., 2005b). Modeling suggests the ice divide was shifted to the west relative to the Andean crest at this time (Hulton et al., 1994).

2.1.2 Tectonic setting

Recent uplift of the Patagonian Andes is thought to have initiated c. 30-26 Ma, corresponding with the breakup of the Farallon plate and an increase in subduction velocity and decrease in obliquity between the Nazca and South American plates (Pardo-Casas and Molnar, 1987; Lonsdale, 2005). This corresponds with an apatite fission-track derived increase in denudation at the western edge of the Patagonian cordillera, suggesting the rapid development of high topography and enhanced orographic precipitation (Thomson et al., 2001). Uplift is further recorded by the Miocene Santa Cruz molasse, which records terrestrial deposition in the developing foreland basin of the modern Andes (Ramos and Ghiglione, 2008). Sedimentation began c. 22 Ma and ceased c. 14 Ma, which has been classically interpreted as representing the development of an orographic barrier and the subsequent aridification of eastern Patagonia (Blisniuk et al., 2005).

The oblique subduction of the Chile spreading ridge has had a profound effect on the nature of Neogene uplift in Patagonia. North of the CTJ, transtensional basin filling during the early Miocene was terminated by a period of transpressional uplift and unroofing along the dextral Liquiñe-Ofqui Fault Zone (LOFZ), beginning between 16-10 Ma and most intense between 7-2 Ma (Thomson, 2002). Additionally, the region north of the CTJ features a reduction in back-arc molasse volume, the lack of a fold and thrust belt in the back-arc, sediment subduction and underplating in the fore-arc, low basement exposure, and lower maximum topography compared to the southern region (Ramos, 1989; Behrmann and Kopf, 2001). South of the CTJ, accelerated denudation has been active since 30 Ma, focused on an eastward-migrating locus presently focused on the topographic divide (Thomson et al., 2001). Here, the foreland features thick Miocene molasse deposits, fold and thrust belts active to the late Miocene, sediment accretion in the fore-arc, high exposure of basement rock, and higher maximum topography compared to the northern region (Ramos, 1989; Behrmann and Kopf, 2001).

Continuing uplift through the Miocene of the Patagonian Andes south of 46°S is suggested by zircon fission track data that indicate uplift associated with crustal shortening and thrusting in the eastern cordillera at 22-18 Ma (Fosdick et al., 2013). This record is coincident with transition from marine to continental deposition in the Centinela-Santa Cruz transition. The Santa Cruz formation, a molasse deposit that records terrestrial deposition between c. 22-14 Ma in the flexural back-arc of the incipient Andes (Ramos and Ghiglione, 2008). The timing of deep exhumation and sediment accumulation suggests this period of uplift is related to stress propagation from transpression along the incipient North Scotia Ridge (Lagabrielle et al., 2009).

The cessation of sedimentation at 14 Ma, in conjunction isotopic changes in eastern Patagonia, have been classically interpreted as consequences of increasing aridity provoked by the development of an orographic barrier and rain shadow effect (Blisniuk et al., 2005). Recent work suggests a weaker orographic rain shadow effect until c. 7 Ma (Palazzesi et al., 2014), suggesting cessation of sedimentation may instead be a consequence of foreland uplift due to the subduction of the Chile spreading ridge and subsequent opening of a slab window (Breitsprecher and Thorkelson, 2009; Guillaume et al., 2009). Subduction of the Chile spreading ridge began at 14-12 Ma at a latitude of 54°S, and the resultant triple junction has subsequently migrated northward in a stepwise fashion to its current position at 46°S (Lagabrielle et al., 2004). As the ridge was subducted, the ~8 cm/yr difference in subduction velocity between the faster Nazca plate and the slower Antarctic plate opened a slab window (Ghiglione et al., 2016), associated with main- and post-plateau lavas across southern Patagonia (Gorring et al., 1997).

North of the CTJ, transtensional basin filling during the early Miocene was terminated by closure of the Pacific connection to the Ñirihuau basin, coeval with the increase in subduction velocity and orthogonality at ~30 Ma (Aragón et al., 2011). Generalized subduction-related uplift was punctuated by a period of transpressional uplift and unroofing along the dextral Liquiñe-Ofqui Fault Zone (LOFZ), beginning between 16-10 Ma and most intense between 7-2 Ma (Thomson, 2002; Adriasola et al., 2006). The extremely young (~2 Ma) AFT and (U-Th)/He closure ages imply rapid and recent uplift of up to 1.5-3mm/yr, in contrast to the southern Patagonian Andes, where exhumation occurred earlier in the Miocene (Thomson et al., 2010; Fosdick et al., 2013). Additionally, the region north of the CTJ exhibits a relatively reduced volume of Santa Crucian molasse, the lack of a fold and thrust belt in the back-arc, lesser basement exposure (Ramos, 1989), sediment subduction and underplating in the fore-arc (Behrmann and Kopf, 2001), and lower maximum topography compared to the southern region (Montgomery et al., 2001).

2.2 Present climatology of Patagonia

> *"Every aspect of the climate of southern Chile and Argentina is determined by the interaction of the westerlies with the Andean Range. The orographic effects are probably as 'pure' and simple as can be found anywhere on earth. The range is relatively narrow and oriented*

perpendicular to the mean flow. The zone would undoubtedly make an excellent "laboratory" for the verification of theoretical models of air flow over mountains and resulting precipitation and cloudiness patterns."

- Miller (1976)

The most prominent feature of southern South American climate is the persistently strong westerly atmospheric flow, and the resultant effects this dominant characteristic has on the region's climate. Advection of moist air from the Pacific results in a concentration of precipitation along the mountainous coast and the development of a pronounced rain shadow effect east of the continental divide (Miller 1976; see also Figure 2.2). The influence of oceanic air masses also limits seasonal temperature variability (Figure 2.3). The resulting climate is cool-maritime climate characterized by temperate broadleaf forests in the west and a cold-desert steppe climate to the east (Olson et al., 2001; Peel et al., 2007), a zonation due primarily to the westerly-modulated precipitation gradient across the region (Figure 2.4).

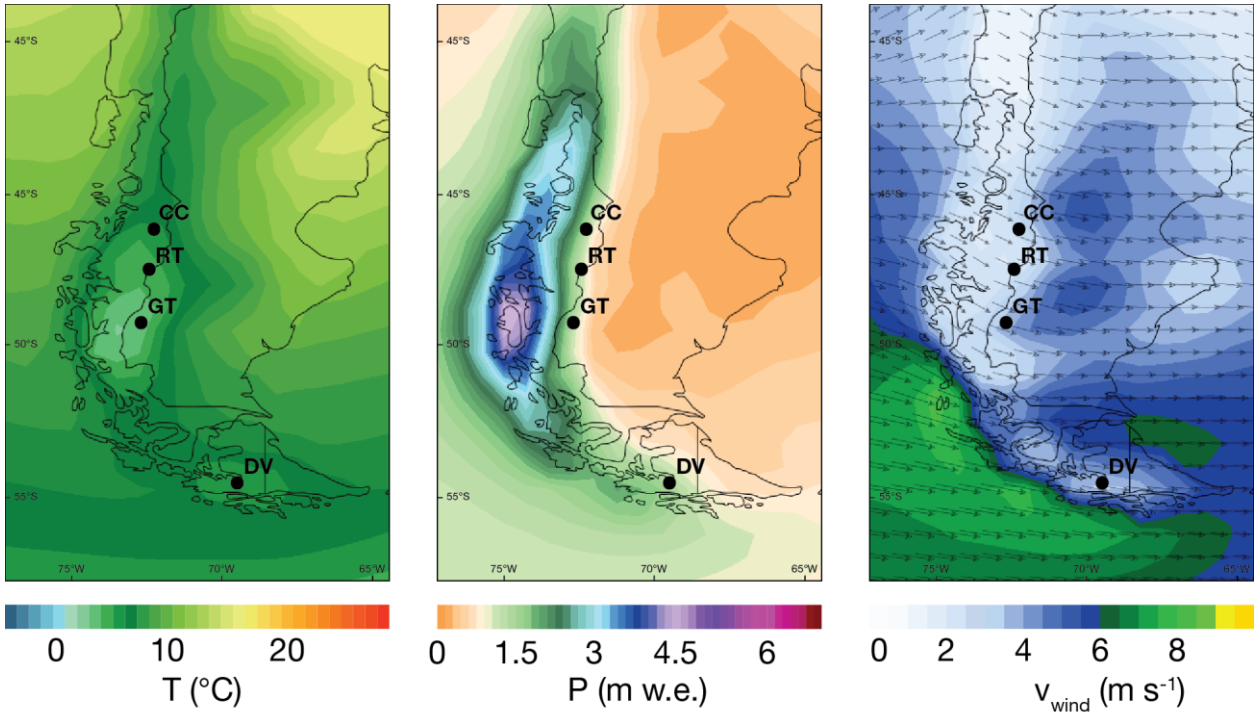

Figure 2.2. Annual temperature, precipitation, and wind speed from the ERA-Interim reanalysis (Dee et al., 2011) for the interval 1979-2015. Location of study areas in this thesis indicated by black dots. CC=Cerro Castillo, RT=Río Tranquilo, GT=Glaciar Torre, DV=Dalla Vedova. Images from Climate Reanalyzer (https://ClimateReanalyzer.org), Climate Change Institute, University of Maine, USA.

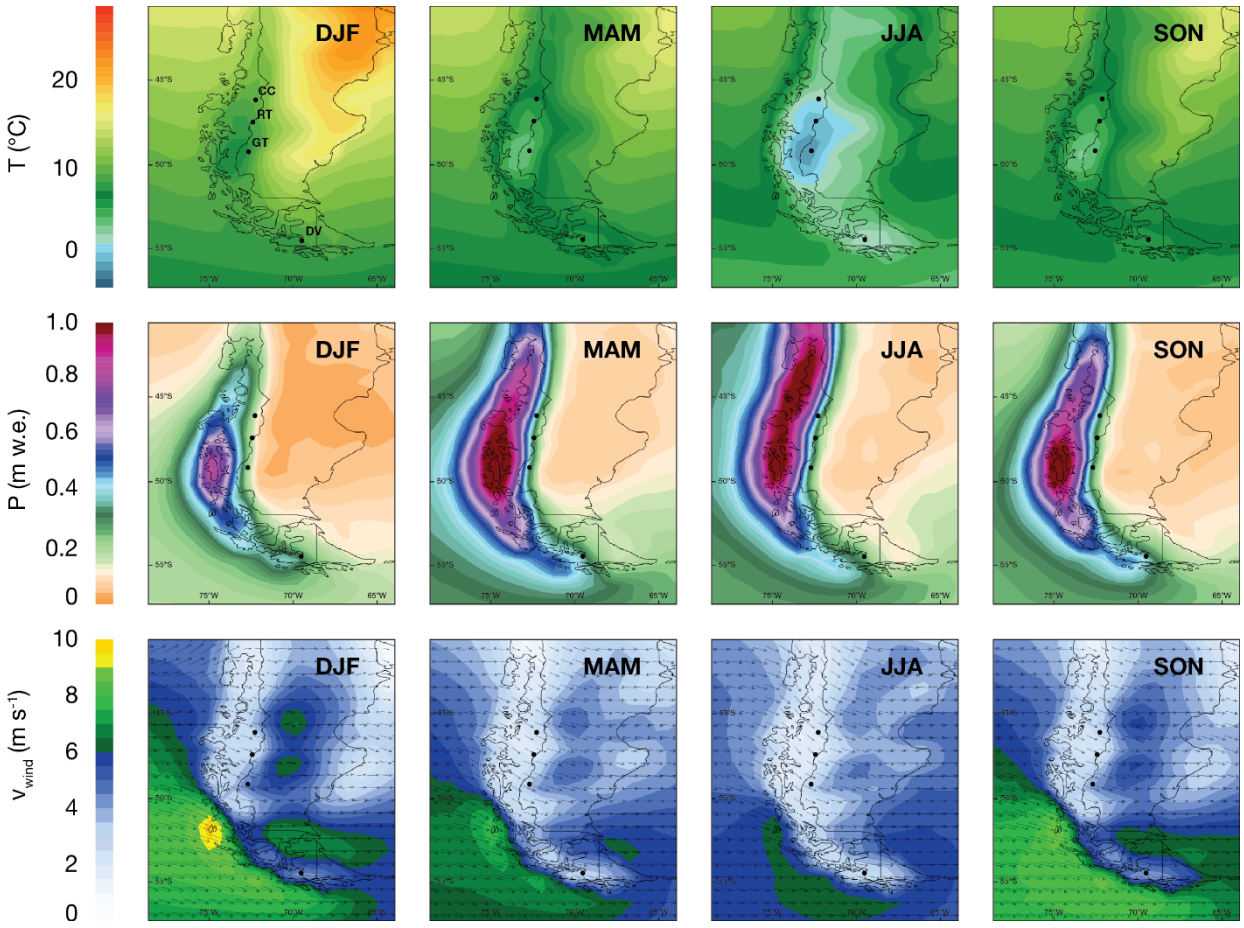

Figure 2.3. Seasonal temperature, precipitation, and wind speed from the ERA-Interim reanalysis (Dee et al., 2011) for the interval 1979-2015. Location of study areas in this thesis indicated by black dots. CC=Cerro Castillo, RT=Río Tranquilo, GT=Glaciar Torre, DV=Dalla Vedova. Images from Climate Reanalyzer (https://ClimateReanalyzer.org), Climate Change Institute, University of Maine, USA.

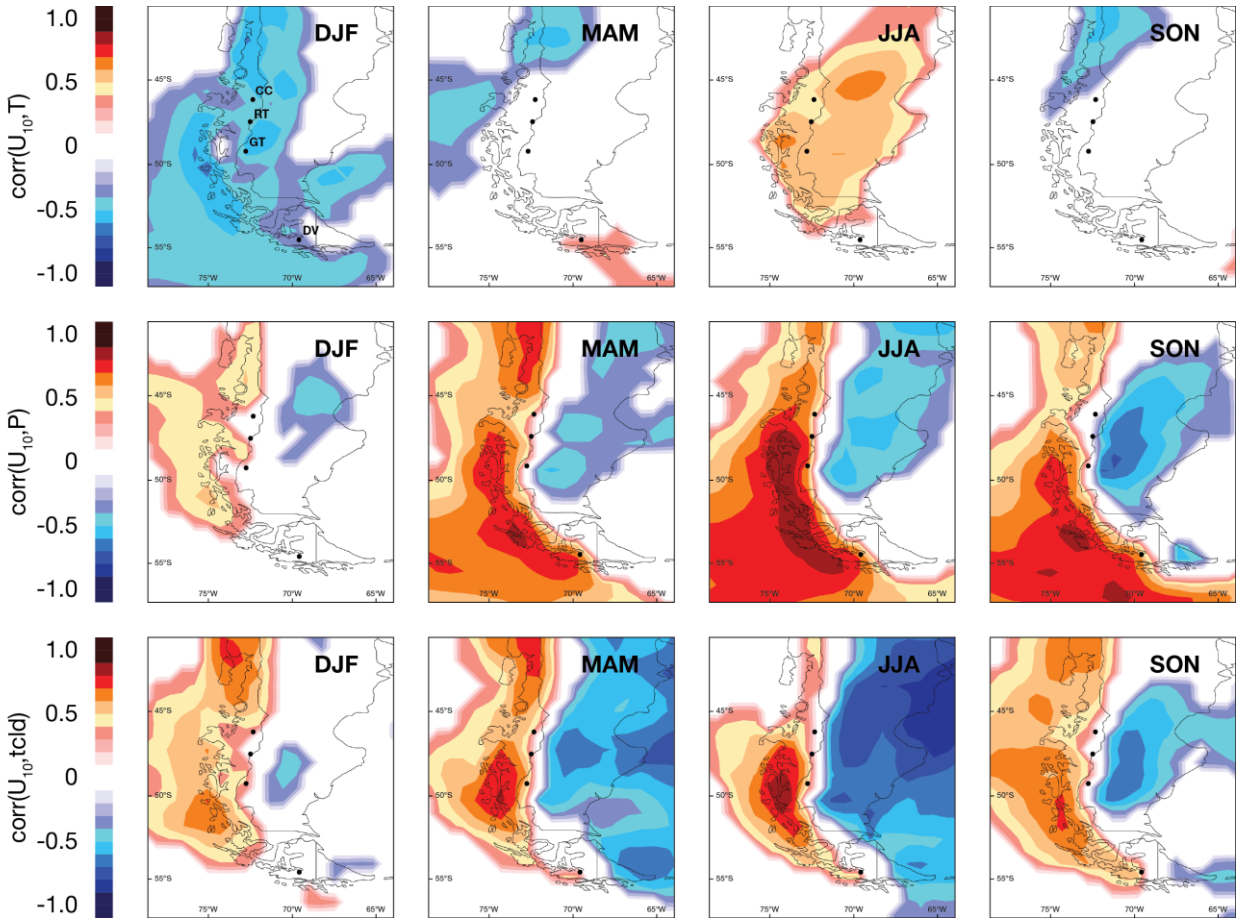

Figure 2.4. Seasonal correlations at the 95th percentile between 10-m zonal wind and temperature (first row), precipitation (second row), and total cloud cover (third row) from the ERA-Interim reanalysis (Dee et al., 2011) for the interval 1979-2015. Location of study areas in this thesis indicated by black dots. CC=Cerro Castillo, RT=Río Tranquilo, GT=Glaciar Torre, DV=Dalla Vedova. Images from Climate Reanalyzer (https://ClimateReanalyzer.org), Climate Change Institute, University of Maine, USA.

Analysis of historical trends in temperature and precipitation are limited by the sparse station data in the region, although some tendencies are apparent. A subtle warming trend over the 20th century is observed in station data (Rosenblüth et al., 1997; Carrasco et al., 2002) and the NCEP-NCAR reanalysis (Rasmussen et al., 2007). Changes in precipitation are regionally distributed: since the 1970's precipitation has declined across Patagonia north of ~48°S, while it has increased in western Patagonia south of this latitude and no trend is apparent to the east (Aravena and Luckman, 2009; Garreaud et al., 2013).

Interannual climate variability shows a strong relationship to the Antarctic Oscillation/Southern Annular Mode (AAO/SAM; hereafter SAM). Classically defined as a zonal pressure differential between 40°S and 65°S (Gong and Wang, 1999; Marshall, 2003), its increasingly-frequent positive mode is associated with the modern strengthening of westerly circulation over the Southern Ocean (Figure 2.5, Thompson and Solomon, 2002). The ring-like—or annular—intensification of westerly circulation over the subantarctic also results in distributed changes in temperature and precipitation. A temperature dipole develops between Patagonia/West Antarctica and

East Antarctica, while the strong correlation between precipitation and westerly circulation is reflected in precipitation anomalies corresponding to the strongly-affected zonal wind field over the Southern Ocean (Figure 2.5).

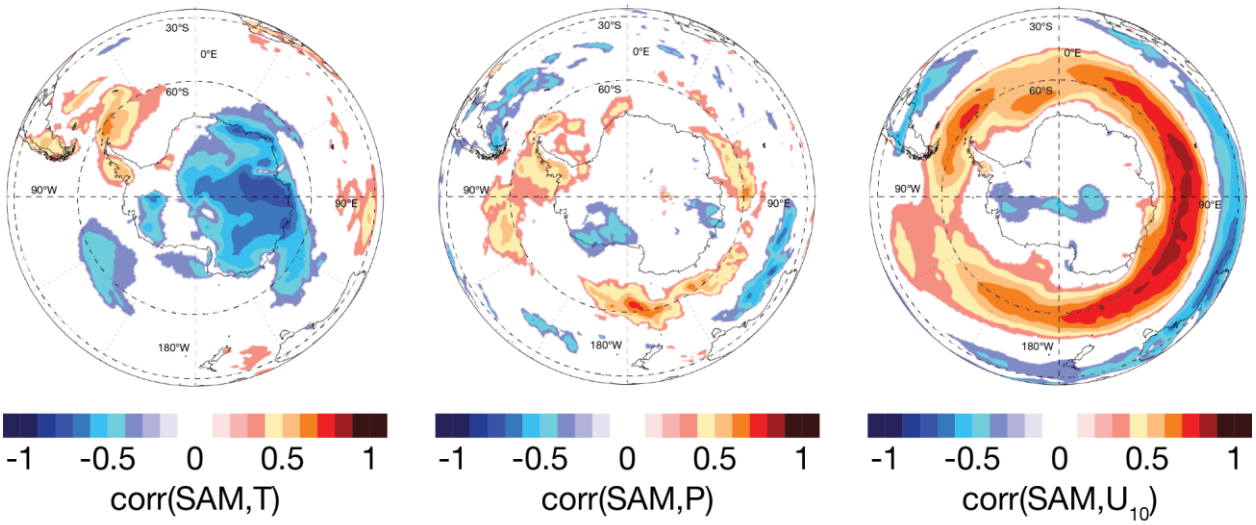

Figure 2.5. Annual correlations at the 95th percentile over the Southern Hemisphere between the Marshall SAM index (Marshall, 2003) and temperature, precipitation, and 10-m zonal wind from the ERA-Interim reanalysis (Dee et al., 2011) for the interval 1979-2017. SAM index values are from realtime station-based mean sea level pressure differentials between 40° and 65°S (https://legacy.bas.ac.uk/met/gjma/sam.html) on methods outlined in (Marshall, 2003). Images from Climate Reanalyzer (https://ClimateReanalyzer.org), Climate Change Institute, University of Maine, USA.

The Southern (and Northern) Annular Modes are strongly influenced by variations in the stratospheric winds (Kidston et al., 2015). Recent trends towards the positive phase of the SAM (Marshall, 2003) have been attributed to the depletion of stratospheric ozone (Thompson et al., 2011) and greenhouse gas emissions (Simpkins and Karpechko, 2012). The SAM is highly correlated with temperature over Patagonia and slightly correlated with precipitation over Tierra del Fuego (Figure 2.6; Garreaud et al., 2009). The trend towards positive SAM is likely linked to regional warming (Rasmussen et al., 2007) and positive precipitation anomalies observed in southernmost Patagonia (Aravena and Luckman, 2009).

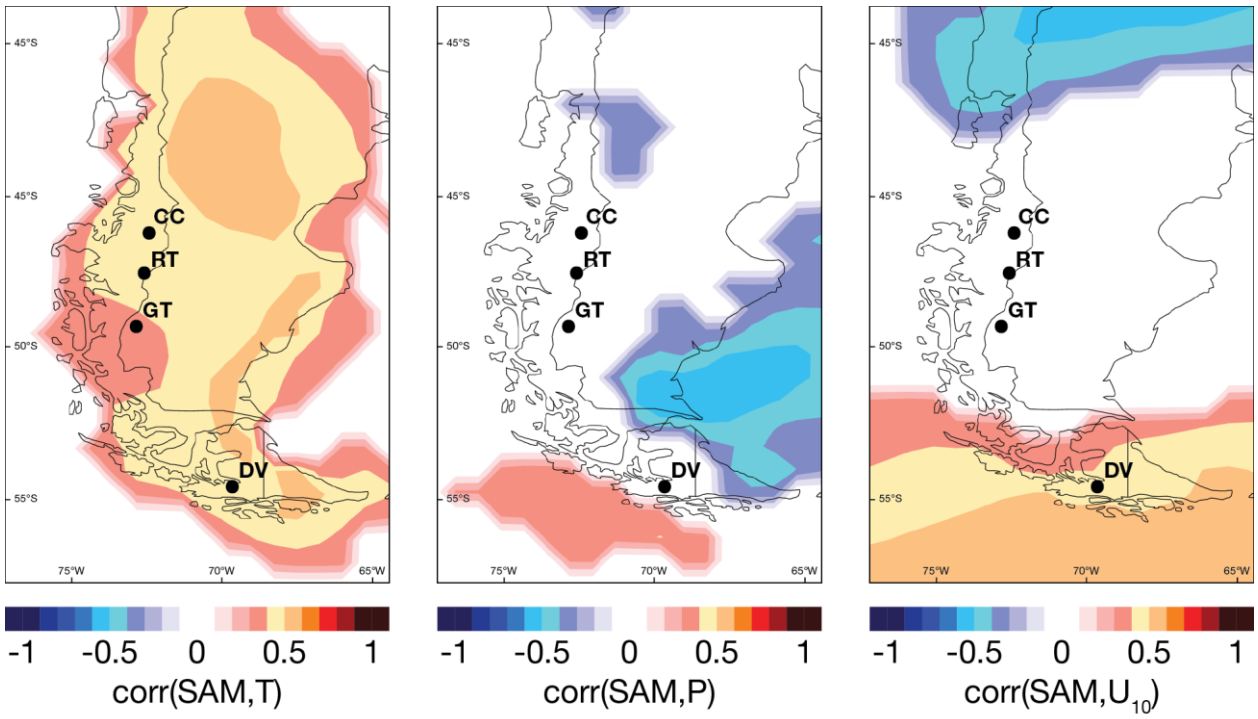

Figure 2.6. Annual correlations at the 95th percentile over Patagonia between the Marshall SAM index (Marshall, 2003) and temperature, precipitation, and 10-m zonal wind from the ERA-Interim reanalysis (Dee et al. 2011) for the interval 1979-2017. Location of study areas in this thesis indicated by black dots. CC=Cerro Castillo, RT=Río Tranquilo, GT=Glaciar Torre, DV=Dalla Vedova. SAM index values are from realtime station-based mean sea level pressure differentials between 40° and 65°S (https://legacy.bas.ac.uk/met/gjma/sam.html) on methods outlined in (Marshall, 2003). Images from Climate Reanalyzer (https://ClimateReanalyzer.org), Climate Change Institute, University of Maine, USA.

2.3 Past climate of Patagonia

2.3.1 Records of paleoclimate in Patagonia

Classically, Holocene climate variability in Patagonia has been attributed to broad changes in the nature of the Southern Westerly Wind (SWW) belt, although the precise nature of the variability remains elusive. Various investigators have invoked changes of the SWW belt's latitudinal position (Moreno et al., 2009), intensity (Mayr et al., 2007), latitudinal breadth (Lamy et al., 2010), or some combination of these factors (Kilian and Lamy, 2012). Although a straightforward relationship between SWW strength and precipitation exists across the region (Garreaud et al., 2013), to date the paleoglacier record has been unable to contribute to the debate as to the nature of SWW variability. This is due in large part to the lack of firm constraints or consensus on the exact timing of Holocene paleoglacier advances in Patagonia and Tierra del Fuego.

2.3.1 State of the science: Paleoglacier records in Patagonia 41°-55°S

Patagonia's potential as the paleoglacial keystone of the southern hemisphere was first acknowledged in the work of Caldenius (1932). While their relative chronology of Patagonian glaciations remains essentially unmodified today, Caldenius' effort to correlate Patagonian glacial events with their northern hemisphere counterparts was

thwarted by the lack of absolute dating techniques available at the time. Significant developments in glacial chronologies did not occur for three decades later, with the onset of radiocarbon dating as a viable technique. Auer (1960) was the first exponent of this method in Patagonia, followed closely thereafter by the works of Heusser (1960) and Mercer in Argentina (1965, 1968) and Chile (1970).

2.3.1.1 LGM and LGT chronologies

Again, the Last Glacial Maximum (LGM) is defined as the global ice volume maximum defined by sea level regression during the last glacial period, between 26.5 and 19 ka (Mix et al., 2001; Clark et al., 2009). Multiple studies indicate a recent PIS maximum that broadly parallels the global LGM. Maximum ice extent of the Bahía Inútil lobe of the Patagonian paleo ice cap on Tierra del Fuego occurred c. 22-20 ka (McCulloch et al., 2005b; Kaplan et al., 2008), while the Magellan lobe reached its maximum extent c. 27 ka (Mcculloch et al., 2005b; Kaplan et al., 2008). Further north, the Lago Pueyrredón lobe reached its maximum slightly earlier at 31 ka (Hein et al., 2010), while the maximum at Lago Buenos Aires has been constrained at c. 27 ka (Kaplan et al., 2005; Douglass et al., 2006). These dates are broadly in accord with the coldest Antarctic paleotemperature during the last glacial period at EPICA Dome C and Vostok (Blunier et al., 1998; Jouzel et al., 2007). However, a number of new studies have suggested the last maximum ice extent along certain parts of the PIS occurred earlier, during MIS 3 (Sagredo et al. 2011; Darvill et al., 2015; Smedley et al., 2016; García et al., 2018).

The weight of literature shows that late Pleistocene glacier maxima occurred during the LGM, although it also appears that earlier local maxima exist. With existing data, no coherent spatial variation appears to exist in the exact timing of the "last glacial maximum" *sensu stricto*, which is in line with global variations in the millennial-scale timing of the LGM. Of note is the great difference in LGM glacier extent between Tierra del Fuego and southern Patagonia. The Bahía Inútil and Magellan lobes each extended almost 200 km north from their source areas within the Cordillera Darwin (Figure 2.1; Rabassa et al., 2000). On the other hand, LGM outlets of the paleo-Southern Patagonian Ice Field extended no further than 100 km from the present outlets. This set the stage for the dramatic collapse of the Patagonian Ice Sheet at the onset of the last glacial-interglacial transition.

2.3.1.2 Last glacial-interglacial transition (~18 ka-11.7 ka)

As in other regions of the globe, the transition out of the LGM appears to have happened simultaneously (within dating uncertainties) in southern Patagonia and Tierra del Fuego, with glacier culmination followed by recession occurring c. 18-17 ka (Mcculloch et al., 2005a; Schaefer et al., 2006; Kaplan et al., 2008; Denton et al., 2010). In both sectors ice sheet collapse was rapid. At Lago Argentino, ice had retreated to within 30 km of the present-day ice margin by c. 16.4 ka (Strelin et al., 2011). Meanwhile, in Tierra del Fuego, northern Cordillera Darwin glaciers retreated to a position near their present-day ice margins by c. 16.8 ka (Hall et al., 2013). Ice sheet collapse is contemporaneous

with the onset of Antarctic warming (Jouzel et al., 2007); however, this gradual warming trend does not in and of itself explain the extremely rapid deglaciation that occurred across southern South America.

Workers in Tierra del Fuego have reported equivocal evidence for a lateglacial readvance of glaciers during the Antarctic Cold Reversal (ACR). Small mountain glaciers near Ushuaia exhibit an advance during this period (Menounos et al., 2013), and Mcculloch et al. (2005a) suggested a readvance of the Cordillera Darwin ice sheet to the Strait of Magellan, at Isla Dawson. However, maritime glaciers along the Cordillera Darwin show no evidence for an advance at this time (Boyd et al., 2008; Hall et al., 2013; Fernández et al., 2017; Bertrand et al., 2017). If a readvance were to have occurred, the magnitude must have been small relative to the LGM extent of the former ice sheet.

On the other hand, significant glacier advances occurred concurrent with the ACR throughout southern Patagonia (Sagredo et al., 2018). Torres del Paine glaciers expanded over 45 km from their present ice margins (García et al., 2012); in Lago Argentino, ice expanded nearly 70 km from its present extent to encompass nearly half of the present lake extent (Mercer, 1965; Ackert et al., 2008; Kaplan et al., 2011; Strelin et al., 2011).

2.3.1.3 The Holocene (11.7 ka-present)

Early Holocene conditions unfavorable for glacier expansion in Patagonia are supported by the current paleoglacier literature, which suggests an early Holocene 'climatic optimum' at 11,000-6000 yr BP was followed by a glacier maximum at c. 6000-5000 yr BP; this mid-Holocene glacier maximum was followed by less-extensive glacier readvances leading up to the modern deglaciation (Mercer, 1976; Porter, 2000). Studies have followed Northern Hemisphere conventions by describing this renewed glacial activity as representative of a "Neoglacial" interval (Porter and Denton, 1967; Porter, 2000). Recent efforts relying on ^{10}Be, supported by ^{14}C, generally conform to the "Hypsithermal-Neoglacial" paradigm (Strelin et al., 2014; Kaplan et al., 2016; Nimick et al., 2016). Nonetheless, scattered evidence has suggested some early Holocene glacial activity in Patagonia (Röthlisberger, 1986; Douglass et al., 2005; Mardones et al., 2011; Harrison et al., 2012; Strelin et al., 2014).

Mercer's chronology of 'Neoglacial' advances beginning c. 5 ka remained the standard chronology for several decades (Porter, 2000), with only slight variations being proposed for the timing of events during this period (Röthlisberger, 1986; Aniya and Sato, 1995b). Glasser et al. (2004) classified the accumulated radiocarbon chronologies as belonging to one of two types. 'Mercer-type' chronologies showed three mid- to late-Holocene advances: between 4700-4200 ^{14}C years BP, 2700-2000 ^{14}C years BP, and during the 'Little Ice Age' from 700-200 years BP. 'Aniya-type' chronologies showed four advances at 3600 ^{14}C years BP, 2300 ^{14}C years BP, between 1600-1400 ^{14}C years BP, and during the 'Little Ice Age.'

While data for the Holocene in Tierra del Fuego are scarce, what studies do exist indicate that Tierra del Fuego glaciers have behaved differently during the Holocene than their northern counterparts. The dated advances of the Ema glacier at Monte Sarmiento indicate a Holocene glacial maximum within the past ~300 yr, during the classic Little Ice Age (LIA; Strelin et al., 2008). The Pía glacier adjacent to the Beagle Channel shows no Little Ice Age maximum, and instead features an apparent Holocene maximum between 940 and 670 yr B.P. (Kuylenstierna et al., 1996). The Marinelli glacier had advanced to its most advanced Holocene position by 8 ka and remained at this location until the mid-1960's, when it commenced a rapid retreat that continues today (Boyd et al., 2008). In the Cordón Martial, only circumstantial evidence exists for pre-LIA Holocene glacier advances; a prominent yet limited glacier advance close to the modern ice limit is assumed to represent the LIA (Menounos et al., 2013). Collectively, these dates suggest a latest Holocene glacier maximum, without apparent evidence for more-extensive glaciations earlier in the Holocene.

Recent technical advances in absolute dating have yielded new insights into the nature of Holocene glaciation. Mounting evidence suggests activity prior to the classical onset of Neoglaciation at 5 ka. Using terrestrial cosmogenic nuclide surface exposure dating (TCN-SED), Douglass et al. (2005) provided ages of ~11 ka and ~8 ka (c. 11 and 8 ka recalculated with the production rate of Kaplan et al., 2011) for moraines south of Lago Buenos Aires, while Glasser et al. (2012) suggests earliest Holocene maxima for outlets of the Northern Patagonian Icefield. Harrison et al. (2012) utilized optically stimulated luminescence (OSL) dating to identify glacier advances of the San Rafael glacier at ~9.5 ka and 5.7 ka. However, the overall body of evidence for early Holocene glaciation in Patagonia remains sparse and has not found universal acceptance within the scientific community (Kaplan et al. 2016).

2.3.1.4 Critically evaluating Holocene chronologies

The bulk of the literature surrounding paleoglacier fluctuations has been conducted using radiocarbon-minimum limiting ages (see section 1.2.3). Such ages give a minimum age of glacier retreat and can be taken either from material overlying glacial sediment or from vegetation between a glacial moraine and the present-day glacier margin. The benefit of this method is that samples are simple to take and relatively inexpensive to process. The drawback is that the minimum age is not often a 'close minimum,' as organic deposition post-glacial retreat can be controlled by factors unrelated to glaciation (e.g. microclimatic variability, time of vegetation establishment, erosion).

Radiocarbon-maximum limiting ages give a maximum age of glacier advance and can be obtained from organic material either underlying glacial sediment, or occasionally embedded within glacial sediment. The latter are especially useful as they typically provide much tighter constraints on glacial activity than minimum limiting ages. However, they are often difficult to obtain, requiring either extensive digging or a preexisting exposure of glacial sediment. They are also limited by their "one-sidedness" in that while they constrain glacial advance, in the absence of a minimum-limiting age

overlying a glacial sequence they cannot give the whole history of a glacial advance-retreat cycle—the elusive bracketed limiting age.

The result of a paleoglacier record based solely upon open-ended chronologies is a record that show little coherence when not interpreted as closely-limiting minimum or maximum ages (Figure 2.7)

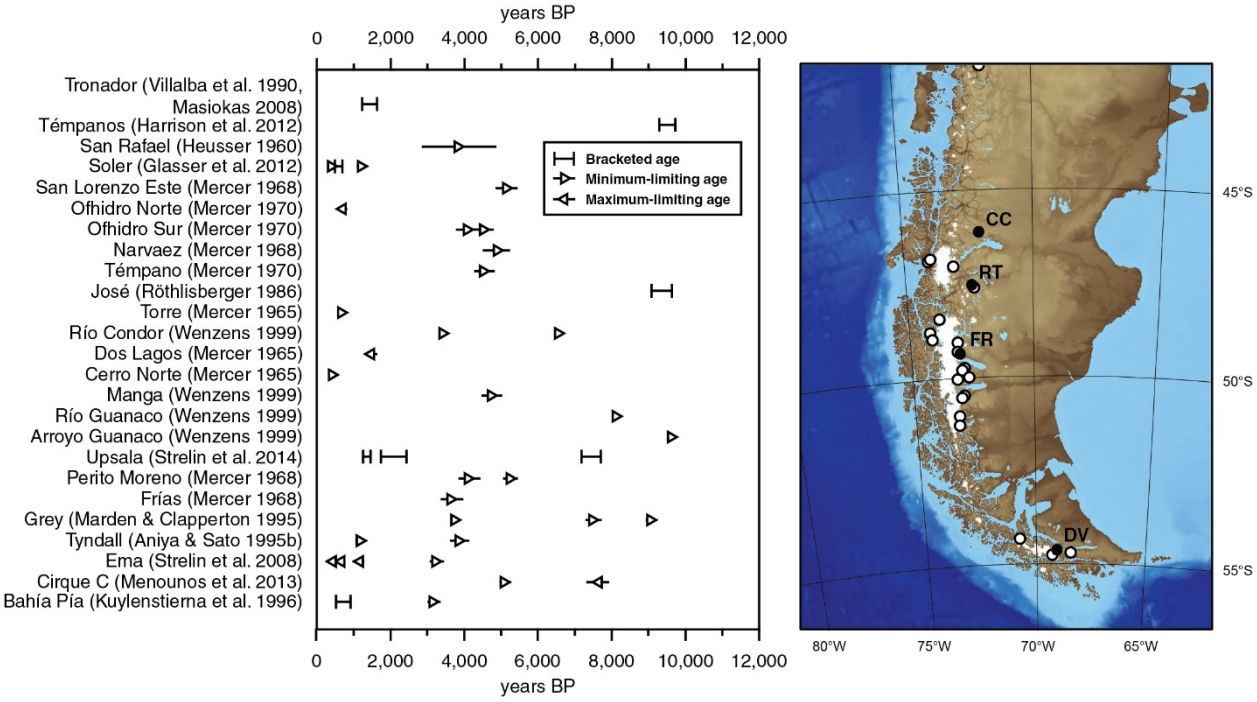

Figure 2.7. Holocene glacier chronologies in Patagonia and Tierra del Fuego published prior to 2015. Sites are ordered by latitude and correspond to white dots in the regional map (right). References in text.

Kaplan et al. (2016) noted that, until recently, the vast majority of prior studies (Heusser, 1960; Mercer, 1982, 1965, 1970, 1976; Röthlisberger, 1986; Aniya and Sato, 1995b, 1995a; Aniya, 1996; Aniya and Naruse, 1999; Wenzens, 1999; Garibotti and Villalba, 2009; Masiokas et al., 2009) had to rely on minimum-limiting age dating of glacial deposits to constrain Holocene glacier advances or retreats. As mentioned in section 1.2.3, minimum-limiting ages are "open-ended," which yield valid results when interpreted solely as minimum-limiting ages of a geologic event (in this case, the formation of said glacial deposits). However, a key assumption for the use of these data as precise indicators of Holocene climate variability is that the time lag between deposition and colonization by vegetation is minimal. Intervals of 10^2 years or greater, or periods of erosion between initial and subsequent colonization, can result in a date that provides a valid limiting age of low precision.

Strelin & Malagnino (Strelin and Malagnino, 2000) reported a minimum-limiting age of 5,730±580 ^{14}C yr BP for the seventh ridge of the Puerto Bandera II moraines at Lago Argentino (51°S); the actual age of the ridge was 11,100±730 ^{14}C yr BP. They cautioned that minimum-age dating in the region could significantly underestimate the actual age

of glacial landforms. Subsequent dating in the Lago Argentino region revealed several significant age discrepancies between the initially-reported single minimum-limiting ages and new chronologies obtained by age bracketing and ^{10}Be surface exposure dating.

- The initial minimum-limiting age of the Herminita moraines of 2,360±90 ^{14}C yr BP (Aniya and Sato, 1995a) significantly underestimated the true age of the late-glacial moraines, which were formed no later than 10,350±45 ^{14}C yr BP (Strelin et al., 2011).
- The outermost Pearson I moraine at Lago Pearson/Anita was assigned a minimum age of 1,995±100 ^{14}C yr BP by Mercer (1965). ^{10}Be surface exposure dating subsequently established that this moraine most likely formed at 4,450±220 yr BP (Kaplan et al., 2016).
- The outermost Pearson I moraine on the Herminita Peninsula (Pearson 1a) was originally interpreted as representing a glacial advance from between 1,600-1,400 ^{14}C yr BP, based on basal radiocarbon ages from dry ponds both inboard and outboard of the Pearson 1a moraine (Aniya and Sato, 1995a). Later studies demonstrated that the Pearson 1a moraine at this location was formed at no later than 4,085±85 cal yr BP, likely between ~6000 and ~4500 yr BP (Strelin et al., 2014; Kaplan et al., 2016).
- Mercer (1976) obtained a minimum-limiting age of >3,465±130 ^{14}C yr BP for the outermost moraine at Glaciar Frías, with maximum Holocene extent prior to this date. Radiocarbon age bracketing and ^{10}Be moraine dating (Strelin et al., 2014; Kaplan et al., 2016) suggested a more precise age of ~6,000 yr BP for this advance.

In each example listed above, the actual landform age predates the originally-reported age, which is consistent with the interpretation of the original ages as minimum-limiting ages. However, in many circumstances the authors assumed that these ages were not open-ended minimum ages, but as close-limiting ages. These ages were subsequently used to construct the active models of Holocene glaciation in Patagonia. Given that more recent studies have demonstrated this assumption to be unsustainable, a critical reevaluation of the preexisting Holocene glacier chronology is warranted.

2.4 Concluding remarks

Southern Patagonia and Tierra del Fuego provide excellent natural laboratories to study the crucial belt of latitude between 46° and 55°S. The nearly-orthogonal strike of the Andes with respect to the dominant westerly flow is unique in the world, and the strong dependence of regional climate upon the westerlies simplifies paleoclimatic interpretation. However, with respect to the extensive paleoglacier record that exists in the region, important ambiguities still exist regarding the timing and spatial distribution of glacier advances and retreats, especially with regards to the Holocene. Rectifying these ambiguities will help to identify the scope of Holocene climate change and better understand the underlying processes behind said climate variability.

* * *

Chapter 3 – Lateglacial to Holocene glacier fluctuations in southern Patagonia

3.1 Introduction

This chapter contains the results of a paleoglacier chronology from Glaciar Torre, Provincia de Santa Cruz, Argentina (49.3°S / 73.0°W). This chronology was established using ^{10}Be terrestrial cosmogenic nuclide surface exposure dating of seven glacier advances spanning the lateglacial and Holocene. A manuscript presenting these results is presented here; it has been accepted for publication by *Quaternary Science Reviews* (June 2019). The chapter concludes with a summary of the glacier chronology and its significance in a paleoclimatic context.

Supplementary material for this publication are located in the Appendix (section 8.1).

3.2 Holocene glacier fluctuations in Patagonia are modulated by summer insolation intensity and paced by Southern Annular Mode-like variability (manuscript accepted for publication by *Quaternary Science Reviews*)

Quaternary Science Reviews 220 (2019) 178–187

Contents lists available at ScienceDirect

Quaternary Science Reviews

journal homepage: www.elsevier.com/locate/quascirev

Holocene glacier fluctuations in Patagonia are modulated by summer insolation intensity and paced by Southern Annular Mode-like variability

Scott A. Reynhout [a, b], Esteban A. Sagredo [b, c, *], Michael R. Kaplan [d, e], Juan Carlos Aravena [e], Mateo A. Martini [f], Patricio I. Moreno [b, g], Maisa Rojas [b, h, j], Roseanne Schwartz [d], Joerg M. Schaefer [d, i]

[a] Departamento de Geología, Facultad de Ciencias Físicas y Matemáticas, Universidad de Chile, Plaza Ercilla 803, 8370450 Santiago, Chile
[b] Núcleo Milenio Paleoclima, Universidad de Chile, Las Palmeras 3425, Ñuñoa, Chile
[c] Instituto de Geografía, Pontificia Universidad Católica de Chile, Avenida Vicuña Mackenna 4860, 7820436 Macul, Chile
[d] Lamont-Doherty Earth Observatory, P.O. Box 1000, 61 Route 9W, Palisades, NY 10964-100, USA
[e] Centro de Investigación Gaia Antártica, Universidad de Magallanes, Avenida Bulnes 01855, 62000009, Punta Arenas, Chile
[f] Centro de Investigaciones en Ciencias de la Tierra (CONICET-Facultad de Ciencias Exactas, Físicas y Naturales, UNC), Vélez Sársfeld 1611, X5016GCA, Córdoba, Argentina
[g] Departamento de Ciencias Ecológicas, Facultad de Ciencias, Universidad de Chile, Las Palmeras 3425, Ñuñoa, Chile
[h] Departamento de Geofísica, Facultad de Ciencias Físicas y Matemáticas, Universidad de Chile, Avenida Blanco Encalada 2002, Santiago, Chile
[i] Department of Earth and Environmental Sciences of Columbia University, New York, NY, 10027, USA
[j] Center for Climate and Resilience Research (CR2), Blanco Encalada 2002, Santiago, Chile

ARTICLE INFO

Article history:
Received 28 January 2019
Received in revised form
27 May 2019
Accepted 30 May 2019

Keywords:
Holocene
Glaciation
Paleoclimatology
South America
Cosmogenic isotopes
Geomorphology
Glacial
Insolation
Southern annular mode

ABSTRACT

Alpine glaciers are sensitive indicators of changes in climate, and their ubiquity in mountainous regions make them valuable proxies for terrestrial climate reconstructions worldwide. However, the timing and extent of glacier change across the South American mid-latitudes through the Holocene are still poorly constrained relative to their counterparts in the Northern Hemisphere. Here we report a new ^{10}Be surface exposure-based chronology of moraines recording a series of progressively less-extensive glacier advances of Glaciar Torre (Argentina, 49.3°S/73.0°W) since the Last Glacial Maximum, with expansions culminating at 17,600 ± 900, 13,500 ± 500, 9700 ± 400, 6900 ± 200, 6100 ± 300, 4500 ± 200, and 530 ± 60 yr BP. The declining magnitude of Holocene glacier expansions parallels a gradual rise in local summer insolation intensity during the Holocene, while individual advances occurred during inferred negative Southern Annular Mode (SAM)-like states at centennial to millennial timescales. These observations suggest that (i) summer insolation intensity modulated antiphased trends in glacier extent in the polar hemispheres during the Holocene, and that (ii) centennial-scale 'SAM-like' temperature and precipitation anomalies paced glacier fluctuations throughout Patagonia. Given the persistence of the inferred 'SAM-like' anomalies throughout the Holocene, the modern measured trend towards positive SAM index conditions could mark the onset of a fundamental shift in the climate of the Southern Hemisphere midlatitudes that warrants consideration in projections of future climate.

1. Introduction

At least five decades of studies on glaciers around the North Atlantic sector have revealed a general pattern of progressively larger glacier expansions during the Holocene, culminating in glacier maxima within the last 600 years (Porter and Denton, 1967; Denton and Karlén, 1973; Ivy-Ochs et al., 2009; Nesje, 2009; Carlson et al., 2014). As alpine glaciers respond to decadal-to millennial-scale climate change (Mackintosh et al., 2017), this pattern has been interpreted to support a warm early-to middle-Holocene, although some glaciers did expand during this period (Nesje, 2009; Schimmelpfennig et al., 2012). Several explanations have been

* Corresponding author. Núcleo Milenio Paleoclima, Universidad de Chile, Las Palmeras 3425, Ñuñoa, Chile.
E-mail address: esagredo@uc.cl (E.A. Sagredo).

https://doi.org/10.1016/j.quascirev.2019.05.029
0277-3791/

proposed for this pattern in Europe and North America; however, if the opposing trend of progressively smaller glacier advances during the Holocene in New Zealand (Schaefer et al., 2009; Putnam et al., 2012; Kaplan et al., 2013) represents a Southern Hemisphere-wide pattern, antiphased trends in summer insolation intensity between the Northern and Southern Hemispheres may be implicated as a 'modulator' of global mid-latitude glacier extent.

Paleoglacier studies in southern Patagonia (defined here as South America between 46° and 53°S) reveal a glacial chronology different from those in New Zealand and the Northern Hemisphere. Several models of "Neoglaciation" have been proposed, often dissimilar from each other, although all suggest that an early Holocene warm period was followed immediately by mid-Holocene glacier maxima and progressively smaller glaciations in the mid-to late-Holocene (Mercer, 1965; Clapperton and Sugden, 1988; Glasser et al., 2004; Aniya, 2013; Strelin et al., 2014; Kaplan et al., 2016). Although this pattern differs from the progressively less- and more-extensive Holocene glaciations in New Zealand and the Northern Hemisphere, respectively, early workers (Porter and Denton, 1967; Mercer, 1982) drew implicit parallels across the polar hemispheres by defining the Patagonian record in terms of a warm "Hypsithermal" followed by a colder "Neoglacial" period (Porter, 2000). The failure of present glacier chronologies to identify coherent hemispheric trends in climate colors our understanding of Holocene climate and suggests no single factor has governed glacier behavior over this time period (Solomina et al., 2015).

An important caveat in Patagonian glacier studies is the continued reliance on chronologies based on minimum-limiting age dating. Kaplan et al. (2016) note that, until recently, most prior studies had to rely on minimum ages to constrain Holocene glacier advances or retreats. A common method involves radiocarbon dating of organic matter overlying glacial deposits. This method yields valid results when interpreted as minimum-limiting ages of a geologic event; however, a key assumption for the use of these data to constrain Holocene climate variability is that the time lag between deposition and colonization by vegetation is minimal. Lags of centuries to millennia—or periods of erosion between initial and subsequent colonization—can result in valid limiting ages of low precision. New age constraints of previously dated moraines in Patagonia have demonstrated that the original minimum-limiting ages often underestimated the true age of the landform by thousands of years, for instance at Peninsula Herminita (Aniya and Sato, 1995; Strelin et al., 2011; Kaplan et al., 2016), Lago Pearson (Mercer, 1965; Kaplan et al., 2016), and at Glaciar Frías (Mercer, 1976; Strelin et al., 2014; Kaplan et al., 2016).

We stress that the original ages reported in such sites are not incorrect; the actual ages of the dated moraines predate the originally-reported ages, which is consistent with the *a priori* implications of minimum-limiting ages. However, the existing models of Holocene glaciation in Patagonia were constructed in part assuming that minimum-limiting ages served as close (e.g. sub-millennial) approximations of the true age of a glacial advance. As multiple studies have now demonstrated that this assumption cannot be universally sustained in this region, a reevaluation of the preexisting Holocene glacier chronology is necessary to evaluate sub-millennial climate variability.

We set out to improve our understanding of the timing and extent of Patagonian glacier fluctuations since the Last Glacial Maximum (LGM) by developing a new ^{10}Be chronology for a sequence of well-preserved moraines deposited by Glaciar Torre in southwestern Patagonia. Using this chronology, we evaluate the regional coherence between published glacier chronologies, the putative role of summer insolation intensity in mid-latitude glacier fluctuations (Kaufman et al., 2004) throughout the Southern Hemisphere, and a suggested link between distinct glacier expansions and quasi-modern climate variability at centennial timescales during the Holocene.

2. Study area

2.1. Setting

Glaciar Torre (~50 km^2, 49.32°S/73.02°W) is located approximately 20 km north of Glaciar Viedma, the eastern outlet of the Southern Patagonian Icefield (SPI) into Lago Viedma (Fig. 1a). Glaciar Torre lies adjacent to, but is independent from the Icefield, separated to the west by a >500 m headwall formed by the Cerro Torre chain of peaks. Lliboutry (1953) identifies the glacier as a compound glacier composed of three tributary ice bodies named Adela, Grande, and Torre; it is sometimes erroneously referred to as the Fitz Roy glacier. We follow the convention established by Masiokas et al. (2009) by referring to the entire glacier system as Glaciar Torre, although the bulk of the present glacier front consists of ice originating from Glaciar Adela. The glacier terminates in an ice-marginal lake (Laguna Torre; Fig. 1c), which formed as ice retreated from the innermost moraine M7. Ice was land-terminating when the moraines we focus on ("M0"-M7) were formed, as evidenced by the extensive system of terminal moraines, meltwater channels, and outwash deposits associated with past glacier highstands (Fig. 1b).

The chronologic potential within the well-preserved series of end moraines of the Torre Glacier system (Fig. 1b) has been recognized for over 60 years (Heim, 1951; Auer, 1956; Lawrence and Lawrence, 1959; Mercer, 1965). However, few studies have been carried out to evaluate the absolute ages of these landforms. Mercer (1965) provided one minimum-limiting radiocarbon age for the "Fitz Roy III moraine" (M3) of 800 ± 85 ^{14}C yr for a basal peat behind the moraine, and a dendrochronologically-derived minimum-limiting age of ~1695 CE for the "outer Fitz Roy IV moraine" (M4). Masiokas et al. (2009) used dendrochronologic surface exposure dating to estimate "Little Ice Age" minimum-limiting ages for moraines M3-M7 but were unable to obtain limiting ages for the older moraines. This chronology formed the basis of a regional *Rhizocarpon* calibration curve (Garibotti and Villalba, 2009), which suggests latest-Holocene ages for all moraines identified in the area.

2.2. Regional climatology

Regional climate is characterized by the dominant influence of the Southern Westerly Winds (SWW) and the orographic forcing imposed by the Patagonian Andes, resulting in a pronounced west-east gradient in several climatic variables. Precipitation reaches Patagonia in the form of westerly frontal systems guided by the upper-level jet, which is largely symmetric across the southern hemisphere (Garreaud et al., 2009). Precipitation varies from up to 10,000 mm/yr west of the Andean divide to less than 300 mm/yr to the east; zonal westerly flow correlates positively (negatively) with precipitation to the west (east) of the divide, consistent with the development of a strong rain-shadow effect (Garreaud et al., 2013). This longitudinal transition is also seen in the progressive increase of incoming solar radiation towards the east (Schaefer et al., 2015) and the sharp transition in vegetation within the study area. From west to east, the dominant ecoregion transitions from polar ice cap conditions near the eastern limit of the SPI, to a narrow belt of Subantarctic evergreen and deciduous forest, to Patagonian steppe, in less than 20 km (Olson et al., 2001).

Meteorological station data are sparse in the region, but the few stations that exist near the limits of the SPI exhibit historical mean annual temperatures of ~6 °C (Miller, 1976; Carrasco et al., 2002). A long-term warming trend is apparent across southern Patagonia

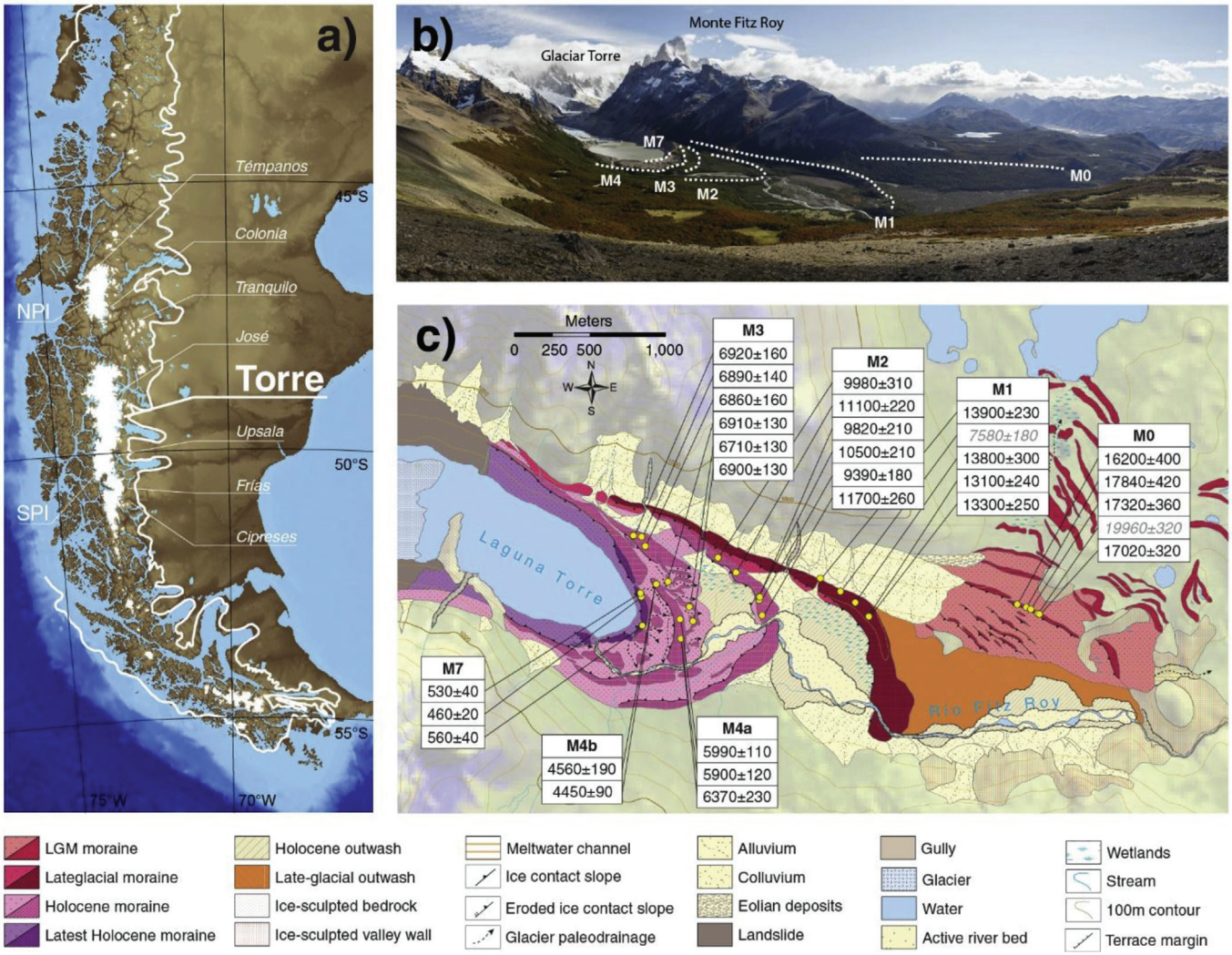

Fig. 1. a) Regional overview with sites mentioned in this paper. White areas represent present ice cover and the white line shows LGM ice extent. SPI = Southern Patagonian Icefield, NPI = Northern Patagonian Icefield. b) Photo of the study area, emphasis on moraine ridge crests. View to the north. c) Glacial geomorphology of the study area and ^{10}Be ages (±1σ internal error) for each dated moraine (yr BP). Ages in gray italics indicate outliers excluded from discussion (see Supplementary Information).

over the 20th century, driven primarily by increases in summer (DJF) temperatures (Villalba et al., 2003). West of the orographic divide, trends in precipitation reflect southerly intensification of the SWW during this period, with a 300–800 mm decade^{-1} decline north of 50°S and a 200–300 mm decade^{-1} increase south of 50°S from 1978 to 2001; east of the divide trends are insignificant (Garreaud et al., 2013). Regional surface energy mass balance modeling of the SPI suggests that increased orographic precipitation—linked with SWW intensification—could have resulted in modelled positive mass balance over the period of 1975–2011 (Schaefer et al., 2015). However, this same study indicates that during this period Glaciar Torre experienced net negative mass balance, incongruent with an increase in precipitation. The negative mass balance trend is better explained as a response to warmer temperatures over the last several decades (Rignot et al., 2003; Rivera and Casassa, 2004; Rasmussen et al., 2007).

Observations of elevated temperatures and a poleward shift and intensification of the SWW are consistent with recent persistently positive phases of the Southern Annular Mode/Antarctic Oscillation (SAM/AAO; hereafter SAM). The SAM is a mode of climatic variability associated with summer (DJF) intensification of the SWW over the Southern Ocean during the latter half of the 20th century (Jones et al., 2016). Positive (negative) phases of the SAM reflect poleward (equatorward) shifts and strengthening (weakening) of the SWW and Antarctic polar vortex, leading to warmer (colder) conditions in Patagonia and increased (decreased) orographic precipitation west of the orographic divide (Gillett et al., 2006; Garreaud et al., 2009; Thompson et al., 2011; Villalba et al., 2012). Registries of the SAM beyond instrumental records indicate multidecadal to centennial trends over the past millennium (Villalba et al., 2012; Abram et al., 2014), and suggest SAM-like variability has existed at centennial timescales through the Holocene (Moreno et al., 2018).

3. Methods

Mapping of glacial landforms enabled us to identify eight well-preserved moraine complexes distal to the modern ice margin of Glaciar Torre (Fig. 1b). These moraines are sharp-crested, variably dissected by paleochannels or modern drainages, with slope angles in the sampled areas below the angle of repose of unconsolidated sediment. Following prior convention (Masiokas et al., 2009), we

label them M0 to M7 in ascending chronostratigraphic order. From these latero-frontal moraines, we collected 30 samples from boulders to establish the age of at least six glacier expansions (Fig. 1c).

Rock samples were taken for ^{10}Be surface exposure dating from large (>1 m^3) boulders rooted in the crests of moraine ridges (Fig. S1). An assumption underlying this method is that boulders deposited at this position were deposited during the final phases of a glacier advance, and their exposure ages will reflect the age of moraine stabilization following glacier retreat. We assume that we sample the final part of the moraine constructed (i.e. the top) and that moraine stabilization occurred immediately after the withdrawal of Glaciar Torre from the moraine-forming position. We also assume advance and retreat of Glaciar Torre was primarily a function of climate; Sagredo et al. (2014) suggested that southern Patagonian glaciers are relatively more sensitive to variations in temperature than precipitation, due to the region's shallower atmospheric lapse rate and greater atmospheric emissivity. We therefore assume the age of moraine stabilization therefore closely dates the inflection point when local climatic conditions—specifically temperature—changed from favorable to unfavorable for glacier advance. Strictly speaking, our moraine ages are considered close minimum-limiting ages marking the end of glacial expansions.

Rhyodacitic and granodioritic lithologies were sampled; total sample quartz content varied between 5 and 35%. Samples >0.5 m tall were preferentially sampled to avoid possible effects of burial and posterior exhumation of boulders. Sampling taller boulders also reduces the likelihood of long-term burial under thick snow, the impact of which we consider minor and for which we do not correct. Rock surfaces presenting few signs of surficial pitting or erosion were preferentially selected, avoiding any surfaces that show obvious signs of erosion (e.g. spalling, flaking), although the effects of *in situ* weathering are assumed to be negligible due to the young age of the samples. We therefore do not correct for erosion in our age calculations. Samples were taken from the top 1–4 cm of planar to gently curved non-vegetated surfaces using a drill and explosive charges. A topographic skyline, as well as surficial strike and dip measurements, were made using a pocket transit and clinometer for shielding corrections. Coordinates and altitude were evaluated relative to the WGS 1984 datum using a handheld commercial GPS with an assumed uncertainty of 5 m in the horizontal plane and 5-10 m in the vertical.

Initial rock crushing took place at the Pontificia Universidad Católica de Chile; mineral separation, beryllium isolation, and final sample preparation occurred at the Cosmogenic Nuclide Laboratory at Lamont-Doherty Earth Observatory following established geochemical protocols (Schaefer et al., 2009; Kaplan et al., 2011). Dating of latest-Holocene boulders is made possible only through recent advances in cosmogenic dating techniques that permit analysis of very low ^{10}Be/^{9}Be ratios (~10^{-16}). The two critical components are 1) the low process blank utilized at the Lamont cosmogenic nuclide laboratory, and 2) a custom ion source utilized for AMS measurements at the Center for Accelerator Mass Spectrometry at Lawrence Livermore National Laboratory. Analytical data are available in Table 1.

^{10}Be ages were calculated based on methods incorporated in the CRONUS-Earth online exposure age calculators (v. 2.2) (Balco et al., 2008), using the time-dependent Lal/Stone scaling model and the regional Patagonian production rate (Kaplan et al., 2011). We report mean moraine ages with the propagation of the analytical uncertainty and local production rate uncertainties (3%) (Kaplan et al., 2011) for comparison with other proxy records. We base our discussion on ages using version 2.2.1 of the constants file, as it is modified with a high-resolution version of the geomagnetic framework (Lifton et al., 2008) to be consistent with calculations made by Kaplan et al. (2011). Our choice of constants file and scaling model does not fundamentally alter our conclusions (see Table S1). Radiocarbon ages presented in the discussion were calculated as cal yr BP using the SHCal13 calibration (Hogg et al., 2013) and CALIB v. 7.0.4 (Stuiver and Reimer, 2018).

4. Results

Six of the eight identified moraine crests in the study area were dated. Moraine ages, along with summary statistics, are presented as summed probability distributions in Figs. S2 and S3. Analytical data pertinent to the computation of ages are presented in Table 1; Table S2 presents individual ages according to different production rate scaling schemes. Geomorphologic interpretations, along with a discussion of outliers, are presented below.

4.1. Moraine M0: 17,100 ± 860 yr BP (n = 4, 1 outlier excluded)

M0 is a relatively small (max. 10 m tall) lateral moraine crest preserved in dense forest on the north slope of the Fitz Roy valley. Five samples were taken from boulders astride the ~10 m ridge crest of M0. Greater evidence of superficial pitting and flaking was evident on the granitic boulders that comprise these samples, which suggest that weathering may have affected them to a greater degree; this would have the net effect of reducing the perceived age of these boulders, suggesting the average age should be considered a minimum. Sample FR14-01-31 was excluded based on a Grubbs' test for outliers (Grubbs, 1969).

The remaining four samples from the lateral yield ages ranging from 17,840 ± 420 to 16,200 ± 400 yr BP, with a mean of 17,100 ± 860 yr BP. Inboard of M0, we recognized a series of intermittent, low-relief moraines and planar surfaces with a pronounced ice-proximal scarp interpreted as kame terraces; we consider these to be recessional features not indicative of major glacier expansions. Their presence suggests ice retreat from M0 was incremental, but the lack of age control prohibits a quantitative interpretation of rate of retreat.

4.2. Moraine M1: 13520 ± 540 yr BP (n = 4, 1 outlier excluded)

The next prominent moraine upriver corresponds to M1, a sharp-crested frontal-lateral moraine (max. 50 m tall) ~4.3 km from the present ice margin. This moraine forms the most prominent moraine in the upper Río Fitz Roy valley. Several generations of outwash lie outboard of this landform, comprising the majority of the valley fill. The moraine is breached in several parts by streams and debris flows originating from the northern valley wall, but the lateral M1 moraine can be followed upriver beyond the current proglacial lake margin.

Five samples were used to constrain the age of this moraine; sample FR14-01-02 was excluded based on a Grubbs' test for outliers (Grubbs, 1969). This sample was taken from a location close to a gully that carried sediment from the slope above, which may have altered the original position of the boulder. The other four samples collected along the moraine front yield an average age of 13,520 ± 540 yr BP.

4.3. Moraine M2: 11,660 ± 260 to 9390 ± 180 yr BP (average 9730 ± 420 yr BP; n = 6)

M2 consists of a max. 30 m tall frontal-lateral moraine bisected by the Río Fitz Roy at about 3.2 km from the present ice margin. The northern lateral consists of a 10–20 m tall sharp-crested moraine cut in several parts by perennial streams originating from the northern valley wall. It grades into an elevated hummocky surface

Table 1
Analytical data for samples, sorted by moraine. An assumed sample density of 2.7 g/cm^3 is used in keeping with the felsic to intermediate lithologies sampled. Carrier concentrations used are 1048 ppm ([a]), 1043 ppm ([b]), and 1045 ppm ([c]). (*)AMS ratios presented as boron-corrected values measured against the 07KNSTD3110 standard material (^{10}Be/^{9}Be = 2.85 × 10^{-12}; Nishiizumi et al. 2007). Ratios are not corrected for background ^{10}Be in procedural blanks. (†) = ^{10}Be concentrations in this column are corrected for background ^{10}Be as recorded by the procedural blanks associated with each sample set, the concentrations of which ranged from 6.7545 × 10^{-17} to 7.6323 × 10^{-16}. (‡) = Moraine ages are reported as mean ages (excluding outliers; see text); reported error incorporates one standard deviation and the propagated 3% error of the production rate of Kaplan et al. (2011).

Moraine	Sample	CAMS	Lat.	Lon.	Elevation	Thickness	Shielding	Mass	Be carrier	^{10}Be/^{9}Be	^{10}Be	Age	1σ
		lab no.	°	°	m amsl	cm		g	g	(10^{-14})*	10^4 atoms/g†	yr BP	yr BP‡
M0	FR14-01-28	BE40834	−49.3274	−72.9433	666	2.5	0.993	10.8042	0.1822[a]	10.0665 ± 0.24422	11.845 ± 0.2876	16200	400
	FR14-01-29	BE40015	−49.3276	−72.9421	666	2.3	0.994	9.2087	0.1816[b]	9.6525 ± 0.22321	13.196 ± 0.3058	17840	420
	FR14-01-30	BE42008	−49.3277	−72.9416	659	2.8	0.994	10.0643	0.1816[c]	10.0434 ± 0.20771	12.581 ± 0.2608	17320	360
	FR14-01-31	*BE40016*	*−49.3281*	*−72.9407*	*667*	*2.2*	*0.994*	*10.8238*	*0.1819[b]*	*12.6727 ± 0.20360*	*14.783 ± 0.2381*	*19960*	*320*
	FR14-01-32	BE41998	−49.3281	−72.9405	668	2.6	0.994	10.0632	0.1820[c]	9.8830 ± 0.18340	12.476 ± 0.2318	17020	320
	Average											**17100**	**860**
M1	FR14-01-01	BE40253	−49.3268	−72.9644	640	2.7	0.983	30.1487	0.1822[b]	23.3169 ± 0.37580	9.803 ± 0.1581	13870	230
	FR14-01-02	*BE41991*	*−49.3258*	*−72.9668*	*631*	*2.7*	*0.981*	*10.0594*	*0.1826[c]*	*4.1679 ± 0.09756*	*5.276 ± 0.1240*	*7580*	*180*
	FR14-01-03	BE41992	−49.3276	−72.9626	623	2.3	0.982	10.6287	0.1819[c]	8.0449 ± 0.17528	9.608 ± 0.2096	13770	300
	FR14-01-04	BE40831	−49.3286	−72.961	625	2.1	0.988	25.0633	0.1825[a]	18.1621 ± 0.33641	9.243 ± 0.1713	13130	240
	FR14-01-05	BE40254	−49.3286	−72.961	621	1.7	0.987	27.3342	0.1817[b]	20.2526 ± 0.37771	9.362 ± 0.1747	13320	250
	Average											**13520**	**540**
M2	FR14-01-09	BE41993	−49.3244	−72.9792	630	2.5	0.973	10.0648	0.1824[c]	5.4675 ± 0.16690	6.912 ± 0.2113	9980	310
	FR14-01-10	*BE41994*	*−49.3255*	*−72.977*	*625*	*2.1*	*0.979*	*10.5112*	*0.1819[c]*	*6.4099 ± 0.12360*	*7.739 ± 0.1497*	*11110*	*215*
	FR14-01-13	BE40255	−49.3273	−72.9741	607	3.4	0.982	35.2886	0.1818[b]	18.6569 ± 0.39435	6.683 ± 0.1414	9820	210
	FR14-01-14	*BE41995*	*−49.3271*	*−72.9742*	*610*	*2.8*	*0.983*	*10.054*	*0.1721[c]*	*6.0254 ± 0.12235*	*7.195 ± 0.1465*	*10480*	*210*
	FR14-01-15	BE40256	−49.3276	−72.9741	605	1.6	0.982	35.0604	0.1813[b]	17.9895 ± 0.33616	6.467 ± 0.1210	9390	180
	FR14-01-16	*BE40832*	*−49.3288*	*−72.9738*	*606*	*2.0*	*0.986*	*25.07*	*0.1824[a]*	*15.8486 ± 0.35158*	*8.057 ± 0.1788*	*11660*	*260*
	Average											**9730**	**420**
M3	FRY16-02-08	BE42000	−49.3228	−72.9894	674	0.8	0.972	13.4369	0.1813[c]	5.3837 ± 0.12178	5.016 ± 0.1143	6910	130
	FRY16-02-09	BE42001	−49.3229	−72.9884	663	2.3	0.972	14.9972	0.1825[c]	5.8200 ± 0.11890	4.895 ± 0.1008	6710	130
	FRY16-02-10	BE42002	−49.3236	−72.9879	676	1.3	0.974	13.0344	0.1813[c]	5.1809 ± 0.11662	4.974 ± 0.1129	6900	130
	FR14-01-24	BE40833	−49.3264	−72.9851	654	1.5	0.982	25.0654	0.1828[a]	9.7240 ± 0.18719	4.948 ± 0.0954	6920	160
	FR14-01-25	BE40257	−49.3283	−72.9825	645	1.6	0.986	34.2906	0.1807[b]	13.0623 ± 0.24407	4.781 ± 0.0895	6890	140
	FR14-01-26	BE40258	−49.3294	−72.982	639	1.9	0.987	30.0048	0.1815[b]	11.6508 ± 0.21774	4.893 ± 0.0916	6860	160
	Average											**6860**	**220**
M4a	FR14-01-17	BE40828	−49.3308	−72.9834	669	2.2	0.988	50.0674	0.1820[a]	17.0830 ± 0.31598	4.340 ± 0.0803	5990	110
	FR14-01-18	BE41996	−49.3293	−72.9836	667	2.0	0.986	15.0561	0.1720[c]	5.3497 ± 0.11209	4.263 ± 0.0896	5900	120
	FR14-01-19	BE41997	−49.3293	−72.9836	667	1.8	0.986	13.9391	0.1729[c]	5.3292 ± 0.19257	4.611 ± 0.1668	6370	230
	Average											**6080**	**310**
M4b	FR14-01-20	BE42003	−49.329	−72.9837	665	2.3	0.982	5.0263	0.1819[c]	1.3499 ± 0.05426	3.258 ± 0.1358	4560	190
	FR14-01-21	BE40829	−49.3266	−72.9865	668	2.7	0.982	28.2396	0.1825[a]	7.0460 ± 0.14780	3.172 ± 0.0667	4450	90
	Average											**4500**	**160**
M7	FRY16-02-01	BE42009	−49.3298	−72.988	658	1.8	0.984	70.3865	0.1824[c]	2.1653 ± 0.13275	0.3781 ± 0.0233	560	40
	FRY16-02-03	BE42010	−49.3284	−72.9878	674	2.6	0.984	71.351	0.1820[c]	1.7775 ± 0.07427	0.3031 ± 0.0129	460	20
	FRY16-02-04	BE42011	−49.3273	−72.9884	675	1.5	0.984	73.9716	0.1816[c]	2.1852 ± 0.16986	0.3616 ± 0.0282	530	42
	Average											**520**	**60**

with no clear single ridge in the frontal section of the moraine.

Six samples from M2 yield ages from 11,700 ± 260 to 9390 ± 180 yr BP. Although these ages collectively do not overlap, and therefore do not provide a mean age (Fig. S2), the three youngest ages form a population with a mean age of 9730 ± 420 yr BP. We tentatively use this population in our discussion but emphasize that these ages solely record with confidence an early Holocene maximum of Glaciar Torre. Possible causes of this spread in ages include a period of glacier margin expansion during the latter interval of our age spread, long-term occupancy of the moraine by Glaciar Torre, or alternatively post-depositional collapse or reworking of the moraine front.

4.4. Moraine M3: 6860 ± 220 yr BP (n = 6)

Less than 700 m upstream, the M3 moraine complex consists of several tightly clustered lateral ridges that collectively rise over 50 m from the valley bottom 2.5 km from the ice margin, consisting of no fewer than three crests. Although these crests are distinct in the northern lateral section of the moraine, the frontal moraines have been mostly dissected by meltwater channels, forming a series of discontinuous ridges, hampering correlation of these frontal ridges with their lateral counterparts.

Three samples collected from boulders on the outermost lateral crest of M3 yield ages of 6920 ± 160, 6890 ± 140 and 6860 ± 160 yr BP. Three additional samples collected from the frontal M3 crest provided ages of 6910 ± 130, 6900 ± 130 and 6710 ± 130 yr BP. We treat samples taken from the frontal moraine fragments (n = 3) as equivalent to samples taken from the exterior lateral crest (n = 3); as they all overlap at 1-sigma, they are statistically indistinguishable and yield a uniform age of 6860 ± 220 yr BP for the entire moraine complex.

4.5. Moraine M4: 6080 ± 310 yr BP (n = 3) and 4510 ± 160 yr BP (n = 2)

M4 is a prominent (~60 m) moraine belt preserved on both sides of the river, 2.4 km from the ice margin. The moraine system partially overprints the M3 complex. The Río Fitz Roy runs parallel to the southern section of the moraine; evident slope retreat and subsequent erosion of the ridge crest led us to focus our sampling efforts only on the north side. The northern crest is continuous as a single mappable body but features a considerable vertical “step” between the higher frontal section and the lower lateral section, suggesting a geomorphic break.

The older frontal section yields ages of 6370 ± 230, 5990 ± 110

and 5900 ± 120 yr BP (M4a; mean age 6080 ± 310 yr BP), whereas the two samples from the lateral-lower section provide ages of 4560 ± 190 and 4,450 ± 90 yr BP (M4b; mean age 4510 ± 160 yr BP). Considered separately, two population clusters appear, the frontal at 6080 ± 310 yr BP, and the lateral at 4510 ± 160 yr BP, suggesting the present landform represents two distinct mid-Holocene glacier maxima. We therefore interpret M4 as a polygenetic landform, formed during two discrete mid-Holocene glacier advances at c. 6100 ka and c. 4500 ka.

4.6. Moraines M5 and M6: No absolute age control

M5 and M6 are represented by remnants of moraine ridges, interpreted by previous workers (Mercer, 1965; Masiokas et al., 2009) as evidence of two separate advances. We have no absolute age control for these moraines due to the poor preservation of these landforms and lack of suitable boulders for sampling. Based on their morphostratigraphic position, M5 and M6 must postdate the M4b advance at 4.5 ka and predate the later M7 advance.

4.7. Moraine M7: 520 ± 60 yr BP (n = 3)

Moraine M7 forms the innermost moraine crest bordering Laguna Torre, 2.1 km from the present ice margin. In the lateral sections the distinction between M6 and M7 is unclear. In parts M7 is recognizable as a trimline interior to the M6 crest, but in other parts the M7 lateral appears to merge or overprint the M6 lateral. M7 is only present north of the Río Fitz Roy. As a result, we did not sample from the M6 lateral, and focused our efforts on the unambiguous frontal crest of M7.

Three samples from boulders atop the sharp-crested frontal section of this moraine provide ages of 560 ± 40, 530 ± 40 and 460 ± 20 yr BP, with a mean age of 520 ± 60 yr BP. We attribute the relatively high chi-squared value of these ages to a) the high absolute precision of these dates, with analytical error on the order of tens of years; and b) the higher relative influence of pre-depositional ^{10}Be accumulated during supraglacial transport (inheritance) on younger age populations in alpine glaciers, a phenomenon discussed by Schaefer et al. (2009). Taken together, these ages indicate glacier advance between 400 and 600 years BP (15th-17th centuries CE). This age represents the most recent major moraine-building event by Glaciar Torre.

5. Discussion

Our results comprise the most comprehensive directly-dated chronology for fluctuations of a single Patagonian glacier spanning the last ~18,000 years. This chronology suggests that Glaciar Torre expanded coeval with a final phase of the LGM (M0: 17,100 ± 860 yr BP) and the Antarctic Cold Reversal (ACR) between 14,500 and 12,700 yr BP (M1: 13,520 ± 540 yr BP). Successively less-extensive expansions of Glaciar Torre reached maxima between 11,600 ± 260 and 9390 ± 180 yr BP (mean age 9730 ± 420 yr BP); and at 6860 ± 220, 6080 ± 310, 4510 ± 160, and 520 ± 60 yr BP; these maxima were separated in parts by millennial-scale periods when glacier advances were not preserved in the moraine record. While the LGM and ACR advances reflect well-documented events in Patagonia (García et al., 2012; Sagredo et al., 2018), the Holocene behavior of Glaciar Torre runs counter to the Hypsithermal/Neoglacial model proposed for the region (Porter, 2000) and demonstrates that previous studies considerably underestimated the ages of glacier advances in the area (Table 2).

5.1. Representativity of moraine ages

Analytical error of individual ages does not, in general, exceed 3% (Table S1). Holocene moraine age populations exhibit error on the order of hundreds of years, with reduced chi-squared values of less than 3 for all moraines save the youngest. For these youngest ages, increased analytical error (6–7%) and increased scatter ($\chi^2 = 6.3$; Supplementary Figs. S2 and S3) can be explained as a consequence of the very low concentrations of beryllium-10 in these samples and inheritance on very young landforms, respectively (Schaefer et al., 2009). While we recognize that moraine stabilization is not necessarily an instantaneous process, the minimal scatter of moraine ages therefore suggests that post-depositional reworking has not been an important factor on most of the dated moraines, giving us confidence that our record is an accurate record of glacier fluctuations at the centennial scale.

Single-glacier records suffer from the doubt that they may experience undue influence from microclimatic effects or even internal dynamics, complicating climatic interpretations of glacier advances. To test the representativity of our record, we compare our chronology to those of two outlet glaciers of the SPI, the Upsala glacier (Herminita and Pearson moraines) and the Frías glacier (Figs. 1a and 51°S). These constitute the most thorough records of directly-dated glacier fluctuations since late-glacial time in the region (Strelin et al., 2014; Kaplan et al., 2016). These records from Lago Argentino show glacier expansions during the ACR and at 6100 ± 390, 4450 ± 220, 2300-2000, 1400 ± 110, 600-500, 360 ± 30, and 240 ± 20 yr BP (Fig. 2b). Moreover, less well-dated positions are at ~5500 and 2300-2000 yr BP (Strelin et al., 2014).

Our records overlap during the ACR (Kaplan et al., 2011) and at 6100, 4500, and 600-500 yr BP. We argue the pre-6000 yr BP events not preserved at Lago Argentino reflect climatic events within a generalized warm period on a scale too brief for the much larger SPI to respond and leave a preserved moraine record (Jóhannesson et al., 1989). Within dating uncertainties, early Holocene glaciers at Lago Argentino remained close to the 20th century limits during this time period (Strelin et al., 2014), suggesting any activity would

Table 2
Moraine ages from this study from Table 1 compared with previous age constraints.

Landform	Age (this study)	Age (previously reported)	Type of measurement	Reference
	yr BP	yr BP (2016)		
M0	17,100 ± 860	–	–	–
M1	13,520 ± 540	>535	Lichenometry	Garibotti and Villalba (2009)
M2	9730 ± 420	>273	Lichenometry	Garibotti and Villalba (2009)
M3	6,860 ± 220	>392	Tree ring surface exposure	Masiokas et al. (2009)
		>800 ± 85 (^{14}C yr BP)	Age of inboard basal peat	Mercer (1965)
M4a	6,080 ± 310	–	–	–
M4b	4,500 ± 160	>360	Tree ring surface exposure	Masiokas et al. (2009)
		~320	Tree ring surface exposure	Mercer (1965)
M7	520 ± 60	>175	Lichenometry	Garibotti and Villalba (2009)

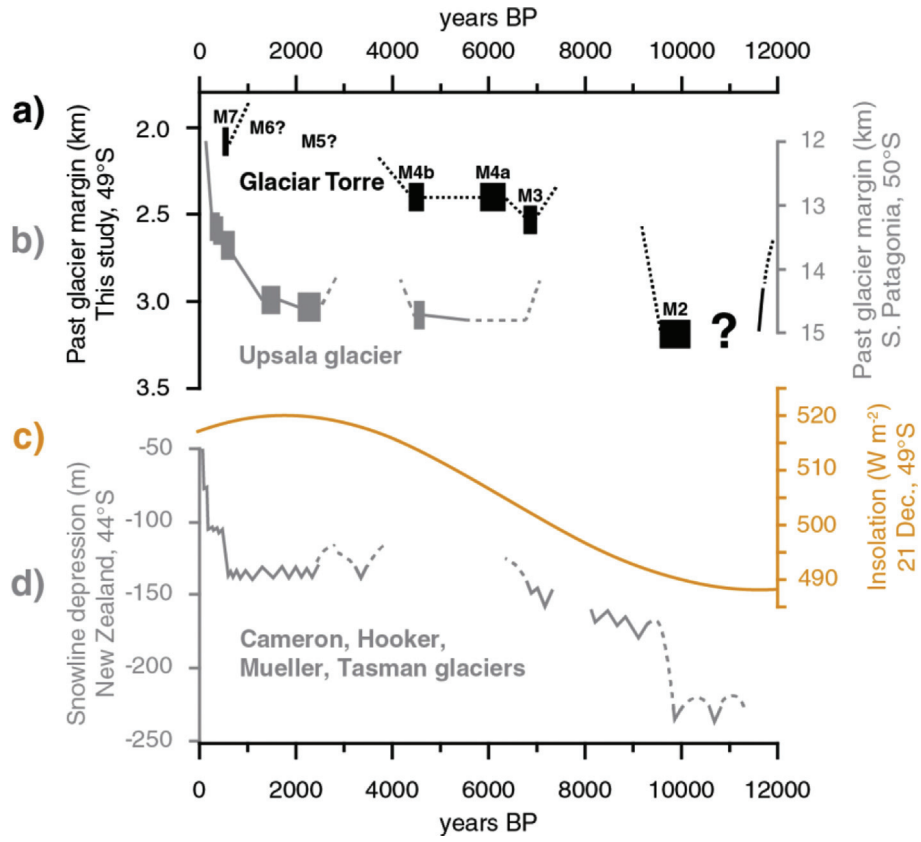

Fig. 2. a) Time-distance diagram of Glaciar Torre moraines. Boxes are mean moraine ages with ±1-sigma uncertainty. Lines indicate inferred glacier behavior; question marks indicate inferred times at which a moraine is found a certain distance from the ice margin. b) Time-distance diagram of Upsala glacier (Kaplan et al., 2016), based on chronologies from Peninsula Herminita and Lago Pearson. c) Summer insolation intensity at 49°S (Laskar et al., 2004). d) Composite snowline depression from the South Island of New Zealand (Putnam et al., 2012). Solid lines correspond to dated glacier advances; dashed lines correspond to inferred glacier retreat.

have been erased by subsequent extensive mid-Holocene glaciers. Glacier advances between 2300-2000 and 1450-1100 yr BP, recorded at Lago Argentino, correspond morphostratigraphically with our M5 and M6 moraines, which were unsuitable for dating. Given the observed parallels between our glacier chronologies, we suggest both glacier systems responded to similar external forcings, rather than internal variability. We merge both chronologies using these advances as tie points to yield a composite Holocene glacier chronology for southern Patagonia. Together, these observations reveal a regional pattern of steadily-declining glacier expansions throughout the Holocene (Fig. 2).

5.2. Insolation as "modulator" of Holocene glaciers

Our composite glacier chronology from southern Patagonia (Fig. 2a and b) mirrors the pattern of progressively less-extensive Holocene glacier advances in New Zealand (Fig. 2d), although the timing of discrete advances differs. We first address the zonally-uniform trend of declining Holocene glacier extent in the southern mid-latitudes, a pattern different to that of the northern mid-latitudes. Summer insolation intensity increases (decreases) from the early to the late Holocene in the Southern (Northern) Hemisphere (Laskar et al., 2004) (Fig. 2c), suggesting that this factor played a key role in modulating global glacier extent during this period. As local summer insolation intensity relates inversely to summer duration (Huybers and Denton, 2008), the former likely is more influential in constraining mid-latitude glacier extent during the latest interglacial.

While parallel trends of insolation and glacier extent could be due to a direct, glacier-specific effect of secular insolation change on glacier mass balance, indirect effects cannot be ruled out. Mid-Holocene glacier reconstructions from Patagonia and New Zealand suggest glaciers in both zones responded to depressed temperatures forced by lower summer insolation (Bravo et al., 2015; Rojas and Moreno, 2011). Modelled cool mid-Holocene conditions in both Patagonia (Wagner et al., 2007) and New Zealand (Ackerley et al., 2013) have been attributed to insolation-modulated changes on the zonal westerlies, meridional temperature gradients, and local land surface temperature. An insolation-modulated migration of the Intertropical Convergence Zone has also been proposed to explain the trend of declining Southern Hemisphere glacier extent during the Holocene (Putnam et al., 2012).

5.3. The SAM as "pacemaker" of Patagonian climate

Progressive change in summer insolation intensity cannot by itself produce the observed repeated glacier advances in Patagonia—a forcing that provides periodic "kicks" to the climate system is necessary. Although the overlap between our record and those at Lago Argentino suggest regionally impactful changes in climate occurred periodically throughout the Holocene, it has been proposed that such variations could be due to effectively random climate excursions on a scale not exceeding that observed on the decadal timeframe (Roe and O'Neal, 2009). As a test of whether our observed glacier variability is observed in other terrestrial paleoclimate proxies, we refer to a recent palynological study of lake sediments from Lago Cipreses, located ~220 km south from Glaciar Torre (Fig. 1a). Here, Moreno et al. (2018) identified warm/dry

secular events with an average duration of 200 ± 60 years since 11,000 yr BP, which alternated with cold/wet phases lasting on average 500 ± 200 years. These phases are tentatively connected to long-term trends in the SAM, the variability of which would also have direct effects on Patagonian glaciers. Modern variability of the SAM drives anomalies in temperature and the SWW during the summer months throughout Patagonia, with positive (negative) SAM indices correlated to higher (lower) summer temperatures (Garreaud et al., 2009) and a corresponding redistribution of precipitation across the orographic divide (Garreaud et al., 2013).

Comparison of our ensemble chronology with the Lago Cipreses non-arboreal pollen (NAP) record (Fig. 3), a proxy for climate-induced intervals of forest canopy opening and closure, suggests that Patagonian glaciers reached their maxima during centennial- to millennial-scale SAM-negative-like phases. Conversely, prolonged SAM-positive-like phases—the Extended Warm Dry Anomaly (EWDA, 9500-7500 yr BP) and the Late Holocene Warm Dry Period (LHWDP, 4100-2800 yr BP)—correspond to periods when Patagonian glaciers were less-extensive (Fig. 3). Other dated moraines from the Colonia valley (Nimick et al., 2016) and Río Tranquilo (Sagredo et al., 2016) (Figs. 1a and 3d), as well as the few closely-bracketed ages of glacial sediment from the historical literature (Fig. 3e; Mercer, 1965; Röthlisberger, 1986; Harrison et al., 2012; Strelin et al., 2014), corroborate this pattern.

The correspondence between our composite glacier chronology and paleoecological changes at Lago Cipreses leads us to suggest that Patagonian glacier advances were paced by centennial-scale climate variability—resembling that of the modern SAM—that resulted in warm or cool periods throughout the Holocene. In this scenario, the hypothesized paleo-SAM would have modulated glacier mass balance via its effect on summer temperature, reflecting the modern climatology. Other potential drivers of Patagonian climate include the modes of climate variability in the south Pacific, the El Niño- Southern Oscillation phenomenon (ENSO) and the Interdecadal Pacific Oscillation/Pacific Decadal Oscillation (IPO/PDO). ENSO and the IPO/PDO, however, have not been shown to significantly affect modern interannual variability of precipitation or temperature in central and southern Patagonia (Garreaud et al., 2009), although a centennial-scale relationship between ENSO and SAM may exist over the Holocene (Moy et al., 2002; Yuan et al., 2018; Moreno et al., 2018). This differs from the New Zealand case, where ENSO and the IPO/PDO currently exert a strong influence in the southwestern Pacific climate (Salinger and Mullan, 1999). Meridional shifts of warm anomalies related to the central and eastern modes of ENSO (Carré et al., 2014) may account for differences in the timing of Holocene glacier advances between Patagonia and New Zealand (Fig. 2).

Our results suggest that Patagonian glaciers responded to two mechanisms during the Holocene: a global, insolation-driven "modulator" governing the magnitude of a glacier response; and a regional, SAM-like "pacemaker" that determines the timing of glacier change. Within this context, summer insolation intensity plays an important role in regulating ice extent in both hemispheres' midlatitudes under interglacial conditions. Future work is

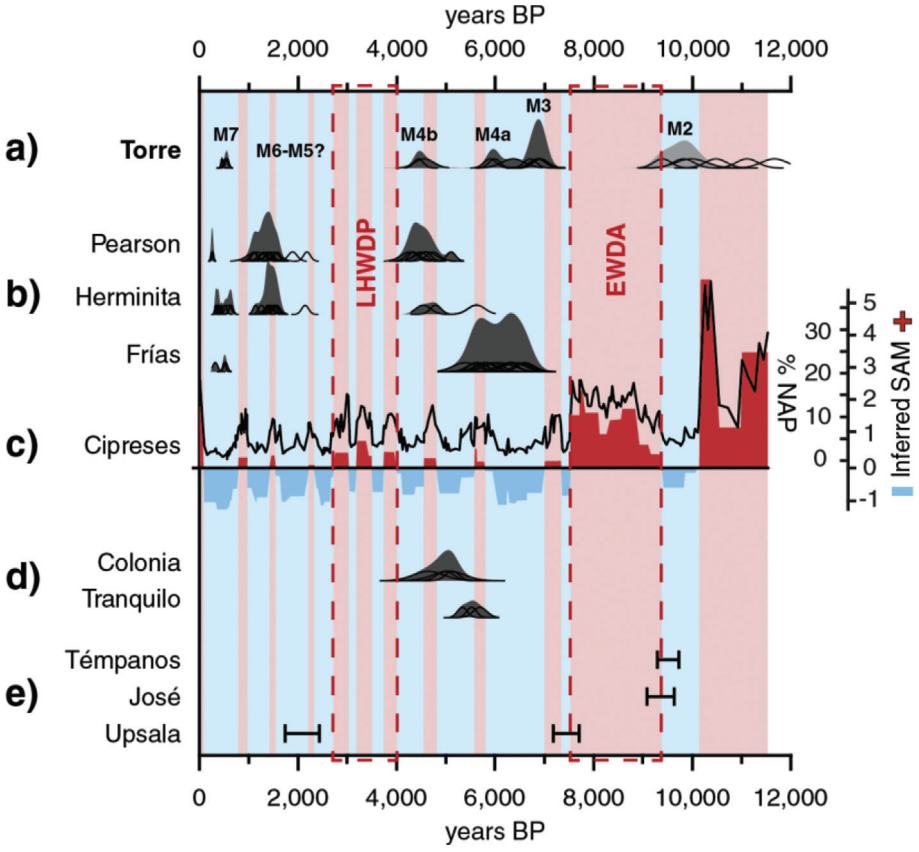

Fig. 3. Southern Patagonian paleoglacier records for a) Glaciar Torre and b) Lago Argentino (Strelin et al., 2014; Kaplan et al., 2016). ^{10}Be ages are presented as normalized standard probability distributions (black curves); cumulative weighted average moraine ages are represented by shaded curves. Shading represents inferred SAM (red = positive; blue = negative) from c) the Lago Cipreses (Moreno et al., 2018) non-arboreal pollen (NAP) record (black line) and regime shift detection z-scores (colored polygons). LHWDP = Late Holocene Warm Dry Period; EWDA = Early Warm Dry Anomaly. d) Other published ^{10}Be moraine ages in southern Patagonia: Colonia (Nimick et al., 2016) and Río Tranquilo (Sagredo et al., 2016). e) All close bracketing ages of glacial deposits from Patagonia: Témpanos (OSL) (Harrison et al., 2012), José (^{14}C) (Röthlisberger, 1986), and Upsala (^{14}C) (Mercer, 1965; Strelin et al., 2014). (For interpretation of the references to color in this figure legend, the reader is referred to the Web version of this article.)

needed to determine the specific avenue through which insolation could have affected glaciers.

The modern trend towards high-index SAM conditions in austral summer has been explained as a consequence of greenhouse gas forcing and stratospheric ozone depletion; future implementation of the Montreal Protocol is postulated to inhibit this positive trend (Thompson et al., 2011). We note, however, that our record suggests the observed trend may be superimposed upon a larger shift in baseline climate (Zhang et al., 2014). The present effects of positive SAM on the southern midlatitudes—the southward shift and intensification of the westerlies, summer warming, and precipitation redistribution (Gillett et al., 2006)—may therefore represent the new normal climate that may persist for hundreds of years, independent of future changes in anthropogenic forcings.

Acknowledgements

This project was supported by the Núcleo Milenio Paleoclima of the Iniciativa Científica Milenio of the Ministerio de Economía, Fomento y Turismo (Chile), FONDECYT 1160488, FONDECYT 1171773, FONDECYT 1180717, FONDAP-CONICYT 15110009, NSF-EAR 09-02363, and NSF-EAR 18–04816. S.A.R. is a recipient of a CONICYT-PCHA Beca de Doctorado Nacional (2015). We thank the Administración de Parques Nacionales and Parque Nacional Los Glaciares (Argentina) for their support. We additionally thank J. Hanley and J. Frisch for laboratory support; and P. Talbot, M. Calabrese, D. Tetzner, C. Sullivan, and G. Sullivan for scientific and logistical support in the field. This is LDEO contribution # 8326.

Appendix A. Supplementary data

Supplementary data to this article can be found online at https://doi.org/10.1016/j.quascirev.2019.05.029.

References

Abram, N.J., Mulvaney, R., Vimeux, F., Phipps, S.J., Turner, J., England, M.H., 2014. Evolution of the southern annular mode during the past millennium. Nat. Clim. Change 4, 564.

Ackerley, D., Lorrey, A., Renwick, J., Phipps, S.J., Wagner, S., Fowler, A., 2013. High-resolution modelling of mid-Holocene New Zealand climate at 6000 yr BP. Holocene 23, 1272–1285. https://doi.org/10.1177/0959683613484612.

Aniya, M., 2013. Holocene glaciations of Hielo Patagónico (Patagonia Icefield), south America: a brief review. Geochem. J. https://doi.org/10.2343/geochemj.1.0171.

Aniya, M., Sato, H., 1995. Holocene glacial chronology of Upsala glacier at Peninsula Herminita, southern Patagonia Icefield. Bull. Glacier Res. 13, 83–96.

Auer, V., 1956. The Pleistocene of Fuego-Patagonia. Part I: the Ice and Interglacial Ages, Series AII. Annales Academia Scientarium Fennicae, Helsinki.

Balco, G., Stone, J.O., Lifton, N.A., Dunai, T.J., 2008. A complete and easily accessible means of calculating surface exposure ages or erosion rates from 10Be and 26Al measurements. Quat. Geochronol. 3, 174–195. https://doi.org/10.1016/J.QUAGEO.2007.12.001.

Bravo, C., Rojas, M., Anderson, B.M., Mackintosh, A.N., Sagredo, E., Moreno, P.I., 2015. Modelled glacier equilibrium line altitudes during the mid-Holocene in the southern mid-latitudes. Clim. Past 11, 1575–1586. https://doi.org/10.5194/cp-11-1575-2015.

Carlson, A.E., Winsor, K., Ullman, D.J., Brook, E.J., Rood, D.H., Axford, Y., LeGrande, A.N., Anslow, F.S., Sinclair, G., 2014. Earliest Holocene south Greenland ice sheet retreat within its late Holocene extent. Geophys. Res. Lett. 41, 5514–5521. https://doi.org/10.1002/2014GL060800.

Carrasco, J.F., Casassa, G., Rivera, A., 2002. Meteorological and Climatological Aspects of the Southern Patagonia Icefield. In: Casassa, G., Sepúlveda, F.V., Sinclair, R.M. (Eds.), The Patagonian Icefields: A Unique Natural Laboratory for Environmental and Climate Change Studies. Springer, Boston, MA, pp. 29–41. https://doi.org/10.1007/978-1-4615-0645-4_4.

Carré, M., Sachs, J.P., Purca, S., Schauer, A.J., Braconnot, P., Falcón, R.A., Julien, M., Lavallée, D., 2014. Holocene history of ENSO variance and asymmetry in the eastern tropical Pacific. Science (80-.) 345, 1045 LP – 1048.

Clapperton, C.M., Sugden, D.E., 1988. Holocene glacier fluctuations in South America and Antarctica. Quat. Sci. Rev. 7, 185–198. https://doi.org/10.1016/0277-3791(88)90005-4.

Denton, G.H., Karlén, W., 1973. Holocene climatic variations-Their pattern and possible cause. Quat. Res. 3, 155–205. https://doi.org/10.1016/0033-5894(73)90040-9.

García, J.L., Kaplan, M.R., Hall, B.L., Schaefer, J.M., Vega, R.M., Schwartz, R., Finkel, R., 2012. Glacier expansion in southern Patagonia throughout the Antarctic cold reversal. Geology 40, 859–862.

Garibotti, I.A., Villalba, R., 2009. Lichenometric dating using Rhizocarpon subgenus Rhizocarpon in the Patagonian Andes, Argentina. Quat. Res. 71, 271–283. https://doi.org/10.1016/J.YQRES.2009.01.012.

Garreaud, R.D., Vuille, M., Compagnucci, R., Marengo, J., 2009. Present-day south American climate. Palaeogeogr. Palaeoclimatol. Palaeoecol. 281, 180–195. https://doi.org/10.1016/j.palaeo.2007.10.032.

Garreaud, R., Lopez, P., Minvielle, M., Rojas, M., 2013. Large-scale control on the Patagonian climate. J. Clim. 26, 215–230. https://doi.org/10.1175/JCLI-D-12-00001.1.

Gillett, N.P., Kell, T.D., Jones, P.D., 2006. Regional climate impacts of the southern annular mode. Geophys. Res. Lett. 33. https://doi.org/10.1029/2006GL027721.

Glasser, N.F., Harrison, S., Winchester, V., Aniya, M., 2004. Late Pleistocene and holocene palaeoclimate and glacier fluctuations in Patagonia. Glob. Planet. Chang. 43, 79–101. https://doi.org/10.1016/J.GLOPLACHA.2004.03.002.

Grubbs, F.E., 1969. Procedures for detecting outlying observations in samples. Technometrics 11, 1–21. https://doi.org/10.1080/00401706.1969.10490657.

Harrison, S., Glasser, N.F., Duller, G.A.T., Jansson, K.N., 2012. Early and mid-holocene age for the tempanos moraines, Laguna san Rafael, Patagonian Chile. Quat. Sci. Rev. 31, 82–92. https://doi.org/10.1016/J.QUASCIREV.2011.10.015.

Heim, A., 1951. Informe sobre un estudio glaciológico en el Parque Nacional Los Glaciares. Anales de Parques Nacionales, Buenos Aires.

Hogg, A.G., Hua, Q., Blackwell, P.G., Niu, M., Buck, C.E., Guilderson, T.P., Heaton, T.J., Palmer, J.G., Reimer, P.J., Reimer, R.W., Turney, C.S.M., Zimmerman, S.R.H., 2013. SHCal13 southern hemisphere calibration, 0–50,000 Years cal BP. Radiocarbon 55, 1889–1903. https://doi.org/10.2458/azu_js_rc.55.16783.

Huybers, P., Denton, G., 2008. Antarctic temperature at orbital timescales controlled by local summer duration. Nat. Geosci. 1, 787.

Ivy-Ochs, S., Kerschner, H., Maisch, M., Christl, M., Kubik, P.W., Schlüchter, C., 2009. Latest Pleistocene and Holocene glacier variations in the European Alps. Quat. Sci. Rev. 28, 2137–2149. https://doi.org/10.1016/j.quascirev.2009.03.009.

Jóhannesson, T., Raymond, C.F., Waddington, E.D., 1989. A Simple Method for Determining the Response Time of Glaciers. Springer, Dordrecht, pp. 343–352. https://doi.org/10.1007/978-94-015-7823-3_22.

Jones, J.M., Gille, S.T., Goosse, H., Abram, N.J., Canziani, P.O., Charman, D.J., Clem, K.R., Crosta, X., de Lavergne, C., Eisenman, I., England, M.H., Fogt, R.L., Frankcombe, L.M., Marshall, G.J., Masson-Delmotte, V., Morrison, A.K., Orsi, A.J., Raphael, M.N., Renwick, J.A., Schneider, D.P., Simpkins, G.R., Steig, E.J., Stenni, B., Swingedouw, D., Vance, T.R., 2016. Assessing recent trends in high-latitude Southern Hemisphere surface climate. Nat. Clim. Change 6, 917.

Kaplan, M.R., Strelin, J.A., Schaefer, J.M., Denton, G.H., Finkel, R.C., Schwartz, R., Putnam, A.E., Vandergoes, M.J., Goehring, B.M., Travis, S.G., 2011. In-situ cosmogenic 10Be production rate at Lago Argentino, Patagonia: implications for late-glacial climate chronology. Earth Planet. Sci. Lett. 309, 21–32. https://doi.org/10.1016/J.EPSL.2011.06.018.

Kaplan, M.R., Schaefer, J.M., Denton, G.H., Doughty, A.M., Barrell, D.J.A., Chinn, T.J.H., Putnam, A.E., Andersen, B.G., Mackintosh, A., Finkel, R.C., Schwartz, R., Anderson, B., 2013. The anatomy of long-term warming since 15 ka in New Zealand based on net glacier snowline rise. Geology 41, 887–890.

Kaplan, M.R., Schaefer, J.M., Strelin, J.A., Denton, G.H., Anderson, R.F., Vandergoes, M.J., Finkel, R.C., Schwartz, R., Travis, S.G., Garcia, J.L., Martini, M.A., Nielsen, S.H.H., 2016. Patagonian and southern South Atlantic view of holocene climate. Quat. Sci. Rev. 141, 112–125. https://doi.org/10.1016/j.quascirev.2016.03.014.

Kaufman, D., Ager, T., Anderson, N., Anderson, P., Andrews, J., Bartlein, P., Brubaker, L., Coats, L., Cwynar, L., Duvall, M., Dyke, A., Edwards, M., Eisner, W., Gajewski, K., Geirsdóttir, A., Hu, F., Jennings, A., Kaplan, M., Kerwin, M., Lozhkin, A., MacDonald, G., Miller, G., Mock, C., Oswald, W., Otto-Bliesner, B., Porinchu, D., Rühland, K., Smol, J., Steig, E., Wolfe, B., 2004. Holocene thermal maximum in the western Arctic (0–180°W). Quat. Sci. Rev. 23, 529–560. https://doi.org/10.1016/J.QUASCIREV.2003.09.007.

Laskar, J., Robutel, P., Joutel, F., Gastineau, M., Correia, A.C.M., Levrard, B., 2004. A long-term numerical solution for the insolation quantities of the Earth. A&A 428, 261–285.

Lawrence, D.B., Lawrence, E.G., 1959. Recent Glacier Variations in Southern South America. American Geographical Society Technical Report.

Lifton, N., Smart, D.F., Shea, M.A., 2008. Scaling time-integrated in situ cosmogenic nuclide production rates using a continuous geomagnetic model. Earth Planet. Sci. Lett. 268, 190–201. https://doi.org/10.1016/J.EPSL.2008.01.021.

Lliboutry, L., 1953. Snow and ice in the Monte Fitz Roy region (Patagonia). J. Glaciol. 2, 255–261. https://doi.org/10.3189/S0022143000025430.

Mackintosh, A.N., Anderson, B.M., Pierrehumbert, R.T., 2017. Reconstructing climate from glaciers. Annu. Rev. Earth Planet Sci. 45, 649–680. https://doi.org/10.1146/annurev-earth-063016-020643.

Masiokas, M.H., Luckman, B.H., Delgado, S., Skvarca, P., Ripalta, A., 2009. Little Ice Age fluctuations of small glaciers in the Monte Fitz Roy and Lago del Desierto areas, south Patagonian Andes, Argentina. Palaeogeogr. Palaeoclimatol. Palaeoecol. 281, 351–362. https://doi.org/10.1016/J.PALAEO.2007.10.031.

Mercer, J.H., 1965. Glacier variations in southern Patagonia. Geogr. Rev. 55, 390–413. https://doi.org/10.2307/213136.

Mercer, J.H., 1976. Glacial history of southernmost South America. Quat. Res. 6,

125–166. https://doi.org/10.1016/0033-5894(76)90047-8.
Mercer, J.H., 1982. Holocene Glacier Variations in Southern South America (Striae).
Miller, A., 1976. The climate of Chile. In: Schwerdtfeger, W. (Ed.), World Survey of Climatology. Elsevier, Amsterdam, pp. 113–130.
Moreno, P.I., Vilanova, I., Villa-Martínez, R., Dunbar, R.B., Mucciarone, D.A., Kaplan, M.R., Garreaud, R.D., Rojas, M., Moy, C.M., De Pol-Holz, R., Lambert, F., 2018. Onset and Evolution of southern annular mode-like changes at centennial timescale. Sci. Rep. 8, 3458. https://doi.org/10.1038/s41598-018-21836-6.
Moy, C.M., Seltzer, G.O., Rodbell, D.T., Anderson, D.M., 2002. Variability of El Niño/southern oscillation activity at millennial timescales during the holocene epoch. Nature 420, 162.
Nesje, A., 2009. Latest Pleistocene and holocene alpine glacier fluctuations in Scandinavia. Quat. Sci. Rev. 28, 2119–2136. https://doi.org/10.1016/j.quascirev.2008.12.016.
Nimick, D.A., McGrath, D., Mahan, S.A., Friesen, B.A., Leidich, J., 2016. Latest Pleistocene and holocene glacial events in the Colonia Valley, northern Patagonia Icefield, southern Chile. J. Quat. Sci. 31, 551–564. https://doi.org/10.1002/jqs.2847.
Olson, D.M., Dinerstein, E., Wikramanayake, E.D., Burgess, N.D., Powell, G.V.N., Underwood, E.C., D'amico, J.A., Itoua, I., Strand, H.E., Morrison, J.C., Loucks, C.J., Allnutt, T.F., Ricketts, T.H., Kura, Y., Lamoreux, J.F., Wettengel, W.W., Hedao, P., Kassem, K.R., 2001. Terrestrial Ecoregions of the World: a New Map of Life on EarthA new global map of terrestrial ecoregions provides an innovative tool for conserving biodiversity. Bioscience 51, 933–938. https://doi.org/10.1641/0006-3568(2001)051[0933:teotwa]2.0.co;2.
Porter, S.C., Denton, G.H., 1967. Chronology of neoglaciation in the north American Cordillera. Am. J. Sci. 265, 177–210. https://doi.org/10.2475/ajs.265.3.177.
Porter, S.C., 2000. Onset of neoglaciation in the southern hemisphere. J. Quat. Sci. 15, 395–408. https://doi.org/10.1002/1099-1417(200005)15:4%3c395::AID-JQS535%3e3.0.CO;2-H.
Putnam, A.E., Schaefer, J.M., Denton, G.H., Barrell, D.J.A., Finkel, R.C., Andersen, B.G., Schwartz, R., Chinn, T.J.H., Doughty, A.M., 2012. Regional climate control of glaciers in New Zealand and Europe during the pre-industrial Holocene. Nat. Geosci. 5, 627.
Rasmussen, L.A., Conway, H., Raymond, C.F., 2007. Influence of upper air conditions on the Patagonia icefields. Glob. Planet. Chang. 59, 203–216. https://doi.org/10.1016/J.GLOPLACHA.2006.11.025.
Rignot, E., Rivera, A., Casassa, G., 2003. Contribution of the Patagonia icefields of south America to Sea level rise. Science (80-.) 302, 434 LP – 437. https://doi.org/10.1126/science.1087393.
Rivera, A., Casassa, G., 2004. Ice Elevation, Areal, and Frontal Changes of Glaciers from National Park Torres del Paine, Southern Patagonia Icefield. Arctic. Antarct. Alp. Res. 36, 379–389. https://doi.org/10.1657/1523-0430(2004)036[0379:IEAAFC]2.0.CO;2.
Roe, G.H., O'Neal, M.A., 2009. The response of glaciers to intrinsic climate variability: observations and models of late-Holocene variations in the Pacific Northwest. J. Glaciol. 55, 839–854. https://doi.org/10.3189/002214309790152438.
Rojas, M., Moreno, P.I., 2011. Atmospheric circulation changes and neoglacial conditions in the Southern Hemisphere mid-latitudes: insights from PMIP2 simulations at 6 kyr. Clim. Dyn. 37, 357–375. https://doi.org/10.1007/s00382-010-0866-3.
Röthlisberger, F., 1986. 1000 Jahre Gletschergeschichte der Erde. Verlag Sauerlander, Salzburg.
Sagredo, E.A., Lowell, T.V., Kelly, M.A., Rupper, S., Aravena, J.C., Ward, D.J., Malone, A.G.O., 2016. Equilibrium line altitudes along the Andes during the Last millennium: Paleoclimatic implications. Holocene 27, 1019–1033. https://doi.org/10.1177/0959683616678458.
Sagredo, E.A., Kaplan, M.R., Araya, P.S., Lowell, T.V., Aravena, J.C., Moreno, P.I., Kelly, M.A., Schaefer, J.M., 2018. Trans-pacific glacial response to the Antarctic Cold Reversal in the southern mid-latitudes. Quat. Sci. Rev. 188, 160–166. https://doi.org/10.1016/J.QUASCIREV.2018.01.011.
Sagredo, E.A., Rupper, S., Lowell, T.V., 2014. Sensitivities of the equilibrium line altitude to temperature and precipitation changes along the Andes. Quat. Res. 81, 355–366. https://doi.org/10.1016/j.yqres.2014.01.008.
Salinger, M.J., Mullan, A.B., 1999. New Zealand climate: temperature and precipitation variations and their links with atmospheric circulation 1930–1994. Int. J. Climatol. 19, 1049–1071. https://doi.org/10.1002/(SICI)1097-0088(199908)19:10%3c1049::AID-JOC417%3e3.0.CO;2-Z.
Schaefer, J.M., Denton, G.H., Kaplan, M., Putnam, A., Finkel, R.C., Barrell, D.J.A., Andersen, B.G., Schwartz, R., Mackintosh, A., Chinn, T., Schlüchter, C., 2009. High-frequency holocene glacier fluctuations in New Zealand differ from the northern signature. Science 84.) 324, 622–625. https://doi.org/10.1126/science.1169312.
Schaefer, M., Machguth, H., Falvey, M., Casassa, G., Rignot, E., 2015. Quantifying mass balance processes on the southern Patagonia Icefield. Cryosph 9, 25–35. https://doi.org/10.5194/tc-9-25-2015.
Schimmelpfennig, I., Schaefer, J.M., Akçar, N., Ivy-Ochs, S., Finkel, R.C., Schlüchter, C., 2012. Holocene glacier culminations in the Western Alps and their hemispheric relevance. Geology 40, 891–894.
Solomina, O.N., Bradley, R.S., Hodgson, D.A., Ivy-Ochs, S., Jomelli, V., Mackintosh, A.N., Nesje, A., Owen, L.A., Wanner, H., Wiles, G.C., Young, N.E., 2015. Holocene glacier fluctuations. Quat. Sci. Rev. https://doi.org/10.1016/j.quascirev.2014.11.018.
Strelin, J.A., Denton, G.H., Vandergoes, M.J., Ninnemann, U.S., Putnam, A.E., 2011. Radiocarbon chronology of the late-glacial Puerto Bandera moraines, southern Patagonian Icefield, Argentina. Quat. Sci. Rev. 30, 2551–2569. https://doi.org/10.1016/J.QUASCIREV.2011.05.004.
Strelin, J.A., Kaplan, M.R., Vandergoes, M.J., Denton, G.H., Schaefer, J.M., 2014. Holocene glacier history of the Lago Argentino basin, southern Patagonian Icefield. Quat. Sci. Rev. 101, 124–145. https://doi.org/10.1016/j.quascirev.2014.06.026.
Stuiver, M., Reimer, P.J., 2018. CALIB.
Thompson, D.W.J., Solomon, S., Kushner, P.J., England, M.H., Grise, K.M., Karoly, D.J., 2011. Signatures of the Antarctic ozone hole in Southern Hemisphere surface climate change. Nat. Geosci. 4, 741.
Villalba, R., Lara, A., Boninsegna, J.A., Masiokas, M., Delgado, S., Aravena, J.C., Roig, F.A., Schmelter, A., Wolodarsky, A., Ripalta, A., 2003. Large-scale temperature changes across the southern Andes: 20th-century variations in the context of the past 400 years. Clim. Change 59, 177–232. https://doi.org/10.1023/A:1024452701153.
Villalba, R., Lara, A., Masiokas, M.H., Urrutia, R., Luckman, B.H., Marshall, G.J., Mundo, I.A., Christie, D.A., Cook, E.R., Neukom, R., Allen, K., Fenwick, P., Boninsegna, J.A., Srur, A.M., Morales, M.S., Araneo, D., Palmer, J.G., Cuq, E., Aravena, J.C., Holz, A., LeQuesne, C., 2012. Unusual southern hemisphere tree growth patterns induced by changes in the southern annular mode. Nat. Geosci. 5, 793.
Wagner, S., Widmann, M., Jones, J., Haberzettl, T., Lücke, A., Mayr, C., Ohlendorf, C., Schäbitz, F., Zolitschka, B., 2007. Transient simulations, empirical reconstructions and forcing mechanisms for the Mid-holocene hydrological climate in southern Patagonia. Clim. Dyn. 29, 333–355. https://doi.org/10.1007/s00382-007-0229-x.
Yuan, X., Kaplan, M.R., Cane, M.A., 2018. The interconnected global climate system-a review of tropical-polar teleconnections. J. Clim. 31, 5765–5792. https://doi.org/10.1175/JCLI-D-16-0637.1.
Zhang, Z., Gong, D., Kim, S., Mao, R., Yang, J., 2014. Is the Antarctic oscillation trend during the recent decades unusual? Antarct. Sci. 26, 445–451. https://doi.org/10.1017/S0954102013000734.

3.3 Conclusions

Glaciar Torre repeatedly expanded at c. 17.1 ka, 13.5 ka, 9.4 ka, 6.8 ka, 6.1 ka, 4.5 ka, and 0.5 ka. While the advances at 17.1 ka and 13.5 ka reflect climate changes recognized across Patagonia at these times, directly dating the early Holocene glacier maximum as presented here—as well as the 6.8 ka advance—is without precedent in the paleoglacier literature of the area. The progressively less-extensive nature of these advances is striking, and while this pattern parallels that of glaciers in New Zealand, it opposes the general trend of Northern Hemisphere glaciers.

A two-component control over Glaciar Torre in the Holocene is presented. The increasing trend of summer insolation intensity throughout the epoch is proposed as the control over trends in glacier extent. The timing of glacier advances as well as their absence are explained as a consequence of centennial-scale cold/wet and warm/dry phases, respectively. Moreno et al (2018) inferred these correspond with "Southern Annular Mode-like" variability throughout the Holocene, in which cold/wet (warm/dry) phases associated with negative (positive) SAM-like conditions. This study suggests this climate variability is additionally responsible for Patagonian glacier advance and retreat throughout the Holocene.

* * *

Chapter 4 – Deglacial history of the Cordillera Darwin

4.1 Introduction

This chapter includes a manuscript in preparation detailing a paleoglacier chronology constructed for this thesis from the Cordillera Darwin, Tierra del Fuego (54.5°S). In this article, a combination of 10Be surface exposure dating, radiocarbon minimum-age dating, and dendroglaciology is used to constrain glacier fluctuations of the Dalla Vedova glacier (54.65°S / 69.15°W). The chapter concludes with a summary of the results and paleoclimatic significance of the glacial record at Dalla Vedova.

4.2 Glacier advance during the Medieval Climate Anomaly in the Cordillera Darwin, southernmost South America (55°S) (manuscript in preparation)

Glacier advance during the Medieval Climate Anomaly in the Cordillera Darwin, southernmost South America (55°S)

Scott A. Reynhout[1,2], Esteban A. Sagredo[2,3], Juan Carlos Aravena[4], Rodrigo Soteres[2,3], Michael R. Kaplan[5], and Joerg M. Schaefer[5,6]

[1]Departamento de Geología, Facultad de Ciencias Físicas y Matemáticas, Universidad de Chile, Plaza Ercilla 803, 8370450 Santiago, Chile

[2]Núcleo Milenio Paleoclima, Universidad de Chile, Las Palmeras 3425, Ñuñoa, Chile

[3]Instituto de Geografía, Pontificia Universidad Católica de Chile, Avenida Vicuña Mackenna 4860, 7820436 Macul, Chile

[4]Centro de Investigación Antártica, Universidad de Magallanes, Avenida Bulnes 01890 6213029, Punta Arenas, Chile

[5]Lamont-Doherty Earth Observatory, P.O. Box 1000, 61 Route 9W, Palisades, NY 10964-100, United States of America

[6]Department of Earth and Environmental Sciences of Columbia University, New York, NY, 10027, USA

4.2.1 Introduction

The Southern Westerly Winds (SWW) currently dominate the climate of southernmost South America between (42°-56°S; hereafter Patagonia), with their variability reflected in zonal and meridional variations in temperature and precipitation (Garreaud et al., 2013). As such, reconstructions of past climate in the region frequently invoke changes in the strength, width, or latitudinal position of the strongest SWW to explain local climate variability (Lamy et al., 2010; Villa-Martínez et al., 2012; Boex et al., 2013, Van Daele et al., 2016; Sagredo et al., 2018). Additionally, SWW behavior has been proposed as a driver of global climate by modulating Southern Ocean upwelling and the degassing of CO_2 from Antarctic bottom water (Anderson et al., 2009; Fletcher and Moreno, 2011). Defining the preindustrial variability of the SWW is therefore of vital importance to understanding future impacts of the SWW on both regional and global climate.

Over the last several decades, a poleward shift of the "core" of the SWW has asymmetrically affected Patagonia. South of ~50°S, westerly circulation has increased over the last several decades, resulting in wetter conditions on the western margin of the continent; north of this limit, weaker westerlies result in drier conditions (Aravena and Luckman, 2009; Carrasco et al., 2008; Garreaud et al., 2013). This trend towards more intense westerly circulation over southwestern Patagonia is primarily driven by persistently-positive phases of the Southern Annular Mode/Antarctic Oscillation (SAM; Thompson et al., 2011), which has been suggested to have varied at the centennial scale over the Holocene (Villalba et al., 2012; Abram et al., 2014; Dätwyler et al., 2018; Moreno et al., 2018).

As the southernmost continental-scale landmass abutting the Southern Ocean, the South American island of Isla Grande de Tierra del Fuego (53°-55°S; hereafter Tierra del Fuego) is uniquely positioned to test the hypothesis of westerly shifts over the Holocene.

Of note are the glaciers mantling the mountainous core of Tierra del Fuego within the Cordillera Darwin, which extended more than 100 km to the north during the Last Glacial Maximum (LGM; Rabassa et al., 2000; McCulloch et al., 2005; Kaplan et al., 2008). Cordillera Darwin glaciers show a general trend of retreat over the last century, albeit with an unusual concentration of glaciers with stationary ice margins (Bown et al., 2014). High-altitude mass gain and glacier advance have occurred at some glaciers in the Cordillera Darwin (Holmlund and Fuenzalida, 1995; Melkonian et al., 2013), the Gran Campo Nevado (53°S; Möller et al., 2007), and the western Southern Patagonian Icefield (SPI) south of 49°S (López et al., 2010; Schaefer et al., 2015). These anomalous trends have been explained as consequences of increased orographic precipitation brought on by enhanced westerly circulation, suggesting that SWW changes play an important role in controlling regional glaciation.

Glaciers are also sensitive to surface air temperature, and it is this factor that is most commonly invoked to explain the observed trend of ice mass loss across Patagonia (Rignot et al. 2003, Rasmussen et al. 2007, Bown et al. 2014). This is in accord with instrumental records showing a long-term warming trend since the beginning of the 20th century (Miller, 1976; Rosenblüth et al., 1997; Villalba et al., 2003; Sagredo and Lowell, 2014), as well as the strong positive correlation between mean annual temperature and the persistently-positive SAM in recent decades (Garreaud et al., 2009; Thompson et al., 2011). However, the lack of trends in the 0°C isotherm at Punta Arenas since the 1970's—in conjunction with slightly increased precipitation—resulted in net lowering of modeled glacier equilibrium-line altitudes (ELAs) over this period (Carrasco et al., 2008). While this tendency fails to explain the prevailing trend of regional glacier recession, it provides a physically-based mechanism that could account for scattered glacier advances throughout the regions.

To summarize:

- The climate of southernmost South America is characterized by a long-term warming trend with a recent southward intensification of the SWW, the latter of which has resulted in increased precipitation over the extreme southwest margin of the continent;
- Intensification of westerly circulation over the Southern Ocean can be explained by persistently-positive phases of the SAM, which also explains at least some regional warming;
- In Tierra del Fuego, at the extreme southern margin of Patagonia, some glaciers exhibit a mass balance response potentially linked to westerly-modulated increases in precipitation, linked to positive tendencies in the SAM;
- If persistent SAM variations over the Holocene function in a similar fashion to the present, then some glaciers in Tierra del Fuego may have advanced (retreated) during inferred periods of positive (negative) SAM.

To test this hypothesis, we investigated the history of past glacier advances of the northeastern Dalla Vedova glacier (54.65°S / 69.15°W). Here, we present a chronology of glacier variations spanning the last glacial termination and Holocene, constructed using terrestrial cosmogenic surface exposure dating, radiocarbon dating, and dendrochronologic surface exposure dating.

4.2.2 Study area

4.2.2.1 Geographic setting

The Dalla Vedova glacier covers ~55 km² at the eastern terminus of the Cordillera Darwin (CD), Tierra del Fuego (Figure 4.1). It is a valley glacier positioned at the end of Bahía Blanca, an arm of Fiordo Parry, a fjord positioned at the far eastern end of Seno Almirantazgo. This glacier forms part of the extensive ice cover mantling the Cordillera Darwin and is bordered by the Stoppani glacier to the east, the Cuevas glacier to the south, and the Nueva Zelandia glacier to the west. It is currently largely land-terminating.

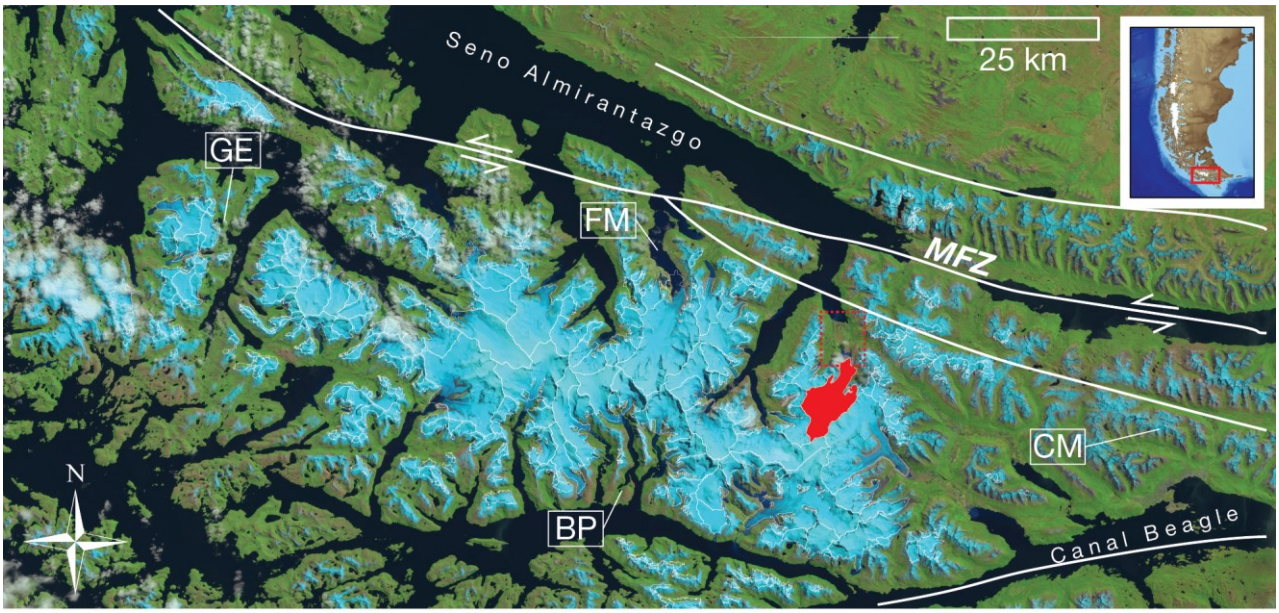

Figure 4.1. Regional context of the study area (see inset for general location). The Dalla Vedova glacier is highlighted in red, while the inset is highlighted by a red box. Major named faults in the region illustrated by thick white lines(Sue and Ghiglione, 2016). Glacier outlines are drawn as narrow white lines adapted from the Randolph Glacier Inventory. Locations mentioned in the text are indicated. BP = Bahía Pía (Kuylenstierna et al. 1996), CM = Cordón Martial (Menounos et al. 2013), FM = Fiordo Marinelli (Boyd et al. 2008), GE = Glaciar Ema (Strelin et al. 2008).

The interior Cordillera Darwin is mantled by over 2,000 km² of ice (Bown et al., 2014). This region is often referred to as the Cordillera Darwin Icefield, although it is perhaps better described as a concentration of adjacent, extensive valley glaciers. Modern equilibrium-line altitudes (ELAs) in the region range from 650-1100 m, increasing to the east (Bown et al., 2014; Strelin and Iturraspe, 2007). These glaciers have undergone generalized retreat since the mid-1950 (Bown et al., 2014), although individual glaciers have experienced highly variable rates of change. For example, the tidewater Marinelli Glacier, 25 km from the study area, has retreated 15 km from its midcentury ice margin (Porter and Santana, 2003), likely due to a combination of accelerated calving flux and unfavorable climate conditions (Koppes and Montgomery, 2009).

The island of Tierra del Fuego is bisected from west to east by the left-lateral Magallanes-Fagnano Fault Zone (MFZ; Figure 4.1), which separates the Scotia plate to

the south from the South American plate to the north. Positioned immediately to the south of the MFZ, the Cordillera Darwin (54°-55°S) forms the mountainous core of Tierra del Fuego. Eocene apatite fission track closure ages for the Cordillera Darwin suggest the high topography of the CD is in part inherited from Paleogene-Neogene uplift events (Nelson, 1982), although raised marine terraces and paleoshorelines indicate localized neotectonic uplift of 15-30m during the Holocene (Bentley and McCulloch, 2005; Bujalesky, 2007). A significant glacial-isostatic component may be influential, as was suggested by previous paleoshoreline analyses (Porter et al., 1984), modelling (Ivins and James, 2004) and GPS measurements in the region (Mendoza et al., 2011).

4.2.2.2 Regional paleoglacier chronologies

Erratic boulders from the Cordillera Darwin have been found associated with Last Glacial Maximum (LGM; 26.5-19 ka; Clark et al., 2009) deposits at Bahía Inútil, >100 km north of the CD, implying the existence of an extensive, conjoined ice sheet at this time that covered much of the region (Figure 1; Darvill et al., 2015; Evenson et al., 2009). Ice retreat at the Last Glacial-Interglacial Transition (LGIT) is thought of as extremely rapid after 17-18 ka (Hall et al., 2013). Glaciers adjacent to the CD advanced during the ACR (García et al., 2012; Menounos et al., 2013); however, the existence of an ACR glacier advance reaching the Strait of Magellan remains contentious (McCulloch et al., 2005a).

Holocene glacier activity in the Cordillera Darwin is preserved solely during the late part of the epoch, although to the east of the CD proper evidence exists for early Holocene advances close to the "Little Ice Age" ice limit ("CM" in Figure 1; Menounos et al., 2013). Kuylenstierna et al. (1996) bracket two late Holocene glacier advances at Bahía Pía ("BP" in Figure 1) to between 1790 and 940 ^{14}C yr BP (1871-1486 and 928-684 cal yr BP; 95% probability) and between 940 and 675 ^{14}C yr BP (928-684 and 683-518 cal yr BP). To the west, at Monte Sarmiento, Strelin et al., (2008) record glacier advances at 1288 ^{14}C yr BP (1297-982 cal yr BP) and from 695 and 379 ^{14}C yr BP (741-506 and 520-155 cal yr BP). Periods of glacier recession are indicated by peat growth on former proglacial lake beds at Bahía Pía between 2605 and 1950 ^{14}C yr BP (2760-2492 and 2035-1620 cal yr BP; Kuylenstierna et al., 1996) and fjord sediments from Seno Almirantazgo between 3200-2500 yr BP and 2000-1100 yr BP (Bertrand et al., 2017). These records of glacier retreat are in agreement with a terrestrial dust record near the study area, indicating elevated dust flux from the Cordillera Darwin—associated with glacier retreat—between 2400-1400 ka (Vanneste et al., 2016).

4.2.2.3 Regional climatology

Climate across southernmost South America is difficult to evaluate given the paucity of long-term meteorological registries in the region, although broad patterns may be observed. Climate is cold-maritime, dominated by interactions between strong and persistent westerly atmospheric flow and the topographic barrier imposed by the Andes (Miller, 1976; Schneider et al., 2003). A strong orographic effect produces a pronounced west-east precipitation gradient (Figure 4.2a), with precipitation of up to 2,000 mm/yr concentrated on the hyperhumid western (windward) slopes of Tierra del Fuego, dropping to 300-400 mm/yr on the eastern steppe. Precipitation west of the topographic

divide scales directly with zonal wind, while east of the divide heightened wind corresponds to lower precipitation (Garreaud et al., 2013).

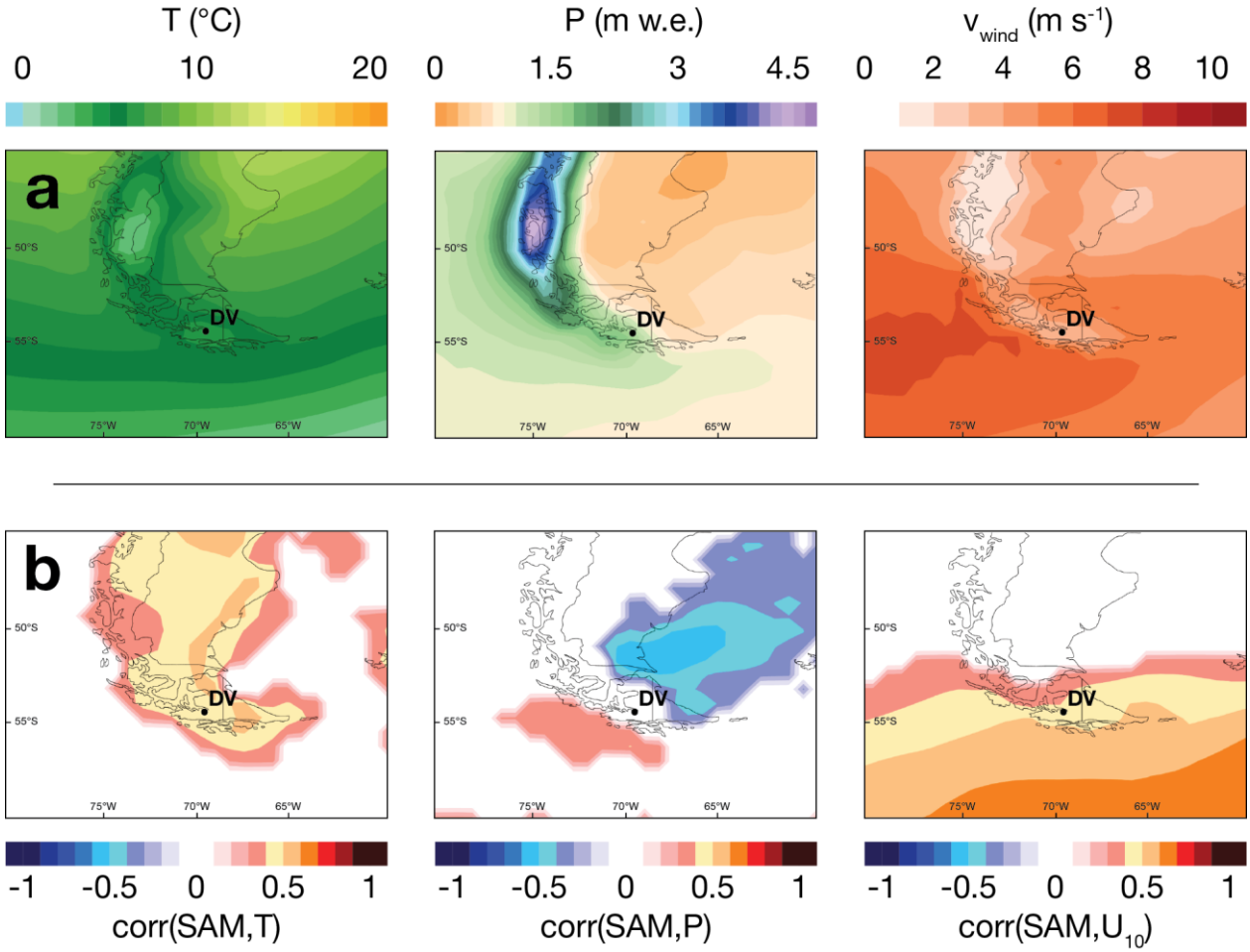

Figure 4.2. Climate parameters over southernmost South America. a) top row shows annual trends in temperature (left), precipitation (center), and wind velocity (right) from the ERA-Interim reanalysis (Dee et al., 2011) for the interval 1979-2015. b) bottom row shows annual correlations at the 95th percentile between temperature, precipitation, and 10-m zonal wind from ERA-Interim and the Marshall (2003) instrumental SAM index.

Tierra del Fuego receives less annual precipitation than the South American coast immediately to the north (Miller, 1976; Carrasco et al., 2002); this precipitation is also distributed more evenly across the year (Sagredo and Lowell, 2012). Since the 1960's, precipitation has increased over southwestern Patagonia (including parts of Tierra del Fuego) by approximately 200 mm per decade. (Garreaud et al., 2013). This trend is directly related to enhanced orographic precipitation brought on by increased westerly circulation over the Southern Ocean, which is in turn associated with a multidecadal trend towards positive SAM (Pohl and Fauchereau, 2012). SAM highly correlates with temperature across southernmost South America, and the strengthening of westerly circulation over the Southern Ocean and Tierra del Fuego is associated with an increase in precipitation over southwestern Tierra del Fuego (Figure 4.2b, Aravena and Luckman, 2009).

4.2.3 Methods

Field work was carried out in November 2014 and April 2015. In addition to analysis of aerial photographs, field mapping was used to elaborate a geomorphologic map of the area, revealing a relative chronology of glacial and paraglacial events in the region. We used a combination of cosmogenic surface exposure dating, dendrochronology, and radiocarbon dating to constrain these events. Cosmogenic dating efforts were focused on the high-elevation relict moraines and the moraine defining the outer limit of the recent moraines. To give chronological control for the more recent dates, a dendrochronological transect was conducted from the ice-distal to ice-proximal sector of the recent moraines. Radiocarbon samples were taken from bog cores in a low-relief topographic high near the coast, to constrain the minimum age of ice retreat from the distal study area.

4.2.3.1 ^{10}Be surface exposure dating

We directly dated glacial moraines using terrestrial cosmogenic nuclides. Rock samples were taken for ^{10}Be surface exposure dating from large (>1 m^3) boulders embedded in the crests of moraine ridges (Figure 4.3a, b). Total sample quartz content varied between 5-35%. Samples >0.5 m tall were preferentially sampled to avoid possible burial effects; erosion is assumed to be negligent due to the young age of the samples and generally good condition of the rock surfaces sampled. We do not correct for shielding effects of snow or vegetation. Samples were taken from the top 1-4 cm of planar to gently curved non-vegetated surfaces using a drill and explosive charges per Kelly (2013). Topographic skyline, as well as surficial strike and dip measurements, were recorded using a handheld transit and clinometer for shielding corrections. Coordinates and altitude were evaluated relative to the WGS 1984 datum using a handheld commercial GPS with an assumed uncertainty of <10 m. We assume ages record the near-final construction and stabilization of an end moraine, near the climatic inflection point when the glacier in question begins to retreat. Ideally these ages represent tight minimum limiting ages of the culmination of a glacial advance.

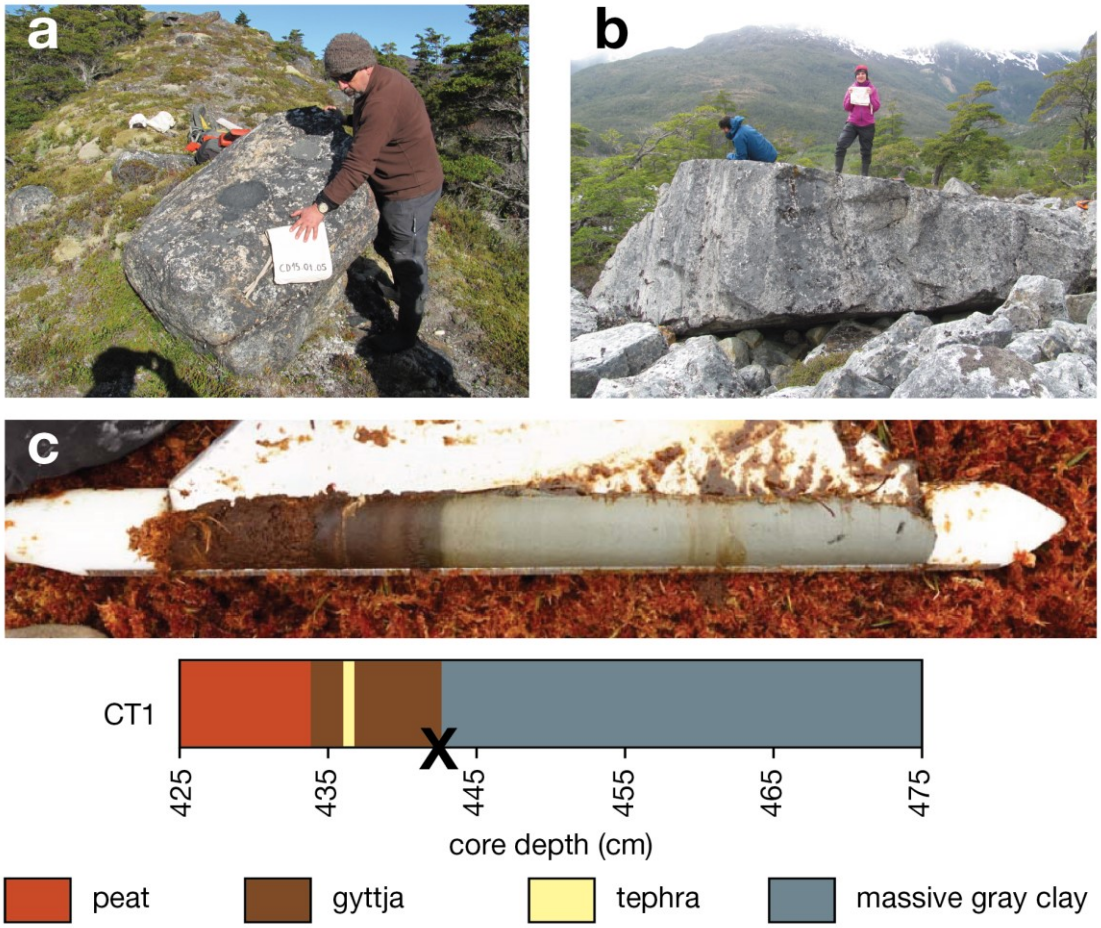

Figure 4.3. a) Sample CD15-01-05 was taken from a 1.5 x 1.5 x 1 m granitic boulder on a sharp-crested moraine fragment, which is located on a topographic high ~160 m amsl approximately 3 km from the modern ice margin. b) Sample CD14-03-04 was taken from the pictured boulder, dimensions 6 x 3 x 2 m, perched on a prominent latero-frontal moraine approximately 2 km from the modern ice margin. c) Core CD14-03-01-CT8, which at a depth of 425-475 cm preserves the transition from peat to gray clay. The X marks the position where samples were taken for radiocarbon dating, although no sample was dated from this core section.

Initial rock crushing took place at the Pontificía Universidad Católica de Chile; mineral separation and final sample preparation occurred at the Cosmogenic Nuclide Laboratory at Lamont-Doherty Earth Observatory (LDEO) following standard geochemical protocols (Schaefer et al., 2009; Kaplan et al., 2011). These include the low process beryllium blank in use at LDEO, which permits measurement of very low concentrations of ^{10}Be (minimum sample ^{10}Be/^{9}Be = 5×10^{-15}), and recent advances at the Center of Accelerator Mass Spectrometry at Lawrence Livermore National Laboratory that permit precise measurements of these low ^{10}Be concentrations. Ages (Table 1) were calculated using the "Lm" scaling scheme and v. 2.2 of the CRONUS calculator (Balco et al., 2008), the v.2.2.1 constants file, and the regional production rate for Patagonia at 50°S (Kaplan et al., 2011). This method is preferred over the more recent v.2.3 or v.3 calculators, as the v. 2.2.1 constants file incorporates a high-resolution geomagnetic framework (Lifton et al., 2008) that is needed for consistency with the regional production rate of Kaplan et al. (2011).

4.2.3.2 Dendroglaciology

To constrain further the glacial history of the area, we conducted dendroglaciological dating of trees growing in the glacier forefield (Figure 4.4). The age of the oldest tree growing on a deglaciated surface will give a minimum-limiting age of glacier retreat (Luckman, 2000; Sigafoos and Hendricks, 1969). We collected 95 increment cores of *Nothofagus betuloides* from 5 stations in the study area. Most samples were taken from 10-50 cm above the surface to minimize height-age error (McCarthy et al., 1991). The samples were prepared following standard procedures at the Instituto Antártico, Universidad de Magallanes (Stokes, 1996); ring counting took place at the Instituto de Geografía, Pontifícia Católica Universidad de Chile. We make no additional correction for ring height nor rotted piths.

Aerial photography from a United States Air Force trimetrogon survey in 1945 established that the Dalla Vedova glacier was land terminating (Figure 2). We collected five discs from saplings within this ice limit to obtain an estimate of local ecesis. The oldest age of this population yielded an age of 29 years, suggesting an approximate ecesis value of 41 years. This value is comparable to ecesis values estimated from the Gran Campo Nevado at 53°S (Koch and Kilian, 2005) and Bahía Pía in the CD at 55°S (Holmlund and Fuenzalida, 1995).

4.2.3.3 Radiocarbon dating

We obtained four sediment cores from an ombotrophic bog in the northern study area for analysis. The deepest section of bog was identified via survey with a steel probe along two orthogonal transects. Using a D-section Russian corer, complete sections were obtained from this section. Field descriptions of core composition and texture were compiled until the bottom of the bog was reached, whereupon 15-cm sections of the overlying material were collected for further analysis. Loss-on-ignition burns for 2 hours at 550°C and 4 hours at 950°C were used to determine the organic, siliciclastic, and carbonate fractions of the bottom sections at 1-cm intervals (Heiri et al., 2001). Plant macrofossils were collected from within 1 cm above the loss-on-ignition defined break between predominantly inorganic and predominantly organic sediments up section for AMS radiocarbon dating. Samples were processed and analyzed at the commercial laboratory of Beta Analytic. We convert all radiocarbon ages to cal years BP using CALIB 7.1 (Stuiver et al., 2019). As the ages pertain to the Holocene, we use the Southern Hemisphere calibration curve of Hogg et al. (2013) in our calibrations.

4.2.4 Results

4.2.4.1 Glacial geomorphology of the study area

The Dalla Vedova is largely land-terminating, with a ~300 m section of the nearly 2 km glacier terminus calving into a proglacial lake (Figure 4.4). Distal to the proglacial lake is a distinct hummocky morainal belt that defines the former glacier forefield. Numerous ($n > 30$) low-relief, discontinuous ridges of diamicton orthogonal to the modern ice terminus characterize the proximal morainal belt; these are interpreted as recessional moraines recording annual glacier stillstands. Trimetrogon imagery from 1945 indicates that at this time the glacier was at or near these moraines, and that the modern proglacial lake had not yet formed.

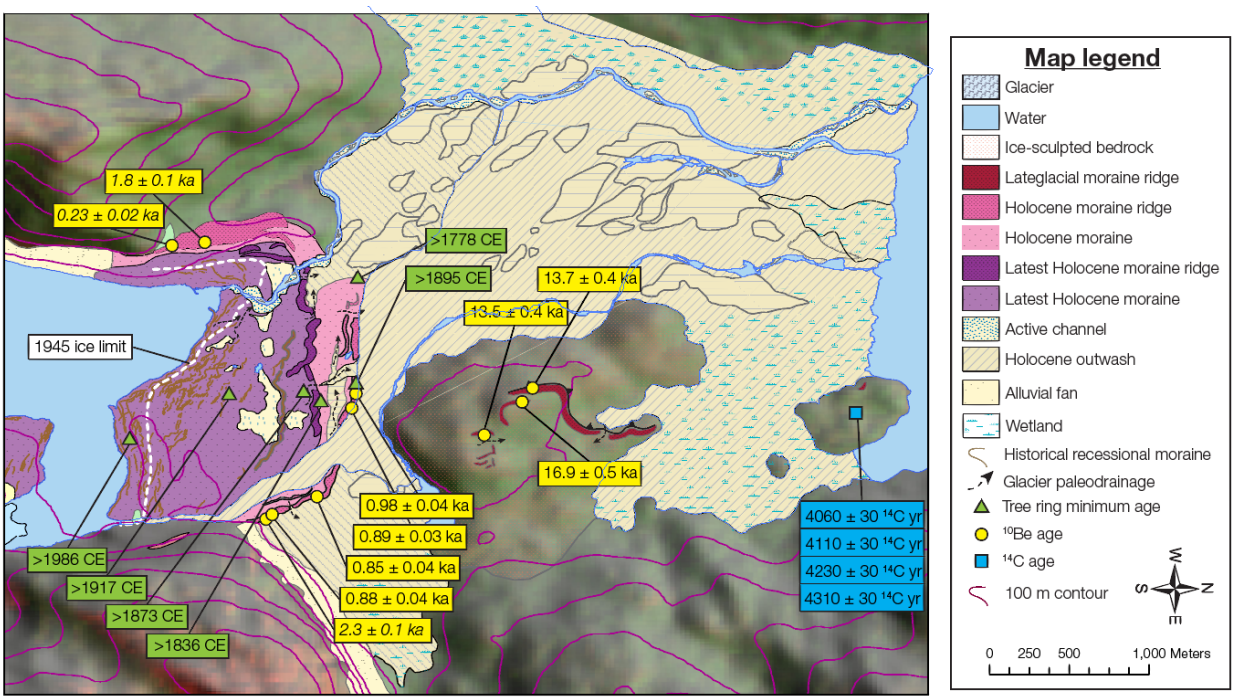

Figure 4.4. Geomorphologic map of the study area with results of the paleoglacier chronology. Elevation is based upon the SRTM 1-arc second digital elevation model. Ages in asterisks are determined to be outliers and are not considered in the discussion.

Outboard of these recessional moraines, several closed depressions currently hold water, whereas others are broken by dry canals interpreted as paleochannels. These are interpreted as paleolake beds, formed by ponding of water between a receding ice margin and the more continuous moraines outboard. These two prominent ridges, approximately 2 km from the modern ice margin, form a pair of well-defined, continuous, sharp-crested latero-frontal moraines between 5 and 60 m in height (Fig. 4.4). The outer and inner moraines are dubbed "H1" and "H2," respectively. Maximum height is achieved on the western lateral; the eastern lateral rises to approximately 20 m, and the frontal moraines do not rise above 10 m. These moraines are cut in several parts by multiple generations of paleochannels, as well as the modern drainage. These channels, along with boulder-sized outwash deposits and hummocky topography, separate the two moraine ridges. Samples for ^{10}Be surface exposure dating were collected from the outer H1 moraine, while dendrochronologic stations were positioned to constrain the age of the inboard landforms.

An extensive outwash plain leads from two breaches in the outer moraine ridge to the ocean, ~3.5 km to the north. Outwash in the study area is defined morphologically as continuous low-angle surfaces with evidence of channelization, and compositionally as moderately sorted deposits of subrounded to rounded clasts ranging in size from coarse sand to boulders < 1 m diameter. Several generations of outwash are defined by vegetation development and morphostratigraphic relations. The 1945 imagery additionally reveals that the prominent abandoned channel to the east was active at that time, although the current drainage was also active. The contemporary active channel forms a pronounced knickpoint as it passes through the outer moraine, and cuts an older outwash surface consisting of imbricated boulders of up to 1 m in diameter. This

suggests that the breaching of the outer moraine prior to 1945 resulted in a glacier lake outburst flood (GLOF).

The outwash plain skirts a ~175 m tall bedrock promontory, from where additional ^{10}Be samples were collected (Fig. 4.4). On top of this topographic feature, two distinct ridges are found at different elevations. The higher ridge, dubbed "L1," forms an approximately 150 x 150 m L-shaped angle, forming the highest point on the bedrock knob, and is composed of sediment with scattered boulders on top. The discontinuous lower ridge, "L2," approximately 10 m below the high ridge at its maximum, has a similar composition. It can be followed to the north as it progressively loses elevation, terminating at approximately 20 m amsl, 10 m above the modern outwash surface. Both ridges are interpreted as relict latero-frontal moraines from an extensive advance of the Dalla Vedova glacier that predates the younger moraine ridges found closer to the modern ice margin. The most probable interpretation is that the bulk of ice flowed to the west of these moraines when they were formed.

Approximately 5.5 km from the modern ice margin, close to the bay, a low-relief (max. 20 m) bedrock promontory forms part of the modern coastline, above the modern outwash surface. The interior of the promontory is mantled by a mixture of mature *Nothofagus* forest and raised bog; a fragmented crest composed of diamict is interpreted as a moraine fragment of indeterminate age. The sediment cores described below were taken from a raised bog at an elevation of ~15 m amsl in the interior of this bedrock outcrop.

Low-lying parts of the study area are covered by shallow (depth 1-2 m) lakes and wetlands. These are associated with damming activity of introduced beavers (*Castor canadiensis*), and are therefore not considered an intrinsic part of the pre-historical geomorphology of the region.

4.2.4.2 Absolute dating of glacial events

Results of the cosmogenic dating of glacial moraines are presented in Table 4.1. Ages show good stratigraphic agreement in that more distal/higher moraines yield older ages than those more proximal to the modern ice limit. These ages can be divided into Lateglacial and Holocene moraines, and are discussed below.

Table 4.1. Analytical data for 10Be terrestrial cosmogenic nuclide surface exposure dating, sorted by moraine. We assume a sample density of 2.7 g/cm^3 and make no corrections for erosion or shielding by sediment, snow, or vegetation. Carrier concentrations used are 1043 ppm ([a]) and 1044 ppm ([b]). (*) AMS ratios are presented as boron-corrected values measured against the 07KNSTD3110 standard material (^{10}Be/^{9}Be = 2.85 × 10^{-12}; Nishiizumi et al., 2007). (†) ^{10}Be concentrations are corrected for background ^{10}Be as recorded by the procedural blanks associated with each sample set, the concentrations of which ranged from 3.4656 × 10^{-16} to 5.0787 × 10^{-16}. (‡) Moraine ages are reported as mean ages (excluding outliers; see text); reported error incorporates one standard deviation and the

propagated 3% error of the production rate of Kaplan et al. (2011).

Moraine	Sample	CAMS lab no.	Lat. °	Lon. °	Elevation m amsl	Thickness cm	Shielding	Mass g	Be carrier g	$^{10}Be/^{9}Be$ (10^{-14})*	^{10}Be 10^{4} atoms/g†	Age yr BP	1σ yr BP
L1	CD15-01-05	BE40013	-54.59076	-69.13718	160	2.19	0.997	10.0604	0.1821	6.8228 ± 0.1930	8.5429 ± 0.2423	16950	480
L2	CD15-01-04	BE40012	-54.59287	-69.13411	174	2.66	0.998	7.2807	0.1814	4.0208 ± 0.1073	6.8935 ± 0.1857	13490	370
	CD15-01-06	BE40014	-54.59013	-69.13834	142	1.89	0.998	10.152	0.1814	5.4898 ± 0.1366	6.7731 ± 0.1695	13670	340
H1 (lateral)	*CD14-03-01*	*BE40260*	*-54.60506*	*-69.12583*	*95*	*2.16*	*0.971*	*56.7273*	*0.1812*	*4.7988 ± 0.1088*	*1.0619 ± 0.02423*	*2310*	*50*
	CD15-01-01	*BE40265*	*-54.61012*	*-69.15239*	*153*	*1.64*	*0.980*	*54.8185*	*0.1823*	*0.4966 ± 0.03742*	*0.1072 ± 0.00851*	*230*	*20*
	CD15-01-02	*BE40266*	*-54.60837*	*-69.1526*	*146*	*2.56*	*0.978*	*55.9677*	*0.1831*	*3.8100 ± 0.1653*	*0.8620 ± 0.03750*	*1790*	*80*
H1 (frontal	CD14-03-02	BE40261	-54.60476	-69.12644	90	2.4	0.965	57.4382	0.1821	1.8172 ± 0.08197	0.3945 ± 0.01799	880	40
	CD14-03-04	BE40262	-54.60229	-69.12824	79	2.69	0.992	54.6026	0.1823	1.6908 ± 0.06931	0.3859 ± 0.01601	850	40
	CD14-03-06	BE40263	-54.60039	-69.13682	60	1.79	0.994	56.7178	0.1822	1.8315 ± 0.06812	0.4028 ± 0.01522	890	30
	CD14-03-07	BE40264	-54.60013	-69.13851	57	2.13	0.994	56.1857	0.1822	1.9690 ± 0.07048	0.4377 ± 0.01591	980	40
	Average											**900**	**60**

4.2.4.3 Lateglacial moraines

Three boulders were sampled from the two moraine ridges (L1 and L2) preserved atop the bedrock promontory, above the modern outwash. A single sample from a boulder atop the L1 moraine fragment, topographically above all other moraines in the study area, yielded an age of 16,950 ± 480 yr BP. The L2 moraine forms a discontinuous moraine crest that is discernable directly inboard of this moraine fragment. Of variable height (max. 10 m), two samples from boulders on top of the L2 ridge crest give ages of 13,490 ± 370 and 13,670 ± 340 yr BP (average age 13,580 ± 430 yr BP). Further age constraint was not possible due to the scarcity of in-situ boulders on top of these moraine crests.

4.2.4.4 Holocene moraines

We dated 7 boulders from the outer H1 moraine, the most prominent latero-frontal moraine system in the field area. Ages show considerable spread from 230 ± 20 yr BP to 2310 ± 50 yr BP. However, four of these ages form a population around 900 ± 60 yr BP (ages: 850 ± 40, 880 ± 40, 890 ± 30, and 980 ± 40 yr BP). These ages overlap at 2-sigma, while the remaining three ages (2310 ± 50, 1790 ± 80, and 230 ± 20 yr BP) overlap neither with each other nor with the population at 900 ± 60 yr BP. We also note that the four ages that form a population comes from the frontal moraine, whereas the three non-conforming ages were taken from the lateral moraine, where repeated advances and paraglacial modification may complicate interpretation of boulders found on these surfaces. We therefore consider the frontal area with the coherent ages as marking a distinct true moraine age with a mean approximated as 900 ± 60 yr BP. The lateral samples are considered part of a compound moraine subject to reworking and erosion. Due to a lack of appropriate boulders, cosmogenic age constraints of the H2 moraine are not possible.

The H1 moraine complex was also included in our dendrochronological transect. Stations 1 and 2 (Table 4.2), located on moraine H1, yielded minimum ages of ice retreat as occurring prior to 1778 and 1895 CE, respectively. Stations 3 and 4, established on the

proximal and distal sides of moraine H2, yield minimum ages of ice retreat as before 1836 and 1873 CE. Station 5, within the belt of recessional moraines, yields a minimum age of ice retreat as before 1917 CE.

Table 4.2. Dendroglaciological data for the study area. The minimum date of landform stabilization is given in years CE, determined by adding a 29-year ecesis correction to the oldest tree age from each station (see text for details).

Site	Code	Latitude °S	Longitude °W	No. sampled trees	Age max years	Date CE
Moraine H1 W	Station 1	54.5996	69.1501	16	196	1778
Moraine H1 E	Station 2	54.6001	69.1386	15	79	1895
Moraine H2 Outer	Station 3	54.6018	69.1373	20	138	1836
Moraine H2 Inner	Station 4	54.6029	69.1381	20	101	1873
Internal moraines	Station 5	54.6071	69.1379	24	57	1917

All ages agree with the absolute constraints provided by the ^{10}Be dating and aerial photos, although it is noteworthy that the dendrochronologic minimum limiting age of ~200 yr BP for the H1 considerably undershoots the ^{10}Be-constrained stabilization age of ~900 yr BP for this landform.

4.2.4.5 Radiocarbon dating of bog formation

Plant macrofossils and bulk organic sediment samples were dated from four bog cores taken from a raised bog on a 15-m tall bedrock platform near the coast, at the extreme north of the study area (Figure 4.4). Until 4 m cores were composed of peat and gyttja, but at depths of 4-5 m we encountered a substantial change in composition, from peat up section to dark brown gyttja and finally bluish-gray clay down section (Figure 4.5). Loss-on-ignition profiles identified this visual transition as reflecting a change from predominantly inorganic to organic sediments up section. A notable feature was a yellowish, grainy, silicic band of no more than 0.5 cm thickness found between 5-10 cm above the visual organic-inorganic transition, interpreted as a tephra.

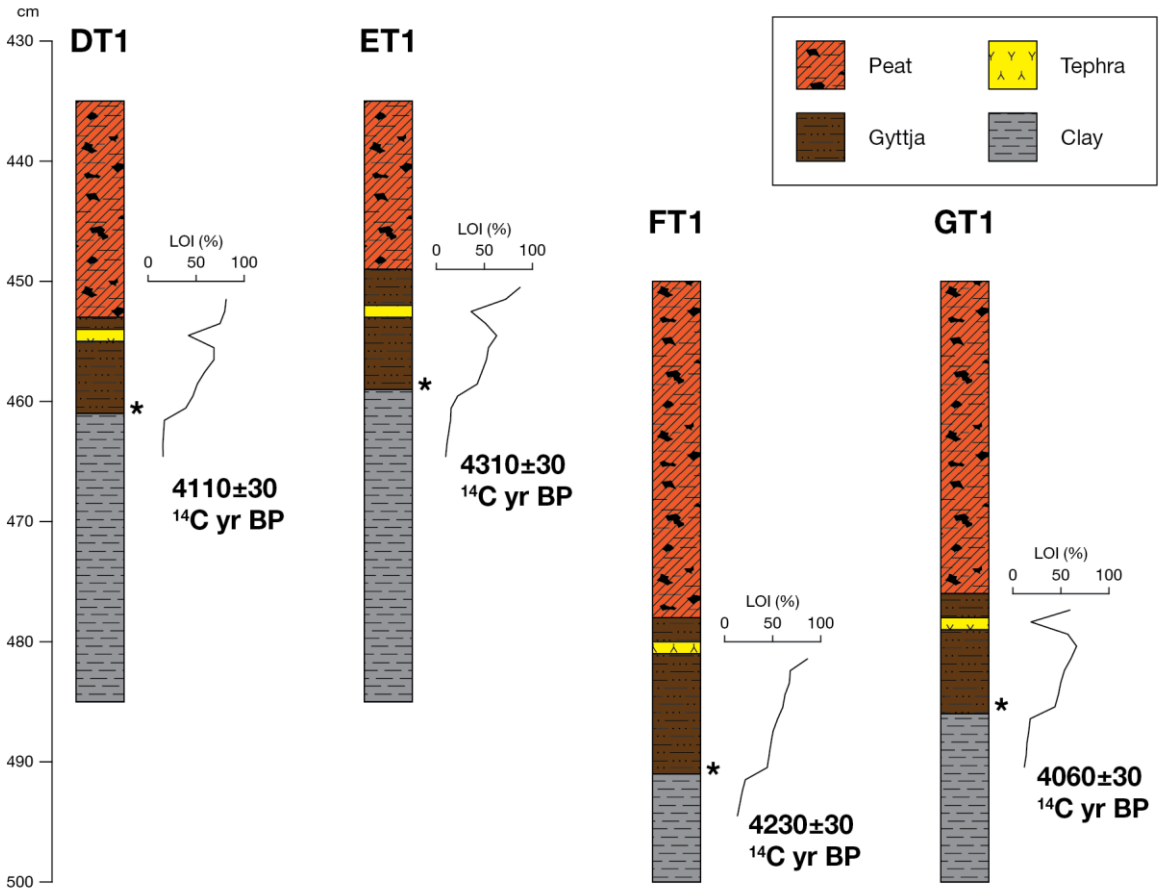

Figure 4.5. Sediment cores dated in this study. Loss-on-ignition profiles are displayed to the right of each core. Radiocarbon sampling sites are indicated by stars.

Radiocarbon dating of the inorganic clay-organic silt transition yielded ages from 4060 ± 30 to 4310 ± 30 ^{14}C yr BP (Table 4.3; 4435-4810 to 4650-4960 cal yr BP). These ages indicate a middle Holocene transition from subaqueous to terrestrial deposition at this bog, and imply that ice has not extended beyond this point (Figure 4.4) since that time.

Table 4.3 Analytical data for radiocarbon samples from the bog in the northern section of the study area. Ages calibrated using CALIB 7.1 and are reported as the 2-sigma age range when calibrated to the SHCal13 curve (Hogg et al., 2013).

Site	Lab code	Material	Depth in core	δ13C	Radiocarbon age	Calibrated age
			cm	‰	(^{14}C years BP)	(cal years BP)
DT1	Beta-420660	Macrofossil	461	-27.9	4110 ± 30	4435 - 4810
ET1	Beta-420661	Macrofossil	459	-26.2	4310 ± 30	4650 - 4960
FT1	Beta-420662	Bulk	489	-27.1	4230 ± 30	4580 - 4840
GT1	Beta-420663	Macrofossil	492	-26.2	4060 ± 30	4420 - 4780

4.2.5 Discussion

Two noteworthy results arise from the chronology of paleoglacier fluctuations of the Dalla Vedova glacier: 1) preliminary evidence for restricted lateglacial ice extent from within the Cordillera Darwin, and 2) a glacier advance culminating in the "Medieval Warm Period" (c. 1100-800 yr BP). We discuss these conclusions, as well as ambiguities in our chronologies below.

4.2.5.1 Evidence for restricted lateglacial ice in the Cordillera Darwin

Collectively, the three lateglacial ages of moraine boulders in our study area suggest ice extent was limited to within the Cordillera Darwin by c. 13,500 yr BP. The single age of 16,950 ± 480 yr BP for the outermost L1 moraine offers tantalizing evidence of similarly limited ice extent during Heinrich Stadial 1. Although nothing can be definitively concluded with a single date, we note that this age—representing moraine abandonment by a glacier—overlaps with the oldest minimum limiting ages of CD deglaciation, at ~16,800 yr BP (Hall et al., 2013).

L2 moraine formation at c. 13.5 ka coincides with the Antarctic Cold Reversal (ACR), a period of relatively cooler temperatures recorded in Antarctic ice cores c. 14.5-12.9 ka associated with moraine formation across the Southern Hemisphere midlatitudes (e.g. Pedro et al., 2016; Sagredo et al., 2018). These ages therefore parallel evidence for ACR glacier advance in the adjacent Cordón Martial to the east near Ushuaia (Menounos et al., 2013). Although the samples dating the ACR moraine were taken from an elevation of approximately 160 m amsl, the moraine itself is laterally continuous down to an elevation of approximately 10 m amsl. While we have no constraints on the length of the glacier at this time, the low elevation of the moraine suggests that ice did not extend more than tens of kilometers beyond the study area.

This interpretation is consistent with the conclusions of previous studies in the area, which suggested ice extent in the eastern Cordillera Darwin during the ACR was restricted to the Cordillera proper (Boyd et al., 2008; Hall et al., 2013; Bertrand et al., 2017; Fernández et al., 2017). This result casts further doubt upon the possibility of an ACR glacier expansion that reached the Strait of Magellan (e.g. McCulloch et al. 2005a), although an alternative possibility is that restricted ice in our study area implies a decoupling of the eastern CD from the western cordillera.

4.2.5.2 Late Holocene glacial maximum

The H1 moraine, which formed c. 900 ± 60 yr BP, represents the most extensive Holocene advance preserved at the Dalla Vedova glacier. This advance corresponds to the so-called "Medieval Climate Anomaly" (MCA, 1000-800 yr BP; Mann et al., 2009), alternatively known as the Medieval Warm Period or Medieval Climate Optimum. Farther north in Patagonia evidence is generally lacking for a glacier advance at c. 900 yr BP (Masiokas et al., 2009), although scattered dates exist at Lago Argentino that may overlap with the MCA within analytical error (Kaplan et al., 2016). Additionally, glaciers reached their maximum Holocene extent either during the Little Ice Age (Koch and Kilian, 2005) or in the early to middle Holocene (Kaplan et al., 2016; Reynhout et al. 2019).

The c. 900 yr BP H1 advance corresponds (within error) to the bracketed Holocene glacier maximum recorded at Bahía Pía, 40 km to the southwest, between 850 ± 70 and 600 ± 50 cal yr BP (Kuylenstierna et al., 1996). Other advances identified in the region between 7-5 ka (Menounos et al., 2013) and in the late Holocene and "Little Ice Age" (LIA; Strelin et al., 2008) do not appear in our chronology. Poor preservation may explain the lack of older advances in our study area, especially given the extensive outwash deposits outboard of H1. The LIA advance at Glaciar Ema ("GE" in Figure 1) may be preserved as the H2 moraine in our study area, an interpretation which conforms to the dendroglaciological constraints on the H2 moraine.

4.2.5.3 Interpreting basal radiocarbon ages

The sediment cores extracted from the northern part of the study area bear visual similarities to the 'transition zone' from glacial clay to lacustrine silt defined by Hall et al. (2013), including a thin tephra stratigraphically above the transition. However, our ages differ significantly, yielding a mid-Holocene age for the transition in our cores. This strongly suggests the tephra observed in our cores is not the Reclus tephra, but rather the MB2 tephra from Mount Burney (3,830 ± 390 ^{14}C yr BP; Stern, 2008) and challenges our a priori interpretation of the core as representing the age of deglaciation from the valley.

One interpretation of these cores is that the ages closely bracket ice retreat from the northern margin of our study area. The transition from inorganic to organic sedimentation does, *sensu strictu*, define a minimum age of deglaciation in the zone. However, no other evidence for extensive Holocene ice exists in this valley. Additionally, such a scenario struggles to explain the geomorphologic position of the L2 moraine ~1 km upvalley, where it extends down to an elevation similar to that of the core site. While it is possible the blue-gray clay represents a proglacial facies associated with lateglacial advances of the Dalla Vedova glacier, this would also imply a depositional hiatus of over 8,000 years, limiting the utility of these ages to constrain the glacial history of our zone.

Instead, we favor the interpretation of this transition as marking a shift from a nearshore lagoonal environment to a terrestrial bog. The transition therefore marks a relative sea level regression between 4.8-4.5 ka, which corresponds well to the regional relative sea level curve of Porter et al. (1984). As the present bog surface lies approximately 15 m amsl, a sample depth of approximately 5 m implies approximately 10 m of local sea level regression over the last 4.5 ka, or an uplift rate of ~2.2 mm/yr. This is similar to, but slightly higher than the maximum uplift rates of 1.5-2.0 mm/yr estimated by dating of raised Holocene beaches in the Beagle Channel (Bujalesky, 2007). Higher rates of coastal uplift adjacent to Seno Almirantazgo could be explained by increased isostatic rebound closer to the "core" of the Cordillera Darwin and/or uplift due to neotectonic influence from the nearby Magallanes Fault Zone (Figure 4.1).

4.2.5.4 Climatic implications

Two sites in the eastern Cordillera Darwin appear to have registered advances during the MCA: this study and Bahía Pía, 45 km to the southwest (Kuylenstierna et al., 1996). No other glacier in Patagonia appears to have left evidence of advance during this time.

Furthermore, advances at both sites appear to have corresponded to a late Holocene glacier maximum, while further north in Patagonia glaciers reached their maxima earlier, at c. 6 ka (Kaplan et al., 2016) or at c. 9.7 ka (Reynhout et al., 2019). What drove these seemingly anomalous glacier advances in the eastern Cordillera Darwin?

We propose that enhanced precipitation over the Cordillera Darwin, associated with an episode of positive-trending SAM during the MCA, strongly influenced glacier advances in the eastern Cordillera Darwin during this time. The MCA corresponded to a period of more-positive SAM (Moreno et al., 2018), whereas the LIA corresponded to several centuries of more-negative SAM (Figure 4.6b). In this scenario, increased advected precipitation above the equilibrium line in the Cordillera Darwin would have been sufficient to counteract generalized warming associated with more-frequent positive SAM and drive glacier advances at Bahía Pía and Dalla Vedova (Figure 4.6c). Furthermore, increased precipitation and cloudiness would reduce incoming solar radiation received by the glacier surface, reducing ablation. However, across the rest of Patagonia, warmer and drier effects dominated (Moreno et al., 2014; Moreno et al., 2018), and prevented glacier expansion during the MCA.

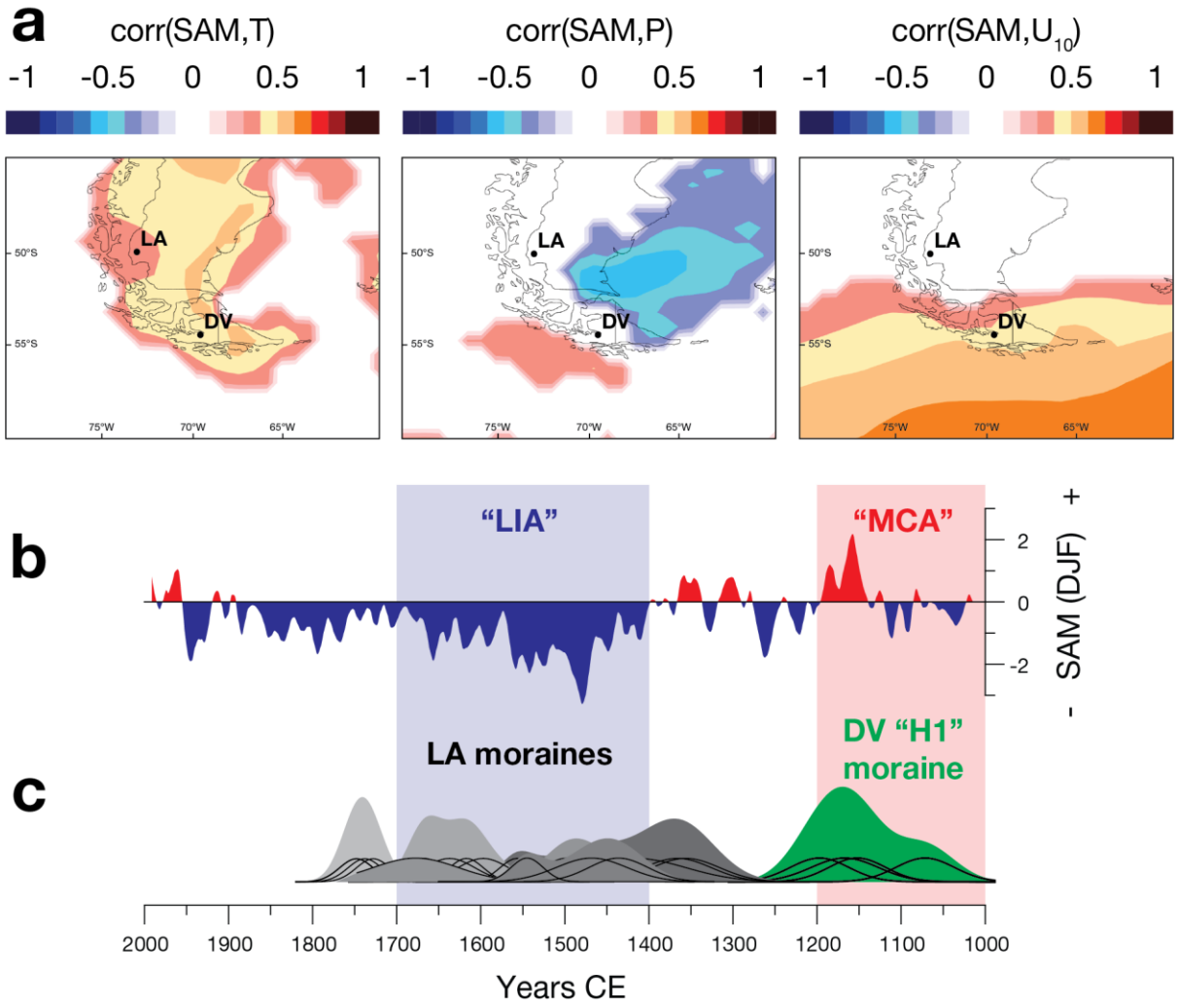

Figure 4.6 Schematic outlining postulated SAM-glacier linkages over the Holocene. a) modern annual correlations at the 95th percentile between temperature, precipitation, and 10-m zonal wind from the ERA-Interim analysis from 1979-2017 (Dee et al., 2011) and the Marshall (2003) instrumental SAM index. DV=Dalla Vedova glacier (this

study); LA=Lago Argentino (Kaplan et al., 2016). b) Long-term variations in the SAM over the last millennium (Dätwyler et al., 2017). The Little Ice Age ("LIA") and Medieval Climate Anomaly ("MCA") are shaded in blue and red, respectively, per the chronological definition of these periods of Mann et al. (2009). c) Cosmogenic ages of glacier advances from LA in grey and the "H1" moraine building event from this study. Individual ages are presented as Gaussian probability distributions (black curves) and whole moraine ages are presented as summed probability plots of individual ages (colored polygons).

An alternative scenario to explain asymmetrical late Holocene glacier advances across Patagonia include a regional cold event in Tierra del Fuego that did not affect Patagonia during the MCA. Additionally, the glacial system at Bahía Pía—while terminating on land during the MCA—was fundamentally a tidewater system, and the advance at this time may not have corresponded to a climatic trigger. Tidewater dynamics are also a factor in explaining the complete lack of Holocene terminus variation of the nearby Marinelli glacier until the 1960s (Boyd et al., 2008). It is also worth noting that existing evidence at Glaciar Ema in the western CD does not register an advance during the MCA (Strelin et al., 2008); instead, the dated Holocene maximum at this site corresponded to the LIA.

The lack of apparent glacier advances in the Cordillera Darwin prior to the late Holocene differs from interpretations in southern Patagonia of progressively less-extensive Southern Hemisphere glacier advances as a consequence of progressive changes in Holocene summer insolation intensity (Reynhout et al., 2019) or southward migration of the Intertropical Convergence Zone, as has been proposed for New Zealand (Putnam et al., 2012). Instead, this result suggests glaciers in Tierra del Fuego in the southernmost tip of the continent were subject to different controls over glacier mass balance than their counterparts further north in Patagonia. This interpretation is supported by modern analysis of glacier climate sensitivity, which demonstrates glaciers in Tierra del Fuego are relatively less sensitive to changes in temperature and precipitation than their mainland counterparts (Sagredo et al., 2014). However, we also highlight, our study involves one of the first in CD to date directly moraine crests with cosmogenic dating; we encourage future studies in the CD as well as in Patagonia to seek additional evidence of advances coincident with the MCA.

4.2.6 Acknowledgements

This project was supported by the Núcleo Milenio Paleoclima of the Iniciativa Científica Milenio of the Ministerio de Economía, Fomento y Turismo (Chile); CONICYT Colaboración Internacional USA2130035; and FONDECYT 1160488. S. Reynhout is a recipient of a CONICYT-PCHA Beca de Doctorado Nacional (year 2015).

4.2.7 References

Abram, N.J., Mulvaney, R., Vimeux, F., Phipps, S.J., Turner, J., England, M.H., 2014. Evolution of the Southern Annular Mode during the past millennium. Nat. Clim. Chang. 4, 564.

Anderson, R.F., Ali, S., Bradtmiller, L.I., Nielsen, S.H.H., Fleisher, M.Q., Anderson, B.E., Burckle, L.H., 2009. Wind-Driven Upwelling in the Southern Ocean and the

Deglacial Rise in Atmospheric CO₂ Science (80-.). 323, 1443 LP – 1448. https://doi.org/10.1126/science.1167441

Aravena, J., Luckman, B.H., 2009. Spatio-temporal rainfall patterns in southern South America. Int. J. Climatol. 29, 2106–2120.

Balco, G., Stone, J.O., Lifton, N.A., Dunai, T.J., 2008. A complete and easily accessible means of calculating surface exposure ages or erosion rates from 10Be and 26Al measurements. Quat. Geochronol. 3, 174–195. https://doi.org/10.1016/J.QUAGEO.2007.12.001

Bentley, M.J., Mcculloch, R.D., 2005. Impact of neotectonics on the record of glacier and sea level fluctuations, strait of magellan, southern chile. Geogr. Ann. Ser. A, Phys. Geogr. 87, 393–402. https://doi.org/10.1111/j.0435-3676.2005.00265.x

Bertrand, S., Lange, C.B., Pantoja, S., Hughen, K., Van Tornhout, E., Wellner, J.S., 2017. Postglacial fluctuations of Cordillera Darwin glaciers (southernmost Patagonia) reconstructed from Almirantazgo fjord sediments. Quat. Sci. Rev. 177, 265–275. https://doi.org/10.1016/J.QUASCIREV.2017.10.029

Boex, J., Fogwill, C., Harrison, S., Glasser, N.F., Hein, A., Schnabel, C., Xu, S., 2013. Rapid thinning of the late Pleistocene Patagonian Ice Sheet followed migration of the Southern Westerlies. Sci. Rep. 3, 2118. https://doi.org/10.1038/srep02118

Bown, F., Rivera, A., Zenteno, P., Bravo, C., Cawkwell, F., 2014. First Glacier Inventory and Recent Glacier Variation on Isla Grande de Tierra Del Fuego and Adjacent Islands in Southern Chile, in: Global Land Ice Measurements from Space. Springer Berlin Heidelberg, Berlin, Heidelberg, pp. 661–674. https://doi.org/10.1007/978-3-540-79818-7_28

Boyd, B.L., Anderson, J.B., Wellner, J.S., Fernández, R.A., 2008. The sedimentary record of glacial retreat, Marinelli Fjord, Patagonia: Regional correlations and climate ties. Mar. Geol. 255, 165–178. https://doi.org/10.1016/J.MARGEO.2008.09.001

Bujalesky, G.G., 2007. Coastal geomorphology and evolution of Tierra del Fuego (Southern Argentina). Geol. Acta 5, 337–362.

Carrasco, J.F., Casassa, G., Rivera, A., 2002. Meteorological and Climatological Aspects of the Southern Patagonia Icefield. Springer, Boston, MA, pp. 29–41. https://doi.org/10.1007/978-1-4615-0645-4_4

Carrasco, J.F., Osorio, R., and Casassa, G., 2008, Secular trend of the equilibrium-line altitude on the western side of the southern Andes, derived from radiosonde and surface observations: Journal of Glaciology, v. 54, p. 538–550.

Clark, P.U., Dyke, A.S., Shakun, J.D., Carlson, A.E., Clark, J., Wohlfarth, B., Mitrovica, J.X., Hostetler, S.W., and McCabe, A.M., 2009, The Last Glacial Maximum: Science, v. 325, p. 710 LP – 714, doi:10.1126/science.1172873.

Darvill, C.M., Bentley, M.J., Stokes, C.R., 2015. Geomorphology and weathering characteristics of erratic boulder trains on Tierra del Fuego, southernmost South America: Implications for dating of glacial deposits. Geomorphology 228, 382–397. https://doi.org/10.1016/J.GEOMORPH.2014.09.017

Dätwyler, C., Neukom, R., Abram, N.J., Gallant, A.J.E., Grosjean, M., Jacques-Coper, M., Karoly, D.J., Villalba, R., 2018. Teleconnection stationarity, variability and trends of the Southern Annular Mode (SAM) during the last millennium. Clim. Dyn. 51, 2321–2339. https://doi.org/10.1007/s00382-017-4015-0

Evenson, E., Burkhart, P., Gosse, J., Baker, G., Jackofsky, D., Meglioli, A., Dalziel, I., Kraus, S., Alley, R., Berti, C., 2009. Enigmatic boulder trains, supraglacial rock avalanches, and the origin of "Darwin's boulders," Tierra del Fuego. GSA Today 4–10. https://doi.org/10.1130/GSATG72A.1

Fernández, R., Gulick, S., Rodrigo, C., Domack, E., Leventer, A., 2017. Seismic stratigraphy and glacial cycles in the inland passages of the Magallanes Region of Chile, southernmost South America. Mar. Geol. 386, 19–31. https://doi.org/10.1016/J.MARGEO.2017.02.006

Fletcher, M.-S., Moreno, P.I., 2011. Zonally symmetric changes in the strength and position of the Southern Westerlies drove atmospheric CO2 variations over the past 14 k.y. Geology 39, 419–422. https://doi.org/10.1130/G31807.1

García, J.L., Kaplan, M.R., Hall, B.L., Schaefer, J.M., Vega, R.M., Schwartz, R., Finkel, R., 2012. Glacier expansion in southern Patagonia throughout the Antarctic cold reversal. Geology 40, 859–862.

Garreaud, R., Lopez, P., Minvielle, M., Rojas, M., 2013. Large-scale control on the Patagonian climate. J. Clim. 26, 215–230. https://doi.org/10.1175/JCLI-D-12-00001.1

Garreaud, R.D., Vuille, M., Compagnucci, R., Marengo, J., 2009. Present-day South American climate. Palaeogeogr. Palaeoclimatol. Palaeoecol. 281, 180–195. https://doi.org/10.1016/j.palaeo.2007.10.032

Hall, B.L., Porter, C.T., Denton, G.H., Lowell, T. V., Bromley, G.R.M., 2013. Extensive recession of Cordillera Darwin glaciers in southernmost South America during Heinrich Stadial 1. Quat. Sci. Rev. 62, 49–55. https://doi.org/10.1016/J.QUASCIREV.2012.11.026

Heiri, O., Lotter, A., and Lemcke, G., 2001, Loss on Ignition as a Method for Estimating Organic and Carbonate Content in Sediments: Reproducibility and Comparability of Results: Journal of Paleolimnology, v. 25, doi:10.1023/A:1008119611481.

Hogg, A.G., Hua, Q., Blackwell, P.G., Niu, M., Buck, C.E., Guilderson, T.P., Heaton, T.J., Palmer, J.G., Reimer, P.J., Reimer, R.W., Turney, C.S.M., Zimmerman, S.R.H., 2013. SHCal13 Southern Hemisphere Calibration, 0–50,000 Years cal BP. Radiocarbon 55, 1889–1903. https://doi.org/DOI: 10.2458/azu_js_rc.55.16783

Holmlund, P., Fuenzalida, H., 1995. Anomalous glacier responses to 20th century climatic changes in Darwin Cordillera, southern Chile. J. Glaciol. 41, 465–473. https://doi.org/10.3189/S0022143000034808

Ivins, E.R., James, T.S., 2004. Bedrock response to Llanquihue Holocene and present-day glaciation in southernmost South America. Geophys. Res. Lett. 31, L24613. https://doi.org/10.1029/2004GL021500

Kaplan, M.R., Fogwill, C.J., Sugden, D.E., Hulton, N.R.J., Kubik, P.W., Freeman, S.P.H.T., 2008. Southern Patagonian glacial chronology for the Last Glacial period and implications for Southern Ocean climate. Quat. Sci. Rev. 27, 284–294. https://doi.org/10.1016/J.QUASCIREV.2007.09.013

Kaplan, M.R., Schaefer, J.M., Strelin, J.A., Denton, G.H., Anderson, R.F., Vandergoes, M.J., Finkel, R.C., Schwartz, R., Travis, S.G., Garcia, J.L., Martini, M.A., Nielsen, S.H.H., 2016. Patagonian and southern South Atlantic view of Holocene climate. Quat. Sci. Rev. 141, 112–125. https://doi.org/10.1016/j.quascirev.2016.03.014

Kaplan, M.R., Strelin, J.A., Schaefer, J.M., Denton, G.H., Finkel, R.C., Schwartz, R., Putnam, A.E., Vandergoes, M.J., Goehring, B.M., Travis, S.G., 2011. In-situ cosmogenic 10Be production rate at Lago Argentino, Patagonia: Implications for late-glacial climate chronology. Earth Planet. Sci. Lett. 309, 21–32. https://doi.org/10.1016/J.EPSL.2011.06.018

Koch, J., Kilian, R., 2005. 'Little Ice Age' glacier fluctuations, Gran Campo Nevado, southernmost Chile. The Holocene 15, 20–28. https://doi.org/10.1191/0959683605hl780rp

Koppes, M.N., Montgomery, D.R., 2009. The relative efficacy of fluvial and glacial erosion over modern to orogenic timescales. Nat. Geosci. 2, 644–647. https://doi.org/10.1038/ngeo616

Kuylenstierna, J.L., Rosqvist, G.C., Holmlund, P., 1996. Late-Holocene glacier variations in the Cordillera Darwin, Tierra del Fuego, Chile. The Holocene 6, 353–358. https://doi.org/10.1177/095968369600600310

Lamy, F., Kilian, R., Arz, H.W., Francois, J.-P., Kaiser, J., Prange, M., Steinke, T., 2010. Holocene changes in the position and intensity of the southern westerly wind belt. Nat. Geosci. 3, 695.

Lifton, N., Smart, D.F., and Shea, M.A., 2008, Scaling time-integrated in situ cosmogenic nuclide production rates using a continuous geomagnetic model: Earth and Planetary Science Letters, v. 268, p. 190–201, doi:10.1016/J.EPSL.2008.01.021.

Lopez, P., Chevallier, P., Favier, V., Pouyaud, B., Ordenes, F., Oerlemans, J., 2010. A regional view of fluctuations in glacier length in southern South America. Glob. Planet. Change 71, 85–108. https://doi.org/10.1016/J.GLOPLACHA.2009.12.009

Luckman, B.H., 2000. The Little Ice Age in the Canadian Rockies. Geomorphology 32, 357–384. https://doi.org/10.1016/S0169-555X(99)00104-X

Mann, M.E., Zhang, Z., Rutherford, S., Bradley, R.S., Hughes, M.K., Shindell, D., Ammann, C., Faluvegi, G., Ni, F., 2009. Global signatures and dynamical origins of the Little Ice Age and Medieval Climate Anomaly. Science 326, 1256–60. https://doi.org/10.1126/science.1177303

Masiokas, M.H., Luckman, B.H., Delgado, S., Skvarca, P., Ripalta, A., 2009. Little Ice Age fluctuations of small glaciers in the Monte Fitz Roy and Lago del Desierto areas, south Patagonian Andes, Argentina. Palaeogeogr. Palaeoclimatol. Palaeoecol. 281, 351–362. https://doi.org/10.1016/J.PALAEO.2007.10.031

McCarthy, D.P., Luckman, B.H., Kelly, P.E., 1991. Sampling Height-Age Error Correction for Spruce Seedlings in Glacial Forefields, Canadian Cordillera. Arct. Alp. Res. 23, 451–455. https://doi.org/10.1080/00040851.1991.12002865

Mcculloch, R.D., Bentley, M.J., Tipping, R.M., Clapperton, C.M., 2005a. Evidence for late-glacial ice dammed lakes in the central strait of magellan and bahía inútil, southernmost south america. Geogr. Ann. Ser. A, Phys. Geogr. 87, 335–362. https://doi.org/10.1111/j.0435-3676.2005.00262.x

Mcculloch, R.D., Fogwill, C.J., Sugden, D.E., Bentley, M.J., Kubik, P.W., 2005b. Chronology of the last glaciation in central strait of magellan and bahía inútil, southernmost south america. Geogr. Ann. Ser. A, Phys. Geogr. 87, 289–312. https://doi.org/10.1111/j.0435-3676.2005.00260.x

Melkonian, A.K., Willis, M.J., Pritchard, M.E., Rivera, A., Bown, F., Bernstein, S.A., 2013. Satellite-derived volume loss rates and glacier speeds for the Cordillera Darwin Icefield, Chile. Cryosph. 7, 823–839. https://doi.org/10.5194/tc-7-823-2013

Mendoza, L., Perdomo, R., Hormaechea, J.L., Cogliano, D. Del, Fritsche, M., Richter, A., Dietrich, R., 2011. Present-day crustal deformation along the Magallanes-Fagnano Fault System in Tierra del Fuego from repeated GPS observations. Geophys. J. Int. 184, 1009–1022. https://doi.org/10.1111/j.1365-246X.2010.04912.x

Menounos, B., Clague, J.J., Osborn, G., Davis, P.T., Ponce, F., Goehring, B., Maurer, M., Rabassa, J., Coronato, A., Marr, R., 2013. Latest Pleistocene and Holocene glacier fluctuations in southernmost Tierra del Fuego, Argentina. Quat. Sci. Rev. 77, 70–79. https://doi.org/10.1016/J.QUASCIREV.2013.07.008

Miller, A., 1976. The Climate of Chile, in: Schwerdtfeger, W. (Ed.), World Survey of Climatology. Elsevier, Amsterdam, pp. 113–130.

Möller, M., Schneider, C., Kilian, R., 2007. Glacier change and climate forcing in recent decades at Gran Campo Nevado, southernmost Patagonia. Ann. Glaciol. 46, 136–144. https://doi.org/10.3189/172756407782871530

Moreno, P.I., Vilanova, I., Villa-Martínez, R., Dunbar, R.B., Mucciarone, D.A., Kaplan, M.R., Garreaud, R.D., Rojas, M., Moy, C.M., De Pol-Holz, R., Lambert, F., 2018. Onset and Evolution of Southern Annular Mode-Like Changes at Centennial Timescale. Sci. Rep. 8, 3458. https://doi.org/10.1038/s41598-018-21836-6

Moreno, P.I., Vilanova, I., Villa-Martínez, R., Garreaud, R.D., Rojas, M., De Pol-Holz, R., 2014. Southern Annular Mode-like changes in southwestern Patagonia at centennial timescales over the last three millennia. Nat. Commun. 5, 4375. https://doi.org/10.1038/ncomms5375

Moy, C.M., Dunbar, R.B., Moreno, P.I., Francois, J.-P., Villa-Martínez, R., Mucciarone, D.M., Guilderson, T.P., Garreaud, R.D., 2008. Isotopic evidence for hydrologic change related to the westerlies in SW Patagonia, Chile, during the last millennium. Quat. Sci. Rev. 27, 1335–1349. https://doi.org/10.1016/J.QUASCIREV.2008.03.006

Nelson, E.P., 1982. Post-tectonic uplift of the Cordillera Darwin orogenic core complex: evidence from fission track geochronology and closing temperature–time relationships. J. Geol. Soc. London. 139, 755–761. https://doi.org/10.1144/gsjgs.139.6.0755

Pedro, J.B., Bostock, H.C., Bitz, C.M., He, F., Vandergoes, M.J., Steig, E.J., Chase, B.M., Krause, C.E., Rasmussen, S.O., Markle, B.R., Cortese, G., 2016. The spatial extent and dynamics of the Antarctic Cold Reversal. Nat. Geosci. 9, 51–55. https://doi.org/10.1038/ngeo2580

Pohl, B., and Fauchereau, N., 2012, The southern annular mode seen through weather regimes: Journal of Climate, v. 25, p. 3336–3354.

Porter, C., Santana, A., 2003. Rapid 20th century retreat of Ventisquero Marinelli in the Cordillera Darwin icefield, in: Anales Del Instituto de La Patagonia. pp. 17–26.

Porter, S.C., Stuiver, M., and Heusser, C.J., 1984, Holocene sea-level changes along the Strait of Magellan and Beagle Channel, southernmost South America: Quaternary Research, v. 22, p. 59–67.

Putnam, A.E., Denton, G.H., Schaefer, J.M., Barrell, D.J.A., Andersen, B.G., Finkel, R.C., Schwartz, R., Doughty, A.M., Kaplan, M.R., Schlüchter, C., 2010. Glacier advance in

southern middle-latitudes during the Antarctic Cold Reversal. Nat. Geosci. 3, 700–704. https://doi.org/10.1038/ngeo962

Putnam, A.E., Schaefer, J.M., Denton, G.H., Barrell, D.J.A., Finkel, R.C., Andersen, B.G., Schwartz, R., Chinn, T.J.H., and Doughty, A.M., 2012, Regional climate control of glaciers in New Zealand and Europe during the pre-industrial Holocene: Nature Geoscience, v. 5, p. 627, https://doi.org/10.1038/ngeo1548.

Rabassa, J., Coronato, A., Bujalesky, G., Salemme, M., Roig, C., Meglioli, A., Heusser, C., Gordillo, S., Roig, F., Borromei, A., Quattrocchio, M., 2000. Quaternary of Tierra del Fuego, Southernmost South America: an updated review. Quat. Int. 68–71, 217–240. https://doi.org/10.1016/S1040-6182(00)00046-X

Rasmussen, L.A., Conway, H., and Raymond, C.F., 2007, Influence of upper air conditions on the Patagonia icefields: Global and Planetary Change, v. 59, p. 203–216, doi:10.1016/J.GLOPLACHA.2006.11.025.

Reynhout, S.A., Sagredo, E.A., Kaplan, M.R., Aravena, J.C., Martini, M.A., Moreno, P.I., Rojas, M., Schwartz, R., and Schaefer, J.M., 2019, Holocene glacier fluctuations in Patagonia are modulated by summer insolation intensity and paced by Southern Annular Mode-like variability: Quaternary Science Reviews, in press.

Rignot, E., Rivera, A., and Casassa, G., 2003, Contribution of the Patagonia Icefields of South America to Sea Level Rise: Science, v. 302, p. 434 LP – 437, doi:10.1126/science.1087393.

Rosenblüth, B., Fuenzalida, H.A., and Aceituno, P., 1997, Recent temperature variations in southern South America: International Journal of Climatology, v. 17, p. 67–85, doi:10.1002/(SICI)1097-0088(199701)17:1<67::AID-JOC120>3.0.CO;2-G.

Sagredo, E.A., Kaplan, M.R., Araya, P.S., Lowell, T. V., Aravena, J.C., Moreno, P.I., Kelly, M.A., Schaefer, J.M., 2018. Trans-pacific glacial response to the Antarctic Cold Reversal in the southern mid-latitudes. Quat. Sci. Rev. 188, 160–166. https://doi.org/10.1016/J.QUASCIREV.2018.01.011

Sagredo, E.A., Lowell, T.V., 2012. Climatology of Andean glaciers: A framework to understand glacier response to climate change. Glob. Planet. Change 86–87, 101–109. https://doi.org/10.1016/J.GLOPLACHA.2012.02.010

Schaefer, J.M., Denton, G.H., Kaplan, M., Putnam, A., Finkel, R.C., Barrell, D.J.A., Andersen, B.G., Schwartz, R., Mackintosh, A., Chinn, T., Schlüchter, C., 2009. High-frequency holocene glacier fluctuations in new zealand differ from the northern signature. Science (80-.). 324, 622–625. https://doi.org/10.1126/science.1169312

Schaefer, M., Machguth, H., Falvey, M., Casassa, G., Rignot, E., 2015. Quantifying mass balance processes on the Southern Patagonia Icefield. Cryosph. 9, 25–35. https://doi.org/10.5194/tc-9-25-2015

Schneider, C., Glaser, M., Kilian, R., Santana, A., Butorovic, N., Casassa, G., 2003. Weather Observations Across the Southern Andes at 53°S. Phys. Geogr. 24, 97–119. https://doi.org/10.2747/0272-3646.24.2.97

Sigafoos, R.S., Hendricks, E.L., 1969. The time interval between stabilization of alpine glacial deposits and establishment of tree seedlings. US Geol. Surv. Prof. Pap. 650, B89–B93.

Stern, C.R., 2008. Holocene tephrochronology record of large explosive eruptions in the southernmost Patagonian Andes. Bull. Volcanol. 70, 435–454. https://doi.org/10.1007/s00445-007-0148-z

Stokes, M.A., 1996. An introduction to tree-ring dating. University of Arizona Press.
Strelin, J., Casassa, G., Rosqvist, G., Holmlund, P., 2008. Holocene glaciations in the Ema Glacier valley, Monte Sarmiento Massif, Tierra del Fuego. Palaeogeogr. Palaeoclimatol. Palaeoecol. 260, 299–314. https://doi.org/10.1016/J.PALAEO.2007.12.002
Strelin, J., Iturraspe, R., 2007. Recent evolution and mass balance of Cordón Martial glaciers, Cordillera Fueguina Oriental. Glob. Planet. Change 59, 17–26. https://doi.org/10.1016/J.GLOPLACHA.2006.11.019
Stuiver, M., Reimer, P.J., Reimer, R.W., 2019. CALIB 7.1 [WWW program].
Thompson, D.W.J., Solomon, S., Kushner, P.J., England, M.H., Grise, K.M., Karoly, D.J., 2011. Signatures of the Antarctic ozone hole in Southern Hemisphere surface climate change. Nat. Geosci. 4, 741.
Van Daele, M., Bertrand, S., Meyer, I., Moernaut, J., Vandoorne, W., Siani, G., Tanghe, N., Ghazoui, Z., Pino, M., Urrutia, R., De Batist, M., 2016. Late Quaternary evolution of Lago Castor (Chile, 45.6°S): Timing of the deglaciation in northern Patagonia and evolution of the southern westerlies during the last 17 kyr. Quat. Sci. Rev. 133, 130–146. https://doi.org/10.1016/J.QUASCIREV.2015.12.021
Vanneste, H., De Vleeschouwer, F., Bertrand, S., Martínez-Cortizas, A., Vanderstraeten, A., Mattielli, N., Coronato, A., Piotrowska, N., Jeandel, C., Roux, G. Le, 2016. Elevated dust deposition in Tierra del Fuego (Chile) resulting from Neoglacial Darwin Cordillera glacier fluctuations. J. Quat. Sci. 31, 713–722. https://doi.org/10.1002/jqs.2896
Villa-Martínez, R., Moreno, P.I., Valenzuela, M.A., 2012. Deglacial and postglacial vegetation changes on the eastern slopes of the central Patagonian Andes (47°S). Quat. Sci. Rev. 32, 86–99. https://doi.org/10.1016/J.QUASCIREV.2011.11.008
Villalba, R., Lara, A., Masiokas, M.H., Urrutia, R., Luckman, B.H., Marshall, G.J., Mundo, I.A., Christie, D.A., Cook, E.R., Neukom, R., Allen, K., Fenwick, P., Boninsegna, J.A., Srur, A.M., Morales, M.S., Araneo, D., Palmer, J.G., Cuq, E., Aravena, J.C., Holz, A., LeQuesne, C., 2012. Unusual Southern Hemisphere tree growth patterns induced by changes in the Southern Annular Mode. Nat. Geosci. 5, 793.

* * *

4.3 Conclusions

The Dalla Vedova glacier advanced at least twice since the Last Glacial Maximum: at some time during the Last Glacial Termination, and at ~0.9 ka. The Last Glacial Termination advances, corresponding to one date at 17 ka and two dates at 13.5 ka, parallel recognized events across southern South America, namely the onset of the Last Glacial Termination and the Antarctic Cold Reversal, respectively. This reinforces the view that these points were times of major climatic significance across the region. The apparent Holocene glacier maximum at 0.9 ka is unusual in that it occurs during a period (the so-called "Medieval Climate Anomaly") when there is scarce evidence for glacier advances in southernmost South America.

While the LGT record appears to have precedent elsewhere in the literature, the latest Holocene maximum of the Dalla Vedova glacier does not have parallels on mainland Patagonia, although it may be synchronous with another glacier in the Cordillera Darwin. Additionally, late Holocene glacier maxima do not reflect the observed pattern of mid or early Holocene glacier maxima elsewhere in Patagonia. It is proposed that enhanced precipitation in the Cordillera Darwin—brought on by strengthened westerly circulation associated with the positive phase of the Southern Annular Mode—can explain glacier advances in Tierra del Fuego that occur out-of-phase with mainland Patagonia. Further differentiating Tierra del Fuego glaciers are differing sensitivities to climate changes than those in Patagonia, which—when combined with locally variable climate conditions—result in apparently out-of-phase behavior between the two regions.

* * *

Chapter 5 – Equilibrium-line reconstructions for Holocene glaciers in Patagonia and Tierra del Fuego, 46°-55°S

5.1 Introduction

This chapter presents a reconstruction of Holocene glacier equilibrium line altitudes (ELAs) for four sites across Patagonia and Tierra del Fuego. ELAs are reconstructed for Glaciar Torre (Chapter 3), the Dalla Vedova glacier (Chapter 4), Cerro Castillo (this chapter), and Río Tranquilo (Sagredo et al. 2016). A preliminary chronology of Holocene glacier advances is presented for Cerro Castillo. This chapter presents and evaluates several methods of ELA estimation and paleosurface interpolation, and discusses implications for the climate zonation of southernmost South America.

5.2 Framing the issue: The importance of ELA

The long-term recession of glaciers in the 20th and 21st centuries forms one of the key pieces of evidence for modern climate change (Dyurgerov and Meier, 2000; Zemp, 2008; Roe et al., 2016). A first-order relationship between glacier mass balance and climate—namely temperature and precipitation—allows for an association between glacier length and climate (Oerlemans, 2005; Andreassen et al., 2005). However, non-climatic factors condition the length response of individual glaciers to a uniform climate change, such as aspect, bed topography, and glacier hypsometry (Furbish and Andrews, 1984). Furthermore, tidewater or surging glaciers can exhibit length variations due to non-climatic dynamic factors internal to the glacier system (Meier and Post, 1987; Raymond, 1987). These factors complicate the use of past glacier extent to interpret paleoclimate, since a uniform climate change can provoke different length responses in different glaciers.

A common alternative metric to glacier length for the interpretation of climate changes is the *equilibrium line altitude (ELA)*, which denotes the averaged elevation on a glacier surface connecting all points where accumulation balances ablation (Oerlemans, 2001). As the ELA is defined by local mass and energy balance, ELA variations are due exclusively to climate, avoiding conceptual uncertainties inherent within the use of glacier length (Kuhn, 1989). Change in equilibrium line altitude (ΔELA, occasionally equated to "snowline change"; Benn and Evans, 2014) can therefore be used to compare climate changes between two glaciers, and therefore evaluate the spatial coherency of climate variability, past or present.

Past glaciers are commonly reconstructed to estimate paleo-ELAs as a means to extrapolate past climate (Porter, 1977; Leonard, 1989; Benn and Lehmkuhl, 2000; Hostetler and Clark, 2000; Hughes et al., 2006). The derivation of past steady-state ELA depends on two components (Benn et al., 2005): 1) delineation of past limits of glaciation, and 2) geometric interpolation of the past ice surface. Furthermore, to pin the ELA reconstructions in time, absolute chronologies for individual glacier highstands are required. A wide variety of methods have been utilized to address the second issue,

ranging in complexity from very simple geomorphic indices to models that integrate surface energy mass balance and glacier physics.

In the Southern Hemisphere midlatitudes, a key question facing paleoclimate researchers is the zonal symmetry or asymmetry of climate variations across the Pacific (Fletcher and Moreno, 2012). Paleoglacier studies in New Zealand and South America may be capable of addressing this question (e.g. Sagredo et al., 2018), but intercomparison between the regions is hampered by the different methods by which past glacier changes are evaluated. Paleoglacier studies in New Zealand have made extensive use of paleoglacier reconstructions and measures of ΔELA to interpret lateglacial and Holocene glacier advances (Porter 1975; Putnam et al., 2012; Kaplan et al., 2013). Studies in southernmost South America have instead used length variation alone to evaluate the magnitude of Holocene glacier length fluctuations (Kaplan et al., 2016; Reynhout et al., 2019).

An exception is Sagredo et al. (2016), who analyzed paleo-ELAs at four sites over the Andes for the last millennium glacial maximum. However, the lack of ELA reconstructions in southernmost South America restricted the conclusions that could be drawn from this dataset. Furthermore, while New Zealand glaciers are reconstructed using glacier flowline-based contouring of past glacier surfaces (Kaplan et al., 2010), Sagredo et al. (2016) use a different method of paleoglacier reconstruction than that which is used in New Zealand, in which paleosurfaces are reconstructed from a linear interpolation between paleoglacier limits. Sagredo et al. (2018) claim that this method is statistically indistinguishable from paleoglacier reconstructions based on manual contouring, but do not attempt further validation of their reconstructions.

New chronologies of Holocene glacier advances in southernmost South America—presented in this thesis—have yielded a population of dated glacier advances of known dimensions that spans the region. ELA reconstructions of these advances could be used to evaluate magnitudes of Holocene ELA change across the region, helping to evaluate the coherence of glacier response to South American climate change. ELA reconstructions would also permit a more robust intercomparison with the New Zealand glacier record.

This chapter aims to accomplish three goals: first, to assess the paleosurface reconstruction methodology outlined in Sagredo et al. (2016); second, to assess common methods of ELA reconstruction from paleoglaciers; and third, to reconstruct paleo-ELAs across southernmost South America. Validation of the paleosurface interpolation will be accomplished by comparing known modern glacier surfaces with glacier surfaces interpolated from the modern ice limit. ELA reconstructions are assessed by applying these methods to six glacier advances at Glaciar Torre (Reynhout et al., 2019) to check for logical consistency within and between each method. All ELA reconstruction methods are applied to four Holocene glacier chronologies spanning Patagonia and Tierra del Fuego to evaluate the magnitude of ΔELA associated with Holocene glacier advance in both regions.

5.3 Theoretical background

5.3.1 Definition of the equilibrium line altitude

The equilibrium line defined as a line on the glacier surface connecting all points where the glacier specific balance is equivalent to zero. As this point changes daily or even hourly, it is always to some extent a theoretical concept that implies a certain degree of averaging over a time period. The equilibrium line's position at the annual scale can be approximated by the transient snowline, which marks the limit between the last ablation season's snow and older snow/ice for temperate glaciers where superimposed ice is not a significant contributor to accumulation (Oerlemans, 2001). As this elevation can also vary interannually, depending on the local climate of the previous hydrological year, a more precise definition of more use for long-term climate study is the *steady-state ELA*, which is the average altitude at which B=0 for a glacier with zero net mass balance (Benn and Evans, 2014).

The steady-state ELA is of particular interest for paleoclimate studies utilizing past glacier extent. Glacial terminal or lateral moraines are often used to delimit the past glacier margin. Their age of stabilization marks the time at which net mass balance changed from dominantly positive to negative; that is, the time at which the past glacier mass balance was zero. The glacier's ELA at that time was therefore equivalent to the steady-state ELA.

Caution must be used when comparing past steady-state ELAs to modern ELAs extrapolated from direct observations of snowline or mass balance studies, as modern ELAs do not necessarily correspond to glaciers in a steady state. A glacier's morphometry does not respond immediately to climate change but is subject to a response time of 10^1-10^2 years until it achieves a new steady-state condition (Jóhannesson et al., 1989). The current phenomenon of global glacier retreat therefore implies that glaciers are adjusting to new equilibrium conditions, and the modern ELA is not characteristic of a steady-state glacier. Specifically, calculations of "steady-state" ELAs on modern glacier surfaces should *underestimate* the elevation of the modern, transient ELA.

5.3.2 Principles of paleoglacier surface interpolation

Some methods of ELA reconstruction, as well as more sophisticated paleoglacier models, require a reconstruction of the glacier surface at a particular time in the past. While geomorphology serves as a first-order control over glacier reconstructions, uncertainty cannot be avoided in surface reconstructions as independent verification of glacier height is generally absent for past glaciers.

Glacier surfaces are often reconstructed manually (Porter, 1975; Meierding, 1982; Kaplan et al., 2010), based on known ice limits and inferred glacier flow direction. The former ice extent is first defined, followed by an interpretation of past glacier flowlines. Contours are drawn perpendicular to flowlines, forming the basis of the ice surface reconstruction. This method has the benefit of allowing for a more detailed interpretation of past ice surfaces in the accumulation area, where no independent

control over ice topography exists but reasonable inferences can be made about the ice surface. This is particularly useful for glaciers with highly irregular topography in the accumulation area. However, the highly interpretive nature of the reconstruction makes quantification of error difficult.

Numerical models of ice thickness offer a physics-based approach to reconstruct past ice surfaces (Hulton et al., 1994; Oerlemans, 2001; Benn and Hulton, 2010), and in this sense such models offer a more robust alternative to manual reconstruction. Such models also involve different assumptions that may be difficult to quantify accurately. Some assumptions, such as those of perfect plasticity and basal shear stress being equal to driving shear stress, may not strictly apply to valley glaciers (Benn and Hulton, 2010). A necessary component for these models is also knowledge of subglacial topography of the past glacier.

It is important to note that methods of surface reconstruction based on past glacier flowlines and numerical models depend heavily upon knowledge of the underlying bed. Early flowline-based reconstructions (e.g. Sissons, 1974; Porter, 1975) were conducted for formerly-glaciated areas that are now completely or mostly free of ice cover. Important criteria, such as subglacial topography and geologic indicators of past flow direction, were therefore readily available; subsequent applications of these methods have also often used previously-glaciated catchments that are now ice-free (e.g. Kaplan et al., 2010; Kaplan et al., 2013). While for extensive former glaciers or ice caps subglacial topography can be reasonably inferred from present topography, paleoglacier reconstructions in currently-glaciated basins require knowledge of the modern glacier bed. This information is rarely available in remote locations. Furthermore, the subglacial topography associated with a glacier advance can be obscured by subsequent glacial modification of the former glacier bed.

An interpolation of past glacier surface based on control points offers another option for paleoglacier reconstruction. The sole inputs are a series of geomorphologically-determined points defining the past glacier margins; a geometric interpolation is then used to generate a surface connecting these points (Sagredo et al., 2016). Surface reconstruction therefore does not depend upon an *a priori* interpretation of ELA, interpreted flowline behavior, nor bed topography. The method also has the potential for automation, the only requisite inputs being an outline of the past glacier margin and surface information. While interpolation simplifies the complex topography of glacier surfaces, it simplifies the surface in a systematic way, producing less concave topography in the accumulation area and less convex topography in the ablation area. This method of reconstruction may therefore offer a viable alternative for glacier reconstruction in areas with well-constrained geomorphology and lacking in parameters necessary to confidently apply numerical models of ice thickness.

5.3.3 Methods of paleo-ELA reconstruction

Common methods of ELA reconstruction are summarized in Table 5.1 and are discussed below.

Table 5.1. Comparative overview of different methods of ELA reconstruction. Compiled in base of Meierding et al. (1982), Nesje (1992), Benn and Lehmkuhl (2000), Porter (2000), Benn et al. (2005), and Osmaston (2005).

Method	Description	Benefits	Limitations
Maximum elevation of lateral moraines (MELM)	The highest position of past lateral moraines of a glacier system	Rapid, purely evidence-based	Highly dependent upon geomorphic evidence available
Toe-to-headwall altitude ratio (THAR)	Obtained by applying an altitudinal ratio to the difference between the highest and lowest points of a glacier	Rapid, does not require	Does not account for glacier hypsometry; assumes temporally constant mass balance relationship
Accumulation-area ratio (AAR)	Uses an assumed ratio of accumulation:ablation area transposed to a reconstructed glacier surface	Better incorporates glacier hypsometry; no climate input necessary	Assumes fixed accumulation:ablation area ratio; no comprehensive treatment of mass balance
Area x altitude (AA)	Calculates the ELA as a function of the distribution of area over elevation, assuming BR = 1	Easily calculable given an interpolated surface.	Assumes a uniform balance ratio (unrealistic for most glaciers).
Area x Altitude Balance Ratio (AABR)	Calculates the ELA as a function of the distribution of area over elevation with a balance ratio	More realistically accounts for altitudinal changes in balance gradient. Allows for "tuning" of reconstructed glaciers to account for regional variability via the balance ratio.	Sensitive to choice of balance ratio (preexisting information regarding mass balance necessary). Modern balance ratio not necessarily representative of past balance ratios
Area x Altitude Balance Index (AABI)	Calculates the ELA as a function of the distribution of area over elevation, with altitudinally-variable mass	Better represents glaciers with nonlinear balance ratios (debris-covered glaciers, avalanche-fed glaciers)	Very sensitive to input model of mass balance distribution. Modern balance ratio not necessarily representative of past conditions.

5.3.3.1 Maximum elevation of lateral moraines (MELM)

On any glacier, ice flow moves inward from the ice margins in the accumulation zone, while in the ablation zone ice flows towards the margins. Flow of ice towards the glacier limit results in the deposition of debris at the ice margin in the form of lateral/frontal moraines throughout the ablation zone; deposition ceases at the equilibrium line. In an ideal glacier environment of total preservation, the maximum elevation of lateral moraines (MELM) marks the position of the equilibrium line associated with the glacier that formed said moraine (Benn et al., 2005).

This method is rapid and simple to ascertain with modern images and elevation products, requiring only geomorphologic interpretation. Indeed, this method is least dependent upon assumptions regarding past glacier morphology or mass balance and is in this sense the least prone to parametrization errors. However, moraines are subject to immediate degradation by paraglacial modification as a glacier retreats from its moraine-forming position, as well as geomorphic constraints on their formation, which would result in lower estimated values relative to the true paleo-ELA. Furthermore, continuous deposition of moraines as a glacier recedes upvalley may confound

geomorphic interpretation, possibly resulting in higher estimated values if recessional moraines are misidentified as terminal moraines (Nesje, 1992). MELM is therefore considered less reliable than other methods (Meierding, 1982).

5.3.3.2 Toe-to-headwall altitude ratio (THAR)

This method assumes that the steady-state ELA achieves a "characteristic" elevation defined as a fraction of the elevational range of the glacier. ELA is calculated as a product of this range, defined as the difference between highest and lowest elevations of the glacier, and a ratio representing the relative elevation of the ELA on a glacier. Meierding (1982) suggested a ratio of 0.35-0.4 to best represent past ELAs in the Colorado Front Range.

Toe and headwall elevations are very simple to determine (although the unknown past upper limit of glaciers may introduce significant error). In addition, this method does not suffer from uncertainties related to surface interpolation. However, like the accumulation-area ratio, this method does not account for heterogeneities in glacier geometry, and suffers when applied to glaciers without an uncomplicated, linear distribution of elevation (Nesje, 1992).

5.3.3.3 Accumulation-area ratio (AAR)

Meier (1962) defined the accumulation-area ratio as the amount of area within the accumulation zone divided by the total area of the glacier. Assuming a glacier in steady-state has a characteristic AAR, this value can be applied to a reconstructed glacier surface to determine the past ELA (Meier and Post, 1962; Meierding, 1982). This is usually accomplished visually by applying the ratio to a cumulative histogram of reconstructed glacier area. Studies using this method on temperate glaciers usually adopt an AAR value of between 0.5-0.8, most frequently a value near 0.65, for paleo-ELA reconstruction (Porter, 1975; Meierding, 1982; Kaplan et al., 2010; Sagredo et al., 2016).

This method benefits from a more rigorous consideration of the altitudinal distribution of area on a glacier and does not assume mass balance gradients when applied to paleoglaciers. However, the method is subject to error introduced by complicated glacier geometry (Nesje, 1992); hence, the method works best for relatively simple glacier geometries. The lack of dependence on a mass balance gradient may oversimplify the relationship between mass balance and elevation (Osmaston, 2005), instead depending heavily upon the chosen AAR. Lastly, like all reconstructions involving geometric reconstructions, the AAR method is subject to errors in surface interpolation, which may be difficult to quantify.

5.3.3.4 Area-Altitude (AA), Area-Altitude Balance Ratio (AABR), and Area-Altitude Balance Index (AABI)

The area-altitude balance ratio (AABR) and area-altitude balance index (AABI) methods derive from the area-altitude (AA) method, which weights elevation above and below a

trial elevation, iteratively solving for the ELA using different trial ELA values (Sissons, 1974; Osmaston, 2005). As it assumes a perfectly linear relationship between elevation and mass balance it does not require an explicit treatment of mass balance gradients; however, this likely is unrealistic, as accumulation and ablation gradients tend to differ (e.g. Mayo, 1984).

The AABR method uses the same iterative methodology as the AA, additionally incorporating a balance ratio (BR; ratio between the ablation and accumulation gradient; Oerlemans and Hoogendoorn, 1989) to account for differential ablation and accumulation gradients (Osmaston, 2005). The unitless ratio, while based on local climate, does not strictly require explicit foreknowledge of climate to be used, and can also be run "backwards" on modern glaciers to derive an unknown balance ratio. The AABI (Osmaston, 2005) allows for an even more careful articulation of mass balance by applying a custom profile of mass balance vs. elevation to the glacier surface. This allows for improved modeling of nonlinear accumulation or ablation gradients (e.g. debris-covered or avalanche-fed glaciers, Benn and Lehmkuhl, 2000).

A major issue with the implementation of the area-altitude methods to paleoglaciers is the heavy dependence upon the choice of balance ratio. While the balance ratios of modern glaciers can be constrained by field data or climate modeling, using balance ratios derived from modern climate to reconstruct past glaciers runs the risk of circularity, as the objective of paleoglacier reconstruction is often to derive past climate. This procedure also assumes a constant balance ratio throughout geologic time, which is dubious particularly for the climate of the Last Glacial Maximum (LGM).

Where a large number of paleoglaciers of known age exist, a subjective evaluation of ideal AABR can be determined by calculating paleo-ELA with varying balance ratios for each glacier. The balance ratio that results in the lowest root-mean squared error (RMSE) across the reconstructed glaciers represents the "best" value for this advance (Osmaston, 2005). Where a dense network of well-constrained glacier chronologies does not exist, however, an assumed value must be used.

5.4 Study area

Four glaciers with directly-dated Holocene advances in southern Patagonia and Tierra del Fuego were selected for reconstruction (Figure 5.1). In this section, salient points of each glacier chronology are detailed, and an unpublished preliminary chronology of glacier fluctuations at PN Cerro Castillo is presented.

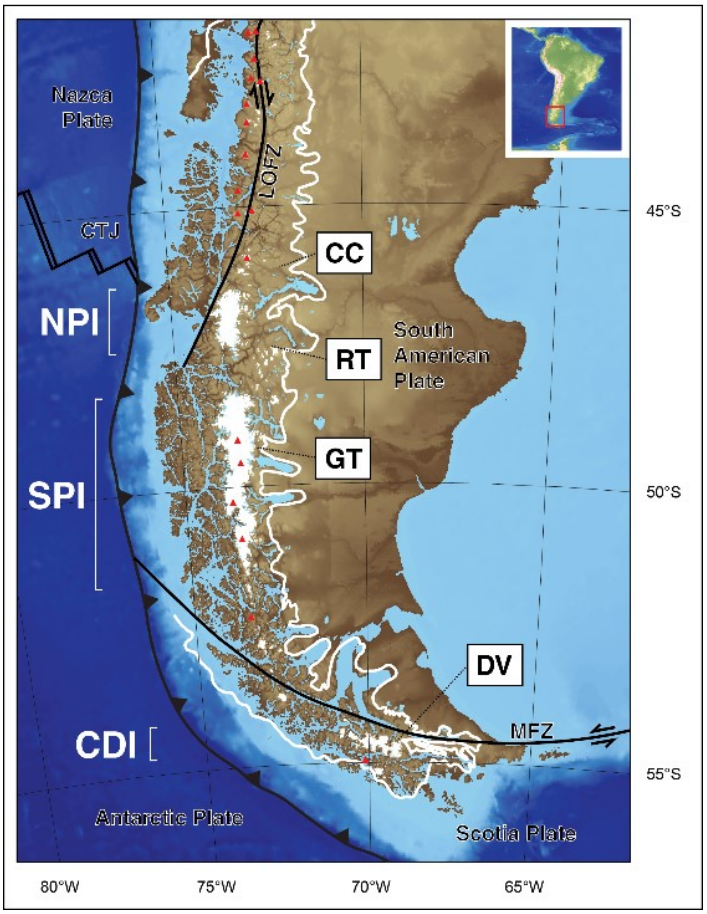

Figure 5.1. Sites evaluated in this text. CC = Cerro Castillo, RT = Río Tranquilo, GT = Glaciar Torre, DV = Dalla Vedova. Note that RT is a glacial system studied in Sagredo et al. (2016) and (2018).

5.4.1 Cerro Castillo (46.1°S)

The "Castillo" glacier (46.07°S / 72.20°W; CL111503019 in the Chilean Inventario Nacional de Glaciares) is a 1.1 km² mountain glacier on the south face of Cerro Castillo, in the National Park of the same name. It is currently land-terminating, although a salient feature of the site is the pronounced proglacial lake and distal overdeepening, which is found more than 200 m below the currently hanging glacier margin (Figure 5.2 a, b).

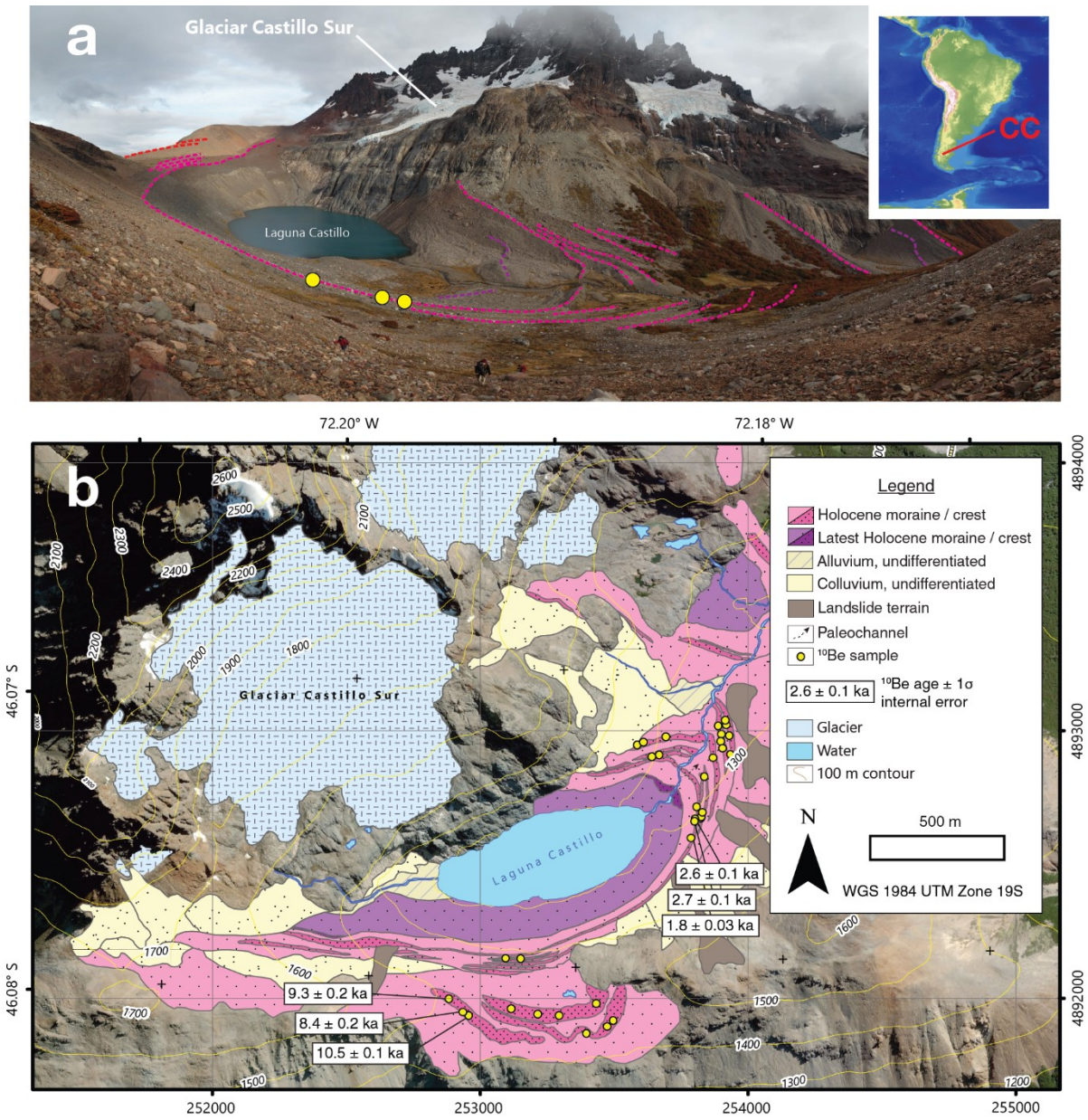

Figure 5.2. a) Photo of the Cerro Castillo study area, view to the north (location in inset). b) Glacial geomorphologic map of Cerro Castillo. The "J6" moraine is the innermost Holocene moraine (outside of the inferred "Latest Holocene" limit) with cosmogenic surface exposure ages of 2.7-1.8 ka. The "V1" moraine is the outermost Holocene moraine with cosmogenic surface exposure ages of 10.6-8.4 ka.

The past ice extent of the Castillo glacier is constrained by no fewer than eight frontal-lateral moraines in the study area. Two broad, low-relief (~1-5 m) moraine sets are found on a shoulder opposite the overdeepened proglacial lake, at an elevation of 1400-1500 m amsl. The ice limit defined by these moraines can be traced down valley along the side of the southern valley wall, where they transition into an intermittently exposed trimline to approximately 1300 m amsl (Figure 5.2b). A series of at six low-relief (~2-10 m), sharp-crested moraines are found inboard of these moraines. The innermost of these moraines is laterally continuous along the southern slope of the valley, while the five more distal moraines are intermittently continuous along the southern valley slope but become well-defined crests down valley. The inner six moraines remain closely spaced throughout the

valley, with a maximum separation between innermost and outermost moraines of not more than 300 m in the frontal moraine section.

Glacial geomorphic mapping and sample collection for cosmogenic dating was carried out in January 2016 and April 2019. Six samples were processed at the Lamont-Doherty Earth Observatory following procedures outlined in the preceding chapters, yielding Holocene ages for all the moraines (Table 5.2).

Table 5.2. Geographical and analytical data for samples processed for cosmogenic dating. We assume a sample density of 2.7 g/cm³ for the granodioritic samples. Carrier concentration is 1045 ppm. (*) AMS ratios are presented as boron-corrected values measured against the 07KNSTD3110 standard material ($^{10}Be/^{9}Be=2.85\times10^{-12}$; Nishiizumi et al., 2007). Ratios are not corrected for background ^{10}Be in procedural blanks. (†) = ^{10}Be concentrations in this column are corrected for background ^{10}Be as recorded by the procedural blanks associated with each sample set, the concentrations of which ranged from 6.0734×10^{-16} to 7.6323×10^{-16} atoms/g.

Moraine	Sample	CAMS lab no.	Lat. °	Lon. °	Elevation m amsl	Thickness cm	Shielding	Mass g	Be carrier g	$^{10}Be/^{9}Be$ (10^{-14})*	^{10}Be 10^{4} atoms/g†	Age yr BP	1σ yr BP
V1	CCA16-01-01	BE42004	-46.0809	-72.1961	1474	0.77	0.965	10.0256	0.1815	9.5934 ± 0.20680	12.053 ± 0.2605	9270	200
	CCA16-01-05	BE42005	-46.0815	-72.1952	1461	1.19	0.965	10.0684	0.181	10.0827 ± 0.20312	13.517 ± 0.2543	10530	200
	CCA16-01-06	BE42006	-46.0814	-72.1955	1466	1.77	0.965	10.1974	0.1812	8.7376 ± 0.23233	10.768 ± 0.2869	8410	220
J6	CCA16-01-02	BE42013	-46.0752	-72.1839	1289	1.5	1	59.5523	0.1816	13.7812 ± 0.32367	29.189 ± 0.0686	2620	60
	CCA16-01-03	BE42014	-46.0758	-72.1841	1306	1.79	1	58.744	0.1817	9.4649 ± 0.17596	20.282 ± 0.0379	1800	30
	CCA16-01-04	BE42015	-46.0753	-72.1839	1293	1.54	1	57.5746	0.1821	13.9158 ± 0.25827	30.573 ± 0.0568	2740	50

Ages for the outermost moraine, the upper "V1" moraine, range from 10,500 ± 200 yr BP to 8410 ± 220 yr BP. Collectively, they define an early Holocene maximum for the Castillo glacier. From the innermost "J6" moraine, three ages were obtained, at 2740 ± 50 yr BP, 2620 ± 60 yr BP, and 1800 ± 30 yr BP. The two older ages overlap at 2-sigma, but given the small sample size these ages are considered collectively to represent a late Holocene glacier advance. No direct age control yet exists for the six intermediate moraines, but they are morphostratigraphically constrained as between the early Holocene and late Holocene.

The glacier highstand associated with the outermost upper V1 moraine was not considered in this analysis, due to the lack of geomorphic control on ice extent on the northern side of the valley and valley bottom. Instead, the innermost J6 moraine was used to define the past late Holocene ice surface at Cerro Castillo. Due to the tight spacing between the J6 moraines and the five moraines distal (often less than the resolution of the digital elevation model used to extract elevation), the reconstructed J6 ice surface is assumed to be representative of these five distal moraines, of presumable late- to mid-Holocene age.

5.4.2 Río Tranquilo (47.5°S)

The Río Tranquilo glacier system has been described and dated using ^{10}Be cosmogenic surface exposure dating in Sagredo et al. (2016) and Sagredo et al. (2018), although most chronological control to date deals with the pre-Holocene record preserved at the site. At

present, modern ice consists of at least eight separate glaciers (total area ~10 km^2) that, in the past, united to form a single ice body. Paleo ice limits are constrained by tall, prominent lateral and frontal moraines dating to the lateglacial (18-11.7 ka). Holocene advances are defined by a minimum of four tightly-spaced, sharp-crested lateral moraines (5-10 m separation at minimum) that reach the modern outwash plain; frontal moraines for the Holocene are largely absent, but can be reasonably interpolated by considering the lowest elevation of the corresponding lateral moraines.

The "RT4" moraine of Sagredo et al. (2018) was used to reconstruct the ice surface at c. 13.7 ka, allowing for a direct intercomparison of Río Tranquilo with Glaciar Torre at this time (see 5.4.3). Furthermore, the site was visited in November 2016 for detailed mapping and sample collection from the Holocene moraine system. The mapping carried out in the field and through photointerpretation allowed for the definition of the third-most distal Holocene ice limit, associated with a glacier highstand at c. 5500 yr BP (Sagredo et al., 2016). This advance was used to reconstruct the ice surface. Similar to Cerro Castillo, it is assumed that due to the tight spacing of the Holocene moraines (sometimes less than the resolution of the digital elevation model used to extract elevation), this reconstruction is characteristic of other undated Holocene advances. It must be stressed that the lack of strong control over the terminal position represents a significant uncertainty associated with this reconstruction.

5.4.3 Glaciar Torre (49.3°S)

Seven dated advances exist at Glaciar Torre (~50 km^2), at c. 17.1 ka, 13.5 ka, 9.7 ka, 6.9 ka, 6.1 ka, 4.5 ka, and 0.5 ka (Reynhout et al., 2019). Each advance corresponds to a well-defined frontal-lateral moraine system, allowing for detailed delineations of each dated glacier highstand. All seven glacier extents are therefore reconstructed. Given that the spacing between Holocene moraines is considerably larger than those at Cerro Castillo or Río Tranquilo (max. 1.5 km), paleoglacier reconstructions at this site alone will allow for an evaluation of the chronological evolution of Holocene ELA depression. ELA reconstructions at this site also provide constraints for the extensive glacier chronology developed at Lago Argentino (50°S; Strelin et al., 2014; Kaplan et al., 2016). There, former outlet lobes advanced in tandem with some advances recorded at Glaciar Torre, but are too complicated for the simplified ELA reconstructions performed in this chapter.

As the site with the most complete chronology included in this chapter, Glaciar Torre is used as the reference site for intercomparisons between methods of ELA reconstruction. Glaciar Torre is therefore considered separately from the other chronologies in the results and discussion.

5.4.4 Dalla Vedova (54.5°S)

One dated glacial advance of the Dalla Vedova glacier (~55 km^2) occurred at 0.9 ka (Chapter 4), corresponding to the prominent "H1" latero-frontal moraine. A younger advance is recorded by the less-prominent "H2" moraine system; dendrochronologic constraints limit the age of this advance to between ~0.13 ka and 0.9 ka. Separation

between these two moraines does not exceed 200 m; the H1 moraine is therefore assumed to be representative of the ice extent associated with the H2 moraine, and is used to delineate past glacier extent for the existing Holocene record.

5.5 Methods

5.5.1 Definition of past ice limits

Former ice margins were defined for dated paleoglacier extents based on field geomorphologic mapping of the four study areas. Dated terminal moraines and associated glacier trimlines were the primary landforms used for ice limit definition, although in areas where there was no distinctive sign of glaciation (e.g. cliffs, recent talus-covered slopes), a series of rules were applied that guided definition:

- Modern ice margins were first drawn based on photointerpretation. Past ice margins were defined in base of latero-frontal moraines or glacier trimlines, or interpolation where no geomorphic limits are available. For instance, for the LGM advance of the Torre glacier—where few trimlines or moraines have been preserved in the Fitz Roy valley—the LGM ice limit was mapped at the change of slope between ice-sculpted bedrock and the steeper sidewalls of the valley.
- Past ice margins were defined up to the modern ELA, approximated by the lower limit between snow and ice at the end of the ablation season. Above this ELA, in the modern accumulation area, ice limits were not changed for subsequent ice limit mapping.
- Interpolated past ice margins must cross contours upwards with distance upvalley; that is, the reconstructed ice margins must define the outline of a surface that plunges downvalley. This is in keeping with the physical principle that ice flows in the direction of ice surface slope (Cuffey and Paterson, 2010).
- Past ice margins defining one glacier advance must not cross other past ice margins, unless clear geomorphic evidence exists that older ice limits were overrun by subsequent advances.
- Ice elevations must correspond from one side of the valley to the other, using modern contours as a guide.

Ice limits were defined in ESRI ArcGIS based on geomorphologic mapping, aerial photos, and contours generated using the JAXA/METI ALOS PALSAR high-resolution, radiometrically terrain corrected digital elevation models (12.5 m resolution DEM). Ice limits were defined as polygons representing the former ice extent at the time of interest (Figure 5.3). Polygon vertices were converted to points and z-values were added based on the ALOS PALSAR DEM values of elevation.

5.5.2 Interpolation and analysis of interpolation methods

Surfaces are interpreted using a natural-neighbor (also known as nearest neighbor, NN) interpolation implemented in ESRI ArcGIS (Sibson, 1981; Childs, 2004). This interpolation weights known values by the proportionate area around an interpolation point. Input values are then weighted by the proportional overlap between the

interpolation polygon and the polygons representing each input value to produce the interpolated value. The result is a smoothed surface strongly related to local data points that neither infers trends nor produces values outside the sample range. Applied to past ice reconstruction, this method is a poor choice for ice features poorly coupled to topography (such as ice domes or ice sheets). However, the method may be effective when applied to valley glaciers, where past ice dimensions can be constrained by geomorphic and topographic limits.

Natural-neighbor interpolation simplifies topography between reference points, introducing error. Other interpolation methods are available in ArcGIS, such as the closely related inverse distance weight (IDW) method, which differs principally in using the distance between points (as opposed to proportional area) to weight input values. More sophisticated geostatistical procedures, such as spline and krige methods, are also available, although it is unclear whether these methods provide advantages over NN interpolation.

To evaluate the suitability of NN interpolation relative to the other tools available, the NN interpolation and two variations each of IDW, krige, and spline interpolation were used to construct synthetic glacier surfaces of the modern Torre glacier. The mean elevation difference between each synthetic surface was calculated to evaluate the magnitude and sign of biases associated with interpolation methods. To evaluate the fidelity of NN-interpolated glacier surfaces relative to an actual glacier surface, NN interpolation between modern glacier limits was used to construct a synthetic glacier surface for all four sites. ELAs were then calculated for both the known, DEM-based glacial surface and the synthetic glacier surface to assess the effect NN interpolation may have on a complex surface.

5.5.3 Paleo-ELA calculation

Paleo-ELAs are calculated using the MELM, THAR, AAR, AA, and AABR methods for dated advances in the Holocene.

MELM

Maximum elevations of lateral moraines at Glaciar Torre and the Dalla Vedova glacier are determined via photointerpretation of aerial imagery. Once the maximum height of a lateral moraine is encountered, the point is projected onto a 12.5 m × 12.5 m ALOS PALSAR digital elevation model (DEM) to extract the elevation.

THAR

For THAR calculation, modern upper ice limits are identified via photointerpretation and are assumed to have been nonvarying through time; lower ice limits are determined as the lowest point on the reconstructed ice surface. Elevations are determined by projection onto an ALOS PALSAR 12.5 m DEM. An altitude ratio of 0.4 is applied to the difference between highest and lowest points to calculate the THAR following Meierding (1982) and (Wright and Porter, 1983).

AAR

Paleoglacier surfaces are constructed by applying nearest-neighbor interpolations to predefined glacier extents (see 5.5.1 and 5.5.2). Hypsometric curves of the interpolated ice surfaces are created to evaluate AAR. These are created by clustering the rasterized interpolated surface into 10-m altitudinal bins and computing a cumulative histogram of elevation above each bin. An AAR of 0.65 is adopted for cross-comparison with other studies that have used a similar value (Meier and Post, 1962; Meierding, 1982; Kaplan et al., 2013; Sagredo et al., 2016). The altitude at which the intersect between the hypsometric curve and AAR=0.65 was identified as the ELA for the specified reconstruction.

AABR

Implementation of the AABR utilizes the same paleosurface reconstructions used for the AAR. Elevation is binned into 100-m "belts," to be applied to the spreadsheet-based iterative solver outlined in Osmaston (2005). A crude sensitivity analysis of the choice of balance ratio was performed by calculating the AABR for both the global average value of 1.75 (Rea, 2009) along with the globally averaged mid-latitude maritime value of 2.0 (Furbish and Andrews, 1984).

Calculation of ΔELA

Derived paleo-ELAs are then compared to two modern values—one calculated using each method of ELA determination, and another derived from satellite imagery—to yield ΔELA. "Calculated" modern ELAs are determined by applying each respective method to a DEM corresponding to the modern ice limit. Ice limits were drawn according to photointerpretation of modern ice using Sentinel-2 and DigitalGlobe imagery; these limits were used to clip the ALOS PALSAR base DEM, which provides a DEM representing the modern ice surface. "Measured" modern ELAs were estimated from satellite imagery based on the principle that end-of-season snowline roughly approximates the interannual ELA of a glacier (Oerlemans, 2001). Snowlines were drawn demarcating the interpreted limit between snow and glacier ice for Sentinel-2 multispectral images acquired from February-April 2019. These lines were converted to points and z-values were assigned from the ALOS PALSAR DEM; average values were calculated, along with the standard deviation, to yield a range of probable modern ELAs.

5.6 Results

5.6.1 Definition of past ice limits

Defined ice limits for the modern glacier extent, as well as those used for paleoglacier reconstruction, are given in Figure 5.3.

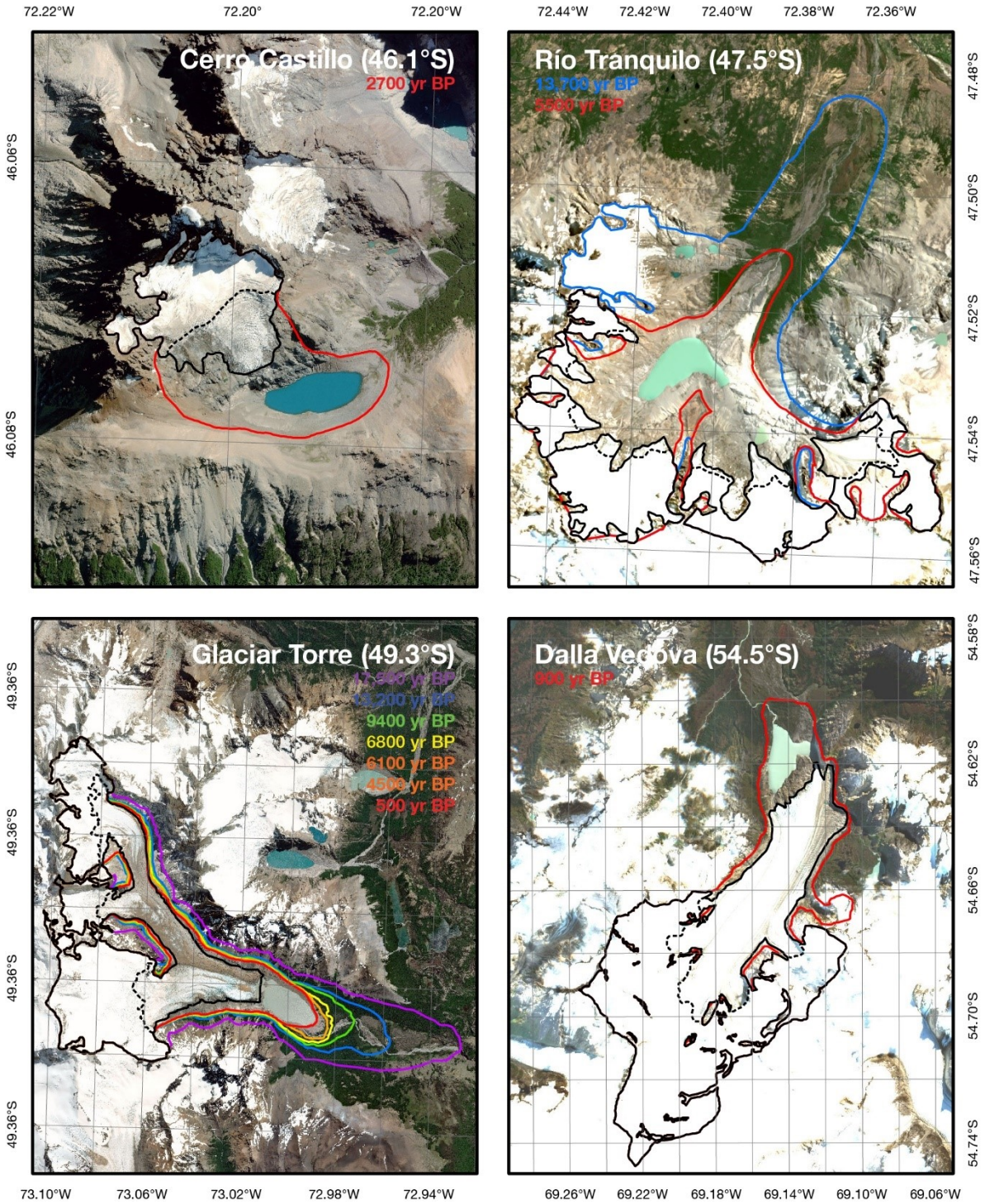

Figure 5.3. Reconstructed paleoglacier limits from the four study areas. Modern ice limits defined in black; paleo ice limits are color coded based on age (indicated in figure). Modern ELA estimated from satellite imagery is marked as a dashed line.

5.6.2 Analysis of interpolation methods

Natural neighbor interpolation, along with two iterations each of IDW, krige, and spline methods, was used to interpolate a surface based on the modern limits of Glaciar Torre. Results of this exercise are presented in Table 5.3. The difference between each

interpolated surface and the known surface was calculated to evaluate the skill of the chosen method. Error is reported as the average of the total pixel differences in meters, with positive values indicating overestimation of interpolated values and negative values indicating underestimation. The arithmetic mean of the absolute difference between the interpolated and reference surface is preferred to the more standard root-mean squared error in this context, as understanding interpolation bias towards over- or underestimated values is important for paleoglacier reconstruction.

Table 5.3. Comparison of interpolation methods for the modern Torre glacier. Average difference is calculated based on the pixel difference between the interpolated DEM and the ALOS PALSAR DEM defining the ice surface; positive (negative) average difference therefore indicates that the interpolation overestimated (underestimated) the ice surface.

Method	Points	Notes	Average diff. (m)	Stdev (m)	Max. (m)	Min. (m)
Natural Neighbor	-		35	68	386	-187
IDW	24	Standard circular search, 1000 m radius	42	143	663	-631
IDW (Geostatistical Analyst)	24	Circular 8-sector search, 1000 m radius	57	101	465	-297
Ordinary kriging	24	Spherical semivariogram, variable search radius	39	140	674	-606
Empirical Bayesian kriging	24	Power semivariogram, circular 8-sector search, variable radius	22	82	440	-191
Spline without barriers	24		-29	213	1380	-1253
Spline with barriers	-		17	70	359	-214

Spline interpolation with barriers produces the lowest average difference from the reference surface, followed by empirical Bayesian kriging (EBK) and then NN interpolation. This result suggests that the more sophisticated interpolations may better replicate the variable topography of the glacier surface; spline interpolation's fitted surface through the input points may be well-suited for mimicking the concave profile of cirque glaciers. However, the average differences between NN, EBK, and spline (barriers) methods do not exceed one standard deviation, differing from each other by no more than 20 m. These methods are therefore considered statistically indistinguishable, and to maintain consistency with previous ELA studies in Patagonia (Sagredo et al., 2016; 2018), NN interpolation is used for all following ELA reconstructions.

Differences between the NN-interpolated surface and the actual glacier surface are distributed unequally along the modern Torre glacier. Maximum deviation occurs in the accumulation area (Figure 5.4), specifically in segments of the glacier that exhibit a great deal of concavity. NN interpolation produces a more planar surface than the reference surface, resulting in a "filling" of concave topography above the equilibrium line. Conversely, NN will "plane off" convex glacier surfaces (Figure 5.5), underestimating surface elevation in the ablation area, although this effect is probably less significant than the effect above the equilibrium line. Interpolation overestimation therefore is biased towards high altitudes.

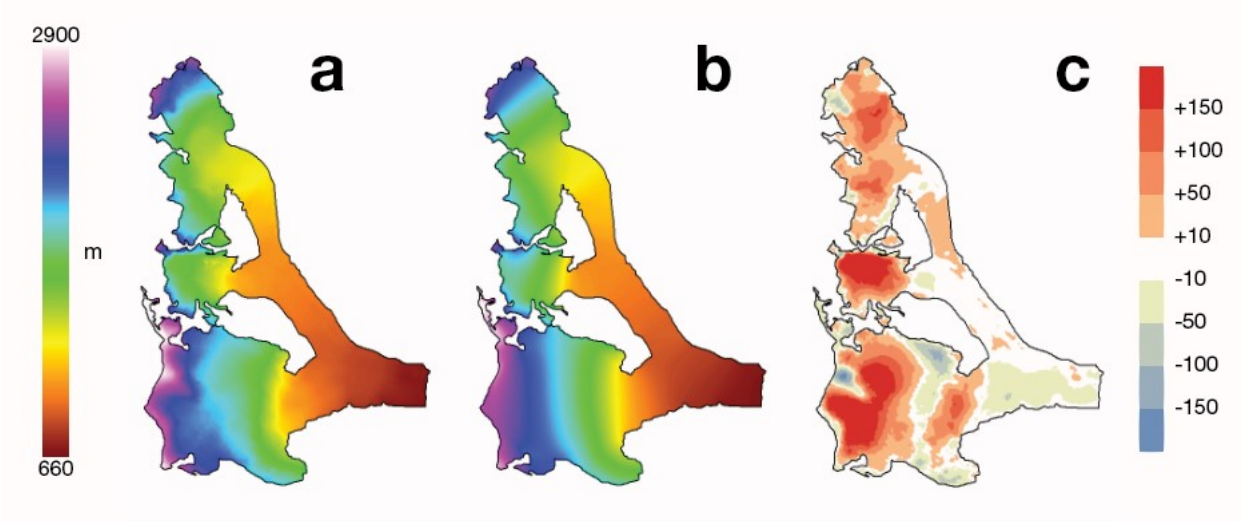

Figure 5.4. a) Digital elevation model of the Torre glacier using the ALOS PALSAR DEM. b) Interpolated ice surface based on the natural neighbor interpolation applied to the glacier outline. c) absolute difference in meters between the interpolated ice surface and the actual ice surface. "Warm" colors indicate areas where the interpolation has overestimated the ice surface.

5.6.3 Effects of interpolation bias on ELA reconstructions

To evaluate the influence that interpolation error has on paleoglacier reconstructions, synthetic glacier surfaces were constructed by applying NN interpolation to modern glacier outlines of all four study glaciers. Hypsometric curves for each surface were generated, and ELA was then calculated using the AAR and AABR methods for both the synthetic glacier surfaces and the known surfaces, as these are the two methods affected by the choice of interpolation (Figure 5.5).

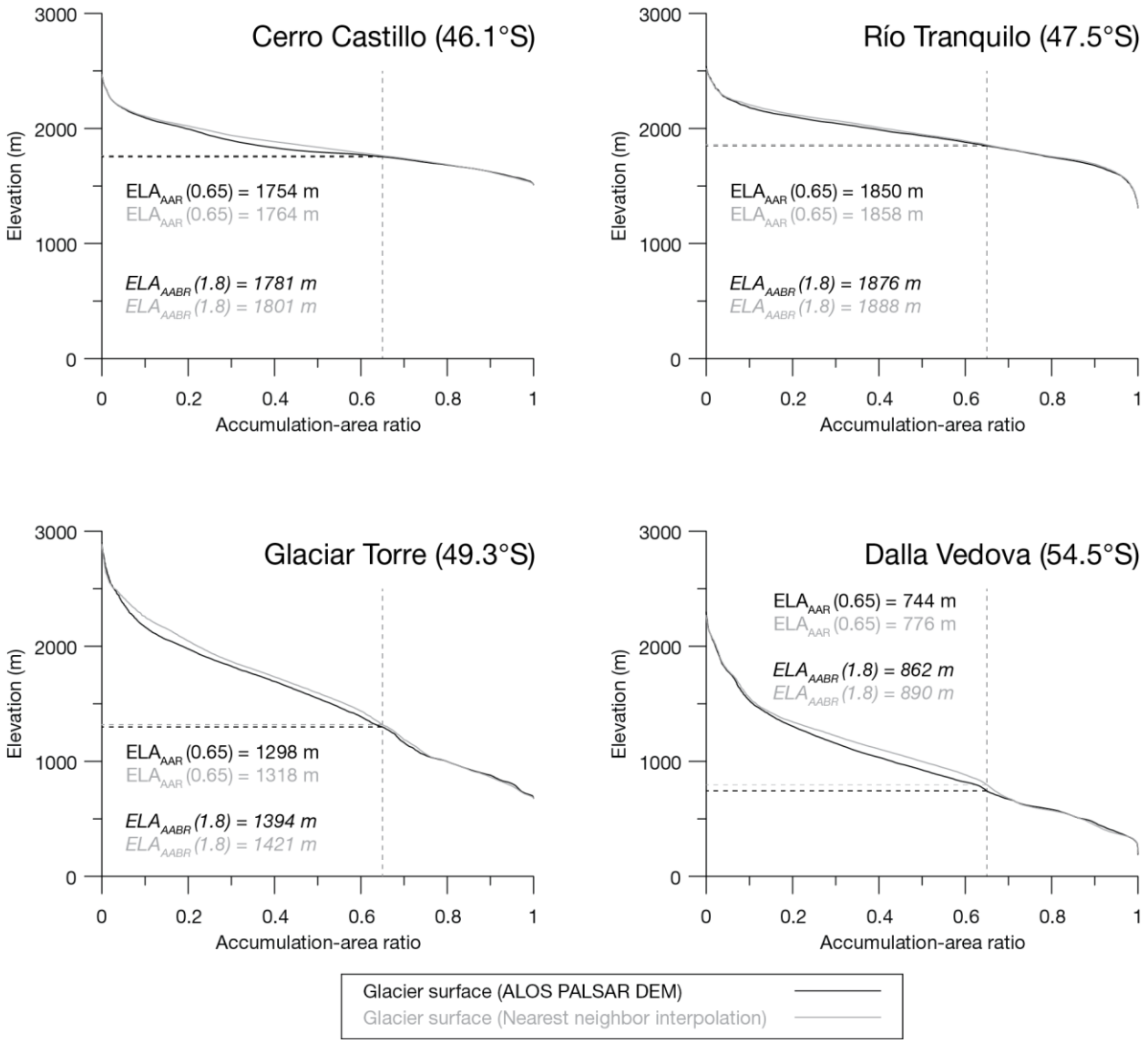

Figure 5.5. Cumulative hypsometric curves of modern glaciers (black curves) and synthetic modern glacier surfaces constructed using NN interpolation. AAR ELAs were calculated for real and synthetic surfaces using these curves and an assumed ratio of 0.65. AABR ELAs are also presented for real and synthetic surfaces.

The interpolated surface consistently overestimates the elevation of the glacier surface in upper half of each glacier; this phenomenon is most pronounced at Glaciar Torre and Dalla Vedova, but is present at each site. This has the effect of producing anomalously high ELA estimates for the interpolated surfaces, which would result in anomalously low ΔELA when applied to past glaciers. Despite the rather large absolute differences between the modern and interpolated surfaces observed at Torre glacier, the ELA derived from both methods does not differ by more than ~30 m at any site. This is similar to the assumed error of 20-50 m for flowline-based reconstructions in New Zealand (Kaplan et al., 2010; Putnam et al., 2012).

5.6.4 Reconstructed ELAs in southernmost South America

Past glacier surfaces are reconstructed using nearest-neighbor interpolation; reconstructions at Glaciar Torre are illustrated in figure 5.6. Reconstructed ELAs for dated moraines at the four study sites by five methods of reconstruction—as well as measured and reconstructed modern ELAs—are given in table 5.4. Hypsometric curves used for calculation of AAR are shown in figure 5.7.

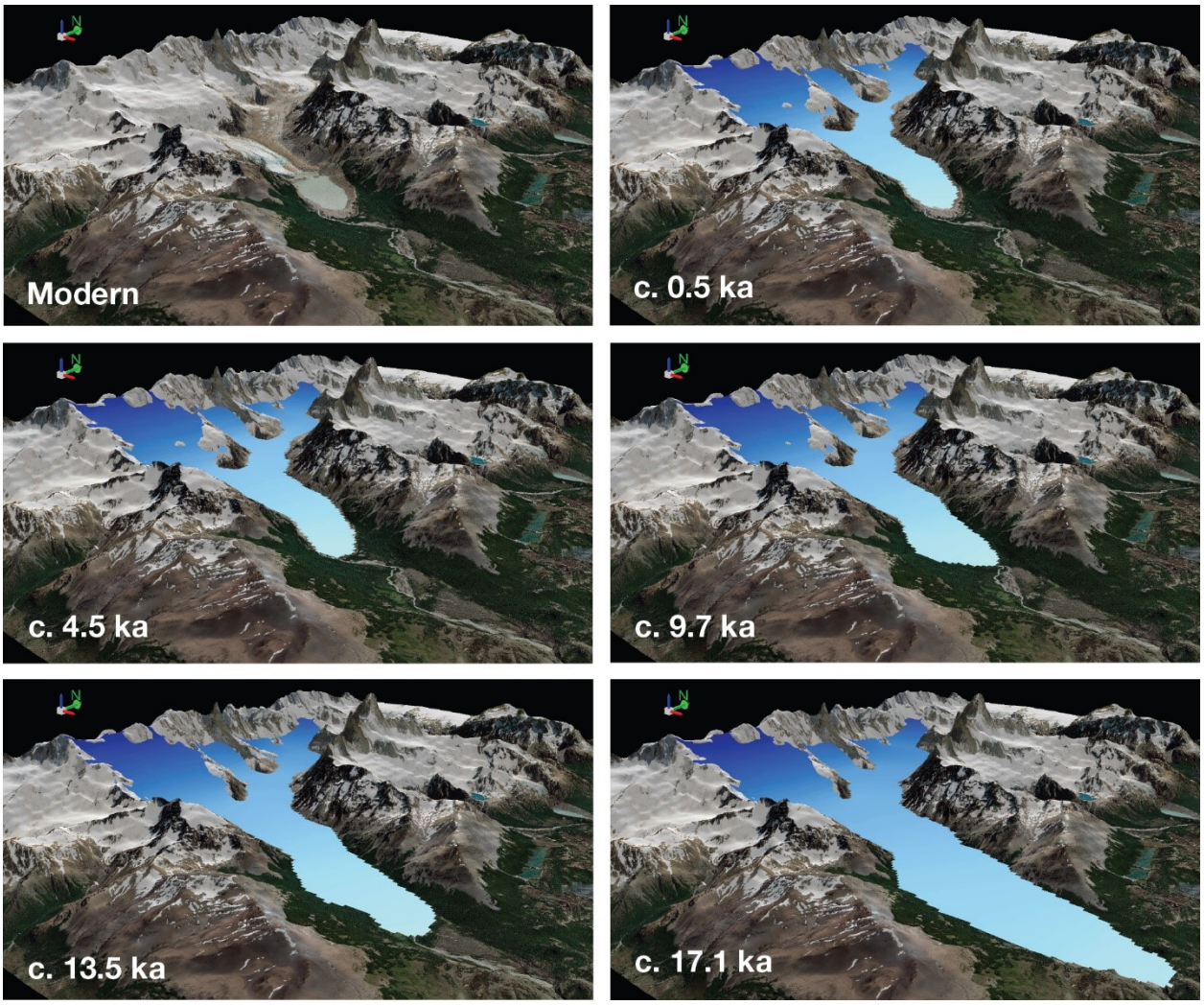

Figure 5.6. Reconstructed paleoglacier surfaces at Glaciar Torre for 5 of the 7 dated glacier advances from Reynhout et al. (2019). Note the "clipping" of modern topography by the paleoglacier surface in the accumulation area of the glacier; this represents underestimation of the past glacier surface by the nearest-neighbor interpolation (e.g. figure 5.4c).

Table 5.4. Observed and calculated ELAs for modern and dated moraines across the four study sites. Ages for Río Tranquilo from Sagredo et al. (2016) and Sagredo et al. (2018); however, the Río Tranquilo paleoglacier was newly reconstructed for each glacial stage.

Site	Age	Observed	ΔELA (m)					
	yr BP		MELM	THAR	AAR (0.65)	AA	AABR (2)	AABR (1.75)
Cerro Castillo (46.1°S)								
Modern	0	1750 ± 10	-	1883	1750	1822	1771	1781
J6	2300	-	1613	1752	1560	1675	1610	1621
Rio Tranquilo (47.5°S)								
Modern	0	1720±100	-	1804	1835	1923	1864	1876
H3	5500	-	1482	1521	1635	1764	1661	1681
RTV4	13,700		1006	1465	1585	1654	1533	1557
Glaciar Torre (49.3°S)								
Modern	0	1410±80	-	1542	1290	1517	1371	1399
M7	500	-	1192	1542	1125	1484	1332	1360
M4b	4500	-	1195	1544	1105	1469	1319	1347
M4a	6100	-	1195	1544	1105	1469	1319	1347
M3	6900	-	1200	1533	1100	1460	1310	1337
M2	9400	-	1179	1519	1110	1440	1291	1318
M1	13,200	-	1204	1504	1100	1409	1261	1282
M0	17,500	-	799	1504	1170	1387	1253	1278
Dalla Vedova (54.5°S)								
Modern	0	770±50	-	1012	715	956	840	862
H1	900	-	729	938	650	923	798	821

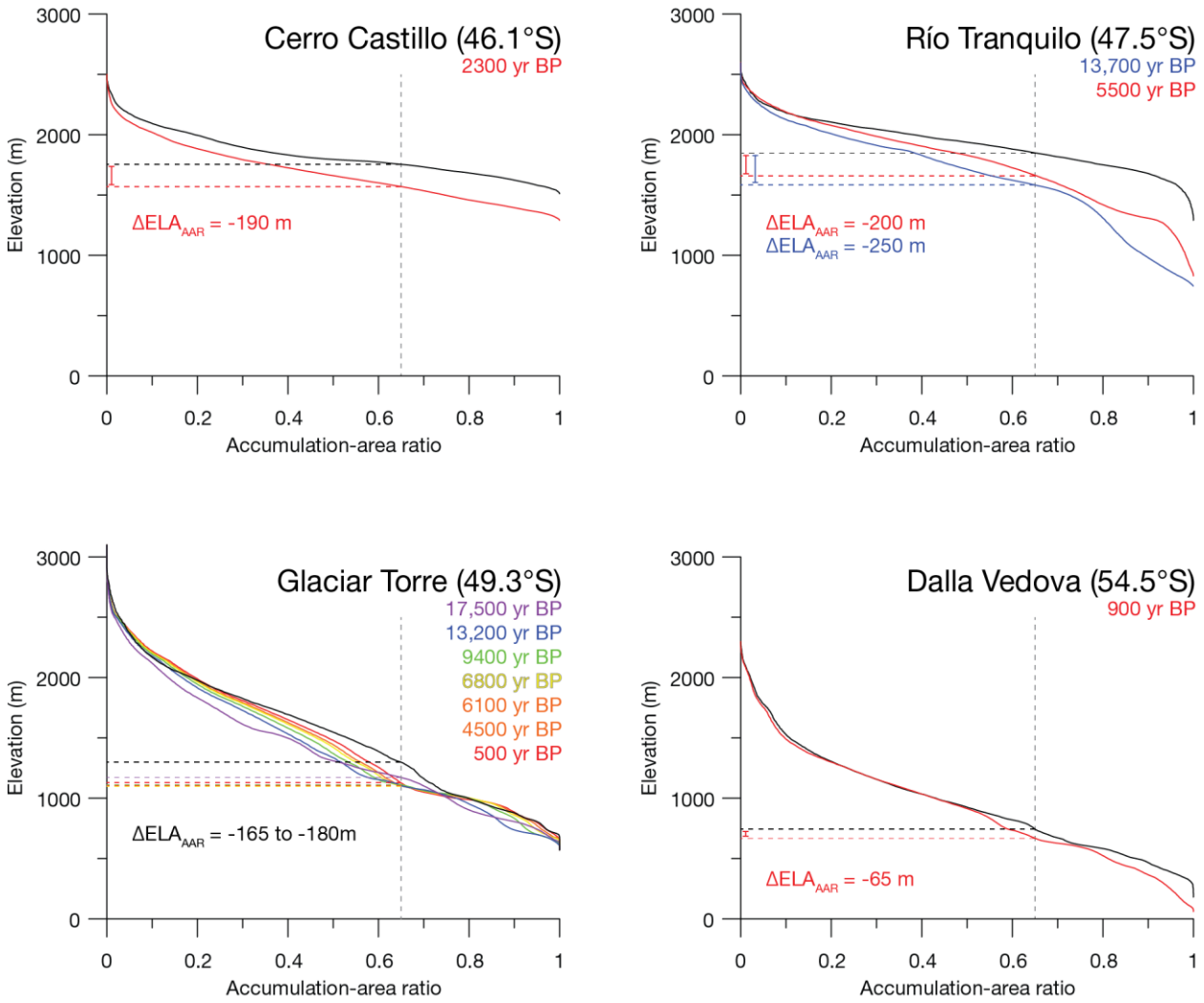

Figure 5.7. Graphic demonstrating AAR reconstruction of paleo-ELA and calculation of ΔELA for the four study sites. Black line represents the modern glacier surface as a cumulative hypsometric curve relative to proportional elevation above a reference point. Colored lines indicate the same, but for the reconstructed surface pertaining to the glacial advance in colored text. Modern and paleo-ELAs are calculated based on an assumed AAR of 0.65; ΔELA is calculated as the difference between modern and prehistoric ELAs as calculated by this method.

5.6.5 Intercomparison of paleo-ELA calculations at Glaciar Torre

Reconstructed ELAs for all seven dated glacier advances at Glaciar Torre are converted to ΔELA by subtracting either the measured modern or reconstructed modern ELA from each reconstructed value. Figure 5.8 presents the results of ΔELA reconstructions for all seven dated advances of Glaciar Torre plotted against time.

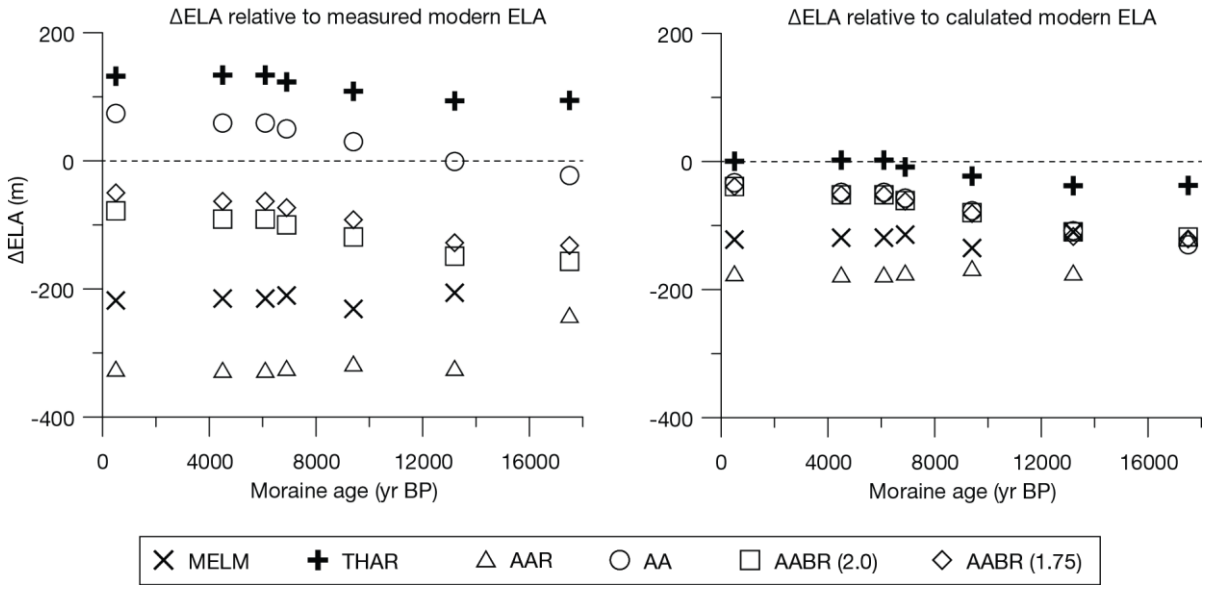

Figure 5.8. ΔELA of Glaciar Torre moraines calculated by subtracting calculated paleo-ELAs from the measured modern ELA (left) or each method's calculated modern ELA (right). Note that the MELM ΔELA for the 17,800-year moraine is not shown, as it falls below the minimum ΔELA value.

Relative to the measured modern ELA, ΔELA varies greatly depending on the method used to calculate paleo-ELA. Two methods, the THAR and the AA, deliver paleo-ELAs *higher* than the observed modern ELA. Most methods yield lower ΔELA values between 0 and -200 m when relative to each method's calculated modern ELA, although the THAR still yields slightly positive values for the Holocene. Of all methods, the AABR (1.75) minimizes the difference between the calculated modern and measured modern ELAs, with a difference of 11 m. The AAR results in the greatest difference between calculated modern and the reference modern ELA (Table 5.4).

The method of ELA calculation also affects the existence of temporal trends. The area-altitude methods (AA and AABR), as well as the THAR, show a rising trend in ELA since the late-glacial. On the other hand, the AAR and MELM methods show no such trends, and indicate an equivalent ΔELA values for each dated advance over the last 13,000 years. Furthermore, while the MELM predicts a 500-600 m ELA depression for the 17,500 yr BP glacier advance, the AAR predicts a relative *increase* in ELA relative to later, less-extensive glacier advances. This is likely a methodological issue with AAR interpolation on complex topography (Nesje 1992, see discussion).

5.6.6 Paleo-ELA calculations across southernmost South America

ΔELA values for Holocene glacier advances in the four studied sites—determined as the difference between the calculated modern ELA and the paleo-ELA—are given in table 5.5. These values are used in the discussion, following the methodology of Sagredo et al. (2016, 2018).

Table 5.5. ΔELAs from four study sites. ΔELA is calculated as the calculated modern ELA estimated by each method minus the paleo-ELA for the glacier reconstruction of the dated glacier limit indicated in the site code, except for the

MELM, which is calculated based on the modern measured ELA. CC = Cerro Castillo, RT = Rio Tranquilo (Sagredo et al. 2016), GT = Glaciar Torre, DV = Dalla Vedova.

Site	Age (yr BP)	ΔELA (m)					
		MELM	THAR	AAR (0.65)	AA	AABR (2)	AABR (1.75)
CC J6 (46.1°S)	2700	-140	-130	-190	-147	-161	-160
RT H3 (47.5°S)	5500	-240	-280	-200	-159	-203	-195
RT RTV4	13,700	-720	-340	-250	-269	-331	-319
GT M7 (49.3°S)	500	-220	0	-165	-33	-39	-39
GT M4b	4500	-220	0	-185	-48	-52	-52
GT M4a	6100	-220	0	-185	-48	-52	-52
GT M3	6900	-210	-10	-190	-57	-61	-62
GT M2	9400	-230	-20	-180	-77	-80	-81
GT M1	13,200	-210	-40	-190	-108	-110	-117
GT M0	17,500	-610	-40	-120	-130	-118	-121
DV H1 (54.5°S)	900	-40	-70	-65	-33	-42	-41

For all reconstruction methods, the greatest Holocene ΔELA occurred at Río Tranquilo (RT; 47.5°S). Considering only the AAR, AA, and AABR methods, Holocene ΔELA was greater in the two northern sites (46.1°S and 47.5°S) compared to the more southern sites (49.3°S and 54.5°S), although the magnitude of this difference strongly depends on the choice of method—AAR yields a mid-Holocene difference in ΔELA of 15 m between Glaciar Torre and Río Tranquilo, while the area-altitude methods give a difference up to an order of magnitude higher.

Other differences in ΔELA across the region depend largely on the choice of ELA reconstruction. At the Dalla Vedova glacier of Cordillera Darwin (DV; 54.5°S), reconstructed ΔELA for the Holocene was smaller than the reconstructed ΔELA at either Cerro Castillo or Río Tranquilo for all methods save the THAR. Dalla Vedova ΔELA is smaller than the latest Holocene (M7) reconstruction at Glaciar Torre when calculated by the MELM and AAR methods; on the other hand, ΔELA is equivalent between the two regions at this time when calculated using the AA or AABR methods, and is greater at Dalla Vedova using the THAR.

5.7 Discussion

ΔELA values vary greatly depending on the method chosen to calculate paleo-ELA. This greatly complicates the climatic interpretation of ΔELA variations across southernmost South America, as the distribution of ΔELA across Patagonia also varies with the method. Before discussing the results, a brief consideration of the relative robustness of

ELA reconstructions is warranted. Both the THAR and AA produced unreasonable ΔELAs when compared to the measured modern ELA (Table 5.4). These methods are not considered further in the discussion, while MELM is treated as a maximum approximation of ΔELA (paleo-ELA should be *higher* than indicated by MELM) and the AAR and AABR ΔELAs are treated as minimum approximations (paleo-ELA should be *lower*).

This discussion will discuss ΔELA values derived from the AAR, as well as the AABR method, so as to allow for a direct comparison with other AAR-based reconstructions throughout the Southern Hemisphere. However, the robustness of AAR-based ΔELA values are called into question by the anomalous results given by AAR reconstruction at Glaciar Torre. This methodological issue is discussed with lateglacial ΔELAs, followed by Holocene ΔELAs and their spatial variability. The discussion concludes with a consideration of systematic uncertainties, and an evaluation of the AAR and AABR methods for future use.

5.7.1 Lateglacial ELA depression at Glaciar Torre

ELA reconstructions at Glaciar Torre indicate ELA depression of ~120 m by both the AAR and AABR methods (Table 5.5). This value is similar to the modeled ELA depression of 160 m for the Southern Patagonian Icefield (SPI) during the LGM at 50°S (Hulton et al., 1994). However, this value differs considerably from their estimated 560 m ELA depression at 40°S, the 900 m LGM ELA depression between 45°-48°S by Hubbard et al. (2005), the 290 m ELA depression at 47°S in the Andean rain shadow (Wolff et al., 2013), and the nearly 1000 m LGM ELA depression in New Zealand (43°-45°S; Porter 1975, Putnam et al. 2013). Furthermore, the AAR-calculated ELA depression is less than that associated with subsequent advances, an impossibility under normal circumstances.

Several scenarios are considered to explain this anomalous result. The first explanation is that lateglacial climate near the SPI favored limited ELA depression. Hulton et al. (1994) explain the relatively small value of LGM ELA depression at 50°S as a consequence of reduced precipitation, provoked by a northerly migration of the westerly wind belt. Precipitation would be further diminished east of the ice divide due to an enhanced rain shadow effect. However, climate alone is cannot explain values of lateglacial ELA depression that are *less* than Holocene values (Kaplan et al., 2013; Sagredo et al., 2016) and, in the case of the AAR, inverted.

A second explanation is that the chosen AAR and AABR values are not representative of the lateglacial Torre glacier. This could be due to either topographic or climatic effects. Glaciar Torre has a concave-up profile, and while marked lateral expansions of the glacier during the lateglacial and Holocene occurred, each expansion reached a similar elevation (Figure 5.6). Meanwhile, these advances also corresponded to substantial vertical gains in surface elevation, resulting in a glacier that became “taller” without a corresponding change in minimum elevation. Application of the AAR to this glacier

would result in anomalously low values of ΔELA, which are compounded by the tendency of concave-up glaciers to underestimate ΔELA (Nesje 1992).

Thomson et al. (2010) proposed that glacial cycles were characterized by widespread cold-based ice beneath large swathes of the ancestral SPI based on trends in long-term exhumation. If this was the case for the last glacial cycle, it would imply that the chosen temperate midlatitude values for the AABR may not be applicable to Glaciar Torre during the lateglacial. Assuming higher AABR values results in higher estimations of past ΔELA, but forms a somewhat circular argument; additionally, little evidence exists to support the assumption of a higher AABR for cold-based glaciers (Rea, 2009), or even if the AABR is an appropriate method for evaluating ELA on such glaciers.

Isostatic rebound could also be a potential confounding factor at Glaciar Torre. ELA reconstructions assume glaciers exist in a fixed environment with zero uplift or subsidence. If the topography supporting Glaciar Torre were depressed during the LGM, seemingly low AAR-derived ΔELA values (Table 5.5) could be explained as reflecting a much greater ELA depression imposed upon a previously sunken surface. If isostatic rebound has affected glacier reconstructions at this site, then estimated ELAs by any method will underestimate ΔELA. Near the Southern Patagonian Icefield, modern rates of viscoelastic isostatic uplift in response to present ice unloading reach upwards of 30 mm/yr (Lange et al., 2014). This has been explained as a result of the opening of a slab window beneath the SPI circa 10 Ma (Breitsprecher and Thorkelson, 2009; Dietrich et al., 2010), which raises the possibility that isostatic depression during the LGM may have affected the interpretation of paleo-ELA at Glaciar Torre. An unrecognized glacio-isostatic effect would particularly affect Glaciar Torre, which is immediately adjacent to the icefield and is very near the zone of modeled maximum viscoelastic response to ice unloading (Lange et al., 2014).

Finally, while it is assumed that the early lateglacial ΔELA_{AAR} of -120 at Glaciar Torre is erroneous, it is also possible that the subsequent values of ΔELA_{AAR} over the Holocene are in error. This would help reconcile the significant differences in Holocene ΔELA_{AAR} and ΔELA_{AABR}, but is considered improbable given the consistency between Holocene ΔELA_{AAR} estimates. The preferred explanation invokes a combination of the aforementioned climatic, topographic, and isostatic factors that produced the anomalously low values of c. 17 ka ΔELA at Glaciar Torre. This value is therefore considered an outlier and not used further in this analysis, and warrants caution when interpreting ΔELA_{AAR} at this site.

Later in the lateglacial period, the M1 advance at Glaciar Torre (13,200±500 yr BP) corresponded to an AAR-derived ELA depression of ~190 m. This ELA depression and age is statistically indistinguishable from the AAR-derived 200±20 m ELA depression that accompanied the ~13,700±500 yr BP RT4 advance at Río Tranquilo (Sagredo et al., 2018), and may suggest a coherent glacier response to a similar climate change between 47°-50°S in Patagonia.

5.7.2 Holocene ELA depression across southernmost South America

While none of the dated Holocene advances in the four sites overlap, the advances at Cerro Castillo and Río Tranquilo are both part of more extensive, tightly-spaced moraine complexes of inferred Holocene age. Some of these moraines are separated by less than 10 meters in parts, which is less than the resolution of the DEM used to match elevation to the paleo-ice limits. It is therefore likely that the calculated ΔELAs for the dated advances at Cerro Castillo, Río Tranquilo, and Dalla Vedova represent close approximations of the ΔELAs of these associated advances and are therefore characteristic of ELA depression during glacial highstands throughout the Holocene.

Measured by the AAR, glaciers in Patagonia (excluding DV, in Tierra del Fuego) advanced at varying times in response to Holocene ELA depressions of 165-200 m. This range of ΔELA is only slightly lower than the -160m ΔELA_{AAR} of the "last millennium maximum" (LMM) glacier advance at Río Tranquilo, as well as other glacier advances across South America (Sagredo et al., 2016). Patagonian ΔELA_{AAR} is also consistent with Holocene snowline depressions of 140-250 m in New Zealand (Putnam et al., 2012; Kaplan et al., 2013). Despite the differences in latitude between Patagonia and New Zealand, as well as differences in the timing of individual advances, glaciers appear to have advanced in response to ELA depressions that were similar in magnitude over the Holocene.

On the other hand, the Dalla Vedova glacier's LMM glacier advance corresponded to a much smaller ELA depression than that which is registered by glaciers further north (ΔELA_{AAR} = -65 m). Measured relative to Cerro Castillo and Río Tranquilo, this difference is consistent across all methods (Table 5.5), suggesting the phenomenon is not a methodological artifact. Smaller Holocene ΔELA values in at the Dalla Vedova glacier could indicate several scenarios in terms of climate. On the one hand, less Holocene ELA lowering in Tierra del Fuego could indicate that glacier advances in the region corresponded to climate variability of a different nature, or lesser magnitude, than the climate variability experienced in Patagonia. On the other hand, if there is a systematic difference in glacier sensitivity to climate change between Tierra del Fuego and Patagonia, a similar climate forcing across the region could result in differential glacier response.

Sagredo et al. (2014) demonstrated that glaciers in Tierra del Fuego are slightly less sensitive to a uniform change in temperature than those in Patagonia. Assuming the observed increase in temperature in southern South America over the last several decades applies uniformly across the region (Rosenblüth et al., 1997; Carrasco et al., 2002; Rasmussen et al., 2007), recent warming will have resulted in less ELA change in Tierra del Fuego than in Patagonia. As our record shows reduced ΔELA in the Tierra del Fuego, differences in glacier sensitivity across the region may be in part responsible for the observed regional differences in Holocene ΔELA.

5.7.3 Systematic uncertainties

Ice limit delineation is subject to mapping error, which affects all methods. This can arise from poorly interpreted geomorphology or errors in the extrapolation of ice limits where direct evidence for glacier extent is not present. Geomorphologic factors will also directly affect the MELM, which—via paraglacial degradation of moraines—will tend to yield lower elevations than the paleo-ELA. This results in an *overestimation* of ΔELA for the MELM method. The resulting ice limits are also subject to DEM error during the assignment of elevation; Shawky et al. (2019) estimated a vertical RMSE of ~5 m for the ALOS PALSAR 12.5m DEM, evaluated in a mountainous environment.

An example of the impact differences in delineation may have are the calculated ΔELAs at Río Tranquilo. ΔELA for the 13,700 advance was calculated using the AAR method (0.67) by Sagredo et al. (2018), who recorded a modern ELA of 1815 m amsl and a paleo-ELA of 1615 m amsl (ΔELA = -200 m). However, the reconstruction in this chapter using almost identical methodology (AAR=0.65, ALOS PALSAR elevation model instead of SRTM) yielded a modern ELA of 1835 m amsl and a paleo-ELA of 1585 m amsl (ΔELA = -250 m; Table 5.4). This difference cannot be explained solely by the choice of AAR and is therefore most likely due to differences in paleoglacier delimitation.

Elevation biases in surface interpolation, or the interpolation method chosen, will have no effect over the solely elevation-dependent indexes (MELM, THAR), nor the AAR, as redistribution of elevation in the accumulation area does not affect the cumulative area at the ELA. The modeled positive bias in the accumulation area (Figure 5.5) will, however, affect the area-altitude methods by placing more relative area in elevation bins with higher net mass balance. This will yield an anomalously high estimated ELA relative to the actual, resulting in *underestimated* ΔELAs for area-altitude reconstructions using linearly interpolated glacier surfaces. AA and AABR-derived ΔELAs should therefore be considered minimum approximations.

All ELA reconstructions assume a glacier is in steady state when it reaches its local limit. Given ongoing glacier recession, modern measured ELAs likely do not represent the steady state ELA and are likely higher than the theoretical steady-state ELA corresponding to a glacier's instantaneous morphology. This should result in more negative values of ΔELA than the real difference. Therefore, higher-than-present paleo-ELAs (such as the THAR and the AA; Figure 5.6) likely indicate faulty assumptions behind the methods. The AA, for instance, assumes a balance ratio of 1, which is likely unrepresentative of the modern distribution of mass balance at Glaciar Torre (Popovnin et al., 1999; De Angelis, 2014). Assuming a larger balance ratio (via the AABR) yields a more realistic result. However, this dependence of both the AABR and the AAR on user-specified ratios to derive ELA is another weakness, although in the case of the AABR the choice of ratio does not appear to significantly affect results (Table 5.4).

Finally, ELA derivations themselves are prone to uncertainty. The AAR method is prone to systematic error when glacier surface topography is not constant. Nesje (1992) demonstrated that glaciers with a concave longitudinal bed profile *underestimate* ΔELA, whereas glaciers with a convex profile overestimate ΔELA. This phenomenon likely

influenced the anomalous ΔELA associated with the 17,500-year advance at Glaciar Torre (Table 5.4 and Figure 5.6).

5.7.4 Evaluation of nearest-neighbor interpolation and ELA reconstruction

In spite of the uncertainties with regard to both surface interpolation and ELA reconstruction, both the nearest-neighbor glacier surface interpolation and the AAR/AABR methods show promise.

Nearest-neighbor interpolation of modern glacier surfaces results in systematic differences of calculated ΔELA similar to those assumed with flowline-based glacier reconstructions. The method is suitable for locations where past glacier margins are well-defined but past subglacial topography is not available due to glacial cover or glacial/paraglacial alteration of the past glacier bed. In such cases, the method possesses a slight advantage over flowline-based glacier reconstructions in that it can be applied to paleoglacier systems that are still extensively glaciated with fewer assumptions about bed topography. Additionally, the method lends itself well to automation and is more replicable than manual flowline-based definition, with the only necessary inputs being the past glacier margin and topography.

At Cerro Castillo and Río Tranquilo, Holocene AAR and AABR values are reasonably consistent with each other and correspond well to previously published estimates (Sagredo et al., 2016). At Dalla Vedova in Tierra del Fuego, AAR and AABR values differ significantly from values reported at Cerro Castillo and Río Tranquilo; the consistency between AAR and AABR estimations at Dalla Vedova suggest that this difference is valid, and reflects a fundamental difference in past climate and/or glacier climate sensitivity between the two regions. However, the persistent difference in ΔELAs calculated by the AAR and AABR methods remains a major concern. While at Cerro Castillo, Río Tranquilo, and Dalla Vedova this difference does not exceed 30 m for Holocene paleoglaciers, at Glaciar Torre the difference is between 100-125 m over the same time scale.

Choice of ΔELA reconstruction at Glaciar Torre therefore has important implications for the interpretation of the data. If ΔELA_{AAR} is preferred, the ELA depressions at Glaciar Torre throughout the Holocene are like those found elsewhere in Patagonia and around the world. However, if ΔELA_{AABR} is used instead, a progressive rise in ELA is seen throughout the Holocene, and late Holocene ELA depression is indistinguishable from that in the Cordillera Darwin. While the AAR produces values of Holocene ΔELA similar to those in New Zealand and elsewhere in Patagonia, this in itself cannot validate the method, especially given the erroneous early lateglacial ΔELA_{AAR} values at the site.

Another possibility is that Glaciar Torre may not be a suitable site for ELA reconstructions with the methods used in this manuscript. This could be due to a combination of size/complexity, given that the glacier is a complex of three separate glaciers, as well as the concavity of the glacial system. Dalla Vedova is also subject to these uncertainties, so the seemingly small values of ΔELA at these sites may be partly a

function of the complexity of the glacier systems. As modern glacier size increases, the difference between the interpolated ELA and the real ELA becomes progressively greater (Figure 5.5), suggesting that larger glacier systems will produce lesser values of ΔELA. However, these differences are not sufficient to explain all of the difference between Cerro Castillo/Río Tranquilo and the more southern glacier systems, suggesting that at least part of the systematic differences between the regions reflect real differences in climate.

Future lines of work on Patagonian ELA reconstruction therefore demand additional reconstructions of smaller dated glacier systems in southernmost Patagonia and Tierra del Fuego. Cross-validation of the interpolation and reconstruction methods with other previously dated paleoglacier systems in New Zealand, would permit a more robust assessment of the method outlined in this thesis with the traditional flowline-based reconstruction. Calibration of ELA parameters, such as the THAR, AAR, and AABR, can be accomplished by performing a suite of simulations on closely-spaced glacier systems with known chronological control; the parameters that result in the lowest RMSE of ΔELAs are the preferred parameters for past glacier advances (Meierding, 1982; Osmaston, 2005). While to some extent this cannot be accomplished until absolute chronologies are refined, with caution these may be applied in areas where extensive work on relative or limiting chronologies have already been carried out. The Glaciar Torre area offers such a site, where multiple adjacent glaciers with limiting ages already exist (Garibotti and Villalba, 2009; Masiokas et al., 2009).

5.8 Conclusions

- Five different methods of paleo-ELA estimation have been applied to age-controlled paleoglaciers reconstructed using natural-neighbor interpolation at four sites in southern Patagonia and Tierra del Fuego.
- At Cerro Castillo and Río Tranquilo, Holocene ΔELA values of -160 m to -200 m coincide with previously reported ΔELA values in the Andes, and are comparable to those reported in New Zealand.
- Dalla Vedova showed consistently lesser Holocene ΔELA values than at Cerro Castillo and Río Tranquilo, suggesting a difference in climate and/or glacier sensitivity between the two regions. Results from Glaciar Torre are ambiguous, and climatic interpretation of the site depends on the choice of reconstruction.
- While application of the AAR method yielded ELA depressions similar to those previously found in Patagonia and New Zealand, in some circumstances the method yielded paradoxical results in Patagonia (e.g. higher ELAs for more extensive advances). This is likely due to elevation biases with highly concave glacier profiles, or unsuitability of these sites for the application of these methods.
- The AABR method shows promise as it yields results most consistent with the observed geomorphology, with low dependence (in this region) on parametrization.
- Future validation of the AABR should focus on applying the method to chronologies to which the AAR was previously applied, and intensive reconstructions of well-dated chronologies at the subregional scale.

* * *

Chapter 6 - Discussion

6.1 Overview

This chapter summarizes results and interpretations from Chapters 3, 4, and 5 to synthesize these new paleoglacier data and place them in the context of regional climate.

Four paleoglacier systems were evaluated in this thesis. Of these, three sites in mainland Patagonia exhibit a pattern of progressively less-extensive advances through the Holocene. On the contrary, one site in Tierra del Fuego shows an opposite tendency, with the most extensive glaciations occurring in the late Holocene. Systematic patterns in the timing, extension, and ELA depression associated with these glacier advances clearly separate the Patagonia and Tierra del Fuego, suggesting the two regions were subject to different regimes of climate variability over the Holocene.

6.2 Integrating these results with the preexisting paleoclimate literature

6.2.1 Lateglacial period

At Glaciar Torre, glacier advances culminated at 17.1 ka and 13.5 ka. These glacier advances correspond to the to the onset of the Last Glacial Termination (LGT; Denton et al., 2010) and the end of the Antarctic Cold Reversal (ACR; Pedro et al., 2016), respectively. Evidence also exists at Dalla Vedova for advances at 17.0 ka and 13.6 ka, although the chronological control for these advances is much less definitive. The glacial system at Río Tranquilo also advanced at 13.7 ka (Sagredo et al., 2018), while no advances at either the ACR or LGT were identified at Cerro Castillo.

Moraine building events from 18-17 ka are recognized across Patagonia (Kaplan et al., 2005; Hein et al., 2010; Moreno et al., 2015) and Tierra del Fuego (McCulloch et al., 2005a; Kaplan et al., 2008; Hein et al., 2010). A prominent glacier advance is recognized during this interval at Lake Ohau in New Zealand (44°S), as well (Putnam et al., 2013). At these sites, this event is considered a final glacier highstand preceding dramatic ice retreat. Advances at c. 17 ka at Glaciar Torre and Dalla Vedova are consistent with the timing and context of these events (e.g. as a final glacier highstand before generalized retreat), and supplement the preexisting evidence suggesting this time represented a crucial turning point in the climate of the lateglacial.

Meanwhile, the ACR is widely recognized as an influential climate event throughout southern Patagonia and New Zealand (Sagredo et al., 2018), although its existence in Tierra del Fuego and within the Cordillera Darwin is less well-established (McCulloch et al., 2005b; Menounos et al., 2013). The ACR advance at Glaciar Torre is therefore consistent with the preexisting literature. While the age constraints on the ACR advance at Dalla Vedova are not firm, they provide early evidence of a glacier advance within the Cordillera Darwin at this time.

To summarize, glaciers across southernmost South America appear to have advanced in near-synchrony at c. 17 ka and c. 13.5 ka. These events are well-recognized across the

region, and suggest that glaciers responded coherently to regional climate events during the LGT. This is in contrast to the Holocene—discussed below—where significant regional variability appears to define styles of glaciation in Patagonia and Tierra del Fuego.

6.2.2 The Holocene

In Patagonia, early Holocene maxima occur at Glaciar Torre (c. 9.7 ka) and Cerro Castillo (c. 10.6-8.4 ka), followed by successively less-extensive glacier advances throughout the epoch. While no chronological control exists for most of the putatively Holocene moraines at Río Tranquilo, relative morphostratigraphic moraine relationships suggest at least two advances occurred prior to a dated advance at c. 5.5 ka (Sagredo et al., 2018). These three sites are thus characterized by less-extensive glacier advances postdating an early Holocene glacier maximum (Figure 6.a), a pattern which is proposed to be characteristic of glaciers in Patagonia (Figure 6.c).

On the other hand, at the Dalla Vedova glacier, the Holocene glacier maximum appears to have occurred later, at c. 0.9 ka. The timing of glaciation here is anomalous in the context of the paleoglacier literature, occurring in only one other site, elsewhere in the Cordillera Darwin (Figure 6.b, Kuylenstierna et al., 1996). Additionally, late Holocene glacier maxima run counter to the model established in Patagonia, although similar patterns appear at the Gran Campo Nevado (Koch and Kilian 2005) and Monte Sarmiento (Strelin et al., 2008). While it is difficult to extrapolate from the limited data set available from Tierra del Fuego, the preexisting literature suggests that more extensive late Holocene advances were characteristic of the region.

Both scenarios, however, differ significantly from the currently accepted model of five Holocene glacial advances—or "Neoglaciations"—at (I) 4.5-4.0 ka, (II) 3.6-3.3 ka, (III) 2.7-2.0 ka, (IV) 1.6-0.9 ka, and (V) 0.4-0.2 ka, wherein the Holocene glacier maximum occurred in the middle Holocene (Figure 6.d; Aniya, 2013). While evidence exists for glacier advances corresponding to some Neoglaciations, the poorly-constrained nature of the chronologies used to define these advances (Figure 6.e) casts doubt on whether they adequately reflect the timing and pattern of glaciation in Patagonia. As the sites presented in this study consistently demonstrate early Holocene glacier maxima in Patagonia, it is proposed that the "Hypsithermal-Neoglacial" model should be abandoned in favor of one that more accurately reflects the behavior of glaciers in the region.

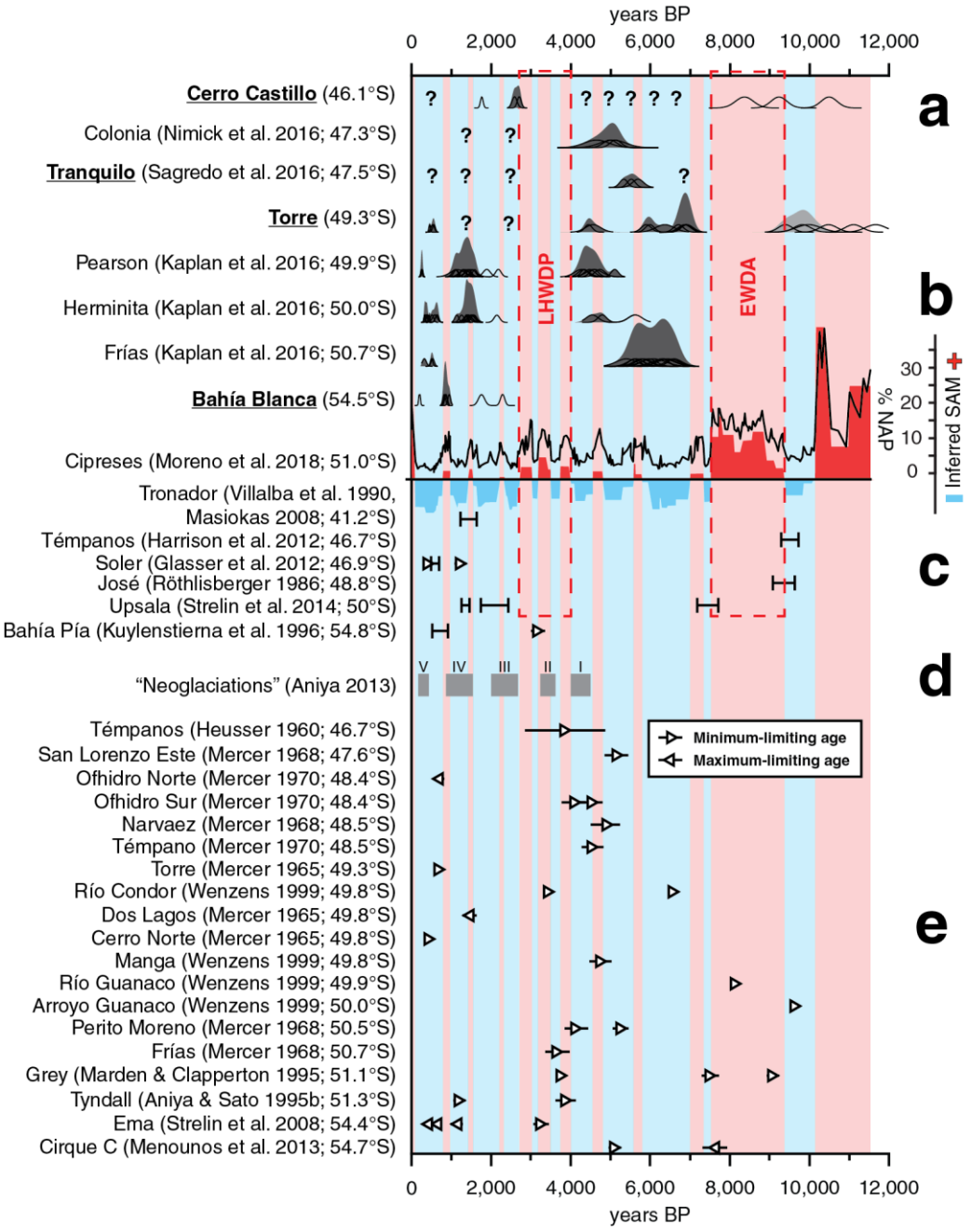

Figure 6.1. a) Holocene glacier chronologies in Patagonia and Tierra del Fuego constructed in base of ^{10}Be surface exposure dating of moraines. b) Lago Cipreses (51°S) percent non-arboreal pollen, showing inferred SAM modes. c) Well-constrained (bracketed) ages of glacier advance in Patagonia and Tierra del Fuego. d) Neoglaciations I-V (Aniya 2013). e) Poorly-constrained (open-ended) ages of glacier advance in Patagonia and Tierra del Fuego.

6.3 Paleoclimatic interpretation of the Holocene glacier record in Patagonia and Tierra del Fuego

6.3.1 Explaining the timing of glacier advances

Placing new ^{10}Be-based chronologies in Patagonia in the context of well-bracketed glacier advances (Figure 6.1a, c), several broad episodes of glacier advance are documented, from c. 10-9 ka, from 7-4.5 ka, from 2.7-1.0 ka, and from 0.7-0.2 ka.

Intriguingly, these advances coincide with periods of generalized cold/wet conditions inferred from paleo-pollen indicators (Figure 6.1b; Moreno et al., 2018); furthermore, our chronology does not reveal advanced glaciers during two periods of generalized warm/dry conditions from c. 9.5-7.5 ka and from 4.0-2.7 ka. Reconstructed Patagonian ELAs using the AAR method show that the magnitude of ELA depression during these Holocene advances was close to uniform throughout the region. This correspondence suggests that Holocene glaciers in Patagonia responded in a coherent fashion to quasi-cyclic climate changes associated with past variations in the Southern Annular Mode (SAM).

The SAM is currently strongly correlated with temperature variations in South America from 42-56°S (Garreaud et al., 2009). The positive (negative) mode of the SAM corresponds to warmer (cooler) temperatures across the region. As the leading mode of climate variability across Patagonia, Moreno et al. (2018) identified the SAM as the most likely mechanism that could explain their observed record of decadal- to centennial-scale cycling between warm/dry and cool/wet conditions in the region. The cross-proxy coherence in "cold" climate proxies—inferred negative SAM from fossil pollen and the glacier advances presented in this thesis—suggest that the SAM served as a "pacemaker" controlling the timing of glacier advance and retreat.

In contrast to Patagonia, where a coherent view of Holocene glacier fluctuations is developing, current chronologies in Tierra del Fuego offer little insight into the Holocene glacier history of the region prior to the last millennium. At the Dalla Vedova glacier, an advance is recorded at 0.9 ka that does not correspond to any recognized advance in southern Patagonia, coinciding only with a bracketed advance elsewhere in the Cordillera Darwin (Bahía Pía, Kuylenstierna et al. 1996).

It is proposed that the offset patterns of glacier advances between Patagonia and Tierra del Fuego can also be attributed to the SAM. The 0.9 ka advance at Dalla Vedova occurred during a centennial-scale episode of positive SAM (Figure 6.1b), which as discussed earlier is associated with generalized retreat across southern South America via warmer temperatures. However, enhanced westerly flow associated with the modern persistence of +SAM index conditions produce locally enhanced precipitation in the Cordillera Darwin, which has provoked modern stillstands or advances in some glaciers in the extreme southwest of South America (Holmlund and Fuenzalida, 1995; Melkonian et al., 2013). In this model, the SAM could provoke a "see-saw" effect on glaciers Tierra del Fuego and Patagonia, in which glacier retreat due to +SAM-induced warming is counteracted by the advance of some glaciers due to localized enhanced precipitation in Tierra del Fuego.

6.3.2 Explaining the extension of glacier advances

Patagonian glaciers exhibit a pattern of progressively less-extensive glacier readvances throughout the Holocene, a pattern that is also observed in New Zealand (Figure 6.2a). Holocene snowline depression using the AAR method yielded ranges of Holocene ELA depression between 165-200 m for dated moraines at Cerro Castillo, Río Tranquilo, and

Glaciar Torre. These values are similar to those observed in the Holocene record at New Zealand (Fig. 6.2a), suggesting that glaciers across the South Pacific responded to Holocene climate changes of similar magnitudes.

The hemispheric-wide trend of early Holocene glacier maxima suggest that this is a common feature of the Southern Hemisphere midlatitudes. Furthermore, this pattern opposes that of many Northern Hemisphere glaciers (Figure 6.2b), which show a broad trend of more-extensive glacier advances during this period, culminating in a Holocene glacier maximum within the last millennium. The opposing patterns of Holocene glacier extent between the Northern and Southern Hemispheres parallel that of summer insolation intensity in both hemispheres. This suggests that, all other factors being equal, summer insolation intensity serves as a "modulator" that governs the maximum extension of a glacier advance to uniform climate changes throughout the Holocene.

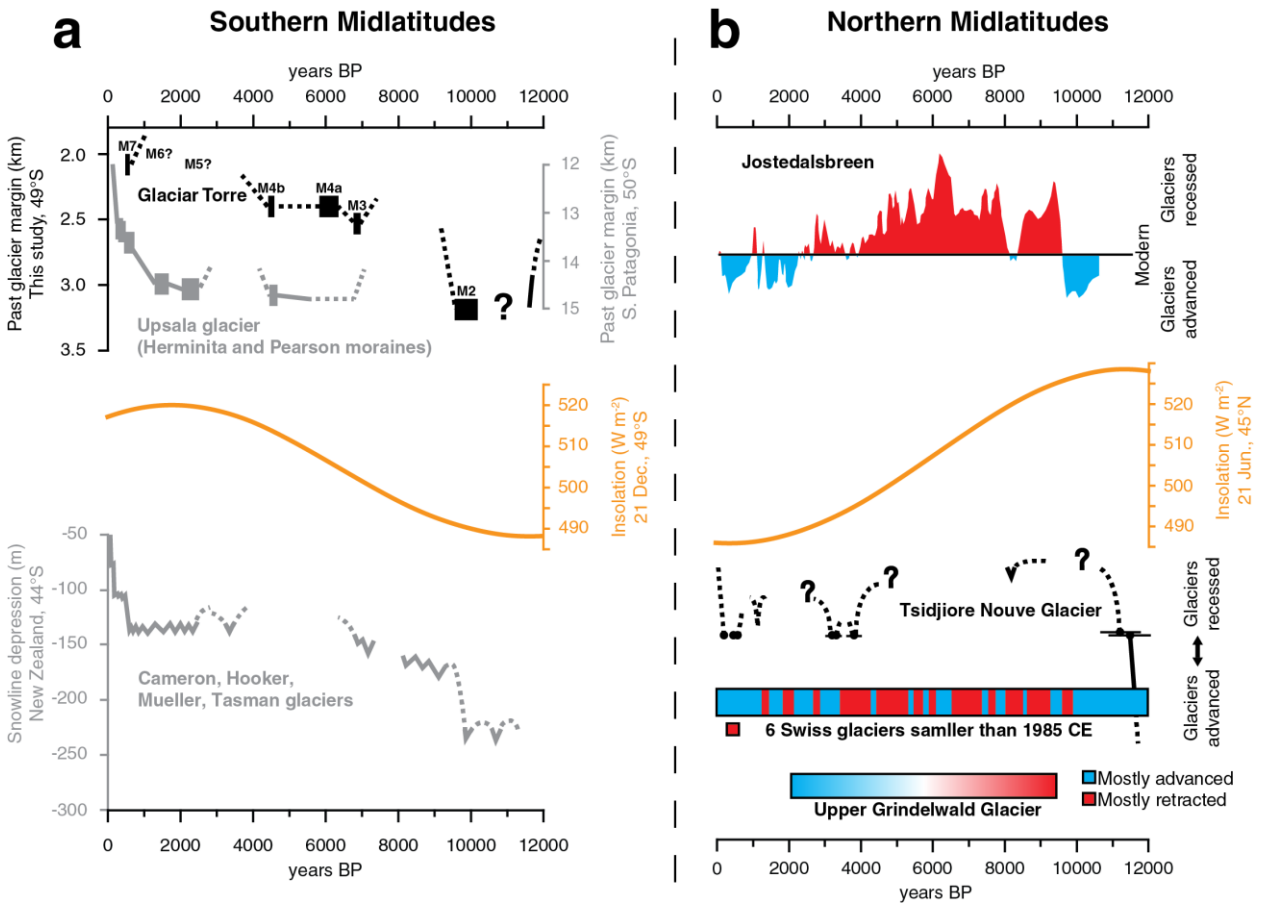

Figure 6.2. a) Multi-moraine Southern Hemisphere paleoglacier chronologies elaborated in base of ^{10}Be moraine dating. Presenting only chronologies from glaciers with more than one sequence of moraines allows for an evaluation of the spatial extension of glacier advances over time. Glaciar Torre time-distance data from Chapter 3. Upsala glacier time-distance data from Kaplan et al. (2016). Summer insolation at Glaciar Torre (49°S) is plotted in orange, above a composite time-distance diagram from New Zealand (Putnam et al. 2012). b) Indicators of paleoglacier extent from Jostedalsbreen, Norway (61°N, Nesje et al., 2001) and the Swiss Alps (46°N, Schimmelpfennig et al., 2014) plotted with summer insolation at 45°N in orange.

The opposite pattern of late Holocene glacier maxima in Tierra del Fuego is not easily explained by trends in summer insolation intensity. Perhaps the simplest explanation of

the lack of middle to early Holocene glacier advances is a lack of preservation of older moraines in the humid Cordillera Darwin, in contrast to the three Patagonian sites which all border the arid eastern margin of the Patagonian Andes. Indeed, some evidence exists of possible mid-Holocene glacier advances at Ema glacier in the CD (Strelin et al., 2008).

The differing pattern of glacier advances between Tierra del Fuego and Patagonia could be explained by differences in the intrinsic climate sensitivity of glaciers in the two regions. As CD glaciers are less sensitive to changes in temperature and precipitation than their Patagonian counterparts (Sagredo et al., 2014), it is possible that the differing pattern in glacier extent in the CD could be due in part to a differential response to similar changes in temperature or precipitation across both regions. Less sensitive glaciers in the CD could also explain lesser values of reconstructed Holocene ELA depression at Dalla Vedova.

6.3.3 Evaluating Holocene climate in southernmost South America

The timing of discrete glacier advances informs sub-millennial variability in the climate of southernmost South America, while trends in glacier extent inform the long-term climate trends across the region. A two-component model of Holocene glaciation in Patagonia is proposed here, wherein the timing of glacier advances is explained by multicentury-scale variation of the Southern Annular Mode (the "pacemaker"), while the pattern of less-extensive advances is explained by summer insolation intensity (the "modulator"). This hypothesis is discussed here.

The association between regional glacier variability and trends in the Southern Annular Mode are based in part on modern observations of strong control of the SAM over temperature and the Southern Westerly Winds at the interannual scale in southernmost South America (Thompson et al., 2011). Other recognized modes of interannual climate variability, such as El Niño-Southern Oscillation (ENSO) and the Pacific Decadal Oscillation (PDO), do not appear to affect temperature in southernmost Patagonia (Garreaud et al., 2009), although one study suggests a weak correlation between ENSO and precipitation at 53°S (Schneider and Gies, 2004). Therefore, while it is possible that the modern correlations between local climate and modes of variability do not represent the past climate of southernmost South America, assuming analogous controls over the climate of the region implicates the SAM as the most likely candidate to have influenced centennial climate variability.

Another key factor implicating the SAM in long-term climate changes is the observed multidecadal trend towards more-positive SAM conditions (Thompson and Solomon, 2002). Recent studies of terrestrial records across southernmost South America and adjacent regions have demonstrated the existence of highly variable Holocene climate over the Holocene (e.g. Van Daele et al., 2016; Oppedal et al., 2018). Additionally, multiple studies have demonstrated that centennial-scale Holocene climate variability over the last millennium in the Southern Hemisphere midlatitudes strongly resembles climate changes associated with positive and negative SAM (Villalba et al., 2012; Abram et al., 2014; Dätwyler et al., 2017; Fletcher et al., 2018; Moreno et al., 2018). On the

other hand, centennial-scale trends in ENSO are less clear (Cobb et al., 2013). Centennial-scale SAM-like variation over the Holocene—resulting in cycling between cold/wet and warm/dry conditions in southwestern Patagonia—is therefore favored as a likely mechanism controlling the timing of glacier advances.

What factors, then, control centennial-scale tendencies in the SAM? The modern trend towards positive SAM index conditions is strongly linked to greenhouse gas forcing and anthropogenic depletion of stratospheric ozone (Thompson and Solomon, 2002; Thompson et al., 2011) via their effects on stratosphere-troposphere temperature gradients (Kidston et al., 2015). Other workers have proposed linkages between the SAM and solar forcing (Kuroda, 2018), volcanic activity (Yang and Xiao, 2018), tropical SST anomalies (Yuan et al., 2018), and ENSO variability (Fogt et al., 2011; Gomez et al., 2011). The driving mechanisms behind preindustrial SAM variability remain poorly understood, and a full exploration of these possibilities is beyond the scope of this thesis. However, if the modern SAM is a model for past variability, it is likely that Holocene SAM variability reflects the southern midlatitude's response to an as-of-yet unidentified forcing of global significance.

SAM-induced variation between generally warm or cold conditions at the centennial scale is proposed as an explanation for the timing of repetitive Patagonian glacier advances during the Holocene. Also observed is a regionally coherent tendency in multiple glacier systems towards less-extensive glacier advances as the Holocene progressed. Viewed in isolation, this pattern could be explained by a progressive decline in the "intensity" of predominantly negative SAM intervals over time, resulting in less-extensive glacier advances. The modern frequency of positive SAM conditions is linked in part to stratospheric greenhouse gas concentrations (Arblaster and Meehl, 2006); Increasing CO_2 during the Holocene (Monnin et al., 2004) could modulate SAM events, resulting in more-intense positive SAM periods and less-intense negative SAM periods over this time period. This model could explain the anomalous pattern of glaciation in the Cordillera Darwin, as glaciers that *gain* mass in response to positive SAM conditions—as has been postulated for Dalla Vedova—would exhibit their greatest advance to CO_2-modulated late Holocene positive SAM conditions. However, it is important to note that such a trend is not reflected by the paleobotanical record of SAM of Moreno et al. (2018).

Viewed in the global context, Patagonian glaciers mirror the tendency of New Zealand glaciers towards less-extensive glacier advances during the Holocene (Kaplan et al., 2013), juxtaposed against the predominant Northern Hemisphere trend towards more extensive glacier advances (Matthews and Briffa 2005). Summer insolation intensity has previously been proposed as a control over glacier extent in the Northern Hemisphere and the tropics (Kaufman et al., 2004; Jomelli et al., 2011). The antiphased trend of summer insolation intensity in the Southern Hemisphere fits well with the observed trends in glacier extent.

Summer insolation intensity likely affected glacier mass balance via its effect on temperature during the ablation season (austral summer for southernmost South

America), and the pattern of glaciation at Glaciar Torre (Figure 6.2.a) matches this trend well. However, Putnam et al. (2012) note that less-extensive glacier advances in New Zealand do not perfectly track the Southern Hemisphere summer insolation curve; they instead propose an indirect insolation control on glaciation via a progressive southward shift of the Intertropical Convergence Zone and Hadley circulation. Das and Alley (2008) demonstrate increasing Holocene summer temperatures in West Antarctica were partially explainable by insolation changes, but note that the timing of observed melt events also does not correspond perfectly to Southern Hemisphere summer insolation. Instead, they propose increasing marine influence over West Antarctica was also responsible for progressively greater warming observed at Siple Dome. Interestingly, this could be explained by more-intense positive SAM periods in the later Holocene, which are associated with warmer temperatures in West Antarctica as well as Patagonia. Such a change in the intensity of positive SAM events could be provoked by increasing atmospheric CO_2 over the Holocene (Monnin et al., 2004).

6.4 Methodological considerations and future work

This thesis presents a new model for glacier advances and retreats across southernmost South America. In Patagonia, many decades of studies have attempted to define glaciation in the region, without recognizing widespread pre-6 ka glacier maxima. It is therefore worth considering why advances identified in this thesis have not yet been observed in prior studies, as well as the representativity of the chronologies developed here.

6.4.1 Radiocarbon dating

As mentioned in Chapter 2, radiocarbon age constraints of some moraines in Patagonia significantly underestimated the actual age of moraines. It bears noting that the first studies to demonstrate this phenomenon also utilized radiocarbon dating (Strelin and Malagnino, 2000; Strelin et al., 2011; Strelin et al., 2014). The principal difference was the number and nature of radiocarbon samples associated with the more modern chronologies.

Previous chronologies generally settled with the use of a single, minimum-limiting radiocarbon sample per moraine, dating organic material that grew directly above glacial sediment. To interpret minimum-limiting ages collected in this manner as closely bracketing the glacial abandonment of the sampling site, certain assumptions must be made. The key assumptions are that a) vegetation growth immediately postdated glacier retreat from a surface; and b) organic matter dated represents the first generation of vegetation growth after the glacial abandonment of the surface. Several biological and geological factors may violate these assumptions. Different plants may experience a colonization delay depending on species, climate, and substrate—for instance, this delay is recognized and corrected for in ecesis calculations for dendroglaciology. Additionally, erosion may strip early generations of vegetation from the surface, meaning that dated material does not closely date deglaciation.

The uncertainties related to the assumptions of immediate colonization and preservation of the first generation of organic material on a surface are very similar to the uncertainties associated with cosmogenic surface exposure age dating. Both methods' uncertainties are very difficult to evaluate in the field, and for this reason standard sampling procedure for cosmogenic surface exposure dating demands taking multiple samples from landforms (Balco et al., 2011). Indeed, newer radiocarbon chronologies used multiple samples from to constrain the age of moraines.

Radiocarbon limiting-ages from stratigraphic sections or cores offer additional advantages over dates obtained from the base of organic material over glacial sediment. Maximum-limiting ages of wood incorporated within glacial sediment more closely brackets glacial advance, as the presence of wood in subglacial till is genetically related to glacial advance. Furthermore, paired minimum-maximum age constraints on glacial sediment provide bracketing ages of glacial advances. In the context of Patagonia, bracketing ages correspond well to the glacial model proposed here (Fig. 6.1c).

6.4.2 Dendroglaciology

At Glaciar Torre and Dalla Vedova, cosmogenic age constraints overlap with dendroglaciological age constraints, revealing in both cases that the tree-ring minimum ages of surface stabilization significantly underestimate the stabilization age of the moraines in question. This is most pronounced at Glaciar Torre, where the youngest c. 0.5 ka M7 moraine is completely barren of vegetation. The age of this moraine is beyond the maximum age of *Nothofagus* in Patagonia (Aravena 2007), suggesting at this site dendroglaciology in its current mode of application is not an effective method for determining the age of glacial advances.

The key assumption in the use of tree ages to constrain surface stabilization is that live trees represent the first living generation on the surface in question. The identification of past generations of trees as deadfall provides a check on this assumption. However, Frangi et al. (1997) demonstrated that *Nothofagus pumilio* boles have a half-life of ~70 years, taking approximately 300 years to lose 95% of their mass. Therefore, it is possible that the existence of prior generations of trees may pass undetected in mature forests. The first living generation assumption may, in certain circumstances, not be possible to evaluate in the field.

Dendroglaciological techniques in southernmost South America are therefore subject to colonization delays that, in some climatic and geologic settings, be unreasonably long. Furthermore, the method is subject to issues regarding the field assessment of first-generation growth. The results of this thesis therefore demand suggest that caution must be used when applying dendrochronology to glacial sequences in the region.

6.4.3 General considerations for the glacial record

Kaplan et al. (2016) dated the Herminita moraines at Lago Argentino using ^{10}Be surface exposure dating, which were also dated using multiple-sample ^{14}C dating (Strelin et al., 2014). Cosmogenic dating cross-dated most ^{14}C-dated moraines, but notably failed to

capture evidence of a ^{14}C-bracketed early Holocene glacier advance of the Upsala glacier between 7.7-7.2 ka. No moraines morphostratigraphically older than c. 6 ka were observed in the area, revealing a key limitation of cosmogenic dating: surface exposure dating cannot constrain glacier advances if associated moraines are overridden or eroded.

Given the dependence of surface exposure dating on the existence of moraines, sites are preferentially selected where greater numbers of moraines are preserved than the average. The implicit assumption here concerns the representativity of the chosen sites. Sites with an uncommon pattern of less-extensive glacier advances are preferentially selected for study. All glaciers in a region are assumed to have advanced at these times; sampling sites hold a complete moraine record of glacier advances, while at other sites glacier moraines were lost as a result of geologic processes. However, this assumption—like the assumptions of instantaneous colonization for ^{14}C and first-generation growth for dendroglaciology—is typically impossible to evaluate in the field.

An alternative explanation is that these glacier systems experienced advances that did not occur at other sites. The absence of these glacier advances at other sites is therefore not due to preservation but due to a fundamental difference in glacier dynamics (e.g. Roe and O'Neal, 2009). The correlation between glacier advances and phases of the SAM presented in this thesis, as well as the described pattern of less-extensive glacier advances, would perhaps be due to coincidence of climate "noise" and independent climate variability. Roe (2011) establish a model-based means by which the likelihood of climatically-significant glacier excursions from the equilibrium can be determined. On the other hand, if multiple glaciers and independent climate proxies show evidence consistent with simultaneous advance and retreat, a climatic forcing can be assigned as the most likely explanation for the observed phenomena. This is the line of argument followed in this thesis, and

It is emphasized that ^{10}Be surface exposure dating need not—and should not—be the definitive method applied to glacier chronologies in southernmost South America. Radiocarbon bracketing ages are superbly valuable in their ability to date glacier advances that were subsequently overridden. Optically-stimulated luminescence dating of stratigraphic sections has also shown some promise in the region (Harrison et al., 2008). Other methods, such as lacustrine sedimentary records frequently used to reconstruct glacier behavior in Scandinavia (Nesje et al., 2001; Bakke et al., 2005; Larsen et al., 2015; Jansen et al., 2016) have not yet been extensively applied in Patagonia, and offer yet another alternative method for future paleoglacier reconstructions.

6.4.4 Equilibrium-line altitude reconstructions

In addition to the aforementioned chronological issues, a comparison of ELA reconstructions revealed significant methodological differences involved in paleoglacier reconstructions for the Holocene. In particular, several methods—the THAR, the AA, and the AAR—yielded results that are physically questionable, such as paleo-ELAs

higher than the modern, or values of ΔELA out of stratigraphic order. These differences pose a substantial hurdle for the quantification of Holocene glacier change in southernmost South America.

Most studies reconstructing ΔELA (snowline depression) in the Southern Hemisphere utilize the AAR method with accumulation-area ratios of 0.65-0.67 (Putnam et al., 2012; Kaplan et al., 2013; Sagredo et al., 2016; Sagredo et al., 2018). Comparison of the record at Glaciar Torre with these AARs is clouded by unviable lateglacial values of ΔELA at this site, although AAR-based Holocene ΔELA values at Glaciar Torre are broadly consistent with Holocene ΔELA values measured elsewhere in the Southern Hemisphere. Apart from the possibility that the AAR is unsuited for glaciers of certain geometric parameters (Nesje 1992), a site-specific factor—such as deglacial isostatic adjustment—could account for inconsistencies in the AAR at Glaciar Torre.

To further verify trends in ΔELA, past studies have reconstructed ELAs for numerous ($n>10$) sites of known age in a restricted geographic location, such as was performed in the Colorado Front Range by Meierding (1982). The method that yielded the lowest root-mean squared error between sites was considered the most robust. A study such as this at previously-studied sites at Glaciar Torre (Garibotti and Villalba, 2009; Masiokas et al., 2009) could help determine if trends at this site are anomalous or represent a coherent pattern. Furthermore, the AABR method produced the most logically-consistent results of all ΔELA reconstructions, although it yields significantly different ΔELA values than the AAR at Glaciar Torre. No other Holocene reconstructions in the Southern Hemisphere use this method, limiting its utility. Therefore, an alternative line of study would reassess previously-reconstructed glaciers using the AABR.

* * *

Chapter 7 – Conclusions

Alpine glacier systems are sensitive indicators of past climate; this work examines four such systems in southernmost South America. A variety of geological, geochronological, and numerical techniques were brought to bear on these locales to constrain the timing of climate changes that forced past glacier behavior in Patagonia and Tierra del Fuego. The glacial geomorphology and paleoglacier history were evaluated for three new sites: Cerro Castillo (46.1°S), Glaciar Torre (49.3°S), and Dalla Vedova (54.5°S). These geochronological data were integrated with a fourth site, Río Tranquilo (47.5°S), to quantify changes in the equilibrium-line altitude associated with Holocene glacier advances.

At Glaciar Torre, glacier advances were dated by extensive application of cosmogenic beryllium-10 surface exposure dating to the moraine sequence preserved at the site. Advances at 17.1 and 13.7 ka were followed by a series of progressively less-extensive glacier advances at 9.7, 6.9, 6.1, 4.5, and 0.5 ka. These advances occur synchronously with other well-dated glacier advances, and parallel independent climate proxies demonstrating shifts between cool/wet and warm/dry conditions. A similar pattern of early Holocene glacier maxima followed by less-extensive readvances is observed at Cerro Castillo and Río Tranquilo, which were partially dated using beryllium-10 dating.

Variations of the Dalla Vedova glacier in Tierra del Fuego were dated using a combination of beryllium-10, radiocarbon, and dendroglaciological techniques. The glacial system advanced at 16.9 and 13.6 ka, coeval with observed advances at Glaciar Torre and Río Tranquilo. The Holocene record at Dalla Vedova differs significantly in the timing and pattern of glacier advance, with a late Holocene maximum at 0.9 ka, and no preserved mid- to early-Holocene glacier activity.

Modeling of paleo-ELAs demonstrated the utility of a new method of paleoglacier surface reconstruction. Nearest-neighbor interpolation of glacier surfaces based on glacier outlines was shown to reproduce modern glaciers with similar error to that associated with conventional flowline-based surface reconstruction. Accumulation-altitude ratio reconstructions based on these paleosurface interpolation showed Patagonian glaciers advanced during the Holocene due to ELA depressions of 160-200 m, while the glacial system studied in Tierra del Fuego responded to a late Holocene ELA depression of 65 m. However, results were highly dependent upon the choice of ELA reconstruction, with ΔELAs calculated by the accumulation-area balance ratio method differing significantly from other methods' estimates when applied to the glacier system preserved at Glaciar Torre.

Glaciers in both Patagonia and Tierra del Fuego advanced during the onset of the Last Glacial Termination and the Antarctic Cold Reversal. These events are widely chronicled throughout the region, and suggest that glaciers in both sectors responded synchronously to dramatic climate changes during the end of the Pleistocene. On the

other hand, trends in Holocene glacier advances differ significantly between Patagonia and Tierra del Fuego.

Patagonian glacier advances during the Holocene are associated with periods of centennial-scale periods of cold/wet conditions that are associated with the negative phase of the modern Southern Annular Mode. The consistent values of ΔELA further suggest these advances occurred in response to a regionally-uniform climate forcing. Meanwhile, the progressively less-extensive glacier advances across the region parallel the evolution of local summer insolation intensity throughout the Holocene. When compared to the similar trends in New Zealand glaciers and the opposing trends in the Northern Hemisphere, summer insolation intensity appears to play a key role in governing Holocene glacier extent across the globe.

In Tierra del Fuego, the latest Holocene glacier advance occurs during a period of inferred warm/dry conditions in southernmost South America, corresponding to phases of positive SAM. This can be explained as a consequence of enhanced advected precipitation to Tierra del Fuego during positive SAM phases, which could cancel or even reverse glacier retreat due to warming. Reduced glacier sensitivity to climate change in Tierra del Fuego may also explain lesser values of ΔELA associated with this advance.

With regards to the objectives of this study, these new data first indicate that Lateglacial advances of glaciers across southernmost South America occurred in synchrony, corresponding well to recognized climate events. Holocene glaciers, however, exhibit a new pattern of less-extensive glacier advances following an early Holocene maximum. This runs counter to the previously-accepted Neoglacial model, and demands reconsideration of this conceptual model behind Patagonian glaciation.

Second, Patagonian glaciers seem to advance and retreat synchronously over the Holocene, following similar trends in glacier extent and ΔELA as well. Glaciers in Tierra del Fuego oppose Patagonian glaciers during this period in timing, extent, and associated ΔELA. This suggests that both regions were subject to differing climate regimes over the Holocene.

Finally, glacier advances correspond well to proxy-based centennial-scale variability of the Southern Annular Mode, suggesting this mode of climate variability dominated the Holocene climate of southernmost South America. Integration of the Patagonian glacier record with global glacier chronologies suggests that summer insolation intensity plays a leading role in governing glacier extent worldwide during interglacials.

* * *

Chapter 8 – References

Abram, N.J., Mulvaney, R., Vimeux, F., Phipps, S.J., Turner, J., and England, M.H., 2014, Evolution of the Southern Annular Mode during the past millennium: Nature Climate Change, v. 4, p. 564, https://doi.org/10.1038/nclimate2235.

Ackert, R.P., Becker, R.A., Singer, B.S., Kurz, M.D., Caffee, M.W., and Mickelson, D.M., 2008, Patagonian Glacier Response During the Late Glacial–Holocene Transition: Science, v. 321, p. 392 LP – 395, doi:10.1126/science.1157215.

Ackert, R.P., Becker, R.A., Singer, B.S., Kurz, M.D., Caffee, M.W., and Mickelson, D.M., 2008, Patagonian Glacier Response During the Late Glacial–Holocene Transition: Science, v. 321, p. 392 LP – 395, doi:10.1126/science.1157215.

Anderson, B., Mackintosh, A., Stumm, D., George, L., Kerr, T., Winter-Billington, A., and Fitzsimons, S., 2010, Climate sensitivity of a high-precipitation glacier in New Zealand: Journal of Glaciology, v. 56, p. 114–128.

Andreassen, L.M., Elvehøy, H., Kjøllmoen, B., Engeset, R. V., and Haakensen, N., 2005, Glacier mass-balance and length variation in Norway: Annals of Glaciology, v. 42, p. 317–325, doi:10.3189/172756405781812826.

Aniya, M., 1996, Holocene variations of Ameghino Glacier, southern Patagonia: The Holocene, v. 6, p. 247–252, doi:10.1177/095968369600600211.

Aniya, M., and Naruse, R., 1999, Late-Holocene glacial advances at Glaciar Soler, Hielo Patagonico Norte, South America: v. 20, 69–83 p.

Aniya, M., and Sato, H., 1995a, Holocene glacial chronology of Upsala Glacier at Peninsula Herminita, Southern Patagonia Icefield: Bulletin of glacier research, v. 13, p. 83–96, https://ci.nii.ac.jp/naid/10002474837/#ref (accessed November 2018).

Aniya, M., and Sato, H., 1995b, Holocene glacier variations at Tyndall Glacier area, southern Patagonia: Bulletin of Glacier Research, v. 13, p. 97–109.

Aniya, M., 2013, Holocene glaciations of Hielo Patagónico (Patagonia Icefield), South America: A brief review: v. 47, 97–105 p., doi:10.2343/geochemj.1.0171.

Aragón, E., Goin, F.J., Aguilera, Y.E., Woodburne, M.O., Carlini, A.A., and Roggiero, M.F., 2011, Palaeogeography and palaeoenvironments of northern Patagonia from the Late Cretaceous to the Miocene: the Palaeogene Andean gap and the rise of the North Patagonian High Plateau: Biological Journal of the Linnean Society, v. 103, p. 305–315, doi:10.1111/j.1095-8312.2011.01684.x.

Aravena, J.-C., 2007, Reconstructing climate variability using tree rings and glacier fluctuations in the southern Chilean Andes: The University of Western Ontario, 220 p.

Aravena, J., and Luckman, B.H., 2009, Spatio-temporal rainfall patterns in southern South America: International Journal of Climatology, v. 29, p. 2106–2120.

Arblaster, J.M., and Meehl, G.A., 2006, Contributions of External Forcings to Southern Annular Mode Trends: Journal of Climate, v. 19, p. 2896–2905, doi:10.1175/JCLI3774.1.

Ascough, P., Cook, G., and Dugmore, A., 2005, Methodological approaches to determining the marine radiocarbon reservoir effect: Progress in Physical Geography, v. 29, p. 532–547.

Auer, V., 1960, The Quaternary history of Fuego-Patagonia: Proceedings of the Royal Society of London. Series B. Biological Sciences, v. 152, p. 507–516, doi:10.1098/rspb.1960.0058.

Bahr, D.B., Pfeffer, W.T., Sassolas, C., and Meier, M.F., 1998, Response time of glaciers

as a function of size and mass balance: 1. Theory: Journal of Geophysical Research: Solid Earth, v. 103, p. 9777–9782.
Bakke, J., Lie, Ø, Nesje, A., Dahl, S.O., and Paasche, Ø, 2005, Utilizing physical sediment variability in glacier-fed lakes for continuous glacier reconstructions during the Holocene, northern Folgefonna, western Norway: The Holocene, v. 15, p. 161–176, doi:10.1191/0959683605hl797rp.
Balco, G., 2011, Contributions and unrealized potential contributions of cosmogenic-nuclide exposure dating to glacier chronology, 1990–2010: Quaternary Science Reviews, v. 30, p. 3–27, doi:https://doi.org/10.1016/j.quascirev.2010.11.003.
Balco, G., Briner, J., Finkel, R.C., Rayburn, J.A., Ridge, J.C., and Schaefer, J.M., 2009, Regional beryllium-10 production rate calibration for late-glacial northeastern North America: Quaternary Geochronology, v. 4, p. 93–107.
Balco, G., Stone, J.O., Lifton, N.A., and Dunai, T.J., 2008, A complete and easily accessible means of calculating surface exposure ages or erosion rates from 10Be and 26Al measurements: Quaternary Geochronology, v. 3, p. 174–195, doi:10.1016/J.QUAGEO.2007.12.001.
Beer, J., Raisbeck, G.M., and Yiou, F., 1991, Time variations of Be-10 and solar activity: IN: The sun in time (A92-46664 19-92). Tucson, AZ, University of Arizona Press, 1991, p. 343-359., p. 343–359, http://adsabs.harvard.edu/abs/1991suti.conf..343B (accessed July 2019).
Behrmann, J., and Kopf, A., 2001, Balance of tectonically accreted and subducted sediment at the Chile Triple Junction: International Journal of Earth Sciences, v. 90, p. 753–768, doi:10.1007/s005310000172.
Bendle, J.M., Thorndycraft, V.R., and Palmer, A.P., 2017, The glacial geomorphology of the Lago Buenos Aires and Lago Pueyrredón ice lobes of central Patagonia: Journal of Maps, v. 13, p. 654–673.
Benn, D.I., and Evans, D.J.A., 2014, Glaciers and glaciation: London, Routledge, 816 p., doi:10.4324/9780203785010.
Benn, D.I., and Hulton, N.R.J., 2010, An ExcelTM spreadsheet program for reconstructing the surface profile of former mountain glaciers and ice caps: Computers & Geosciences, v. 36, p. 605–610, doi:10.1016/J.CAGEO.2009.09.016.
Benn, D.I., and Lehmkuhl, F., 2000, Mass balance and equilibrium-line altitudes of glaciers in high-mountain environments: Quaternary International, v. 65–66, p. 15–29, doi:10.1016/S1040-6182(99)00034-8.
Benn, D.I., Owen, L.A., Osmaston, H.A., Seltzer, G.O., Porter, S.C., and Mark, B., 2005, Reconstruction of equilibrium-line altitudes for tropical and sub-tropical glaciers: Quaternary International, v. 138, p. 8–21.
Benn, D.I., Warren, C.R., and Mottram, R.H., 2007, Calving processes and the dynamics of calving glaciers: Earth-Science Reviews, v. 82, p. 143–179.
Benson, L., Madole, R., Phillips, W., Landis, G., Thomas, T., and Kubik, P., 2004, The probable importance of snow and sediment shielding on cosmogenic ages of north-central Colorado Pinedale and pre-Pinedale moraines: Quaternary Science Reviews, v. 23, p. 193–206.
Bertrand, S., Lange, C.B., Pantoja, S., Hughen, K., Van Tornhout, E., and Wellner, J.S., 2017, Postglacial fluctuations of Cordillera Darwin glaciers (southernmost Patagonia) reconstructed from Almirantazgo fjord sediments: Quaternary Science Reviews, v. 177, p. 265–275, doi:10.1016/J.QUASCIREV.2017.10.029.
Blisniuk, P.M., Stern, L.A., Chamberlain, C.P., Idleman, B., and Zeitler, P.K., 2005, Climatic and ecologic changes during Miocene surface uplift in the Southern

Patagonian Andes: Earth and Planetary Science Letters, v. 230, p. 125–142, doi:https://doi.org/10.1016/j.epsl.2004.11.015.
Blunier, T. et al., 1998, Asynchrony of Antarctic and Greenland climate change during the last glacial period: Nature, v. 394, p. 739–743, doi:10.1038/29447.
Boulton, G.S., and Eyles, N., 1979, Sedimentation by valley glaciers: a model and genetic classification: Moraines and varves, v. 33, p. 11–23.
Boyd, B.L., Anderson, J.B., Wellner, J.S., and Fernández, R.A., 2008, The sedimentary record of glacial retreat, Marinelli Fjord, Patagonia: Regional correlations and climate ties: Marine Geology, v. 255, p. 165–178, doi:10.1016/J.MARGEO.2008.09.001.
Braithwaite, R.J., 1981, On glacier energy balance, ablation, and air temperature: Journal of Glaciology, v. 27, p. 381–391.
Breitsprecher, K., and Thorkelson, D., 2009, Neogene kinematic history of Nazca–Antarctic–Phoenix slab windows beneath Patagonia and the Antarctic Peninsula: v. 464, 10–20 p., doi:10.1016/j.tecto.2008.02.013.
Broecker, W.S., and Denton, G.H., 1990, What drives glacial cycles? Scientific American, v. 262, p. 43–48.
Caldenius, C.C., 1932, Las Glaciaciones Cuaternarias en la Patagonia y Tierra del Fuego: Geografiska Annaler, v. 14, p. 1, doi:10.2307/519583.
Carrasco, J.F., Casassa, G., and Rivera, A., 2002, Meteorological and Climatological Aspects of the Southern Patagonia Icefield, *in* Springer, Boston, MA, p. 29–41, doi:10.1007/978-1-4615-0645-4_4.
Cerling, T.E., and Craig, H., 1994, GEOMORPHOLOGY AND IN-SITU COSMOGENIC ISOTOPES: Annual Review of Earth and Planetary Sciences, v. 22, p. 273–317, doi:10.1146/annurev.ea.22.050194.001421.
Childs, C., 2004, Interpolating surfaces in ArcGIS spatial analyst: ArcUser, July-September, v. 3235, p. 569.
Clark, P.U., Dyke, A.S., Shakun, J.D., Carlson, A.E., Clark, J., Wohlfarth, B., Mitrovica, J.X., Hostetler, S.W., and McCabe, A.M., 2009, The Last Glacial Maximum: Science, v. 325, p. 710 LP – 714, doi:10.1126/science.1172873.
Cobb, K.M., Westphal, N., Sayani, H.R., Watson, J.T., Di Lorenzo, E., Cheng, H., Edwards, R.L., and Charles, C.D., 2013, Highly variable El Niño–southern oscillation throughout the Holocene: Science, v. 339, p. 67–70.
Cuffey, K.M., and Paterson, W.S.B., 2010, The physics of glaciers: Burlington, Butterworth-Heinemann, 693 p.
Darvill, C.M., Bentley, M.J., Stokes, C.R., Hein, A.S., and Rodés, Á., 2015, Extensive MIS 3 glaciation in southernmost Patagonia revealed by cosmogenic nuclide dating of outwash sediments: Earth and Planetary Science Letters, v. 429, p. 157–169, doi:10.1016/J.EPSL.2015.07.030.
Das, S.B., and Alley, R.B., 2008, Rise in frequency of surface melting at Siple Dome through the Holocene: Evidence for increasing marine influence on the climate of West Antarctica: Journal of Geophysical Research: Atmospheres, v. 113.
Dätwyler, C., Neukom, R., Abram, N.J., Gallant, A.J.E., Grosjean, M., Jacques-Coper, M., Karoly, D.J., and Villalba, R., 2018, Teleconnection stationarity, variability and trends of the Southern Annular Mode (SAM) during the last millennium: Climate Dynamics, v. 51, p. 2321–2339, doi:10.1007/s00382-017-4015-0.
De Angelis, H., 2014, Hypsometry and sensitivity of the mass balance to changes in equilibrium-line altitude: the case of the Southern Patagonia Icefield: Journal of Glaciology, v. 60, p. 14–28.

Dee, D.P. et al., 2011, The ERA-Interim reanalysis: configuration and performance of the data assimilation system: Quarterly Journal of the Royal Meteorological Society, v. 137, p. 553–597, doi:10.1002/qj.828.
Denton, G.H., Anderson, R.F., Toggweiler, J.R., Edwards, R.L., Schaefer, J.M., and Putnam, A.E., 2010, The last glacial termination: Science, v. 328, p. 1652–1656.
Denton, G.H., Heusser, C.J., Lowel, T. V, Moreno, P.I., Andersen, B.G., Heusser, L.E., Schlühter, C., and Marchant, D.R., 1999, Interhemispheric linkage of paleoclimate during the last glaciation: Geografiska Annaler: Series A, Physical Geography, v. 81, p. 107–153.
Denton, G.H., and Karlén, W., 1973, Holocene climatic variations-Their pattern and possible cause: Quaternary Research, v. 3, p. 155–205, doi:10.1016/0033-5894(73)90040-9.
Desilets, D., and Zreda, M., 2003, Spatial and temporal distribution of secondary cosmic-ray nucleon intensities and applications to in situ cosmogenic dating: Earth and Planetary Science Letters, v. 206, p. 21–42, doi:10.1016/S0012-821X(02)01088-9.
Desilets, D., Zreda, M., and Prabu, T., 2006, Extended scaling factors for in situ cosmogenic nuclides: New measurements at low latitude: Earth and Planetary Science Letters, v. 246, p. 265–276, doi:https://doi.org/10.1016/j.epsl.2006.03.051.
Dietrich, R., Ivins, E.R., Casassa, G., Lange, H., Wendt, J., and Fritsche, M., 2010, Rapid crustal uplift in Patagonia due to enhanced ice loss: Earth and Planetary Science Letters, v. 289, p. 22–29, doi:10.1016/J.EPSL.2009.10.021.
Douglass, D.C., Singer, B.S., Kaplan, M.R., Ackert, R.P., Mickelson, D.M., and Caffee, M.W., 2005, Evidence of early Holocene glacial advances in southern South America from cosmogenic surface-exposure dating: Geology, v. 33, p. 237, doi:10.1130/G21144.1.
Douglass, D.C., Singer, B.S., Kaplan, M.R., Mickelson, D.M., and Caffee, M.W., 2006, Cosmogenic nuclide surface exposure dating of boulders on last-glacial and late-glacial moraines, Lago Buenos Aires, Argentina: Interpretive strategies and paleoclimate implications: Quaternary Geochronology, v. 1, p. 43–58, doi:10.1016/J.QUAGEO.2006.06.001.
Duller, G.A.T., 2004, Luminescence dating of Quaternary sediments: recent advances: Journal of Quaternary Science, v. 19, p. 183–192.
Dunai, T.J., 2001, Influence of secular variation of the magnetic field on production rates of in situ produced cosmogenic nuclides: v. 193, 197–212 p., doi:10.1016/S0012-821X(01)00503-9.
Dunai, T.J., 2010, Cosmogenic Nuclides: Principles, concepts and applications in the Earth surface sciences: Cambridge, Cambridge University Press, 187 p.
Dyurgerov, M.B., and Meier, M.F., 2000, Twentieth century climate change: evidence from small glaciers.: Proceedings of the National Academy of Sciences of the United States of America, v. 97, p. 1406–11, doi:10.1073/pnas.97.4.1406.
Egholm, D.L., Nielsen, S.B., Pedersen, V.K., and Lesemann, J.-E., 2009, Glacial effects limiting mountain height: Nature, v. 460, p. 884.
Eyles, N., Eyles, C.H., and Miall, A.D., 1983, Lithofacies types and vertical profile models; an alternative approach to the description and environmental interpretation of glacial diamict and diamictite sequences: Sedimentology, v. 30, p. 393–410.
Fernández, R., Gulick, S., Rodrigo, C., Domack, E., and Leventer, A., 2017, Seismic stratigraphy and glacial cycles in the inland passages of the Magallanes Region of

Chile, southernmost South America: Marine Geology, v. 386, p. 19–31, doi:10.1016/J.MARGEO.2017.02.006.
Fletcher, M.-S., Benson, A., Bowman, D.M.J.S., Gadd, P.S., Heijnis, H., Mariani, M., Saunders, K.M., Wolfe, B.B., and Zawadzki, A., 2018, Centennial-scale trends in the Southern Annular Mode revealed by hemisphere-wide fire and hydroclimatic trends over the past 2400 years: Geology, v. 46, p. 363–366, doi:10.1130/G39661.1.
Fletcher, M.-S., and Moreno, P.I., 2012, Have the Southern Westerlies changed in a zonally symmetric manner over the last 14,000 years? A hemisphere-wide take on a controversial problem: Quaternary International, v. 253, p. 32–46, doi:10.1016/J.QUAINT.2011.04.042.
Fontijn, K. et al., 2016, Synchronisation of sedimentary records using tephra: A postglacial tephrochronological model for the Chilean Lake District: Quaternary Science Reviews, v. 137, p. 234–254, doi:10.1016/J.QUASCIREV.2016.02.015.
Fosdick, J.C., Grove, M., Hourigan, J.K., and Calderón, M., 2013, Retroarc deformation and exhumation near the end of the Andes, southern Patagonia: Earth and Planetary Science Letters, v. 361, p. 504–517, doi:https://doi.org/10.1016/j.epsl.2012.12.007.
Foster, D., Brocklehurst, S.H., and Gawthorpe, R.L., 2008, Small valley glaciers and the effectiveness of the glacial buzzsaw in the northern Basin and Range, USA: Geomorphology, v. 102, p. 624–639.
Frangi, J.L., Richter, L.L., Barrera, M.D., and Aloggia, M., 1997, Decomposition of Nothofagus fallen woody debris in forests of Tierra del Fuego, Argentina: Canadian Journal of Forest Research, v. 27, p. 1095–1102.
Furbish, D., and Andrews, J.T., 1984, The Use of Hypsometry to Indicate Long-Term Stability and Response of Valley Glaciers to Changes in Mass Transfer: Journal of Glaciology, v. 30, p. 199–211, doi:10.3189/S0022143000005931.
García, J.-L., Hein, A.S., Binnie, S.A., Gómez, G.A., González, M.A., and Dunai, T.J., 2018, The MIS 3 maximum of the Torres del Paine and Última Esperanza ice lobes in Patagonia and the pacing of southern mountain glaciation: Quaternary Science Reviews, v. 185, p. 9–26, doi:https://doi.org/10.1016/j.quascirev.2018.01.013.
García, J.L., Kaplan, M.R., Hall, B.L., Schaefer, J.M., Vega, R.M., Schwartz, R., and Finkel, R., 2012, Glacier expansion in southern Patagonia throughout the Antarctic cold reversal: Geology, v. 40, p. 859–862, http://dx.doi.org/10.1130/G33164.1.
García, J.-L., Maldonado, A., de Porras, M.E., Delaunay, A.N., Reyes, O., Ebensperger, C.A., Binnie, S.A., Lüthgens, C., and Méndez, C., 2019, Early deglaciation and paleolake history of Río Cisnes Glacier, Patagonian Ice Sheet (44° S): Quaternary Research, v. 91, p. 194–217.
Garibotti, I.A., and Villalba, R., 2009, Lichenometric dating using Rhizocarpon subgenus Rhizocarpon in the Patagonian Andes, Argentina: Quaternary Research, v. 71, p. 271–283, doi:10.1016/J.YQRES.2009.01.012.
Garreaud, R., Lopez, P., Minvielle, M., and Rojas, M., 2013, Large-scale control on the Patagonian climate: Journal of Climate, v. 26, p. 215–230, doi:10.1175/JCLI-D-12-00001.1.
Garreaud, R.D., Vuille, M., Compagnucci, R., and Marengo, J., 2009, Present-day South American climate: Palaeogeography, Palaeoclimatology, Palaeoecology, v. 281, p. 180–195, doi:10.1016/j.palaeo.2007.10.032.
Ghiglione, M.C., Ramos, V.A., Cuitiño, J., and Barberón, V., 2016, Growth of the Southern Patagonian Andes (46–53°S) and Their Relation to Subduction Processes, *in* Springer, Cham, p. 201–240, doi:10.1007/978-3-319-23060-3_10.

Glasser, N.F., Hambrey, M.J., and Aniya, M., 2002, An advance of Soler Glacier, North Patagonian Icefield, at c. AD 1222–1342: The Holocene, v. 12, p. 113–120, doi:10.1191/0959683602hl526rr.
Glasser, N.F., Harrison, S., Schnabel, C., Fabel, D., and Jansson, K.N., 2012, Younger Dryas and early Holocene age glacier advances in Patagonia: Quaternary Science Reviews, v. 58, p. 7–17, doi:https://doi.org/10.1016/j.quascirev.2012.10.011.
Glasser, N.F., Harrison, S., Winchester, V., and Aniya, M., 2004, Late Pleistocene and Holocene palaeoclimate and glacier fluctuations in Patagonia: Global and Planetary Change, v. 43, p. 79–101, doi:10.1016/J.GLOPLACHA.2004.03.002.
Godwin, H., 1962, Half-life of radiocarbon: Nature, v. 195, p. 984.
Gomez, B., Carter, L., Orpin, A.R., Cobb, K.M., Page, M.J., Trustrum, N.A., and Palmer, A.S., 2011, ENSO/SAM interactions during the middle and late Holocene: The Holocene, v. 22, p. 23–30, doi:10.1177/0959683611405241.
Gong, D., and Wang, S., 1999, Definition of Antarctic Oscillation index: Geophysical Research Letters, v. 26, p. 459–462, doi:10.1029/1999GL900003.
Gorring, M.L., Kay, S.M., Zeitler, P.K., Ramos, V.A., Rubiolo, D., Fernandez, M.I., and Panza, J.L., 1997, Neogene Patagonian plateau lavas: Continental magmas associated with ridge collision at the Chile Triple Junction: Tectonics, v. 16, p. 1–17, doi:10.1029/96TC03368.
Gosse, J.C., and Phillips, F.M., 2001, Terrestrial in situ cosmogenic nuclides: theory and application: Quaternary Science Reviews, v. 20, p. 1475–1560, doi:https://doi.org/10.1016/S0277-3791(00)00171-2.
Guillaume, B., Martinod, J., Husson, L., Roddaz, M., and Riquelme, R., 2009, Neogene uplift of central eastern Patagonia: Dynamic response to active spreading ridge subduction? Tectonics, v. 28, doi:10.1029/2008TC002324.
Guyodo, Y., and Valet, J.-P., 1999, Global changes in intensity of the Earth's magnetic field during the past 800 kyr: Nature, v. 399, p. 249–252, doi:10.1038/20420.
Hajdas, I., Kull, C., and Kiefer, T., 2006, 14C-Chronology: PAGES News, v. 14, p. 32, https://core.ac.uk/download/pdf/43658360.pdf#page=2.
Hall, B.L., Porter, C.T., Denton, G.H., Lowell, T. V., and Bromley, G.R.M., 2013, Extensive recession of Cordillera Darwin glaciers in southernmost South America during Heinrich Stadial 1: Quaternary Science Reviews, v. 62, p. 49–55, doi:10.1016/J.QUASCIREV.2012.11.026.
Hallet, B., Hunter, L., and Bogen, J., 1996, Rates of erosion and sediment evacuation by glaciers: A review of field data and their implications: Global and Planetary Change, v. 12, p. 213–235.
Harrison, S., Glasser, N.F., Duller, G.A.T., and Jansson, K.N., 2012, Early and mid-Holocene age for the Tempanos moraines, Laguna San Rafael, Patagonian Chile: Quaternary Science Reviews, v. 31, p. 82–92, doi:10.1016/J.QUASCIREV.2011.10.015.
Hay, J.E., and Fitzharris, B.B., 1988, A comparison of the energy-balance and bulk-aerodynamic approaches for estimating glacier melt: Journal of Glaciology, v. 34, p. 145–153.
Hein, A.S., Cogez, A., Darvill, C.M., Mendelova, M., Kaplan, M.R., Herman, F., Dunai, T.J., Norton, K., Xu, S., and Christl, M., 2017, Regional mid-Pleistocene glaciation in central Patagonia: Quaternary Science Reviews, v. 164, p. 77–94.
Hein, A.S., Hulton, N.R.J., Dunai, T.J., Sugden, D.E., Kaplan, M.R., and Xu, S., 2010, The chronology of the Last Glacial Maximum and deglacial events in central Argentine Patagonia: Quaternary Science Reviews, v. 29, p. 1212–1227,

doi:10.1016/J.QUASCIREV.2010.01.020.
Heusser, C.J., 1960, Late-Pleistocene Environments of the Laguna de San Rafael Area, Chile: Geographical Review, v. 50, p. 555, doi:10.2307/212310.
Hock, R., 2005, Glacier melt: a review of processes and their modelling: Progress in physical geography, v. 29, p. 362–391.
Hogg, A.G. et al., 2013, SHCal13 Southern Hemisphere Calibration, 0–50,000 Years cal BP: Radiocarbon, v. 55, p. 1889–1903, doi:DOI: 10.2458/azu_js_rc.55.16783.
Hooker, B.., and Fitzharris, B.., 1999, The correlation between climatic parameters and the retreat and advance of Franz Josef Glacier, New Zealand: Global and Planetary Change, v. 22, p. 39–48, doi:10.1016/S0921-8181(99)00023-5.
Holmlund, P., and Fuenzalida, H., 1995, Anomalous glacier responses to 20th century climatic changes in Darwin Cordillera, southern Chile: Journal of Glaciology, v. 41, p. 465–473, doi:10.3189/S0022143000034808.
Hostetler, S.W., and Clark, P.U., 2000, Tropical climate at the last glacial maximum inferred from glacier mass-balance modeling.: Science (New York, N.Y.), v. 290, p. 1747–50, doi:10.1126/science.290.5497.1747.
Hubbard, A., Hein, A.S., Kaplan, M.R., Hulton, N.R.J., and Glasser, N., 2005, A Modelling Reconstruction of the Last Glacial Maximum Ice Sheet and Its Deglaciation in the Vicinity of the Northern Patagonian Icefield, South America: Geografiska Annaler. Series A, Physical Geography, v. 87, p. 375–391, doi:10.2307/3554244.
Hughes, P.D., Woodward, J.C., and Gibbard, P.L., 2006, Late Pleistocene glaciers and climate in the Mediterranean: Global and Planetary Change, v. 50, p. 83–98, doi:10.1016/J.GLOPLACHA.2005.07.005.
Hulton, N., Sugden, D., Payne, A., and Clapperton, C., 1994, Glacier Modeling and the Climate of Patagonia during the Last Glacial Maximum: Quaternary Research, v. 42, p. 1–19, doi:10.1006/QRES.1994.1049.
Huybers, P., 2006, Early Pleistocene glacial cycles and the integrated summer insolation forcing: science, v. 313, p. 508–511.
Ivy-Ochs, S., Kerschner, H., Maisch, M., Christl, M., Kubik, P.W., and Schlüchter, C., 2009, Latest Pleistocene and Holocene glacier variations in the European Alps: Quaternary Science Reviews, v. 28, p. 2137–2149, doi:10.1016/j.quascirev.2009.03.009.
Jansen, H.L., Simonsen, J.R., Dahl, S.O., Bakke, J., and Nielsen, P.R., 2016, Holocene glacier and climate fluctuations of the maritime ice cap Høgtuvbreen, northern Norway: The Holocene, v. 26, p. 736–755, doi:10.1177/0959683615618265.
Jóhannesson, T., Raymond, C.F., and Waddington, E.D., 1989, A Simple Method for Determining the Response Time of Glaciers, in Glacier Fluctuations and Climate Change, Springer, Dordrecht, p. 343–352, doi:10.1007/978-94-015-7823-3_22.
Jomelli, V., Khodri, M., Favier, V., Brunstein, D., Ledru, M.-P., Wagnon, P., Blard, P.-H., Sicart, J.-E., Braucher, R., and Grancher, D., 2011, Irregular tropical glacier retreat over the Holocene epoch driven by progressive warming: Nature, v. 474, p. 196.
Jouzel, J. et al., 2007, Orbital and Millennial Antarctic Climate Variability over the Past 800,000 Years: Science, v. 317, p. 793 LP – 796, doi:10.1126/science.1141038.
Kaplan, M.R. et al., 2016, Patagonian and southern South Atlantic view of Holocene climate: Quaternary Science Reviews, v. 141, p. 112–125, doi:10.1016/j.quascirev.2016.03.014.
Kaplan, M.R. et al., 2013, The anatomy of long-term warming since 15 ka in New Zealand based on net glacier snowline rise: Geology, v. 41, p. 887–890,

http://dx.doi.org/10.1130/G34288.1.
Kaplan, M.R., Fogwill, C.J., Sugden, D.E., Hulton, N.R.J., Kubik, P.W., and Freeman, S.P.H.T., 2008, Southern Patagonian glacial chronology for the Last Glacial period and implications for Southern Ocean climate: Quaternary Science Reviews, v. 27, p. 284–294, doi:10.1016/J.QUASCIREV.2007.09.013.
Kaplan, M.R., Strelin, J.A., Schaefer, J.M., Denton, G.H., Finkel, R.C., Schwartz, R., Putnam, A.E., Vandergoes, M.J., Goehring, B.M., and Travis, S.G., 2011, In-situ cosmogenic ^{10}Be production rate at Lago Argentino, Patagonia: Implications for late-glacial climate chronology: Earth and Planetary Science Letters, v. 309, p. 21–32, doi:10.1016/J.EPSL.2011.06.018.
Kaufman, D.. et al., 2004, Holocene thermal maximum in the western Arctic (0–180°W): Quaternary Science Reviews, v. 23, p. 529–560, doi:10.1016/J.QUASCIREV.2003.09.007.
Kelley, S., 2002, K-Ar and Ar-Ar dating: Reviews in Mineralogy and Geochemistry, v. 47, p. 785–818.
Kidston, J., Scaife, A.A., Hardiman, S.C., Mitchell, D.M., Butchart, N., Baldwin, M.P., and Gray, L.J., 2015, Stratospheric influence on tropospheric jet streams, storm tracks and surface weather: Nature Geoscience, v. 8, p. 433.
Kilian, R., and Lamy, F., 2012, A review of Glacial and Holocene paleoclimate records from southernmost Patagonia (49–55°S): Quaternary Science Reviews, v. 53, p. 1–23, doi:https://doi.org/10.1016/j.quascirev.2012.07.017.
Koch, J., and Kilian, R., 2005, 'Little Ice Age' glacier fluctuations, Gran Campo Nevado, southernmost Chile: The Holocene, v. 15, p. 20–28, doi:10.1191/0959683605hl780rp.
Kuhn, M., 1989, The Response of the Equilibrium Line Altitude to Climate Fluctuations: Theory and Observations, *in* Springer, Dordrecht, p. 407–417, doi:10.1007/978-94-015-7823-3_26.
Kuroda, Y., 2018, On the Origin of the Solar Cycle Modulation of the Southern Annular Mode: Journal of Geophysical Research: Atmospheres, v. 123, p. 1959–1969, doi:10.1002/2017JD027091.
Kuylenstierna, J.L., Rosqvist, G.C., and Holmlund, P., 1996, Late-Holocene glacier variations in the Cordillera Darwin, Tierra del Fuego, Chile: The Holocene, v. 6, p. 353–358, doi:10.1177/095968369600600310.
Lagabrielle, Y., Goddéris, Y., Donnadieu, Y., Malavieille, J., and Suarez, M., 2009, The tectonic history of Drake Passage and its possible impacts on global climate: Earth and Planetary Science Letters, v. 279, p. 197–211, doi:https://doi.org/10.1016/j.epsl.2008.12.037.
Lagabrielle, Y., Suárez, M., Rossello, E.A., Hérail, G., Martinod, J., Régnier, M., and de la Cruz, R., 2004, Neogene to Quaternary tectonic evolution of the Patagonian Andes at the latitude of the Chile Triple Junction: Tectonophysics, v. 385, p. 211–241, doi:https://doi.org/10.1016/j.tecto.2004.04.023.
Lal, D., 1987, 10Be in polar Ice: Data reflect changes in cosmic ray flux or polar meteorology: Geophysical Research Letters, v. 14, p. 785–788, doi:10.1029/GL014i008p00785.
Lal, D., 1991, Cosmic ray labeling of erosion surfaces: in situ nuclide production rates and erosion models: Earth and Planetary Science Letters, v. 104, p. 424–439, doi:10.1016/0012-821X(91)90220-C.
Lal, D., 1988, In Situ-Produced Cosmogenic Isotopes in Terrestrial Rocks: Annual Review of Earth and Planetary Sciences, v. 16, p. 355–388,

doi:10.1146/annurev.ea.16.050188.002035.
Lamy, F., Kilian, R., Arz, H.W., Francois, J.-P., Kaiser, J., Prange, M., and Steinke, T., 2010, Holocene changes in the position and intensity of the southern westerly wind belt: Nature Geoscience, v. 3, p. 695, https://doi.org/10.1038/ngeo959.
Lange, H., Casassa, G., Ivins, E.R., Schröder, L., Fritsche, M., Richter, A., Groh, A., and Dietrich, R., 2014, Observed crustal uplift near the Southern Patagonian Icefield constrains improved viscoelastic Earth models: Geophysical Research Letters, v. 41, p. 805–812, doi:10.1002/2013GL058419.
Larsen, D.J., Geirsdóttir, Á., and Miller, G.H., 2015, Precise chronology of Little Ice Age expansion and repetitive surges of Langjökull, central Iceland: Geology, v. 43, p. 167–170.
Laskar, J., Robutel, P., Joutel, F., Gastineau, M., Correia, A.C.M., and Levrard, B., 2004, A long-term numerical solution for the insolation quantities of the Earth : A&A, v. 428, p. 261–285, https://doi.org/10.1051/0004-6361:20041335.
Lavielle, B., Marti, K., Jeannot, J.-P., Nishiizumi, K., and Caffee, M., 1999, The 36Cl–36Ar–40K–41K records and cosmic ray production rates in iron meteorites: Earth and Planetary Science Letters, v. 170, p. 93–104, doi:https://doi.org/10.1016/S0012-821X(99)00099-0.
Lange, H., Casassa, G., Ivins, E.R., Schröder, L., Fritsche, M., Richter, A., Groh, A., and Dietrich, R., 2014, Observed crustal uplift near the Southern Patagonian Icefield constrains improved viscoelastic Earth models: Geophysical Research Letters, v. 41, p. 805–812, doi:10.1002/2013GL058419.
Libby, W.F., 1961, Radiocarbon dating: Science, v. 133, p. 621–629.
Lifton, N.A., Bieber, J.W., Clem, J.M., Duldig, M.L., Evenson, P., Humble, J.E., and Pyle, R., 2005, Addressing solar modulation and long-term uncertainties in scaling secondary cosmic rays for in situ cosmogenic nuclide applications: Earth and Planetary Science Letters, v. 239, p. 140–161, doi:10.1016/J.EPSL.2005.07.001.
Lifton, N., Sato, T., and Dunai, T.J., 2014, Scaling in situ cosmogenic nuclide production rates using analytical approximations to atmospheric cosmic-ray fluxes: Earth and Planetary Science Letters, v. 386, p. 149–160, doi:10.1016/J.EPSL.2013.10.052.
Lonsdale, P., 2005, Creation of the Cocos and Nazca plates by fission of the Farallon plate: Tectonophysics, v. 404, p. 237–264, doi:https://doi.org/10.1016/j.tecto.2005.05.011.
Lopez, P., Chevallier, P., Favier, V., Pouyaud, B., Ordenes, F., and Oerlemans, J., 2010, A regional view of fluctuations in glacier length in southern South America: Global and Planetary Change, v. 71, p. 85–108, doi:10.1016/J.GLOPLACHA.2009.12.009.
Luckman, B.H., 2000, The Little Ice Age in the Canadian Rockies: Geomorphology, v. 32, p. 357–384, doi:10.1016/S0169-555X(99)00104-X.
MacGregor, K.R., Anderson, R.S., Anderson, S.P., and Waddington, E.D., 2000, Numerical simulations of glacial-valley longitudinal profile evolution: Geology, v. 28, p. 1031–1034, doi:10.1130/0091-7613(2000)28<1031:NSOGLP>2.0.CO;2.
Mackintosh, A.N., Anderson, B.M., and Pierrehumbert, R.T., 2017, Reconstructing Climate from Glaciers: Annual Review of Earth and Planetary Sciences, v. 45, p. 649–680, doi:10.1146/annurev-earth-063016-020643.
Marden, C.J., and Clapperton, C.M., 1995, Fluctuations of the South Patagonian Ice-field during the last glaciation and the Holocene: Journal of Quaternary Science, v. 10, p. 197–209, doi:10.1002/jqs.3390100302.
Mardones, M., González, L., King, R., and Campos, E., 2011, Variaciones glaciales durante el Holoceno en Patagonia Central, Aisén, Chile: evidencias geomorfológicas:

Andean Geology, v. 38, p. 371–392.
Marshall, G.J., 2003, Trends in the Southern Annular Mode from Observations and Reanalyses: Journal of Climate, p. 4134–4143, doi:10.1175/1520-0442(2003)016<4134:TITSAM>2.0.CO;2.
Martin, J.R. V, Davies, B.J., and Thorndycraft, V.R., 2019, Glacier dynamics during a phase of Late Quaternary warming in Patagonia reconstructed from sediment-landform associations: Geomorphology, v. 337, p. 111–133.
Masiokas, M.H., Luckman, B.H., Delgado, S., Skvarca, P., and Ripalta, A., 2009, Little Ice Age fluctuations of small glaciers in the Monte Fitz Roy and Lago del Desierto areas, south Patagonian Andes, Argentina: Palaeogeography, Palaeoclimatology, Palaeoecology, v. 281, p. 351–362, doi:10.1016/J.PALAEO.2007.10.031.
Masiokas, M.H., Villalba, R., Luckman, B.H., Lascano, M.E., Delgado, S., and Stepanek, P., 2008, 20th-century glacier recession and regional hydroclimatic changes in northwestern Patagonia: Global and Planetary Change, v. 60, p. 85–100, doi:https://doi.org/10.1016/j.gloplacha.2006.07.031.
Matthews, J.A., and Briffa, K.R., 2005, The 'Little Ice Age': re-evaluation of an evolving concept: Geografiska Annaler: Series A, Physical Geography, v. 87, p. 17–36.
Mayo, L.R., 1984, Glacier Mass Balance and Runoff Research in the U.S.A.: Geografiska Annaler: Series A, Physical Geography, v. 66, p. 215–227, doi:10.1080/04353676.1984.11880110.
Mayo, L.R., and March, R.S., 1990, Air temperature and precipitation at Wolverine Glacier, Alaska; Glacier growth in a warmer, wetter climate: Annals of Glaciology, v. 14, p. 191–194.
Mayr, C. et al., 2007, Holocene variability of the Southern Hemisphere westerlies in Argentinean Patagonia (52°S): Quaternary Science Reviews, v. 26, p. 579–584, doi:https://doi.org/10.1016/j.quascirev.2006.11.013.
McCarthy, D.P., Luckman, B.H., and Kelly, P.E., 1991, Sampling Height-Age Error Correction for Spruce Seedlings in Glacial Forefields, Canadian Cordillera: Arctic and Alpine Research, v. 23, p. 451–455, doi:10.1080/00040851.1991.12002865.
McCulloch, R.D., Bentley, M.J., Tipping, R.M., and Clapperton, C.M., 2005a, Evidence for late-glacial ice dammed lakes in the central strait of magellan and bahía inútil, southernmost south america: Geografiska Annaler: Series A, Physical Geography, v. 87, p. 335–362, doi:10.1111/j.0435-3676.2005.00262.x.
McCulloch, R.D., Fogwill, C.J., Sugden, D.E., Bentley, M.J., and Kubik, P.W., 2005b, Chronology of the last glaciation in central strait of magellan and bahía inútil, southernmost south america: Geografiska Annaler: Series A, Physical Geography, v. 87, p. 289–312, doi:10.1111/j.0435-3676.2005.00260.x.
Meier, M.F., 1962, Proposed definitions for glacier mass budget terms: Journal of Glaciology, v. 4, p. 252–263.
Meier, M.F., and Post, A.S., 1962, Recent variations in mass net budgets of glaciers in western North America: International Association of Hydrological Sciences Publication, v. 58, p. 63–77.
Meier, M.F., and Post, A., 1987, Fast tidewater glaciers: Journal of Geophysical Research, v. 92, p. 9051, doi:10.1029/JB092iB09p09051.
Meierding, T.C., 1982, Late Pleistocene Glacial Equilibrium-Line Altitudes in the Colorado Front Range: A Comparison of Methods: Quaternary Research, v. 18, p. 289–310, doi:10.1016/0033-5894(82)90076-X.
Melkonian, A.K., Willis, M.J., Pritchard, M.E., Rivera, A., Bown, F., and Bernstein, S.A., 2013, Satellite-derived volume loss rates and glacier speeds for the Cordillera

Darwin Icefield, Chile: The Cryosphere, v. 7, p. 823–839, doi:10.5194/tc-7-823-2013.
Menounos, B., Clague, J.J., Osborn, G., Davis, P.T., Ponce, F., Goehring, B., Maurer, M., Rabassa, J., Coronato, A., and Marr, R., 2013, Latest Pleistocene and Holocene glacier fluctuations in southernmost Tierra del Fuego, Argentina: Quaternary Science Reviews, v. 77, p. 70–79, doi:10.1016/J.QUASCIREV.2013.07.008.
Menounos, B., Osborn, G., Clague, J.J., and Luckman, B.H., 2009, Latest Pleistocene and Holocene glacier fluctuations in western Canada: Quaternary Science Reviews, v. 28, p. 2049–2074, doi:https://doi.org/10.1016/j.quascirev.2008.10.018.
Mercer, J.H., 1965, Glacier Variations in Southern Patagonia: Geographical Review, v. 55, p. 390–413, doi:10.2307/213136.
Mercer, J.H., 1968, Variations of some Patagonian glaciers since the Late-Glacial: American Journal of Science, v. 266, p. 91–109, doi:10.2475/ajs.266.2.91.
Mercer, J.H., 1970, Variations of some Patagonian glaciers since the Late-Glacial; II: American Journal of Science, v. 269, p. 1–25, doi:10.2475/ajs.269.1.1.
Mercer, J.H., 1976, Glacial history of southernmost South America: Quaternary Research, v. 6, p. 125–166, doi:10.1016/0033-5894(76)90047-8.
Mercer, J.H., 1982, Holocene glacier variations in southern South America.: v. 18, 35–40 p.
Mercer, J.H., Fleck, R.J., Mankinen, E.A., and Sander, W., 1975, Southern Patagonia—Glacial events between 4 m.y. and 1 m.y. ago: Royal Society of New Zealand Bulletin, v. 13, p. 223–230, http://pubs.er.usgs.gov/publication/70197180.
Miller, A., 1976, The Climate of Chile, *in* Schwerdtfeger, W. ed., World Survey of Climatology, Amsterdam, Elsevier, p. 113–130.
Mitchell, S.G., and Montgomery, D.R., 2006, Influence of a glacial buzzsaw on the height and morphology of the Cascade Range in central Washington State, USA: Quaternary Research, v. 65, p. 96–107.
Mix, A.C., Bard, E., and Schneider, R., 2001, Environmental processes of the ice age: land, oceans, glaciers (EPILOG): Quaternary Science Reviews, v. 20, p. 627–657.
Monnin, E., Steig, E.J., Siegenthaler, U., Kawamura, K., Schwander, J., Stauffer, B., Stocker, T.F., Morse, D.L., Barnola, J.-M., and Bellier, B., 2004, Evidence for substantial accumulation rate variability in Antarctica during the Holocene, through synchronization of CO2 in the Taylor Dome, Dome C and DML ice cores: Earth and Planetary Science Letters, v. 224, p. 45–54.
Montgomery, D.R., 2002, Valley formation by fluvial and glacial erosion: Geology, v. 30, p. 1047–1050.
Montgomery, D.R., Balco, G., and Willett, S.D., 2001, Climate, tectonics, and the morphology of the Andes: Geology, v. 29, p. 579–582, doi:10.1130/0091-7613(2001)029<0579:CTATMO>2.0.CO;2.
Moreno, P.I. et al., 2018, Onset and Evolution of Southern Annular Mode-Like Changes at Centennial Timescale: Scientific Reports, v. 8, p. 3458, doi:10.1038/s41598-018-21836-6.
Moreno, P.I., Denton, G.H., Moreno, H., Lowell, T. V, Putnam, A.E., and Kaplan, M.R., 2015, Radiocarbon chronology of the last glacial maximum and its termination in northwestern Patagonia: Quaternary Science Reviews, v. 122, p. 233–249.
Moreno, P.I., François, J.P., Villa-Martínez, R.P., and Moy, C.M., 2009, Millennial-scale variability in Southern Hemisphere westerly wind activity over the last 5000 years in SW Patagonia: Quaternary Science Reviews, v. 28, p. 25–38, doi:https://doi.org/10.1016/j.quascirev.2008.10.009.

Naranjo, J.A., and Stern, C.R., 2004, Holocene tephrochronology of the southernmost part (42°30'-45°S) of the Andean Southern Volcanic Zone: Revista geológica de Chile, v. 31, p. 224–240, doi:10.4067/S0716-02082004000200003.
Nesje, A., 1992, Topographical effects on the equilibrium-line altitude on glaciers: Geojournal, v. 27, doi:10.1007/BF00185102.
Nesje, A., 2009, Latest Pleistocene and Holocene alpine glacier fluctuations in Scandinavia: Quaternary Science Reviews, v. 28, p. 2119–2136, doi:10.1016/j.quascirev.2008.12.016.
Nesje, A., and Matthews, J.A., 2012, The Briksdalsbre Event: A winter precipitation-induced decadal-scale glacial advance in southern Norway in the ad 1990s and its implications: The Holocene, v. 22, p. 249–261.
Nesje, A., Matthews, J.A., Dahl, S.O., Berrisford, M.S., and Andersson, C., 2001, Holocene glacier fluctuations of Flatebreen and winter-precipitation changes in the Jostedalsbreen region, western Norvay, based on glaciolacustrine sediment records: The Holocene, v. 11, p. 267–280, doi:10.1191/095968301669980885.
Nimick, D.A., McGrath, D., Mahan, S.A., Friesen, B.A., and Leidich, J., 2016, Latest Pleistocene and Holocene glacial events in the Colonia valley, Northern Patagonia Icefield, southern Chile: Journal of Quaternary Science, v. 31, p. 551–564, doi:10.1002/jqs.2847.
Nishiizumi, K., Winterer, E.L., Kohl, C.P., Klein, J., Middleton, R., Lal, D., and Arnold, J.R., 1989, Cosmic ray production rates of 10Be and 26Al in quartz from glacially polished rocks: Journal of Geophysical Research: Solid Earth, v. 94, p. 17907–17915, doi:10.1029/JB094iB12p17907.
Nishiizumi, K., Imamura, M., Caffee, M.W., Southon, J.R., Finkel, R.C., and McAninch, J., 2007, Absolute calibration of 10Be AMS standards: Nuclear Instruments and Methods in Physics Research Section B: Beam Interactions with Materials and Atoms, v. 258, p. 403–413, doi:10.1016/J.NIMB.2007.01.297.
Oerlemans, J., 2001, Glaciers and climate change: CRC Press.
Oerlemans, J., 2005, Extracting a Climate Signal from 169 Glacier Records: Science, v. 308, p. 675–677, doi:10.1126/science.1107046.
Oerlemans, J., and Fortuin, J.P.F., 1992, Sensitivity of glaciers and small ice caps to greenhouse warming: Science, v. 258, p. 115–117.
Oerlemans, J., and Hoogendoorn, N.C., 1989, Mass-balance gradients and climatic change: Journal of Glaciology, v. 35, p. 399–405.
Ohmura, A., Kasser, P., and Funk, M., 1992, Climate at the equilibrium line of glaciers: Journal of Glaciology, v. 38, p. 397–411.
Olley, J., Caitcheon, G., and Murray, A., 1998, The distribution of apparent dose as determined by optically stimulated luminescence in small aliquots of fluvial quartz: implications for dating young sediments: Quaternary Science Reviews, v. 17, p. 1033–1040.
Olson, D.M. et al., 2001, Terrestrial Ecoregions of the World: A New Map of Life on Earth: BioScience, v. 51, p. 933–938, doi:10.1641/0006-3568(2001)051[0933:teotwa]2.0.co;2.
Oppedal, L.T., Bakke, J., Paasche, Ø., Werner, J.P., and van der Bilt, W.G.M., 2018, Cirque Glacier on South Georgia Shows Centennial Variability over the Last 7000 Years : Frontiers in Earth Science , v. 6, p. 2, https://www.frontiersin.org/article/10.3389/feart.2018.00002.
Osmaston, H., 2005, Estimates of glacier equilibrium line altitudes by the Area× Altitude, the Area× Altitude Balance Ratio and the Area× Altitude Balance Index

methods and their validation: Quaternary International, v. 138, p. 22–31.
Pardo-Casas, F., and Molnar, P., 1987, Relative motion of the Nazca (Farallon) and South American Plates since Late Cretaceous time: Tectonics, v. 6, p. 233–248, doi:10.1029/TC006i003p00233.
Pedro, J.B. et al., 2016, The spatial extent and dynamics of the Antarctic Cold Reversal: Nature Geoscience, v. 9, p. 51–55, doi:10.1038/ngeo2580.
Peel, M.C., Finlayson, B.L., and McMahon, T.A., 2007, Updated world map of the Köppen-Geiger climate classification: Hydrology and earth system sciences discussions, v. 4, p. 439–473.
Popovnin, V. V, Danilova, T.A., and Petrakov, D.A., 1999, A pioneer mass balance estimate for a Patagonian glacier: Glaciar De los Tres, Argentina: Global and Planetary Change, v. 22, p. 255–267.
Porter, S.C., 1975, Equilibrium-line Altitudes of Late Quaternary Glaciers in the Southern Alps, New Zealand: Quaternary Research, v. 5, p. 27–47, doi:10.1016/0033-5894(75)90047-2.
Porter, S.C., 1977, Present and Past Glaciation Threshold in the Cascade Range, Washington, U.S.A.: Topographic and Climatic Controls, and Paleoclimatic Implications: Journal of Glaciology, v. 18, p. 101–116, doi:10.3189/S0022143000021559.
Porter, S.C., 2000, Onset of Neoglaciation in the Southern Hemisphere: Journal of Quaternary Science, v. 15, p. 395–408, doi:10.1002/1099-1417(200005)15:4<395::AID-JQS535>3.0.CO;2-H.
Porter, S.C., and Denton, G.H., 1967, Chronology of neoglaciation in the North American Cordillera: American Journal of Science , v. 265, p. 177–210, doi:10.2475/ajs.265.3.177.
Putnam, A.E., Denton, G.H., Schaefer, J.M., Barrell, D.J.A., Andersen, B.G., Finkel, R.C., Schwartz, R., Doughty, A.M., Kaplan, M.R., and Schlüchter, C., 2010, Glacier advance in southern middle-latitudes during the Antarctic Cold Reversal: Nature Geoscience, v. 3, p. 700–704, doi:10.1038/ngeo962.
Putnam, A.E., Schaefer, J.M., Denton, G.H., Barrell, D.J.A., Birkel, S.D., Andersen, B.G., Kaplan, M.R., Finkel, R.C., Schwartz, R., and Doughty, A.M., 2013, The last glacial maximum at 44°S documented by a ^{10}Be moraine chronology at Lake Ohau, Southern Alps of New Zealand: Quaternary Science Reviews, v. 62, p. 114–141.
Putnam, A.E., Schaefer, J.M., Denton, G.H., Barrell, D.J.A., Finkel, R.C., Andersen, B.G., Schwartz, R., Chinn, T.J.H., and Doughty, A.M., 2012, Regional climate control of glaciers in New Zealand and Europe during the pre-industrial Holocene: Nature Geoscience, v. 5, p. 627, https://doi.org/10.1038/ngeo1548.
Rabassa, J. et al., 2000, Quaternary of Tierra del Fuego, Southernmost South America: an updated review: Quaternary International, v. 68–71, p. 217–240, doi:10.1016/S1040-6182(00)00046-X.
Ramos, V.A., 1989, Andean Foothills Structures in Northern Magallanes Basin, Argentina: AAPG Bulletin, v. 73, p. 887–903, http://archives.datapages.com/data/bulletns/1988-89/data/pg/0073/0007/0850/0887.htm?doi=10.1306%2F44B4A28A-170A-11D7-8645000102C1865D (accessed July 2019).
Ramos, V.A., 2005, Seismic ridge subduction and topography: Foreland deformation in the Patagonian Andes: Tectonophysics, v. 399, p. 73–86, doi:10.1016/J.TECTO.2004.12.016.
Ramos, V.A., and Ghiglione, M.C., 2008, Tectonic Evolution of the Patagonian Andes, *in*

Rabassa, J.B.T.-D. in Q.S. ed., The Late Cenozoic of Patagonia and Tierra del Fuego, Elsevier, v. 11, p. 57–71, doi:https://doi.org/10.1016/S1571-0866(07)10004-X.
Rasmussen, L.A., Conway, H., and Raymond, C.F., 2007, Influence of upper air conditions on the Patagonia icefields: Global and Planetary Change, v. 59, p. 203–216, doi:10.1016/J.GLOPLACHA.2006.11.025.
Raymond, C.F., 1987, How do glaciers surge? A review: Journal of Geophysical Research: Solid Earth, v. 92, p. 9121–9134, doi:10.1029/JB092IB09P09121@10.1002/(ISSN)2169-9356.CHAPMAN2.
Rea, B.R., 2009, Defining modern day Area-Altitude Balance Ratios (AABRs) and their use in glacier-climate reconstructions: Quaternary Science Reviews, v. 28, p. 237–248, doi:10.1016/J.QUASCIREV.2008.10.011.
Reichert, B.K., Bengtsson, L., and Oerlemans, J., 2002, Recent glacier retreat exceeds internal variability: Journal of Climate, v. 15, p. 3069–3081.
Reimer, P.J., Baillie, M.G.L., Bard, E., Bayliss, A., Beck, J.W., Blackwell, P.G., Ramsey, C.B., Buck, C.E., Burr, G.S., and Edwards, R.L., 2009, IntCal09 and Marine09 radiocarbon age calibration curves, 0–50,000 years cal BP: Radiocarbon, v. 51, p. 1111–1150.
Reimer, P.J., Bard, E., Bayliss, A., Beck, J.W., Blackwell, P.G., Ramsey, C.B., Buck, C.E., Cheng, H., Edwards, R.L., and Friedrich, M., 2013, IntCal13 and Marine13 radiocarbon age calibration curves 0–50,000 years cal BP: Radiocarbon, v. 55, p. 1869–1887.
Rhodes, E.J., 2011, Optically stimulated luminescence dating of sediments over the past 200,000 years: Annual Review of Earth and Planetary Sciences, v. 39, p. 461–488.
Rivera, A., and Casassa, G., 1999, Volume changes on Pio XI glacier, Patagonia: 1975–1995: Global and Planetary Change, v. 22, p. 233–244.
Rodgers, K.B., Mikaloff-Fletcher, S.E., Bianchi, D., Beaulieu, C., Galbraith, E.D., Gnanadesikan, A., Hogg, A.G., Iudicone, D., Lintner, B.R., and Naegler, T., 2011, Interhemispheric gradient of atmospheric radiocarbon reveals natural variability of Southern Ocean winds: Climate of the Past, v. 7, p. 1123–1138.
Roe, G.H., 2011, What do glaciers tell us about climate variability and climate change? Journal of Glaciology, v. 57, p. 567–578, doi:10.3189/002214311796905640.
Roe, G.H., and O'Neal, M.A., 2009, The response of glaciers to intrinsic climate variability: observations and models of late-Holocene variations in the Pacific Northwest: Journal of Glaciology, v. 55, p. 839–854, doi:10.3189/002214309790152438.
Rosenblüth, B., Fuenzalida, H.A., and Aceituno, P., 1997, Recent temperature variations in southern South America: International Journal of Climatology, v. 17, p. 67–85, doi:10.1002/(SICI)1097-0088(199701)17:1<67::AID-JOC120>3.0.CO;2-G.
Röthlisberger, F., 1986, 10,000 Jahre Gletschergeschichte der Erde: Ein Vergleich zwischen Nord- und Südhemisphäre: Aarau, Verlag Sauerländer, 416 p.
Sagredo, E.A., Kaplan, M.R., Araya, P.S., Lowell, T. V., Aravena, J.C., Moreno, P.I., Kelly, M.A., and Schaefer, J.M., 2018, Trans-pacific glacial response to the Antarctic Cold Reversal in the southern mid-latitudes: Quaternary Science Reviews, v. 188, p. 160–166, doi:10.1016/J.QUASCIREV.2018.01.011.
Sagredo, E.A., Lowell, T. V, Kelly, M.A., Rupper, S., Aravena, J.C., Ward, D.J., and Malone, A.G.O., 2016, Equilibrium line altitudes along the Andes during the Last millennium: Paleoclimatic implications: The Holocene, v. 27, p. 1019–1033, doi:10.1177/0959683616678458.
Sagredo, E.A., Rupper, S., and Lowell, T. V., 2014, Sensitivities of the equilibrium line

altitude to temperature and precipitation changes along the Andes: Quaternary Research, v. 81, p. 355–366, doi:10.1016/j.yqres.2014.01.008.
Sato, T., Yasuda, H., Niita, K., Endo, A., and Sihver, L., 2008, Development of PARMA: PHITS-based Analytical Radiation Model in the Atmosphere: Radiation Research, v. 170, p. 244–259, https://doi.org/10.1667/RR1094.1.
Schaefer, J.M., Denton, G.H., Barrell, D.J.A., Ivy-Ochs, S., Kubik, P.W., Andersen, B.G., Phillips, F.M., Lowell, T. V., and Schlüchter, C., 2006, Near-synchronous interhemispheric termination of the last glacial maximum in mid-latitudes: Science, v. 312, p. 1510–1513, doi:10.1126/science.1122872.
Schaefer, J.M. et al., 2009, High-frequency holocene glacier fluctuations in new zealand differ from the northern signature: Science, v. 324, p. 622–625, doi:10.1126/science.1169312.
Schimmelpfennig, I., Schaefer, J.M., Akçar, N., Koffman, T., Ivy-Ochs, S., Schwartz, R., Finkel, R.C., Zimmerman, S., and Schlüchter, C., 2014, A chronology of Holocene and Little Ice Age glacier culminations of the Steingletscher, Central Alps, Switzerland, based on high-sensitivity beryllium-10 moraine dating: Earth and Planetary Science Letters, v. 393, p. 220–230, doi:https://doi.org/10.1016/j.epsl.2014.02.046.
Shawky, M., Moussa, A., Hassan, Q.K., El-Sheimy, N., Shawky, M., Moussa, A., Hassan, Q.K., and El-Sheimy, N., 2019, Pixel-Based Geometric Assessment of Channel Networks/Orders Derived from Global Spaceborne Digital Elevation Models: Remote Sensing, v. 11, p. 235, doi:10.3390/rs11030235.
Sibson, R., 1981, A brief description of natural neighbour interpolation, in Barnett, V. ed., Interpreting multivariate data, John Wiley & Sons, p. 374.
Sigafoos, R.S., and Hendricks, E.L., 1969, The time interval between stabilization of alpine glacial deposits and establishment of tree seedlings: US Geological Survey Professional Paper, v. 650, p. B89–B93.
Simpkins, G.R., and Karpechko, A.Y., 2012, Sensitivity of the southern annular mode to greenhouse gas emission scenarios: Climate dynamics, v. 38, p. 563–572.
Sissons, J.B., 1974, A Late-Glacial Ice Cap in the Central Grampians, Scotland: Transactions of the Institute of British Geographers, p. 95, doi:10.2307/621517.
Smedley, R.K., Glasser, N.F., and Duller, G.A.T., 2016, Luminescence dating of glacial advances at Lago Buenos Aires (~46 °S), Patagonia: Quaternary Science Reviews, v. 134, p. 59–73, doi:10.1016/J.QUASCIREV.2015.12.010.
Solomina, O.N. et al., 2015, Holocene glacier fluctuations: Quaternary Science Reviews, v. 111, p. 9–34, doi:10.1016/j.quascirev.2014.11.018.
Steinhilber, F., Abreu, J.A., and Beer, J., 2008, Solar modulation during the Holocene: Astrophys. Space Sci. Trans., v. 4, p. 1–6, doi:10.5194/astra-4-1-2008.
Steinhilber, F., Beer, J., and Fröhlich, C., 2009, Total solar irradiance during the Holocene: Geophysical Research Letters, v. 36.
Stern, C.R., 2008, Holocene tephrochronology record of large explosive eruptions in the southernmost Patagonian Andes: Bulletin of Volcanology, v. 70, p. 435–454, doi:10.1007/s00445-007-0148-z.
Stone, J.O., 2000, Air pressure and cosmogenic isotope production: Journal of Geophysical Research: Solid Earth, v. 105, p. 23753–23759, doi:10.1029/2000JB900181.
Strelin, J., Casassa, G., Rosqvist, G., and Holmlund, P., 2008, Holocene glaciations in the Ema Glacier valley, Monte Sarmiento Massif, Tierra del Fuego: Palaeogeography, Palaeoclimatology, Palaeoecology, v. 260, p. 299–314,

doi:10.1016/J.PALAEO.2007.12.002.
Strelin, J.A., Denton, G.H., Vandergoes, M.J., Ninnemann, U.S., and Putnam, A.E., 2011, Radiocarbon chronology of the late-glacial Puerto Bandera moraines, Southern Patagonian Icefield, Argentina: Quaternary Science Reviews, v. 30, p. 2551–2569, doi:10.1016/J.QUASCIREV.2011.05.004.
Strelin, J.A., Kaplan, M.R., Vandergoes, M.J., Denton, G.H., and Schaefer, J.M., 2014, Holocene glacier history of the Lago Argentino basin, Southern Patagonian Icefield: Quaternary Science Reviews, v. 101, p. 124–145, doi:10.1016/j.quascirev.2014.06.026.
Strelin, J.A., and Malagnino, E.C., 2000, Late-Glacial History of Lago Argentino, Argentina, and Age of the Puerto Bandera Moraines: Quaternary Research, v. 54, p. 339–347, https://www.sciencedirect.com/science/article/pii/S0033589400921781 (accessed November 2018).
Stuiver, M., Reimer, P.J., Bard, E., Beck, J.W., Burr, G.S., Hughen, K.A., Kromer, B., McCormac, G., Van Der Plicht, J., and Spurk, M., 1998, INTCAL98 radiocarbon age calibration, 24,000–0 cal BP: Radiocarbon, v. 40, p. 1041–1083.
Sugden, D.E., Hulton, N.R.J., and Purves, R.S., 2002, Modelling the inception of the Patagonian icesheet: Quaternary International, v. 95, p. 55–64.
Templeton, D.H., 1953, Nuclear Reactions Induced by High Energy Particles: Annual Review of Nuclear Science, v. 2, p. 93–104, doi:10.1146/annurev.ns.02.120153.000521.
Thompson, D.W.J., and Solomon, S., 2002, Interpretation of Recent Southern Hemisphere Climate Change: Science, v. 296, p. 895 LP – 899, doi:10.1126/science.1069270.
Thompson, D.W.J., Solomon, S., Kushner, P.J., England, M.H., Grise, K.M., and Karoly, D.J., 2011, Signatures of the Antarctic ozone hole in Southern Hemisphere surface climate change: Nature Geoscience, v. 4, p. 741, https://doi.org/10.1038/ngeo1296.
Thomson, S.N., 2002, Late Cenozoic geomorphic and tectonic evolution of the Patagonian Andes between latitudes 42°S and 46°S: An appraisal based on fission-track results from the transpressional intra-arc Liquiñe-Ofqui fault zone: GSA Bulletin, v. 114, p. 1159–1173, doi:10.1130/0016-7606(2002)114<1159:LCGATE>2.0.CO;2.
Thomson, S.N., Brandon, M.T., Tomkin, J.H., Reiners, P.W., Vásquez, C., and Wilson, N.J., 2010, Glaciation as a destructive and constructive control on mountain building: Nature, v. 467, p. 313, https://doi.org/10.1038/nature09365.
Thomson, S.N., Hervé, F., and Stöckhert, B., 2001, Mesozoic-Cenozoic denudation history of the Patagonian Andes (southern Chile) and its correlation to different subduction processes: Tectonics, v. 20, p. 693–711, doi:10.1029/2001TC900013.
Van Daele, M. et al., 2016, Late Quaternary evolution of Lago Castor (Chile, 45.6°S): Timing of the deglaciation in northern Patagonia and evolution of the southern westerlies during the last 17 kyr: Quaternary Science Reviews, v. 133, p. 130–146, doi:10.1016/J.QUASCIREV.2015.12.021.
Vargo, L.J., Galewsky, J., Rupper, S., and Ward, D.J., 2018, Sensitivity of glaciation in the arid subtropical Andes to changes in temperature, precipitation, and solar radiation: Global and Planetary Change, v. 163, p. 86–96, doi:10.1016/J.GLOPLACHA.2018.02.006.
Villalba, R., 1990, Climatic Fluctuations in Northern Patagonia during the Last 1000 Years as Inferred from Tree-Ring Records: Quaternary Research, v. 34, p. 346–360, doi:DOI: 10.1016/0033-5894(90)90046-N.

Villalba, R. et al., 2012, Unusual Southern Hemisphere tree growth patterns induced by changes in the Southern Annular Mode: Nature Geoscience, v. 5, p. 793, https://doi.org/10.1038/ngeo1613.
Wallinga, J., 2002, Optically stimulated luminescence dating of fluvial deposits: a review: Boreas, v. 31, p. 303–322.
Wenzens, G., 1999, Fluctuations of Outlet and Valley Glaciers in the Southern Andes (Argentina) during the Past 13,000 Years: Quaternary Research, v. 51, p. 238–247, doi:10.1006/QRES.1999.2043.
Wolff, I.W., Glasser, N.F., and Hubbard, A., 2013, The reconstruction and climatic implication of an independent palaeo ice cap within the Andean rain shadow east of the former Patagonian ice sheet, Santa Cruz Province, Argentina: Geomorphology, v. 185, p. 1–15, doi:https://doi.org/10.1016/j.geomorph.2012.10.018.
Wright, H.E., and Porter, S.C., 1983, Late Quaternary Environments of the United States: The Late Pleistocene: U of Minnesota Press, v. 1.
Yang, J., and Xiao, C., 2018, The evolution and volcanic forcing of the southern annular mode during the past 300 years: International Journal of Climatology, v. 38, p. 1706–1717, doi:10.1002/joc.5290.
Yuan, X., Kaplan, M.R., and Cane, M.A., 2018, The interconnected global climate system-a review of tropical-polar teleconnections: Journal of Climate, v. 31, p. 5765–5792, doi:10.1175/JCLI-D-16-0637.1.
Zárate, M.A., 2003, Loess of southern south america: Quaternary Science Reviews, v. 22, p. 1987–200.
Zemp, M., 2008, Global glacier changes: facts and figures: UNEP/Earthprint.

* * *

Appendix A – Supplementary material for "Holocene glacier fluctuations in Patagonia are modulated by summer insolation intensity and paced by Southern Annular Mode-like variability"

Supplementary Information for

Holocene glacier fluctuations in Patagonia are modulated by summer insolation intensity and paced by Southern Annular Mode-like variability

Scott A. Reynhout[1,2], Esteban A. Sagredo*[2,3], Michael R. Kaplan[4,5], Juan Carlos Aravena[2,5], Mateo A. Martini[6,7], Patricio I. Moreno[2,8], Maisa Rojas[2,9], Roseanne Schwartz[4], and Joerg M. Schaefer[4,10]

[1]*Departamento de Geología, Facultad de Ciencias Físicas y Matemáticas, Universidad de Chile, Plaza Ercilla 803, 8370450 Santiago, Chile*
[2]*Núcleo Milenio Paleoclima, Universidad de Chile, Las Palmeras 3425, Ñuñoa, Chile*
[3]*Instituto de Geografía, Pontificia Universidad Católica de Chile, Avenida Vicuña Mackenna 4860, 7820436 Macul, Chile*
[4]*Lamont-Doherty Earth Observatory, P.O. Box 1000, 61 Route 9W, Palisades, NY 10964-100, United States of America*
[5]*Centro de Investigación Gaia Antártica, Universidad de Magallanes, Avenida Bulnes 01855 62000009, Punta Arenas, Chile*
[6]*Centro de Investigaciones en Ciencias de la Tierra (CONICET-UNC), Vélez Sársfeld 1611, X5016GCA, Córdoba, Argentina*
[7]*Facultad de Ciencias Exactas, Físicas y Naturales (Universidad Nacional de Córdoba), Vélez Sársfled 1611, X5016GCA, Córdoba, Argentina*
[8]*Departamento de Ciencias Ecológicas, Facultad de Ciencias, Universidad de Chile, Las Palmeras 3425, Ñuñoa, Chile*
[9]*Departamento de Geofísica, Facultad de Ciencias Físicas y Matemáticas, Universidad de Chile, Avenida Blanco Encalada 2002, Santiago, Chile*
[10]*Department of Earth and Environmental Sciences of Columbia University, New York, NY, 10027, USA*

This file includes:

Comparison of results with historical records

Of the seven moraines dated in our study, six have previously-reported age constraints. The ages we obtained for moraines M1-M7 differ significantly from the radiocarbon, lichenometric, and dendrochronologic age constraints obtained by previous workers (Garibotti and Villalba, 2009; Masiokas et al., 2009; Mercer, 1965) (Table S2). In the case of M3 and M4 this was not unexpected, as the ~400-year-old ages of *Nothofagus betuloides* used by Masiokas et al. (2009) approached the maximum living age of these trees in such climate conditions. However, it is noteworthy that our c. 1500 CE age for the treeless M7 moraine predates the oldest trees in the study area. As growth has not begun on this moraine, which is older than the maximum age of *Nothofagus betuloides*, this suggests that previously-suggested ecesis intervals for this region must be applied with caution.

Mercer (1965) obtained a minimum-limiting age for the M3 complex of 800 ± 85 ^{14}C yr (730 ± 100 cal yr BP; Hogg et al. 2013; Stuiver and Reimer 2018) from a basal peat overlying till between moraines M3 and M4, recognizing that the age was likely not a close limiting age. Although not inaccurate, the minimum-limiting age differs significantly from our reported age of 6,860 ± 140 yr for M3. This pattern of 'loose' constraining ages has been observed previously in the region, where minimum limiting ages for peat overlying till have been shown to greatly underestimate the true age of the landform. The assumption underlying the use of basal peat on glacial sediment is often that its development begins soon after a surface has been deglaciated, and that there have been no episodes of erosion or unfavorable climate that could strip initial growth and "reset" the date. The results from this study suggest that minimum ages obtained in this fashion must be treated with caution.

Although workers have studied the paleoglacial chronology of Patagonia for almost seventy years, prior studies have not revealed a pattern of progressively less-extensive Holocene glacier advances since late-glacial time, including in the early Holocene. We consider several reasons for the novelty of our finding:

a) Until recently, prior efforts could not directly date moraines and thus glacier expansions. The common assumption that radiocarbon-based minimum-limiting ages tightly constrain deglaciation in Patagonia. Many "late Holocene" moraines dated using this method may actually correspond to earlier times;
b) The few studies that obtained bracketing ages for glacial advances (close maximum, as well as minimum, ages of a glacial sequence) do show evidence for early Holocene glacier activity, although of uncertain extent (Harrison et al., 2012; Mercer, 1965; Röthlisberger, 1986; Strelin et al., 2014);
c) In areas studied previously, erosion may have partially to completely removed evidence of middle to early Holocene glacier advances, as appears to be the case in certain sites in New Zealand (Schaefer et al., 2009);

Recent work has focused on outlet glaciers of the Patagonian Icefields, including recent efforts directly dating moraines using ^{10}Be (Kaplan et al., 2016). During the early Holocene, we infer that climate shifts favorable for glacier advance may have been relatively short; the South Patagonian Icefield and its associated outlet glaciers, although climatically sensitive (Strelin et al., 2014), may not have had enough time to respond (Jóhannesson et al., 1989) and leave a preserved geomorphic record on the landscape

that was greater than subsequent expansions. That is, in the early Holocene such cool periods occurred as brief excursions from what was still a generally warm period.

Fig. S1. Samples and geomorphology of the Torre Glacier area. a) Sample FRY16-02-03 (460 ± 20 yr BP) yields the youngest age in the region, from the granitic boulder (1.2 m x 1.0 m x 0.6 m) perched atop a quartz diorite block embedded in the sharp frontal ridge crest of M7. The Torre Glacier is in the background, behind Laguna Torre. b) Sample FR14-01-24 (6,910 ± 130 yr BP) is a granodiorite block perched on top of a sinuous ridge relatively free of vegetation, interpreted as the frontal moraine of M3. c) Sample FRY16-02-08 (6,920 ± 160 yr BP) was taken from an angular quartz diorite block on top of the outermost lateral of the M3 complex; this date is statistically indistinguishable from FR14-01-24. d) View to the northwest from the frontal ridge crest of M4. An inactive meltwater paleochannel is developed in the base of this moraine. Vegetation increases significantly on the leeward (right) side of this moraine, where a mature Nothofagus forest is encountered. M7 is the bare moraine ridge in the left background; the hummocky topography between M4 and M7 represents the dissected M5 and M6 advances.

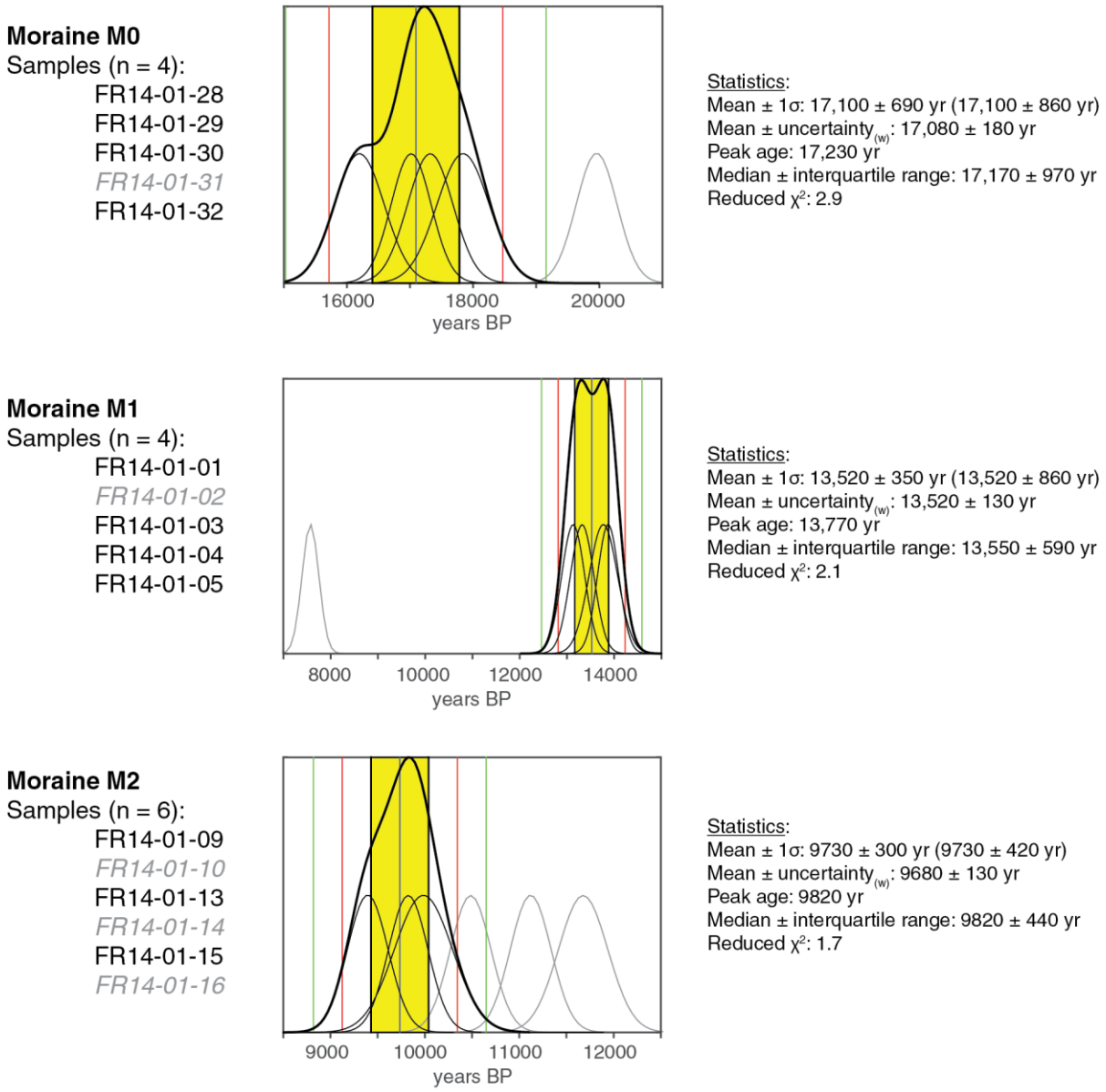

Fig. S2. Relative probability plots of moraine ages (thick curves) for M0, M1, and M2 moraines as the sum of the Gaussian probability density functions of individual dates (thin curves). Outliers are identified as samples that do not overlap with the mean at 2-sigma and are excluded from our analysis (gray curves, samples noted with gray italics). Blue central line represents the arithmetic mean value, and the parallel black, red, and green lines represent one, two, and three standard deviations from this value, respectively. The yellow band represents one standard deviation from the arithmetic mean. Moraine ages are reported as the arithmetic mean ± 1 sigma, but the population weighted means and medians of these moraines show good agreement and each could be used to represent moraine ages. We provide the reduced chi-squared statistic associated with each population; a value of <2 suggests analytical uncertainty alone is sufficient to explain observed variability (Bevington et al., 1993).

Moraine M3
Samples (n = 6):
FR14-01-24
FR14-01-25
FR14-01-26
FRY16-02-08
FRY16-02-09
FRY16-02-10

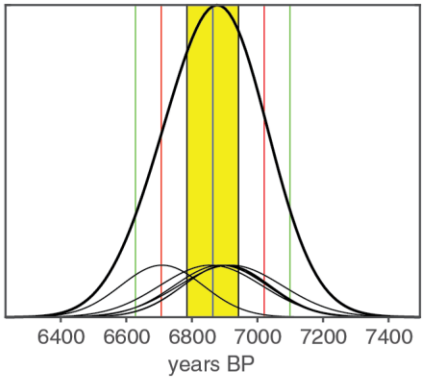

Statistics:
Mean ± 1σ: 6860 ± 80 yr (6860 ± 220 yr)
Mean ± uncertainty$_{(w)}$: 6860 ± 60 yr
Peak age: 6880 yr
Median ± interquartile range: 6900 ± 50 yr
Reduced χ^2: 0.4

Moraine M4a
Samples (n = 3):
FR14-01-17
FR14-01-18
FR14-01-19

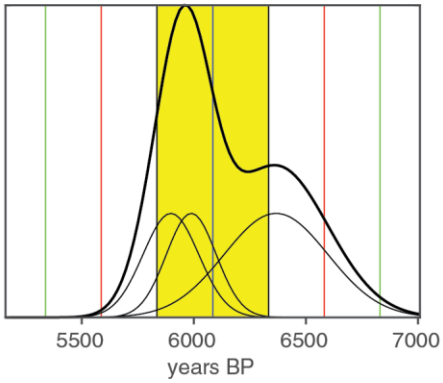

Statistics:
Mean ± 1σ: 6080 ± 250 yr (6080 ± 310 yr)
Mean ± uncertainty$_{(w)}$: 6000 ± 80 yr
Peak age: 5950 years
Median ± interquartile range: 5990 ± 350 yr
Reduced χ^2: 2.3

Moraine M4b
Samples (n = 2):
FR14-01-20
FR14-01-21

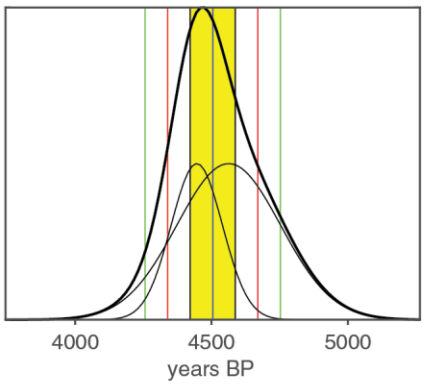

Statistics:
Mean ± 1σ: 4500 ± 80 yr (4500 ± 160 yr)
Mean ± uncertainty$_{(w)}$: 4470 ± 80 yr
Peak age: 4470 years
Median ± interquartile range: 4500 ± 120 yr
Reduced χ^2: 0.5

Moraine M7
Samples (n = 3):
FRY16-02-01
FRY16-02-03
FRY16-02-04

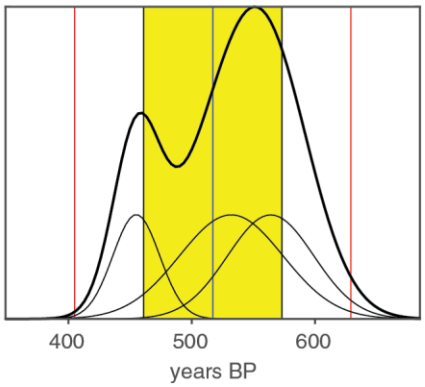

Statistics:
Mean ± 1σ: 520 ± 60 yr (520 ± 60 yr)
Mean ± uncertainty$_{(w)}$: 490 ± 20 yr
Peak age: 550 yr
Median ± interquartile range: 530 ± 80 yr
Reduced χ^2: 6.3

Fig. S3. Same as Fig. S2, but for moraines M3, M4a, M4b, and M7.

TABLES

Table S1. Age results

Sample	**Lm v. 2.2.1**	% uncertainty	v. 2.3. Lm	% of Lm v. 2.2.1	v. 3 Lm	% of Lm v. 2.2.1	v. 3 LSD	% of Lm v. 2.2.1
Moraine M0								
FR14-01-28	**16199 ± 395**	2.44%	15887	98.07%	15803	97.56%	15666	96.71%
FR14-01-29	**17843 ± 415**	2.33%	17489	98.02%	17365	97.32%	17198	96.39%
FR14-01-30	**17322 ± 361**	2.08%	16994	98.11%	16882	97.46%	16728	96.57%
FR14-01-31	***19958 ± 323***	*1.62%*	*19566*	*98.04%*	*19380*	*97.10%*	*19166*	*96.03%*
FR14-01-32	**17019 ± 318**	1.87%	16691	98.07%	16587	97.46%	16434	96.56%
M0 Average	**17100 ± 860**		16770	98.07%	16660	97.45%	16510	96.55%
Moraine M1								
FR14-01-01	**13873 ± 225**	1.62%	13609	98.10%	13595	98.00%	13527	97.51%
FR14-01-02	***7575 ± 178***	*2.35%*	*7410*	*97.82%*	*7473*	*98.65%*	*7479*	*98.73%*
FR14-01-03	**13771 ± 302**	2.19%	13507	98.08%	13494	97.99%	13436	97.57%
FR14-01-04	**13133 ± 244**	1.86%	12877	98.05%	12888	98.13%	12851	97.85%
FR14-01-05	**13322 ± 249**	1.87%	13058	98.02%	13061	98.04%	13019	97.73%
M1 Average	**13520 ± 540**		13260	98.06%	13260	98.04%	13210	97.66%
Moraine M2								
FR14-01-09	**9979 ± 306**	3.07%	9778	97.99%	9868	98.89%	9884	99.05%
FR14-01-10	***11109 ± 215***	*1.94%*	*10884*	*97.97%*	*10965*	*98.70%*	*10983*	*98.87%*
FR14-01-13	**9819 ± 208**	2.12%	9629	98.06%	9717	98.96%	9740	99.20%
FR14-01-14	***10477 ± 214***	*2.04%*	*10270*	*98.02%*	*10336*	*98.65%*	*10339*	*98.68%*
FR14-01-15	**9392 ± 176**	1.87%	9195	97.90%	9273	98.73%	9292	98.94%
FR14-01-16	***11662 ± 260***	*2.23%*	*11429*	*98.00%*	*11480*	*98.44%*	*11478*	*98.42%*
M2 Average	**9730 ± 420**		9530	97.99%	9620	98.86%	9640	99.06%
Moraine M3								
FR14-01-24	**6906 ± 133**	1.93%	6743	97.64%	6833	98.94%	6886	99.71%
FR14-01-25	**6709 ± 126**	1.88%	6551	97.64%	6646	99.06%	6709	100.00%
FR14-01-26	**6903 ± 130**	1.88%	6744	97.70%	6831	98.96%	6888	99.78%
FRY16-02-08	**6918 ± 158**	2.28%	6752	97.60%	6844	98.93%	6892	99.62%
FRY16-02-09	**6888 ± 142**	2.06%	6731	97.72%	6822	99.04%	6874	99.80%
FRY16-02-10	**6858 ± 156**	2.27%	6695	97.62%	6789	98.99%	6838	99.71%
M3 Average	**6860 ± 220**		6700	97.65%	6790	98.99%	6850	99.77%
Moraine M4a								
FR14-01-17	**5988 ± 111**	1.85%	5842	97.56%	5938	99.16%	6010	100.37%
FR14-01-18	**5897 ± 124**	2.10%	5754	97.58%	5842	99.07%	5916	100.32%
FR14-01-19	**6366 ± 231**	3.63%	6212	97.58%	6318	99.25%	6388	100.35%
M4a Average	**6080 ± 310**		5940	97.57%	6030	99.16%	6100	100.35%
Moraine M4b								
FR14-01-20	**4563 ± 190**	4.16%	4451	97.55%	4491	98.42%	4536	99.41%
FR14-01-21	**4446 ± 94**	2.11%	4337	97.55%	4375	98.40%	4416	99.33%
M4b Average	**4500 ± 160**		4390	97.55%	4400	98.41%	4480	99.37%
Moraine M7								
FRY16-02-01	**564 ± 35**	6.21%	532	94.33%	556	98.58%	570	101.06%
FRY16-02-03	**455 ± 19**	4.18%	424	93.19%	448	98.46%	469	103.08%
FRY16-02-04	**532 ± 42**	7.89%	501	94.17%	525	98.68%	541	101.69%
M7 Average	**520 ± 60**		490	93.94%	510	98.58%	530	101.87%

^{10}Be ages for Glaciar Torre samples, sorted by moraine, using the time-dependent Lal/Stone scaling model (Balco et al., 2008; Lal, 1991; Stone, 2000), the regional Patagonian production rate (Kaplan et al., 2011), and v. 2.2.1 of the constants file. We also present ages using the Lm scaling and the v. 2.3 calculator, the Lm scaling and the v. 3 calculator, and the Lifton/Sato/Dunai "LSD" scaling (Lifton et al., 2014) and the v. 3 calculator. The percent difference in age between each alternative calculation and the

v.2.2.1/Lm calculation is given in adjoining columns. The maximum difference between calculations is <4%; we conclude the choice of calculator does not fundamentally affect our conclusions.

References

Balco, G., Stone, J.O., Lifton, N.A., Dunai, T.J., 2008. A complete and easily accessible means of calculating surface exposure ages or erosion rates from 10Be and 26Al measurements. Quat. Geochronol. 3, 174–195. https://doi.org/10.1016/J.QUAGEO.2007.12.001

Bevington, P.R., Robinson, D.K., Bunce, G., 1993. Data Reduction and Error Analysis for the Physical Sciences, 2nd ed. Am. J. Phys. 61, 766–767. https://doi.org/10.1119/1.17439

Garibotti, I.A., Villalba, R., 2009. Lichenometric dating using Rhizocarpon subgenus Rhizocarpon in the Patagonian Andes, Argentina. Quat. Res. 71, 271–283. https://doi.org/10.1016/J.YQRES.2009.01.012

Harrison, S., Glasser, N.F., Duller, G.A.T., Jansson, K.N., 2012. Early and mid-Holocene age for the Tempanos moraines, Laguna San Rafael, Patagonian Chile. Quat. Sci. Rev. 31, 82–92. https://doi.org/10.1016/J.QUASCIREV.2011.10.015

Hogg, A.G., Hua, Q., Blackwell, P.G., Niu, M., Buck, C.E., Guilderson, T.P., Heaton, T.J., Palmer, J.G., Reimer, P.J., Reimer, R.W., Turney, C.S.M., Zimmerman, S.R.H., 2013. SHCal13 Southern Hemisphere Calibration, 0–50,000 Years cal BP. Radiocarbon 55, 1889–1903. https://doi.org/DOI: 10.2458/azu_js_rc.55.16783

Jóhannesson, T., Raymond, C.F., Waddington, E.D., 1989. A Simple Method for Determining the Response Time of Glaciers. Springer, Dordrecht, pp. 343–352. https://doi.org/10.1007/978-94-015-7823-3_22

Kaplan, M.R., Strelin, J.A., Schaefer, J.M., Denton, G.H., Finkel, R.C., Schwartz, R., Putnam, A.E., Vandergoes, M.J., Goehring, B.M., Travis, S.G., 2011. In-situ cosmogenic 10Be production rate at Lago Argentino, Patagonia: Implications for late-glacial climate chronology. Earth Planet. Sci. Lett. 309, 21–32. https://doi.org/10.1016/J.EPSL.2011.06.018

Lal, D., 1991. Cosmic ray labeling of erosion surfaces: in situ nuclide production rates and erosion models. Earth Planet. Sci. Lett. 104, 424–439. https://doi.org/10.1016/0012-821X(91)90220-C

Lifton, N., Sato, T., Dunai, T.J., 2014. Scaling in situ cosmogenic nuclide production rates using analytical approximations to atmospheric cosmic-ray fluxes. Earth Planet. Sci. Lett. 386, 149–160. https://doi.org/10.1016/J.EPSL.2013.10.052

Masiokas, M.H., Luckman, B.H., Delgado, S., Skvarca, P., Ripalta, A., 2009. Little Ice Age fluctuations of small glaciers in the Monte Fitz Roy and Lago del Desierto areas, south Patagonian Andes, Argentina. Palaeogeogr. Palaeoclimatol. Palaeoecol. 281, 351–362. https://doi.org/10.1016/J.PALAEO.2007.10.031

Mercer, J.H., 1965. Glacier Variations in Southern Patagonia. Geogr. Rev. 55, 390–413. https://doi.org/10.2307/213136

Röthlisberger, F., 1986. 1000 Jahre Gletschergeschichte der Erde. Verlag Sauerlander, Salzburg.

Schaefer, J.M., Denton, G.H., Kaplan, M., Putnam, A., Finkel, R.C., Barrell, D.J.A., Andersen, B.G., Schwartz, R., Mackintosh, A., Chinn, T., Schlüchter, C., 2009. High-frequency holocene glacier fluctuations in new zealand differ from the northern signature. Science (80-.). 324, 622–625. https://doi.org/10.1126/science.1169312

Stone, J.O., 2000. Air pressure and cosmogenic isotope production. J. Geophys. Res. Solid Earth 105, 23753–23759. https://doi.org/10.1029/2000JB900181

Strelin, J.A., Kaplan, M.R., Vandergoes, M.J., Denton, G.H., Schaefer, J.M., 2014.

Holocene glacier history of the Lago Argentino basin, Southern Patagonian Icefield. Quat. Sci. Rev. 101, 124–145. https://doi.org/10.1016/j.quascirev.2014.06.026
Stuiver, M., Reimer, P.J., 2018. CALIB.

* * *